THE REGULATION OF MITOCHONDRIAL FUSION TO EXTEND LONGEVITY AND THE EXOGENOUS REGULATION OF GERM CELL PROLIFERATION IN *CAENORHABTIDIS ELEGANS*

by

SNEHAL NITIN CHAUDHARI

(Under the Direction of EDWARD T. KIPREOS)

ABSTRACT

Mitochondria are dynamic organelles that undergo fusion and fission events in all eukaryotic cells. Mitochondrial dynamics are required for mitochondrial viability and serve as indicators of cellular health and bioenergetic status. Here we describe a pathway that regulates mitochondrial fusion in the nematode *Caenorhabditis elegans*. In this pathway, the ubiquitin ligase SCF^{LIN-23} and its exchange factor CAND-1 promote the activity of the AKT-1 kinase, which inactivates the FOXO transcription factor DAF-16. DAF-16 represses the expression of the mitochondrial proteases SPG-7 and PPGN-1, which inhibit the mitochondrial fusion protein EAT-3. Altering components of the pathway to increase mitochondrial fusion is associated with increased lifespan. We further show that diverse long-lived *C. elegans* mutants exhibit increased mitochondrial fusion, and that the fusion is essential for their longevity. Interestingly, physical exertion in *C. elegans* induces mitochondrial fusion, which requires DAF-16 activity. Furthermore, a daily exercise regimen in *C. elegans* extends lifespan by 60% compared

to animals that are not subjected to exercise. Overall, these results demonstrate the regulation and importance of mitochondrial fusion in physical exertion and longevity. *C. elegans* germ cells are syncytial and cannot be isolated and cultured. However, the germ cells from tumorous mutants can be cellularized and isolated from the animals, and cultured. Using this culture system, we found that the steroid hormone dafachronic acid inhibits *C. elegans* germ cell proliferation in vitro and in vivo, and requires the steroid hormone receptor DAF-12 for this function. We also identified bacterial folates as positive regulators of germ cell proliferation. Folates are B-complex vitamins that are required for the de novo synthesis of amino acids and nucleosides. We show that a bacterial folate – 10-formyl-tetrahydrofolate-Glu^n – signals germ cells to proliferate in vitro and in vivo. The bacterial folate precursor dihydropteroate also promotes germ cell proliferation in vitro and in vivo, despite its inability to promote one-carbon metabolism. The folate receptor homolog FOLR-1 is required for the stimulation of germ cells by 10-formyl-tetrahydrofolate-Glu^n and dihydropteroate.

INDEX WORDS: mitochondria, fusion, exercise, longevity, germ cells, dafachronic acid, folate, cancer.

THE REGULATION OF MITOCHONDRIAL FUSION TO EXTEND LONGEVITY AND THE EXOGENOUS REGULATION OF GERM CELL PROLIFERATION IN *CAENORHABTIDIS ELEGANS*

by

SNEHAL NITIN CHAUDHARI

MS, Pennsylvania State University, 2010

BS, Dr. D. Y. Patil Institute of Biotechnology and Bioinformatics, India, 2009

A Dissertation Submitted to the Graduate Faculty of The University of Georgia in Partial Fulfillment of the Requirements for the Degree

DOCTOR OF PHILOSOPHY

ATHENS, GEORGIA

2017

© 2017

Snehal Nitin Chaudhari

All Rights Reserved

THE REGULATION OF MITOCHONDRIAL FUSION TO EXTEND LONGEVITY AND THE EXOGENOUS REGULATION OF GERM CELL PROLIFERATION IN *CAENORHABTIDIS ELEGANS*

by

SNEHAL NITIN CHAUDHARI

Major Professor:	Edward T. Kipreos
Committee:	Jacek Gaertig
	Marcus Fechheimer
	Scott Dougan

Electronic Version Approved:

Suzanne Barbour
Dean of the Graduate School
The University of Georgia
August 2017

DEDICATION

I dedicate this dissertation to my husband, Zachary Detwiler, for his unconditional love, encouragement, patience, and support throughout graduate school. Thanks for helping, caring, and always being there for me. I would not have achieved any of this without you.

ACKNOWLEDGEMENTS

I thank Edward for teaching me how to think like a scientist, and giving me the freedom to pursue my project where it led me. I also want to thank my committee members for their guidance and encouragement, and members of the Kipreos lab for tolerating me, and helping me all these years. I thank my family- mom, dad, my grandparents, and Megz for all the love and support throughout my life; and Zach's parents- Michele and Bob for encouraging me to continue doing good work. Grad school has been the best 6 years of my life because of my friends- Zach, Vasudha, Cat, Justin, Robert, Riju, Diana, Anjana, Priyanka, Mayukh, Sarah, Gautam, Madhumati, and Penny. I extend my gratitude towards the labs of Dr. Dougan, Dr. Gaertig, Dr. Lechtreck, Dr. Meagher, Dr. Mensa-Wilmot, Dr. Schulz, Dr. Shields, Dr. Stabb, Dr. Striepen, and Dr. Kandasamy for help with reagents and equipment.

TABLE OF CONTENTS

Page

LIST OF TABLES

Page

LIST OF FIGURES

Page

CHAPTER 1

INTRODUCTION AND LITERATURE REVIEW

Since its discovery over 50 years ago, *Caenorhabtidis elegans* has proven to be an important model organism in biological research owing to its small size, simplicity, and short lifespan. *C. elegans* research has led to the discovery of many molecular and genetic pathways that are conserved in higher eukaryotes and mammals [1]. This dissertation focuses on 2 major discoveries made in the *C. elegans* field, which if conserved in other animals could transcend the existing paradigms on germline signaling and aging. Chapter 1 presents a literature review on key information and findings that qualify the reader to understand the results and discussions. In Chapter 2, I will discuss a new molecular signaling pathway that regulates *C. elegans* mitochondrial fusion, and its link to insulin signaling, physical exercise, and aging. In Chapter 3, I will describe the role of bacterial folates in inducing germ cell proliferation. Chapter 4 focuses on the role of the steroid hormone dafachronic acid in inhibiting germ cell proliferation. This will be followed by conclusions and discussions in Chapter 5.

The Ubiquitin Proteasome System (UPS)

The vast majority of proteins in the cell are degraded by the ubiquitin proteasome system (UPS). In this system, substrate proteins are tagged with a small protein called ubiquitin [2]. In the UPS, the cascade of E1-activating, E2-conjugating, and E3-ligating enzymes

efficiently tag substrate proteins with a polyubiquitin chain to target them for degradation by the 26S proteasome (Fig. 1.1A). The ubiquitin-activating enzyme E1 binds ubiquitin in an ATP-dependent process via a thiolester linkage. The activated ubiquitin is then transferred to the E2-conjugating enzyme, which interacts with the E3-ligating enzyme. E3 enzymes bind substrate proteins that are to be ubiquitinated, and facilitate the transfer of ubiquitin from the E2 to the substrate protein [3]. E3 ubiquitin ligases provide the specificity that attaches ubiquitin to intended substrate proteins. Polyubiquitination, predominantly through the ubiquitin lysine 48, generally targets proteins for proteolysis. A chain of at least four ubiquitins are a primary signal for targeting proteins for degradation [4]. In contrast, ubiquitination of proteins through the ubiquitin lysine 63 are associated with cellular functions including protein transport, signaling, and shuttling of proteins in the endoplasmic reticulum [5]. The polyubiquitinated proteins are then degraded via the proteasome, which is a large multisubunit protein that can recognize ubiquitinated substrates and proteolytically degrade them. The ubiquitin monomers do not enter the proteasome, and are 'recycled' to label other proteins for transport or degradation [6]. Malfunctioning of the UPS system has been linked to several neurodegenerative diseases primarily due to accumulation of unfolded proteins [7]. Reduction in proteasome function is associated with protein aggregation, defects in protein degradation, and autophagic cell death [8]. Clinical observations and animal experiments have suggested that proteasome functional insufficiency plays an important role in the genesis of congenital diseases [8]. Importantly, the inability to degrade unfolded proteins accelerates aging, while increases in proteasome activity and

proteolysis extends lifespan [4]. Therefore, understanding the mechanisms of protein degradation is important in the context of health and lifespan.

Cullin-RING ubiquitin ligases (CRLs) and their regulation

Mammals have only two E1 enzymes, around 40 E2s, and over 500 different E3 enzymes [9, 10]. The E3 enzymes act to maintain specificity for the large number of protein substrates. The largest group of E3 ubiquitin-ligating enzyme class are the cullin-RING ubiquitin ligases (CRLs) that comprise over 200 members, and are responsible for proteasome-mediated degradation of over 20% of the proteins in cells [11]. CRLs are multi-subunit complexes that include a cullin, a RING H2 finger protein, a substrate-recognition subunit (SRS), and an adaptor subunit that links the SRS to the complex (Fig. 1.1B) [12]. Eukaryotes have 5 cullins- CUL1, 2, 3, 4 and 5 that are widely-observed in animals, and 2 cullins – CUL7 and PARC (Parkin-like cytoplasmic protein) that appear to be vertebrate-specific. *C. elegans* has 6 cullins (CUL-1 to CUL-6) [13]. Crystal studies have shown that the RING H2 finger protein- RBX1 binds the C-terminal domain of all cullins, while RBX1's paralog- RBX2 preferentially associates with CUL5 [14]. Tight binding of cullins with RBX1/2 results in the formation of a single globular CRL unit, existing in a "closed" conformation [14]. Binding of the regulatory protein NEDD8 to the C-terminal domain of cullin/RBX1/2 complex results in "opening" of the CRL complex [14]. NEDD8 binding (neddylation) is a process where NEDD8 is post-translationally attached to cullins via a cascade of E1-E2 and E3 enzymes similar to ubiquitination [15]. Neddylation stimulates the recruitment of ubiquitin-activated E2 enzyme, and enhances the formation of polyubiquitin chains on the substrate proteins bound to the cullin N-

terminal domain (Fig. 1.1B) [16]. Neddylation enhances the activity of CRL complexes independent of the F-box proteins or the substrate proteins [17]. RBX1 binding with CRL is required for neddylation. It has been proposed that NEDD8 and RBX1/2 form a platform for binding of the E2 enzyme, and NEDD8 increases flexibility of the cullin C-terminal domain to allow formation of polyubiquitin chains on substrate proteins [12, 18]. RBX-1 mutants undergo embryonic arrest in *C. elegans*, suggesting that its function is essential.

CRLs are modular structures that utilize cullins as scaffold proteins that bind interchangeable adaptors, SRSs and regulator proteins (such as NEDD8, RBX1/2 discussed above, and CAND1, CSN discussed below) to enable assembly of functionally diverse E3 ligase complexes. This diversity in the ligase complexes allows CRLs to regulate diverse cellular processes including multiple aspects of the cell cycle, transcription, signal transduction, and developmental programming. Perturbation of CRL activity has been linked to severe developmental growth defects, and cancer [11, 12]. Therefore, CRLs have become a sought-after target for drug discovery and therapeutics for a variety of human diseases.

Post-translational modifications of CRL substrates

As discussed above, polyubiquitination of substrate proteins facilitates their degradation. Accumulating evidence suggests that CRL E3 ubiquitin ligases and SRSs generally recognize and bind substrate proteins when they are post-translationally modified [19]. These modifications that target substrate proteins for degradation occur in specific motifs of the proteins called degrons [20]. Degrons can be post-translationally modified by

phosphorylation, acetylation, glycosylation, or hydroxylation. Except for acetylation, all of these modifications have been shown to be important for the regulation of protein degradation by CRL complexes, especially the most extensively studied SCF complexes, named for the core components Skp1 adaptor – cullin 1 – F-box protein SRSs [21, 22]. Phosphorylation of proteins is a major mechanism by which proteins are specified for degradation to regulate cell cycle progression [12]. Phosphorylation of substrate proteins can stabilize them or induce their degradation depending on the SRS, and is regulated by kinases and phosphatases [22, 23]. Hydroxylation of HIF1-α (hypoxia-induced factor 1 α) under normoxic (normal oxygen) conditions facilitates its degradation by the von Hippel–Lindau tumor suppressor (pVHL) CUL2 E3 ligase complex ($CRL2^{VHL}$) [24]. Recent studies have shown that CUL1 ubiquitin ligases with Fbx2 as the SRS (SCF^{Fbx2}) ubiquitinate and degrade *N*-glycosylated proteins that are translocated from the endoplasmic reticulum (ER) to the cytosol [25]. This serves as a quality control mechanism in the ER-associated degradation (ERAD) pathway to proteasomally degrade misfolded proteins. HECT-domain containing E3 ubiquitin ligases have been shown to specifically degrade the cell growth protein Ras when it is acetylated [26]. Additionally, interactions between the substrate and non-peptide hormones, small molecules and cofactors also regulates the recruitment and binding of SRSs to these proteins [21].

CUL1, CUL3, and CUL4-containing CRL complexes can form dimers in vivo [12]. CRLs are neddylated when active, and can dimerize via their SRS proteins [12]. SRS-mediated dimerization occurs via interaction between SRS proteins, and has been observed for some F-box proteins [12]. Dimerization of CRL complexes has been shown to enhance ubiquitination and degradation of substrate proteins [17].

CRL regulation by the CSN complex and CAND1

The COP9 Signalosome (CSN) is a conserved 8-subunit protein complex that is associated with phosphorylation, deneddylation, and deubiquitination, all of which can regulate CRL complexes. The CSN complex inhibits CRLs by deneddylating cullins preventing them from binding substrate proteins (Fig. 1.1C). But while doing so, the CSN complex stabilizes the fully assembled CRL complex by inactivating the cullin (by deneddylation) thus preventing the autoubiquitination of SRS proteins, which can lead to their degradation in the absence of a substrate. This protective mechanism that stabilizes SRS proteins in the absence of a substrate is conserved amongst various eukaryotes, from yeast to humans. Consistently, loss of CSN activity in vivo causes a decrease in CRL activity.

CAND1 (cullin-associated and neddylation-dissociated-1) is an evolutionarily conserved protein that binds CRL complexes, and is required for CRL activity in vivo [27]. Initially identified as an inhibitor of CRL complexes in vitro, CAND1 'hugs' the CRL complexes and binds its C- and N-terminal domains, thus preventing assembly of CRL complexes (Fig. 1.1C). However, in vivo experiments showed that this CAND1 binding to cullins is essential for its function [27]. Depletion of CAND1 results in alterations in abundances of specific CRL complexes [28]. It has been proposed that CAND1 acts as an exchange factor that allows the interchanging of SRSs with CRL complexes [28, 29]. Like the CSN complex, CAND1 only binds and sequesters unneddylated cullins, however unlike the CSN complex, CAND1 cannot remove neddylation from cullins. Therefore, it has been proposed that CAND1 and CSN complex work together, where CSN deneddylates cullins before CAND1 can bind and exchange

the SRS subunit for another one. CAND1 and CSN potentially work together to regulate the repertoire of SRSs and F-box proteins that cullins bind in vivo. The regulation of CAND1, and its functions in vivo are still largely unknown.

C. elegans CAND-1 and CSN

The CAND1 homolog in *C. elegans* has significant sequence identity with the CAND1 proteins across eukaryotes [27]. Our laboratory has previously demonstrated the importance of CAND-1 in the model organism *C. elegans* wherein CAND-1 inactivation leads to developmental delay, altered cell divisions, and morphological defects [27]. Other labs have shown that *C. elegans csn* mutants have muscle contraction defects and germline defects [30, 31]. CSN inactivation in *cand-1* mutants exacerbates the *cand-1* mutant phenotype and leads to embryonic arrest. These observations suggest that in *C. elegans*, both CAND-1 and CSN are important. Specifically, CAND-1 affects the activity of CUL-1 bound to the F-box protein LIN-23, which is the *C. elegans* ortholog of the human ß-TRCP [27]. Consistently, *cand-1*, *cul-1*, and *lin-23* mutants share phenotypes of increased number of seam cells, protruding vulva, defective alae formation, and accumulation of the glutamate receptor GLR-1, a target of the SCF^{LIN-23} complex [27]. In this dissertation, I will discuss a novel pathway that links CAND-1/ SCF^{LIN-23} to insulin signaling, and the regulation of mitochondrial fusion in *C. elegans* muscle cells.

Mitochondrial dynamics and their function

Historically considered as rigid organelles that produce ATP, mitochondria have been identified as dividing, fusing, and moving organelles in the past few decades [32].

Mitochondrial dynamics are important in maintaining the health of the cell [33]. Constant cycles of fusion and fission are required for the function, structure, and genetic integrity of the mitochondrial population in a cell [33]. Mitochondrial fusion and fission events counterbalance each other, and defects in fusion and/or fission are associated with lethality in some animal models and with several human genetic disorders [34, 35].

Mitochondrial fusion is required for genetic complementation, wherein mitochondrial contents are exchanged and mixed to ensure that in situations where certain mitochondria have defective genes, every organelle has the correct proteins and genes required for its function [35]. Fusion enables mtDNA repair and equal distribution of crucial metabolites [36, 37]. Mitochondrial fission is required for mitochondrial transport to sub-cellular compartments such as lamellipodia and dendrites, and to ensure equal segregation of mitochondria to daughter cells during cell division [36]. Fission has also been shown to be important in isolating dysfunctional mitochondria, which can be targeted for degradation (mitophagy) [38]. Mitochondrial fission is required for inducing cell death [39]. When apoptosis is induced in the cell, mitochondria undergo fragmentation, inhibition of which prevents release of cytochrome c, thus inhibiting apoptosis [39]. Therefore, perturbation of mitochondrial dynamics can cause cellular dysfunction, and has been linked to many human genetic diseases including neuropathies such as Optic Atrophy, Parkinson's disease, and cardiovascular disorders such as Ventricular-associated Congenital Heart disease, Hibernating Myocardium, and cardiomyopathies [35, 40]. Mutations in mitochondrial fusion proteins have been known to cause neurodegenerative diseases such as Charcot-Marie Tooth type 2A and Kjer

disease/autosomal dominant optic atrophy, and have been linked to type 2 diabetes [40-42].

Regulation of mitochondrial dynamics

Three categories of proteins are involved in mediating mitochondrial fusion and fission events: 1) outer membrane fusion proteins mitofusins (Mfns) in humans (FZO-1 in *C. elegans*); 2) inner membrane fusion proteins like Opa1 (optic atrophy) in humans (EAT-3 in *C. elegans*); and 3) mitochondrial fission protein Drp1 in humans (DRP-1 in *C. elegans*) [35, 43, 44]. All of these proteins are self-assembling GTPases that perform their fusion or fission events independently of each other [45]. Mitochondrial fusion and fission machinery are subjected to post-translational modifications that affect their abundance, stability, location, and binding and tethering properties, thus regulating mitochondrial morphology and function [45]. Opa1 is proteolytically cleaved by mitochondrial proteases into short isoforms, and various studies in cell lines have shown that both long and short isoforms of Opa1 are required for mitochondrial fusion [45]. These GTPases are highly conserved from yeasts to humans, and link various cellular cues to mitochondrial form and function in order to adapt to environmental changes. For example, dissipation of membrane potential results in inhibition of mitochondrial fusion proteins. This allows dysfunctional fragmented organelles that cannot undergo fusion to be isolated and degraded via mitochondrial autophagy (mitophagy) [46]. On the other hand, cellular stress (such as DNA damage, oxidative stress, etc.) induces mitochondrial fusion as a protective mechanism to increase ATP production, and to allow containment of superoxide radicals emerging from the mitochondria from destroying other organelles

[47-49]. Inactivation of either fusion or fission proteins has been shown to cause cell death in yeast, *Drosophila*, and *C. elegans* [35, 44]. Despite the importance of mitochondrial fusion and fission in human disease, their regulatory mechanisms and pathways are not fully understood.

Mitochondrial DNA and aging

Mitochondria have been considered a central player in aging for over 4 decades, and is the organelle most affected in an aging cell [50, 51]. It has been well documented that as animals age, they accumulate mitochondrial mutations. However, whether mtDNA mutations are causal to aging, or simply correlate with aging was a subject of debate for many years. In the past decade, many groups have probed this relationship between mtDNA mutations and aging, and have generally found that mtDNA mutations cause aging [52]. This was perhaps most directly demonstrated in engineered mice with a proofreading-deficient mtDNA polymerase which accumulated mutations at much higher rate than normal, and had accelerated aging [53].

Since mtDNA encodes for only 13 proteins, all of which are components of the electron transport chain (ETC), it is generally believed that ETC dysfunction causes aging [50]. Furthermore, the ETC is a major hub for reactive oxygen species (ROS) production in the cell. The Mitochondria Free Radical Theory of Aging (MRFTA) attributes aging to increased oxidative damage in the mitochondria [54, 55]. According to the MFRTA, the ROS players that are responsible for aging arise from the ETC and account for over 90% of superoxides ($O_2^{\bullet -}$), peroxides (H_2O_2) and the highly reactive hydroxyl ($^{\bullet}OH$) species of ROS in the cell [50, 56]. ROS especially causes mutations in

mtDNA, thus the MFRTA considers mitochondria at the center of a vicious cycle, where aging causes an increase in mtDNA mutations, causing ETC dysfunction, causing ROS-mediated oxidative damage to mtDNA, leading to further increase in ROS production [56]. However, the MFRTA has been largely refuted recently, the reasons for which will be discussed in the sections below.

Mitohormesis

The MFRTA is based on the observation that mtDNA mutations and ROS production increase with age, while mitochondrial function and ROS-scavenging enzymes decrease with age [57]. Even though these observations are true in all animals tested, recent findings have disputed the MFRTA. Mainly stemming from work done in *C. elegans*, researchers have found that a partial reduction in ETC can slow aging and increase longevity [58]. In a concept termed mitochondrial hormesis or mitohormesis, low amounts of ROS act as signaling molecules to trigger stress-induced responses in the cell that are protective and cause an increase in healthspan and lifespan [59]. These protective mechanisms include stress resistance, unfolded protein response (UPR), proteostasis, etc. that help increase gene expression of detoxifying proteins, superoxide dismutatse (SOD), and increase chaperone production and antioxidant enzymes to improve health of the cell [59]. Apart from *C. elegans*, the concept of mitohormesis has been observed in yeasts, *Drosophila*, and rodents. Another argument against the MFRTA is the species-to-species variations in the relationship between ROS levels and lifespan. For example, naked-mole rats, that live for 25 to 30 years have similar levels of mitochondrial ROS production compared to mice that live only 3-4 years [57]. However, as predicted by the MFRTA, a

complete inhibition of ETC components is detrimental to health and survival. Too much oxidative stress, arising from complete inhibition of ETC can cause disease and lethality in *C. elegans* and mammals, including humans [58, 60]. Therefore, severe ETC dysfunction and ROS production can contribute to aging, but is not the primary mechanism by which mtDNA mutations cause aging.

Mitochondrial function and aging

Studying the effect of mtDNA mutations that occur with age is difficult considering the heteroplasmic nature of mtDNA, wherein every cell has a mixture of wild-type and mutated mtDNA [61]. However, since mtDNA expression is required for oxidative phosphorylation, increases in mtDNA mutations have been shown to predominantly affect ATP production [62]. Aging mice and humans show an age-related decrease in ATP production, with human ATP production decreasing by 8% per decade [63]. Therefore, mtDNA mutations may induce aging by decreasing ATP production in older animals.

It must be noted that mtDNA mutations have effects that are not directly related to oxidative phosphorylation, which also correlate with aging. For example, mtDNA mutations have been shown to be associated with increased apoptosis/cell death [63]. Mitochondria release cytochrome c and other factors that induce the apoptotic caspase cascade leading to cell death [64]. Therefore, mitochondrial dysfunction due to mtDNA mutations triggers apoptosis in aging mice, rodents, and humans by mechanisms that are not fully understood [63].

Another hallmark of aging is muscle loss, also called sarcopenia [65]. Older humans and mice with mitochondrial disorders have increased mitochondrial mass in their skeletal muscle cells [66]. This increase in mitochondrial mass can be caused by a reduction in autophagic clearance of old mitochondria (mitophagy) [61]. Alternatively, experiments in mice have shown that a decrease in ATP production, caused by mtDNA mutations can activate mitochondrial biogenesis, to compensate for the deficient mitochondrial function [66]. This could contribute to the increase in mitochondrial mass in skeletal muscle cells in older humans. Impairment of mitophagy also occurs with age, and can influence accumulation of damaged mitochondria with mtDNA mutations [67]. Therefore, increased mitophagy is protective for mitochondrial health and is associated with increased lifespan as shown in *C. elegans*, *Drosophila*, mice, and humans [67].

Lastly, mitochondrial dynamics have been shown to be linked to aging. With age, mitochondria in yeasts, *C. elegans*, and mice have been shown to fragment [68-70]. This fragmentation is linked to changes in expression of mitochondrial fusion and fission proteins [70].

In conclusion, the role of mitochondria in aging is undisputed. However, the mechanisms that tie the various effects of aging in different species, animals and tissues are yet to be discovered.

Insulin signaling

Insulin and insulin-like growth factor (IGF) are hormones that bind the tyrosine kinase insulin receptor mainly in adipose tissues, liver, and muscle cells [71, 72]. The main function of insulin signaling is to induce the uptake of glucose, and other nutrients such

as amino acids and fatty acids from the blood, and stimulate their storage into tissues in the form of glycogen, proteins and lipids respectively [73]. Reduced insulin production by the pancreatic islets leads to Type-1 diabetes, while reduced insulin signaling is the cause of Type-2 diabetes typically characterized by insulin resistance [73]. Apart from the canonical role of nutrient uptake of insulin signaling, the insulin signaling pathway has been shown to be important for growth and differentiation; impairment of insulin signaling is linked to various metabolic, cardiovascular, and neurodegenerative diseases [74, 75]. The insulin/IGF signaling (IIS) pathway is highly conserved from yeasts to humans [76]. The IIS pathway has been extensively studied in *C. elegans*. Briefly, binding of insulin and IGF ligands to the insulin receptor (DAF-2 in *C. elegans*) activates a signaling cascade that leads to transcriptional changes in the cell. After ligand binding, the activated receptor recruits and activates phosphatidylinositol 3-kinase (PI3-kinase, also AGE-1 in *C. elegans*) at the plasma membrane, allowing it to interact with its membrane-bound physiological substrate PIP_2. PI3-kinase converts PIP_2 into the second messenger PIP_3. Elevated levels of PIP_3 activate the 3-phosphoinositide dependent protein kinase-1 (PDPK1 or PDK1). PDK1 is a master kinase, which when activated can in turn activate many kinases such as Protein Kinase B (PKB/Akt), Protein Kinase C (PKC), cyclic AMP-dependent protein kinase (PRKACA), glucocorticoid-inducible kinase (SGK1), and can turn on multiple signaling cascades in the cell [77]. PDK-1 in *C. elegans* can activate the kinases AKT-1, AKT-2, and SGK-1. Active AKT-1 directly phosphorylates and inactivates FOXO transcription factor DAF-16, which prevents nuclear localization of DAF-16. When insulin signaling is off, DAF-16 in the unphosphorylated (active) state is in the nucleus, and acts as a master regulator, inducing

the expression of genes required for stress response and cell survival [78]. Insulin/IGF signaling (IIS) pathway, and its regulation in aging, growth, and differentiation is conserved amongst metazoans [79].

IIS in dauer formation and aging

C. elegans has four larval stages (L1 to L4) prior to adulthood, but under unfavorable conditions such as limited food availability, high temperatures, or increased population density, *C. elegans* L2-stage larvae will undergo a dauer arrest [80]. The dauer state is morphologically, metabolically, and physiologically distinct compared to larval stages, with exceptionally high resistance to heat, stress, and other environmental insults [81]. *C. elegans* dauers also live up to eight times longer than non-dauer animals [80]. *daf-2* and *age-1* mutants were identified in a screen for constitutive dauer formation (daf), while *daf-16* mutants were identified as dauer defective mutants [82, 83]. Simultaneously, the most striking discovery made in *C. elegans* was that reduced insulin signaling via *daf-2* extends lifespan [84]. *C. elegans daf-2* mutants live twice as long as wild-type animals, and this lifespan extension is dependent on the activity of DAF-16 [85]. Consistently, IIS pathway mutants *pdk-1*, *age-1*, and *akt-1* have extended lifespans that require DAF-16 activity, whereas *daf-16* mutants have a shorter lifespan compared to wild-type animals [86, 87]. A contributing mechanism that allows IIS pathway mutants to live long is their remarkable ability to combat stress. DAF-16 transcriptionally activates superoxide dismutase (*sod-3*) to allow resistance to oxidative stress [88]. Furthermore, reduced IIS recapitulates constitutive dauer-formation phenotypes. Strong mutants of *daf-2*, *age-1*,

and *akt-1* live long, are resistant to stress, and can arrest as dauers, and all of these phenotypes can be reversed by inhibiting DAF-16 activity [89-91].

In addition to *C. elegans*, reduced insulin signaling has been shown to extend lifespan in yeasts, *Drosophila*, and rodents [92]. However, the effects of reduced insulin signaling in human longevity is conflicting. Reduced insulin signaling, a hallmark of diabetes, reduces the average human lifespan by a decade [93]. With age, insulin sensitivity declines, and increases the risk of developing type 2 diabetes in older people [81]. Interestingly, the increase in insulin resistance reaches a peak at the age of 80, after which insulin resistance decreases sharply [94]. Surprisingly, this reduction in insulin resistance in nonagenarians and centenarians and is also accompanied by a sharp reduction in pancreatic β-cell function [94]. Additionally, older humans have increased insulin sensitivity, use insulin more efficiently, and have higher glucose uptake, but overall reduced IIS pathway activation [95, 96]. Mutations in AKT and the insulin receptor are associated with longevity in multiple cohorts of humans, while mutations in FOXO3A and FOXO1A have been consistently associated with mortality in many human cohorts [81, 97]. Therefore, it is apparent that reduced insulin signaling appears to increase human lifespan if counterbalanced by efficient glucose uptake. However, the biological mechanism linking reduced insulin signaling to increased lifespan in humans is unknown.

Dafachronic acid signaling

In screens to identify dauer formation (daf) mutants, two genes – *daf-9* and *daf-12* were identified, which also have pleiotropic phenotypes for *C. elegans* gonad migration,

specifically the migration of the distal tip cell (DTC) [98]. The *C. elegans* gonad is made of 2 U-shaped arms, with mitotic germ cells in the distal gonad, capped by the DTC [99]. The dauer-constitutive gene *daf-9* encodes for a Cytochrome P450 enzyme required to produce a bile-like steroid hormone called dafachronic acid (DA), while the dauer-defective gene *daf-12* encodes a nuclear receptor that is bound by DA [100, 101]. DA has been shown to act via DAF-12 to prevent entry into dauer and reduce *C. elegans* lifespan in wild-type animals. Under unfavorable conditions, such as starvation, peptide signaling pathways are suppressed, and animals move into the dauer state and have longer lifespans [102]. Starvation also dramatically reduces *C. elegans* germ cell numbers and gonad size, subsequently also reducing the number of proliferative germ cells in the gonad [103]. *daf-9* mutants do not have a starvation-induced reduction in germ cells, but adding DA to *daf-9* mutants rescues this phenotype and reduces germ cell numbers upon starvation. Therefore, DA induces dauer formation, starvation-induced lifespan extension and a reduction in germ cell numbers in starved adults.

Folates – sources and absorption into cells

Folates are water-soluble B-vitamins that are essential for all eukaryotes [104]. Humans obtain folates from plants, yeast, and bacteria in their diet [104]. Folates consist of a pteridine ring joined by a methylene bridge to para-aminobenzoic acid (PABA), which is attached to glutamic acid residues by a peptide bond [105]. Natural dietary folates mainly consist of 5-methyl tetrahydrofolate (5-methyl-THF) and 10-formyltetrahydrofolate (10-formyl-THF) in their polyglutamated forms, with one to six glutamate molecules [106]. Folates are essential for *de novo* purine, thymidylate, and methionine synthesis in a

process termed one-carbon metabolism (Fig. 1.2). Methionine is subsequently used for the synthesis of S-adenosylmethionine (SAM), which is a methyl donor that is required for the methylation of DNA, proteins, lipids, and other molecules [107]. The human colon microbiota represents a major source of folate, and contributes more to host folate levels than folates obtained from diet [108]. The gut microbiota predominantly makes and secretes folates in the form of 5-formyl-THF, 5,10-methenyl-THF, and 10-formyl-THF with up to 8 Glu residues, but the precise number of Glu residues is species specific [109-111]. Polyglutamylated folates from the diet and microbiota folates in the gut are hydrolyzed into monoglutamates in the intestine prior to absorption by other cells and tissues [106]. Once monoglutamylated folates are taken up by cells, the folates are glutamylated with up to 9 glutamate residues, or longer [107]. Polyglutamated folates accumulate in cells because they do not cross cellular membranes and are therefore retained in cells. Polyglutamylated folates also have a higher affinity for enzymes involved in one-carbon metabolism than their monoglutamate counterparts. [106]

Folates in one-carbon metabolism

Folate-mediated *one-carbon metabolism* (OCM) is the enzymatic transfer of chemically-activated one-carbons onto folates, which are then used for the *de novo* synthesis of biomolecules in the cell [107]. In the cell, one-carbon metabolism is compartmentalized. Polyglutamated folates in the mitochondria and cytoplasm are two distinct pools that contribute activated cofactors with each other, but are not in equilibrium through folate exchange [106]. Mitochondria contribute around 40% of total cellular folates, and is required primarily for the production of formate from catabolism of choline [106].

Formate serves as a primary source of one-carbon units for cytoplasmic OCM (Fig. 1.2) [107]. Mitochondrial folate metabolism also contributes glycine and ^{fmet}tRNA from the catabolism of serine, and glycine [106]. In the cytoplasm, folates are involved in three metabolic pathways that include homocysteine remethylation, purine biosynthesis and dTMP biosynthesis [106]. 5-methyl-THF functions as a methyl donor for homocysteine remethylation for methionine production via the enzyme methionine synthase [104, 106]. The resulting THF can be converted into 5,10-methylene-THF, 10-formyl-THF, and 5,10-methenyl-THF, by the trifunctional enzyme methylenetetrahydrofolate dehydrogenase (MTHFD1) (Fig. 1.2) [106]. 10-formyl-THF can donate one-carbon groups for purine biosynthesis. The purine biosynthetic machinery exclusively utilizes 10-formyl-THF as the folate cofactor for the biosynthesis of the purine ring in a 10-step pathway [106, 107]. Whereas 5,10-methylene-THF can be used as a cofactor for thymidylate synthesis where dUMP is converted into dTMP [107]. Folate is particularly important during periods of rapid cell division in proliferating cells when purine, dTMP, and methionine synthesis, and DNA replication, methylation, and repair are needed the most. For example, high amounts of folate prove beneficial for cell proliferation in embryonic neural tube closure, the proliferation of leucocytes, erythrocytes and enterocytes, or progression of cancer [107, 108, 111]. Therefore, supplementation with the synthetic monoglutamylated folic acid alleviates neural tube defects (NTD) in developing embryos by inducing folate-mediated one-carbon metabolism [106]. DNA methylation has been largely considered to play an important role in NTD etiology, leading to the hypothesis that impairments in the homocysteine remethylation cycle were causal in NTD pathogenesis [106].

Folate transporters

Monoglutamylated folates are transported into mammalian cells and tissues by specialized membrane transport systems and receptors [108, 112]. RFC (reduced folate carrier) is ubiquitously expressed in many mammalian cells and tissues, and is the major folate transporter [113]. RFC1 is a facilitative anion exchanger that has a high affinity for reduced folates, such as the primary physiologic substrate, 5-methyl-THF [114]. PCFT (proton-coupled folate transporter) is a proton-folate symporter that facilitates uptake of folates by coupling the flow of protons down the electrochemical gradient. PCFT functions optimally at acidic pH [115]. Therefore, PCFT is predominantly expressed in the intestine, allowing absorption of folates in the acidic intestinal environment [116]. Recent studies have also shown expression of PCFT in the placenta, choroid plexus (transporting folates into the cerebrospinal fluid), and kidney tubules [117-119]. PCFT, together with the Folate Receptor mediates endocytosis and release of folates in the cell as discussed below.

Folate receptor (also known as the folate binding protein (FBP), Folbp1 and Folbp2 in mice and FRα, FRβ, and FRγ in humans) is a GPI-anchored protein that has a high affinity for 5-methyl-THF and folic acid [114, 120]. FR is ubiquitously expressed in many tissues in mammals, albeit at very low levels compared to RFC, but FR is expressed at high levels in most cancers [121]. Even though FR has higher affinity for folic acid and 5-methyl-THF compared to RFC, RFC is responsible for the transport of the bulk of folates into the cell, and predominantly contributes to the folate pool in the cell for one-carbon metabolism. This is demonstrated by the fact that PCFT- null mice as well as FRα-deficient mice can both be rescued by prenatal and/or postnatal folate

supplementation [114, 122]. On the contrary, RFC1-/- mice, while also embryonic lethal, cannot be rescued to offspring viability by supplementation with various folate sources [114, 123]. Folr1, the FR ortholog in *Xenopus*, is required for neural tube closure in the developing frog embryo, but does not contribute to the overall level of folates in the cells [124]. Recent evidence suggests that FRα, when activated by binding to a folate, is endocytosed along with PCFT via vesicles that colocalize with multivesicular bodies (MVBs) in the cell [122]. MVBs are known to be sites for intracellular sorting of proteins between recycling, degradation, and secretion pathways [125]. In late endosomes, when the pH drops, the folate is released into the cell via PCFT which functions optimally at acidic pHs [126]. The folate receptor can then be recycled back to the plasma membrane [126, 127]. Thus, folates are taken up by cells and tissues in animals via conserved folate transporters and receptors.

Folate transporters and cancer

In Chapter 3, I will be discussing a new role of FR in inducing *C. elegans* germ stem cell proliferation. This section of the literature review highlights the known roles of folate transporters in signaling and cancer. Since folates are critical in rapidly proliferating cells, many studies have probed the link between folate transporters and cancer. Even though RFC predominantly contributes to the folate reservoir in the cell, it does not correlate with cancer prognosis. Cancer cells exist in a low pH and hypoxic environment [128]. RFC function decreases at pH < 7, whereas PCFT works maximally at lower pH [129]. FR can bind folates at lower pH found in endosomes, but as the pH drops further, FR releases the folate which is then transported into the cell via activated PCFT [130].

Therefore, FR and PCFT may play an important role in the uptake of folates by cancer cells, and not RFC. Also, many studies have ruled out the role of RFC in cancer proliferation and tumor progression in cancers of ovarian, colon, breast, and in leukemia [114, 131-133]. On the contrary, RFC has been shown to be tumor suppressive, especially in conditions of low folate, where RFC can induce folate efflux, causing cell death [114, 131, 132]. Therefore, RFC could potentially function as a unidirectional folate exporter under low folate conditions [132].

In contrast to RFC, many studies in vitro and in vivo have linked FR to cancer. Firstly, FR is overexpressed in many cancers, and can be higher in cancer cells by up to two orders of magnitude compared to normal cells [134]. Secondly, this increase in FR expression is associated with an increase in cell growth, proliferation, and tumor progression in ovarian, lung, colon, nasopharyngeal, pituitary cancers [125, 131, 135-140]. Lastly, stemming largely from cell line studies, it has been observed that FR expression is dependent on levels of folate in the media- with low levels of folate inducing expression of FR transcriptionally, translationally, and by gene amplification [120, 131, 133, 134]. Despite its link to cancer, FR does not significantly add to the folate reservoir in the cells. As discussed above, RFC predominantly contributes to the folate pool in the cell and, thus, to one-carbon metabolism. Therefore, it has been suggested that FR induced in cancer cells performs alternate functions to increase cell proliferation by mechanisms that differ from folate internalization [136]

[135]. It has been shown that FR induces cell signaling via STAT activation in HeLa cells, MAPK activation in *Dictyostelium discoideum*, and upregulation of NOTCH-signaling target genes in pituitary adenomas [135, 141, 142]. Furthermore, FR has been

shown to associate in lipid rafts on the plasma membrane, and can interact with signaling molecules when activated by folates [135]. Recently, a study showed that when FRα binds folic acid, it is internalized in a caveolar vesicle, folic acid is released in the lysosome, and free FRα translocates to the nucleus and binds to cis-regulatory elements of target genes and directly activates transcription [143].

Folate in cancer - cell line studies

Cell lines are convenient to study folate transporter binding affinities to folates, and to study the effect of folates on signaling cascades and the transcriptome. However, studying the effect of different folates on cell proliferation, migration, and cancer has generally produced varying results. For example, in colon epithelial cell lines, one group showed that folic acid inhibits DNA synthesis and cell proliferation in colon epithelial COLO-205 cells [144]. In contrast, other groups observed that folic acid causes an increase in cell proliferation in HCEC, NCM356, and NCM460 colon epithelial cell lines [145]. Even with gene expression studies and underlying pathways that control cell proliferation, the results vary tremendously. One group showed that folic acid inhibits cell proliferation via activation of NFkB [144]. Another group observed that folic acid upregulates NFkB and induces cell proliferation in HCT116 cells [146]. Folate was shown to cause an increase in cell proliferation in fetal neural stem cells via activation of ERK1/2 phosphorylation [147]. Another group observed that folate inhibits endothelial cell proliferation and migration via activation of ERK1/2 phosphorylation [148, 149]. Therefore, a general conclusion of the effect of folate on cancer cannot be drawn by studies involving cell lines. This is largely because how the cell lines were created

(immortalized) can have a big effect on cell proliferation studies. For example, HCECs were immortalized using the SV40-T antigen, which is known to bind and inhibit p53 protein function [145]. Additionally, folate-mediated activation of numerous signaling cascades, as summarized above, could have different functional outcomes in normal cells. Also, especially for studies involving folate, cell culture media have high concentrations of folates, with non-physiological mM concentrations of folic acid. Additionally, DMEM used for many cultures have a high level of methionine. Therefore, studying the effect of folates on cancer using cell lines may not be the ideal strategy, and no generalized conclusion about the effect of folates on cancer can be drawn by taking all cell line studies into consideration [146]. Also, drawing conclusions concerning the effect of folate or folate deficiency on gene expression across different cell lines may not be appropriate because of cell-specific gene regulation in response to folate. Human cell lines, grown in vitro, also exhibit elevated concentrations of DHFR activity compared with that of human tumors or cells obtained in situ, potentially as a consequence of the traditional use of high concentrations of folic acid in tissue culture medium [150]. Therefore, folate studies should be performed in in vivo model systems that can recapitulate physiological conditions, mimicking physiological levels of folate, their absorption via the intestine, and their effect on cancer prognosis. Nonetheless, there is a consensus amongst lots of data suggesting that folic acid triggers signaling cascades in cells in vitro.

Folate studies in mice

Cell lines do not provide reliable studies that could mimic cancer in vivo. Therefore, there appears to be a need for animal models to study folate metabolism and their role in signaling and cancer which can be recapitulated in humans. However, even amongst animal models, mice are better suited to study folates than rats, because rats have significantly higher concentrations of DHFR than humans, which make rats a poor model for studying human folic acid metabolism [150]. An obvious limitation in extrapolating data from rats and mice to humans is that rats and mice are coprophagic, and folates absorbed in the intestine can be secreted in the feces [151, 152]. Despite these limitations, mouse studies may be more reliable than rat studies when comparing to humans. Epidemiological and clinical studies in mice have shown that folate deficiency causes cancer [153]. In two genetic models of colorectal cancer (CRC), moderate dietary folate deficiency enhanced, whereas modest levels of folic acid supplementation (4–10 times the basal daily dietary requirement) suppressed, the development and progression of CRC, if folate intervention was started before the establishment of neoplastic foci in the intestine [154]. However, if folate intervention was started after the establishment of neoplastic foci, dietary folate suppressed the development and progression of CRC, while supplemented folate enhanced CRC progression [155]. Therefore, supraphysiologic doses of folate in mouse models of colon carcinoma and in clinical studies of older human populations with leukemia showed progressive worsening of cancer [133]. Notwithstanding the limitations associated with animal models, these animal studies suggest that the appropriate dosage and timing of folate supplementation is critical in providing safe and effective chemoprevention [133, 153, 154]. In conclusion, animal

studies suggest that folate possesses dual modulatory effect on carcinogenesis, where a deficiency enhances cancer predisposition, while excessive folate can worsen already formed cancers and tumors [153].

Folate studies in humans

Neural tube defects (NTDs) are severe birth defects arising from the failure of embryonic neural tube closure, causing brain and spine malformations in the newborn [156]. To prevent NTDs, United States and a few other countries mandate fortification of grains with folic acid, which has vastly reduced NTD occurrence [145]. In addition to folate supplementation, periconceptional folate intake can prevent about 19% to 70% of NTDs in the various countries that have mandated fortification [157]. However, the reduction in NTDs did not reduce proportionally to the amount of fortification. For example, United States and Chile had approximately 40% reduction in occurrence of NTDs, even though Chile mandated a 2-fold higher amount of folate fortification [157, 158]. In contrast, the rate of colon cancer in older males has more than doubled in Chile since fortification [158]. A similar trend is observed in Canada [145]. Therefore, there appears to be a great need to study the effects of excess folate consumption in predisposing humans to cancer prognosis.

The human gut has a very efficient capacity to convert reduced dietary folates to 5-methy-THF but limited ability to reduce folic acid [150]. Folic acid has only one glutamic residue and first needs to be reduced to the naturally bioactive form tetrahydrofolate (THF), through two reduction reactions catalyzed by dihydrofolate reductase (DHFR) (Fig. 1.2) [106]. Therefore, large amounts of unmodified folic acid

circulate in the portal vein [150]. Despite correlations drawn by epidemiological studies, direct clinical studies in humans show no protective function of folic acid in preventing cancer. One randomized clinical trial study concluded that folic acid administrations for up to six years, does not decrease the risk of adenoma formation in the large intestine. This study showed a moderate increase, although not very significant, in cancer incidence in patients receiving folate supplements [159]. A meta-analysis of eight different studies demonstrated that folic acid supplementation had no protective effect on colorectal cancer risk [160]. Similar results were obtained in randomized clinical trials for prostate cancer, where high folic acid levels promoted prostate cancer [161]. This study was the most illuminative regarding the role of folates in cancer because it distinguished the effect of natural, dietary folates from folic acid supplements, and demonstrated that folic acid supplementation increases the risk of cancer. However dietary folates are protective against cancer [161]. In view of the fortification of the US food supply with folate, and circulation of unmodified folate in the blood, many studies show that folate could conceivably increase the risk of neoplasia even outside the colorectum [159].

C. elegans – a model system to study folate metabolism and signaling

To summarize the above, studies on folate transporters and receptor affinities were largely performed on immortalized cell lines in vitro. However, to study the effect of folates in tumor progression and cell proliferation, in vivo studies and the use of animal models provide better systems that can produce results that can be recapitulated in humans as seen in randomized clinical investigations. Recently, the use of *C. elegans* has gained popularity in the study of folates in vivo. Apart from the convenience of studying

C. elegans, the main reason is that under standard conditions, *C. elegans* diet consists of a single microbe – the human gut bacteria *E. coli* [162]. Like mammals, *C. elegans* is unable to synthesize folate and acquires the metabolite through its diet [163]. *C. elegans* have their own orthologs of the human RFC (FOLT-1), FR (FOLR-1) and PCFT (PCFT) [164-166]. FOLT-1 in *C. elegans* appears to work in similar ways to the folate uptake process that operates in the human intestine, being more active at acidic compared with alkaline buffer pHs, having similar affinity to reduced and substituted folate derivatives [164].

Knockout of the folate transporter *folt-1* causes germline and somatic defects in *C. elegans.* Spermatogenesis is attenuated, and oogenesis is nearly absent in *folt-1* knockout hermaphrodites [167]. Perhaps the most widely performed folate-related research in *C. elegans* has been the effect of Metformin on lifespan. Metformin is a first-line diabetes treatment drug that is FDA approved, and is currently the only drug recommended for preventing type 2 diabetes [168]. Metformin not only reduces the onset of diabetes, but also improves healthspan by combating age-related diseases, and aging itself in *C. elegans*, rodents and humans [169]. It was observed that treatment of *C. elegans* with metformin increases lifespan through a mechanism similar to dietary restriction (DR) [170]. This DR-like mechanism, distinct from the insulin/IGF signaling pathway, induces longevity via activation of the energy sensor AMPK and the conserved oxidative stress-responsive transcription factor SKN-1/Nrf2 [171, 172]. Interestingly, in mammals metformin treatment also induces health benefits by mimicking dietary restriction, and is associated with activation of AMPK [173, 174]. Thus, *C. elegans* has

been considered a promising model organism to study the effect of folates, human microbiota, and mechanisms of action of metformin [164, 172, 175, 176].

Folate studies in *C. elegans*

We have identified a new role of bacterial folates in signaling *C. elegans* germ cells to proliferate. Here, I would like to summarize the known roles of folates on *C. elegans* development and lifespan. *C. elegans* lifespan is shortened by increased folates in their diet [177]. Folates derived from bacteria have been shown to accelerate aging in *C. elegans* without affecting the folate pool in the animal. Lifespan is unaffected by *C. elegans* folate cycle inhibition by Methotrexate, or by supplementation of vitamin B12, which is a critical key step in the folate cycle [177]. Inhibiting bacterial folate production by Trimethoprim (DHFR inhibitor) increased lifespan in a dose dependent manner, and consistently blocked metformin-induced increase in *C. elegans* lifespan, suggesting that metformin and trimethoprim share redundant functions of inhibiting the bacterial folate pathway [176]. Interestingly, in an elegant study by Cabreiro et. al., it was shown that metformin induces longevity in *C. elegans* by altering folate metabolism in *E. coli* [176]. An active bacterial folate metabolism is important for *C. elegans* nutrition, the absence of which delays development and increases lifespan [178]. Cabreiro et. al. show that metformin alters bacterial metabolism by reducing methionine and folate levels in *E. coli*, while metformin-treated *E. coli* increases *C. elegans* lifespan by decreasing methionine levels without affecting levels of folates [176]. Adding metformin to axenic media (media lacking bacteria) or to UV-irradiated dead *E. coli* does not increase lifespan, but rather decreases it, proving that metformin exerts its effects on *C. elegans* lifespan via *E.*

coli metabolism [176]. Therefore, metformin may induce a DR-like state in *C. elegans* indirectly, since it exerts its effects on the bacteria that *C. elegans* eats, without affecting the folate pool in the animal [176]. Thus, folates affect *C. elegans* development and lifespan independently of their role in one-carbon metabolism.

References

1. Kaletta, T. and M.O. Hengartner, *Finding function in novel targets: C. elegans as a model organism.* Nat Rev Drug Discov, 2006. **5**(5): p. 387-98.
2. Willis, M.S., et al., *The role of ubiquitin ligases in cardiac disease.* J Mol Cell Cardiol, 2014. **71**: p. 43-53.
3. Glickman, M.H. and A. Ciechanover, *The ubiquitin-proteasome proteolytic pathway: destruction for the sake of construction.* Physiol Rev, 2002. **82**(2): p. 373-428.
4. Vilchez, D., I. Saez, and A. Dillin, *The role of protein clearance mechanisms in organismal ageing and age-related diseases.* Nat Commun, 2014. **5**: p. 5659.
5. Nguyen, L.K., et al., *Polyubiquitin chain assembly and organization determine the dynamics of protein activation and degradation.* Front Physiol, 2014. **5**: p. 4.
6. Sorokin, A.V., E.R. Kim, and L.P. Ovchinnikov, *Proteasome system of protein degradation and processing.* Biochemistry (Mosc), 2009. **74**(13): p. 1411-42.
7. Paul, S., *Dysfunction of the ubiquitin-proteasome system in multiple disease conditions: therapeutic approaches.* Bioessays, 2008. **30**(11-12): p. 1172-84.

8. Day, S.M., *The ubiquitin proteasome system in human cardiomyopathies and heart failure.* Am J Physiol Heart Circ Physiol, 2013. **304**(10): p. H1283-93.

9. Valimberti, I., et al., *E2 superfamily of ubiquitin-conjugating enzymes: constitutively active or activated through phosphorylation in the catalytic cleft.* Sci Rep, 2015. **5**: p. 14849.

10. Dikic, I. and M. Robertson, *Ubiquitin ligases and beyond.* BMC Biol, 2012. **10**: p. 22.

11. Bulatov, E. and A. Ciulli, *Targeting Cullin-RING E3 ubiquitin ligases for drug discovery: structure, assembly and small-molecule modulation.* Biochem J, 2015. **467**(3): p. 365-86.

12. Bosu, D.R. and E.T. Kipreos, *Cullin-RING ubiquitin ligases: global regulation and activation cycles.* Cell Div, 2008. **3**: p. 7.

13. Sarikas, A., T. Hartmann, and Z.Q. Pan, *The cullin protein family.* Genome Biol, 2011. **12**(4): p. 220.

14. Duda, D.M., et al., *Structural insights into NEDD8 activation of cullin-RING ligases: conformational control of conjugation.* Cell, 2008. **134**(6): p. 995-1006.

15. Huang, D.T., et al., *A unique E1-E2 interaction required for optimal conjugation of the ubiquitin-like protein NEDD8.* Nat Struct Mol Biol, 2004. **11**(10): p. 927-35.

16. Calabrese, M.F., et al., *A RING E3-substrate complex poised for ubiquitin-like protein transfer: structural insights into cullin-RING ligases.* Nat Struct Mol Biol, 2011. **18**(8): p. 947-9.

17. Merlet, J., et al., *Regulation of cullin-RING E3 ubiquitin-ligases by neddylation and dimerization.* Cell Mol Life Sci, 2009. **66**(11-12): p. 1924-38.

18. Sakata, E., et al., *Direct interactions between NEDD8 and ubiquitin E2 conjugating enzymes upregulate cullin-based E3 ligase activity.* Nat Struct Mol Biol, 2007. **14**(2): p. 167-8.

19. Mahon, C., et al., *Cullin E3 ligases and their rewiring by viral factors.* Biomolecules, 2014. **4**(4): p. 897-930.

20. Ravid, T. and M. Hochstrasser, *Diversity of degradation signals in the ubiquitin-proteasome system.* Nat Rev Mol Cell Biol, 2008. **9**(9): p. 679-90.

21. Skaar, J.R., J.K. Pagan, and M. Pagano, *Mechanisms and function of substrate recruitment by F-box proteins.* Nat Rev Mol Cell Biol, 2013. **14**(6): p. 369-81.

22. Petroski, M.D. and R.J. Deshaies, *Function and regulation of cullin-RING ubiquitin ligases.* Nat Rev Mol Cell Biol, 2005. **6**(1): p. 9-20.

23. Craney, A. and M. Rape, *Dynamic regulation of ubiquitin-dependent cell cycle control.* Curr Opin Cell Biol, 2013. **25**(6): p. 704-10.

24. Jaakkola, P., et al., *Targeting of HIF-alpha to the von Hippel-Lindau ubiquitylation complex by O2-regulated prolyl hydroxylation.* Science, 2001. **292**(5516): p. 468-72.

25. Yoshida, Y., et al., *E3 ubiquitin ligase that recognizes sugar chains.* Nature, 2002. **418**(6896): p. 438-42.

26. Suryaraja, R., et al., *The E3 ubiquitin ligase Itch regulates tumor suppressor protein RASSF5/NORE1 stability in an acetylation-dependent manner.* Cell Death Dis, 2013. **4**: p. e565.

27. Bosu, D.R., et al., *C. elegans CAND-1 regulates cullin neddylation, cell proliferation and morphogenesis in specific tissues.* Dev Biol, 2010. **346**(1): p. 113-26.

28. Olma, M.H. and I. Dikic, *Cullins getting undressed by the protein exchange factor Cand1.* Cell, 2013. **153**(1): p. 14-6.

29. Yogosawa, S., et al., *Induced expression, localization, and chromosome mapping of a gene for the TBP-interacting protein 120A.* Biochem Biophys Res Commun, 1999. **266**(1): p. 123-8.

30. Brockway, H., et al., *The CSN/COP9 signalosome regulates synaptonemal complex assembly during meiotic prophase I of Caenorhabditis elegans.* PLoS Genet, 2014. **10**(11): p. e1004757.

31. Miller, R.K., et al., *CSN-5, a component of the COP9 signalosome complex, regulates the levels of UNC-96 and UNC-98, two components of M-lines in Caenorhabditis elegans muscle.* Mol Biol Cell, 2009. **20**(15): p. 3608-16.

32. DiMauro, S. and C. Garone, *Historical perspective on mitochondrial medicine.* Dev Disabil Res Rev, 2010. **16**(2): p. 106-13.

33. Hales, K.G., *The machinery of mitochondrial fusion, division, and distribution, and emerging connections to apoptosis.* Mitochondrion, 2004. **4**(4): p. 285-308.

34. Picard, M., et al., *Mitochondrial morphology transitions and functions: implications for retrograde signaling?* Am J Physiol Regul Integr Comp Physiol, 2013. **304**(6): p. R393-406.

35. Chen, H. and D.C. Chan, *Mitochondrial dynamics--fusion, fission, movement, and mitophagy--in neurodegenerative diseases.* Hum Mol Genet, 2009. **18**(R2): p. R169-76.

36. Bereiter-Hahn, J. and M. Voth, *Dynamics of mitochondria in living cells: shape changes, dislocations, fusion, and fission of mitochondria.* Microsc Res Tech, 1994. **27**(3): p. 198-219.

37. Chen, H., et al., *Mitofusins Mfn1 and Mfn2 coordinately regulate mitochondrial fusion and are essential for embryonic development.* J Cell Biol, 2003. **160**(2): p. 189-200.

38. Detmer, S.A. and D.C. Chan, *Functions and dysfunctions of mitochondrial dynamics.* Nat Rev Mol Cell Biol, 2007. **8**(11): p. 870-9.

39. Frank, S., et al., *The role of dynamin-related protein 1, a mediator of mitochondrial fission, in apoptosis.* Dev Cell, 2001. **1**(4): p. 515-25.

40. Lechner-Scott, J.S., et al., *[Hereditary motor and sensory neuropathies. Clinical and molecular genetic aspects].* Schweiz Arch Neurol Psychiatr (1985), 1995. **146**(4): p. 157-67.

41. Chen, L. and A.A. Knowlton, *Mitochondrial dynamics in heart failure.* Congest Heart Fail, 2011. **17**(6): p. 257-61.

42. Hwang, S.J. and W. Kim, *Mitochondrial dynamics in the heart as a novel therapeutic target for cardioprotection.* Chonnam Med J, 2013. **49**(3): p. 101-7.

43. Rolland, S.G., et al., *The BCL-2-like protein CED-9 of C. elegans promotes FZO-1/Mfn1,2- and EAT-3/Opa1-dependent mitochondrial fusion.* J Cell Biol, 2009. **186**(4): p. 525-40.

44. Labrousse, A.M., et al., *C. elegans dynamin-related protein DRP-1 controls severing of the mitochondrial outer membrane.* Mol Cell, 1999. **4**(5): p. 815-26.

45. Praefcke, G.J. and H.T. McMahon, *The dynamin superfamily: universal membrane tubulation and fission molecules?* Nat Rev Mol Cell Biol, 2004. **5**(2): p. 133-47.

46. Youle, R.J. and D.P. Narendra, *Mechanisms of mitophagy.* Nat Rev Mol Cell Biol, 2011. **12**(1): p. 9-14.

47. Tondera, D., et al., *SLP-2 is required for stress-induced mitochondrial hyperfusion.* EMBO J, 2009. **28**(11): p. 1589-600.

48. Ryan, M.T. and D. Stojanovski, *Mitofusins 'bridge' the gap between oxidative stress and mitochondrial hyperfusion.* EMBO Rep, 2012. **13**(10): p. 870-1.

49. Rolland, S.G., et al., *Impaired complex IV activity in response to loss of LRPPRC function can be compensated by mitochondrial hyperfusion.* Proc Natl Acad Sci U S A, 2013. **110**(32): p. E2967-76.

50. Trifunovic, A., *Mitochondrial DNA and ageing.* Biochim Biophys Acta, 2006. **1757**(5-6): p. 611-7.

51. Sandhu, S.K. and G. Kaur, *Mitochondrial electron transport chain complexes in aging rat brain and lymphocytes.* Biogerontology, 2003. **4**(1): p. 19-29.

52. Sun, N., R.J. Youle, and T. Finkel, *The Mitochondrial Basis of Aging.* Mol Cell, 2016. **61**(5): p. 654-66.

53. Kujoth, G.C., et al., *Mitochondrial DNA mutations, oxidative stress, and apoptosis in mammalian aging.* Science, 2005. **309**(5733): p. 481-4.

54. Harman, D., *Aging: a theory based on free radical and radiation chemistry.* J Gerontol, 1956. **11**(3): p. 298-300.

55. Gruber, J., et al., *Mitochondrial changes in ageing Caenorhabditis elegans--what do we learn from superoxide dismutase knockouts?* PLoS One, 2011. **6**(5): p. e19444.

56. Maklashina, E. and B.A. Ackrell, *Is defective electron transport at the hub of aging?* Aging Cell, 2004. **3**(1): p. 21-7.

57. Bratic, A. and N.G. Larsson, *The role of mitochondria in aging.* J Clin Invest, 2013. **123**(3): p. 951-7.

58. Hamilton, B., et al., *A systematic RNAi screen for longevity genes in C. elegans.* Genes Dev, 2005. **19**(13): p. 1544-55.

59. Ristow, M. and K. Schmeisser, *Mitohormesis: Promoting Health and Lifespan by Increased Levels of Reactive Oxygen Species (ROS).* Dose Response, 2014. **12**(2): p. 288-341.

60. Wei, Y.H., et al., *Mitochondrial theory of aging matures--roles of mtDNA mutation and oxidative stress in human aging.* Zhonghua Yi Xue Za Zhi (Taipei), 2001. **64**(5): p. 259-70.

61. Park, C.B. and N.G. Larsson, *Mitochondrial DNA mutations in disease and aging.* J Cell Biol, 2011. **193**(5): p. 809-18.

62. Zeviani, M. and S. Di Donato, *Mitochondrial disorders.* Brain, 2004. **127**(Pt 10): p. 2153-72.

63. Chistiakov, D.A., et al., *Mitochondrial aging and age-related dysfunction of mitochondria.* Biomed Res Int, 2014. **2014**: p. 238463.

64. Jeong, S.Y. and D.W. Seol, *The role of mitochondria in apoptosis.* BMB Rep, 2008. **41**(1): p. 11-22.

65. Walston, J.D., *Sarcopenia in older adults.* Curr Opin Rheumatol, 2012. **24**(6): p. 623-7.

66. Wredenberg, A., et al., *Increased mitochondrial mass in mitochondrial myopathy mice.* Proc Natl Acad Sci U S A, 2002. **99**(23): p. 15066-71.

67. Diot, A., K. Morten, and J. Poulton, *Mitophagy plays a central role in mitochondrial ageing.* Mamm Genome, 2016. **27**(7-8): p. 381-95.

68. Bernhardt, D., et al., *Simultaneous impairment of mitochondrial fission and fusion reduces mitophagy and shortens replicative lifespan.* Sci Rep, 2015. **5**: p. 7885.

69. Regmi, S.G., S.G. Rolland, and B. Conradt, *Age-dependent changes in mitochondrial morphology and volume are not predictors of lifespan.* Aging (Albany NY), 2014.

70. Kam, J.H. and G. Jeffery, *To unite or divide: mitochondrial dynamics in the murine outer retina that preceded age related photoreceptor loss.* Oncotarget, 2015. **6**(29): p. 26690-701.

71. Chang, L., S.H. Chiang, and A.R. Saltiel, *Insulin signaling and the regulation of glucose transport.* Mol Med, 2004. **10**(7-12): p. 65-71.

72. Werner, H., D. Weinstein, and I. Bentov, *Similarities and differences between insulin and IGF-I: structures, receptors, and signalling pathways.* Arch Physiol Biochem, 2008. **114**(1): p. 17-22.

73. Lizcano, J.M. and D.R. Alessi, *The insulin signalling pathway.* Curr Biol, 2002. **12**(7): p. R236-8.

74. Rask-Madsen, C. and C.R. Kahn, *Tissue-specific insulin signaling, metabolic syndrome, and cardiovascular disease.* Arterioscler Thromb Vasc Biol, 2012. **32**(9): p. 2052-9.

75. de la Monte, S.M. and J.R. Wands, *Alzheimer-associated neuronal thread protein mediated cell death is linked to impaired insulin signaling.* J Alzheimers Dis, 2004. **6**(3): p. 231-42.

76. Barbieri, M., et al., *Insulin/IGF-I-signaling pathway: an evolutionarily conserved mechanism of longevity from yeast to humans.* Am J Physiol Endocrinol Metab, 2003. **285**(5): p. E1064-71.

77. Zabkiewicz, J., et al., *The PDK1 master kinase is over-expressed in acute myeloid leukemia and promotes PKC-mediated survival of leukemic blasts.* Haematologica, 2014. **99**(5): p. 858-64.

78. Murphy, C.T., et al., *Genes that act downstream of DAF-16 to influence the lifespan of Caenorhabditis elegans.* Nature, 2003. **424**(6946): p. 277-83.

79. Pinero Gonzalez, J., et al., *Conservation of key members in the course of the evolution of the insulin signaling pathway.* Biosystems, 2009. **95**(1): p. 7-16.

80. Klass, M. and D. Hirsh, *Non-ageing developmental variant of Caenorhabditis elegans.* Nature, 1976. **260**(5551): p. 523-5.

81. van Heemst, D., *Insulin, IGF-1 and longevity.* Aging Dis, 2010. **1**(2): p. 147-57.

82. Riddle, D.L., M.M. Swanson, and P.S. Albert, *Interacting genes in nematode dauer larva formation.* Nature, 1981. **290**(5808): p. 668-71.

83. Vowels, J.J. and J.H. Thomas, *Genetic analysis of chemosensory control of dauer formation in Caenorhabditis elegans.* Genetics, 1992. **130**(1): p. 105-23.

84. Kenyon, C., et al., *A C. elegans mutant that lives twice as long as wild type.* Nature, 1993. **366**(6454): p. 461-4.

85. Kenyon, C., *The first long-lived mutants: discovery of the insulin/IGF-1 pathway for ageing.* Philos Trans R Soc Lond B Biol Sci, 2011. **366**(1561): p. 9-16.

86. Paradis, S., et al., *A PDK1 homolog is necessary and sufficient to transduce AGE-1 PI3 kinase signals that regulate diapause in Caenorhabditis elegans.* Genes Dev, 1999. **13**(11): p. 1438-52.

87. Chen, A.T., et al., *Effects of Caenorhabditis elegans sgk-1 mutations on lifespan, stress resistance, and DAF-16/FoxO regulation.* Aging Cell, 2013. **12**(5): p. 932-40.

88. Henderson, S.T., M. Bonafe, and T.E. Johnson, *daf-16 protects the nematode Caenorhabditis elegans during food deprivation.* J Gerontol A Biol Sci Med Sci, 2006. **61**(5): p. 444-60.

89. Kimura, K.D., et al., *daf-2, an insulin receptor-like gene that regulates longevity and diapause in Caenorhabditis elegans.* Science, 1997. **277**(5328): p. 942-6.

90. Oh, S.W., et al., *JNK regulates lifespan in Caenorhabditis elegans by modulating nuclear translocation of forkhead transcription factor/DAF-16.* Proc Natl Acad Sci U S A, 2005. **102**(12): p. 4494-9.

91. Alam, H., et al., *EAK-7 controls development and life span by regulating nuclear DAF-16/FoxO activity.* Cell Metab, 2010. **12**(1): p. 30-41.

92. Kaletsky, R. and C.T. Murphy, *The role of insulin/IGF-like signaling in C. elegans longevity and aging.* Dis Model Mech, 2010. **3**(7-8): p. 415-9.

93. Kalra, S., J.J. Jacob, and Y. Gupta, *Newer antidiabetic drugs and calorie restriction mimicry.* Indian J Endocrinol Metab, 2016. **20**(1): p. 142-6.

94. Paolisso, G., et al., *Low insulin resistance and preserved beta-cell function contribute to human longevity but are not associated with TH-INS genes.* Exp Gerontol, 2001. **37**(1): p. 149-56.

95. Paolisso, G., et al., *Glucose tolerance and insulin action in healty centenarians.* Am J Physiol, 1996. **270**(5 Pt 1): p. E890-4.

96. van Heemst, D., et al., *Reduced insulin/IGF-1 signalling and human longevity.* Aging Cell, 2005. **4**(2): p. 79-85.

97. Pawlikowska, L., et al., *Association of common genetic variation in the insulin/IGF1 signaling pathway with human longevity.* Aging Cell, 2009. **8**(4): p. 460-72.

98. Antebi, A., J.G. Culotti, and E.M. Hedgecock, *daf-12 regulates developmental age and the dauer alternative in Caenorhabditis elegans.* Development, 1998. **125**(7): p. 1191-205.

99. Wong, M.C. and J.E. Schwarzbauer, *Gonad morphogenesis and distal tip cell migration in the Caenorhabditis elegans hermaphrodite.* Wiley Interdiscip Rev Dev Biol, 2012. **1**(4): p. 519-31.

100. Gerisch, B., et al., *A bile acid-like steroid modulates Caenorhabditis elegans lifespan through nuclear receptor signaling.* Proc Natl Acad Sci U S A, 2007. **104**(12): p. 5014-9.

101. Antebi, A., et al., *daf-12 encodes a nuclear receptor that regulates the dauer diapause and developmental age in C. elegans.* Genes Dev, 2000. **14**(12): p. 1512-27.

102. Ludewig, A.H., et al., *A novel nuclear receptor/coregulator complex controls C. elegans lipid metabolism, larval development, and aging.* Genes Dev, 2004. **18**(17): p. 2120-33.

103. Thondamal, M., et al., *Steroid hormone signalling links reproduction to lifespan in dietary-restricted Caenorhabditis elegans.* Nat Commun, 2014. **5**: p. 4879.

104. Blom, H.J. and Y. Smulders, *Overview of homocysteine and folate metabolism. With special references to cardiovascular disease and neural tube defects.* J Inherit Metab Dis, 2011. **34**(1): p. 75-81.

105. Tam, C., D. O'Connor, and G. Koren, *Circulating unmetabolized folic Acid: relationship to folate status and effect of supplementation.* Obstet Gynecol Int, 2012. **2012**: p. 485179.

106. Imbard, A., J.F. Benoist, and H.J. Blom, *Neural tube defects, folic acid and methylation.* Int J Environ Res Public Health, 2013. **10**(9): p. 4352-89.

107. Beaudin, A.E. and P.J. Stover, *Insights into metabolic mechanisms underlying folate-responsive neural tube defects: a minireview.* Birth Defects Res A Clin Mol Teratol, 2009. **85**(4): p. 274-84.

108. Liu, Z., et al., *Combined inadequacies of multiple B vitamins amplify colonic Wnt signaling and promote intestinal tumorigenesis in BAT-LacZxApc1638N mice.* FASEB J, 2011. **25**(9): p. 3136-45.

109. Graber, J.R. and J.A. Breznak, *Folate cross-feeding supports symbiotic homoacetogenic spirochetes.* Appl Environ Microbiol, 2005. **71**(4): p. 1883-9.

110. Sybesma, W., et al., *Effects of cultivation conditions on folate production by lactic acid bacteria.* Appl Environ Microbiol, 2003. **69**(8): p. 4542-8.

111. Ogwang, S., et al., *Bacterial conversion of folinic acid is required for antifolate resistance.* J Biol Chem, 2011. **286**(17): p. 15377-90.

112. Sirotnak, F.M. and B. Tolner, *Carrier-mediated membrane transport of folates in mammalian cells.* Annu Rev Nutr, 1999. **19**: p. 91-122.

113. Matherly, L.H., M.R. Wilson, and Z. Hou, *The major facilitative folate transporters solute carrier 19A1 and solute carrier 46A1: biology and role in antifolate chemotherapy of cancer.* Drug Metab Dispos, 2014. **42**(4): p. 632-49.

114. Boyd, C., S. Abraham, and J. Kellow, *Psychological features are important predictors of functional gastrointestinal disorders in patients with eating disorders.* Scand J Gastroenterol, 2005. **40**(8): p. 929-35.

115. Desmoulin, S.K., et al., *The human proton-coupled folate transporter: Biology and therapeutic applications to cancer.* Cancer Biol Ther, 2012. **13**(14): p. 1355-73.

116. Qiu, A., et al., *Identification of an intestinal folate transporter and the molecular basis for hereditary folate malabsorption.* Cell, 2006. **127**(5): p. 917-28.

117. Williams, P.J., H.D. Mistry, and L. Morgan, *Folate transporter expression decreases in the human placenta throughout pregnancy and in pre-eclampsia.* Pregnancy Hypertens, 2012. **2**(2): p. 123-31.

118. Geller, J., et al., *Hereditary folate malabsorption: family report and review of the literature.* Medicine (Baltimore), 2002. **81**(1): p. 51-68.

119. Umapathy, N.S., et al., *Cloning and functional characterization of the proton-coupled electrogenic folate transporter and analysis of its expression in retinal cell types.* Invest Ophthalmol Vis Sci, 2007. **48**(11): p. 5299-305.

120. Elnakat, H. and M. Ratnam, *Distribution, functionality and gene regulation of folate receptor isoforms: implications in targeted therapy.* Adv Drug Deliv Rev, 2004. **56**(8): p. 1067-84.

121. Parker, N., et al., *Folate receptor expression in carcinomas and normal tissues determined by a quantitative radioligand binding assay.* Anal Biochem, 2005. **338**(2): p. 284-93.

122. Grapp, M., et al., *Choroid plexus transcytosis and exosome shuttling deliver folate into brain parenchyma.* Nat Commun, 2013. **4**: p. 2123.

123. Zhao, R., et al., *Rescue of embryonic lethality in reduced folate carrier-deficient mice by maternal folic acid supplementation reveals early neonatal failure of hematopoietic organs.* J Biol Chem, 2001. **276**(13): p. 10224-8.

124. Balashova, O.A., O. Visina, and L.N. Borodinsky, *Folate receptor 1 is necessary for neural plate cell apical constriction during Xenopus neural tube formation.* Development, 2017. **144**(8): p. 1518-1530.

125. Evans, C.O., et al., *Folate receptor expression in pituitary adenomas cellular and molecular analysis.* Vitam Horm, 2008. **79**: p. 235-66.

126. Zhao, R., et al., *A role for the proton-coupled folate transporter (PCFT-SLC46A1) in folate receptor-mediated endocytosis.* J Biol Chem, 2009. **284**(7): p. 4267-74.

127. Birn, H., J. Selhub, and E.I. Christensen, *Internalization and intracellular transport of folate-binding protein in rat kidney proximal tubule.* Am J Physiol, 1993. **264**(2 Pt 1): p. C302-10.

128. Swietach, P., et al., *The chemistry, physiology and pathology of pH in cancer.* Philos Trans R Soc Lond B Biol Sci, 2014. **369**(1638): p. 20130099.

129. Diop-Bove, N.K., et al., *Hypermethylation of the human proton-coupled folate transporter (SLC46A1) minimal transcriptional regulatory region in an antifolate-resistant HeLa cell line.* Mol Cancer Ther, 2009. **8**(8): p. 2424-31.

130. Lee, R.J., S. Wang, and P.S. Low, *Measurement of endosome pH following folate receptor-mediated endocytosis.* Biochim Biophys Acta, 1996. **1312**(3): p. 237-42.

131. Hou, Z., et al., *Identification and functional impact of homo-oligomers of the human proton-coupled folate transporter.* J Biol Chem, 2012. **287**(7): p. 4982-95.

132. Ifergan, I., G. Jansen, and Y.G. Assaraf, *The reduced folate carrier (RFC) is cytotoxic to cells under conditions of severe folate deprivation. RFC as a double edged sword in folate homeostasis.* J Biol Chem, 2008. **283**(30): p. 20687-95.

133. Kelemen, L.E., *The role of folate receptor alpha in cancer development, progression and treatment: cause, consequence or innocent bystander?* Int J Cancer, 2006. **119**(2): p. 243-50.

134. Antony, A., et al., *Translational upregulation of folate receptors is mediated by homocysteine via RNA-heterogeneous nuclear ribonucleoprotein E1 interactions.* J Clin Invest, 2004. **113**(2): p. 285-301.

135. Miotti, S., et al., *Interaction of folate receptor with signaling molecules lyn and G(alpha)(i-3) in detergent-resistant complexes from the ovary carcinoma cell line IGROV1.* J Cell Sci, 2000. **113 Pt 2**: p. 349-57.

136. Corona, G., et al., *Role of folate receptor and reduced folate carrier in the transport of 5-methyltetrahydrofolic acid in human ovarian carcinoma cells.* Int J Cancer, 1998. **75**(1): p. 125-33.

137. Bottero, F., et al., *Gene transfection and expression of the ovarian carcinoma marker folate binding protein on NIH/3T3 cells increases cell growth in vitro and in vivo.* Cancer Res, 1993. **53**(23): p. 5791-6.

138. Bailey, L.B., et al., *Biomarkers of Nutrition for Development-Folate Review.* J Nutr, 2015. **145**(7): p. 1636S-1680S.

139. Fleet, J.C., et al., *Gene expression profiling of Caco-2 BBe cells suggests a role for specific signaling pathways during intestinal differentiation.* Physiol Genomics, 2003. **13**(1): p. 57-68.

140. Leamon, C.P. and A.L. Jackman, *Exploitation of the folate receptor in the management of cancer and inflammatory disease.* Vitam Horm, 2008. **79**: p. 203-33.

141. Hansen, M.F., et al., *Folic acid mediates activation of the pro-oncogene STAT3 via the Folate Receptor alpha.* Cell Signal, 2015. **27**(7): p. 1356-68.

142. Moreno, C.S., et al., *Novel molecular signaling and classification of human clinically nonfunctional pituitary adenomas identified by gene expression profiling and proteomic analyses.* Cancer Res, 2005. **65**(22): p. 10214-22.

143. Boshnjaku, V., et al., *Nuclear localization of folate receptor alpha: a new role as a transcription factor.* Sci Rep, 2012. **2**: p. 980.

144. Kuo, C.T., C. Chang, and W.S. Lee, *Folic acid inhibits COLO-205 colon cancer cell proliferation through activating the FRalpha/c-SRC/ERK1/2/NFkappaB/TP53 pathway: in vitro and in vivo studies.* Sci Rep, 2015. **5**: p. 11187.

145. Crott, J.W., et al., *Moderate folate depletion modulates the expression of selected genes involved in cell cycle, intracellular signaling and folate uptake in human colonic epithelial cell lines.* J Nutr Biochem, 2008. **19**(5): p. 328-35.

146. Novakovic, P., et al., *Effects of folate deficiency on gene expression in the apoptosis and cancer pathways in colon cancer cells.* Carcinogenesis, 2006. **27**(5): p. 916-24.

147. Fu, D., et al., *Cell-cycle-dependent PC-PLC regulation by APC/C(Cdc20)-mediated ubiquitin-proteasome pathway.* J Cell Biochem, 2009. **107**(4): p. 686-96.

148. Anderson, R.A., et al., *Cinnamon counteracts the negative effects of a high fat/high fructose diet on behavior, brain insulin signaling and Alzheimer-associated changes.* PLoS One, 2013. **8**(12): p. e83243.

149. Aras, U., et al., *Chemopreventive and anti-angiogenic effects of dietary phenethyl isothiocyanate in an N-methyl nitrosourea-induced breast cancer animal model.* Biopharm Drug Dispos, 2013. **34**(2): p. 98-106.

150. Patanwala, I., et al., *Folic acid handling by the human gut: implications for food fortification and supplementation.* Am J Clin Nutr, 2014. **100**(2): p. 593-9.

151. Hollister, E.B., C. Gao, and J. Versalovic, *Compositional and functional features of the gastrointestinal microbiome and their effects on human health.* Gastroenterology, 2014. **146**(6): p. 1449-58.

152. Kim, T.H., et al., *A large pool of available folate exists in the large intestine of human infants and piglets.* J Nutr, 2004. **134**(6): p. 1389-94.

153. Kim, Y.I., *Role of folate in colon cancer development and progression.* J Nutr, 2003. **133**(11 Suppl 1): p. 3731S-3739S.

154. Song, J., et al., *Chemopreventive effects of dietary folate on intestinal polyps in Apc+/-Msh2-/- mice.* Cancer Res, 2000. **60**(12): p. 3191-9.

155. Kim, Y.I., *Folate: a magic bullet or a double edged sword for colorectal cancer prevention?* Gut, 2006. **55**(10): p. 1387-9.

156. Cavalli, P., *Prevention of Neural Tube Defects and proper folate periconceptional supplementation.* J Prenat Med, 2008. **2**(4): p. 40-1.

157. Crider, K.S., L.B. Bailey, and R.J. Berry, *Folic acid food fortification-its history, effect, concerns, and future directions.* Nutrients, 2011. **3**(3): p. 370-84.

158. Dunlap, B., et al., *Folic acid and human reproduction-ten important issues for clinicians.* J Exp Clin Assist Reprod, 2011. **8**: p. 2.

159. Cole, B.F., et al., *Folic acid for the prevention of colorectal adenomas: a randomized clinical trial.* JAMA, 2007. **297**(21): p. 2351-9.

160. Qin, T., et al., *Folic acid supplements and colorectal cancer risk: meta-analysis of randomized controlled trials.* Sci Rep, 2015. **5**: p. 12044.

161. Figueiredo, J.C., et al., *Folic acid and risk of prostate cancer: results from a randomized clinical trial.* J Natl Cancer Inst, 2009. **101**(6): p. 432-5.

162. Brenner, S., *The genetics of Caenorhabditis elegans.* Genetics, 1974. **77**(1): p. 71-94.

163. Nguyen, T.P. and C.F. Clarke, *Folate status of gut microbiome affects Caenorhabditis elegans lifespan.* BMC Biol, 2012. **10**: p. 66.

164. Balamurugan, K., et al., *Cloning and functional characterization of a folate transporter from the nematode Caenorhabditis elegans.* Am J Physiol Cell Physiol, 2007. **293**(2): p. C670-81.

165. Chaudhari, S.N., et al., *Bacterial Folates Provide an Exogenous Signal for C. elegans Germline Stem Cell Proliferation.* Dev Cell, 2016. **38**(1): p. 33-46.

166. Ortbauer, M., et al., *Folate deficiency and over-supplementation causes impaired folate metabolism: Regulation and adaptation mechanisms in Caenorhabditis elegans.* Mol Nutr Food Res, 2016. **60**(4): p. 949-56.

167. Austin, M.U., et al., *Knockout of the folate transporter folt-1 causes germline and somatic defects in C. elegans.* BMC Dev Biol, 2010. **10**: p. 46.

168. Hostalek, U., M. Gwilt, and S. Hildemann, *Therapeutic Use of Metformin in Prediabetes and Diabetes Prevention.* Drugs, 2015. **75**(10): p. 1071-94.

169. Barzilai, N., et al., *Metformin as a Tool to Target Aging.* Cell Metab, 2016. **23**(6): p. 1060-5.

170. Onken, B. and M. Driscoll, *Metformin induces a dietary restriction-like state and the oxidative stress response to extend C. elegans Healthspan via AMPK, LKB1, and SKN-1.* PLoS One, 2010. **5**(1): p. e8758.

171. Canto, C. and J. Auwerx, *Calorie restriction: is AMPK a key sensor and effector?* Physiology (Bethesda), 2011. **26**(4): p. 214-24.

172. Bishop, N.A. and L. Guarente, *Two neurons mediate diet-restriction-induced longevity in C. elegans.* Nature, 2007. **447**(7144): p. 545-9.

173. Hawley, S.A., et al., *The antidiabetic drug metformin activates the AMP-activated protein kinase cascade via an adenine nucleotide-independent mechanism.* Diabetes, 2002. **51**(8): p. 2420-5.

174. Ingram, D.K., et al., *Calorie restriction mimetics: an emerging research field.* Aging Cell, 2006. **5**(2): p. 97-108.

175. Storelli, G., M. Tefit, and F. Leulier, *Metformin, microbes, and aging.* Cell Metab, 2013. **17**(6): p. 809-11.

176. Cabreiro, F., et al., *Metformin retards aging in C. elegans by altering microbial folate and methionine metabolism.* Cell, 2013. **153**(1): p. 228-39.

177. Virk, B., et al., *Folate Acts in E. coli to Accelerate C. elegans Aging Independently of Bacterial Biosynthesis.* Cell Rep, 2016. **14**(7): p. 1611-20.

178. Lenaerts, I., et al., *Dietary restriction of Caenorhabditis elegans by axenic culture reflects nutritional requirement for constituents provided by metabolically active microbes.* J Gerontol A Biol Sci Med Sci, 2008. **63**(3): p. 242-52.

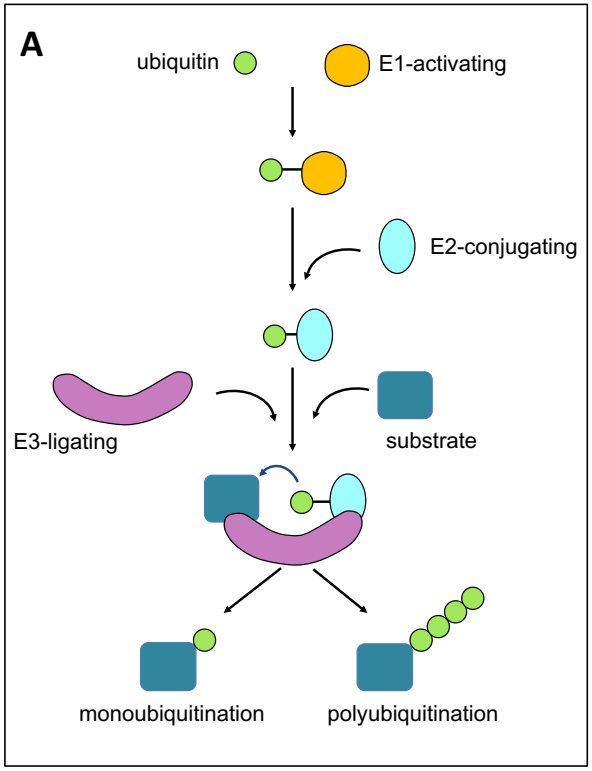
A
ubiquitin
E1-activating
E2-conjugating
E3-ligating
substrate
monoubiquitination
polyubiquitination

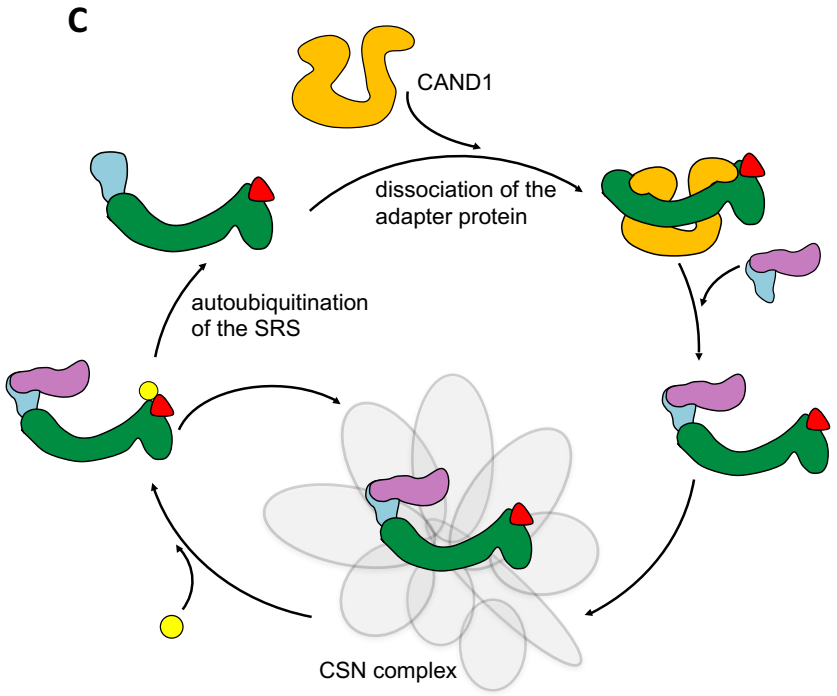
C
CAND1
dissociation of the
adapter protein
autoubiquitination
of the SRS
CSN complex

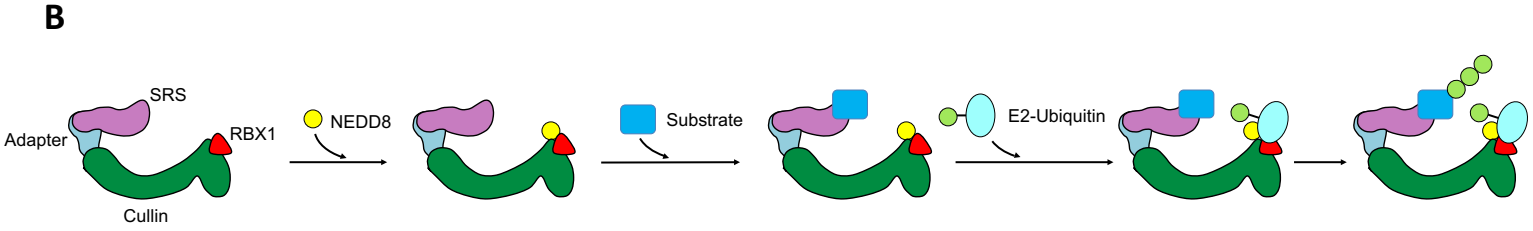
B
SRS
Adapter
RBX1
Cullin
NEDD8
Substrate
E2-Ubiquitin

Figure 1.1 The ubiquitination process; structure and regulation of CRL complexes

(A) The cascade of E1-E2-E3 enzymes tag substrates with ubiquitin. (B) Structure of CRL E3 ubiquitin ligases, and the process of assembly of structural components, recruitment of the E2 enzyme, and ubiquitination of substrate proteins. (C) Regulation of CRLs by CAND1 and the CSN complex.

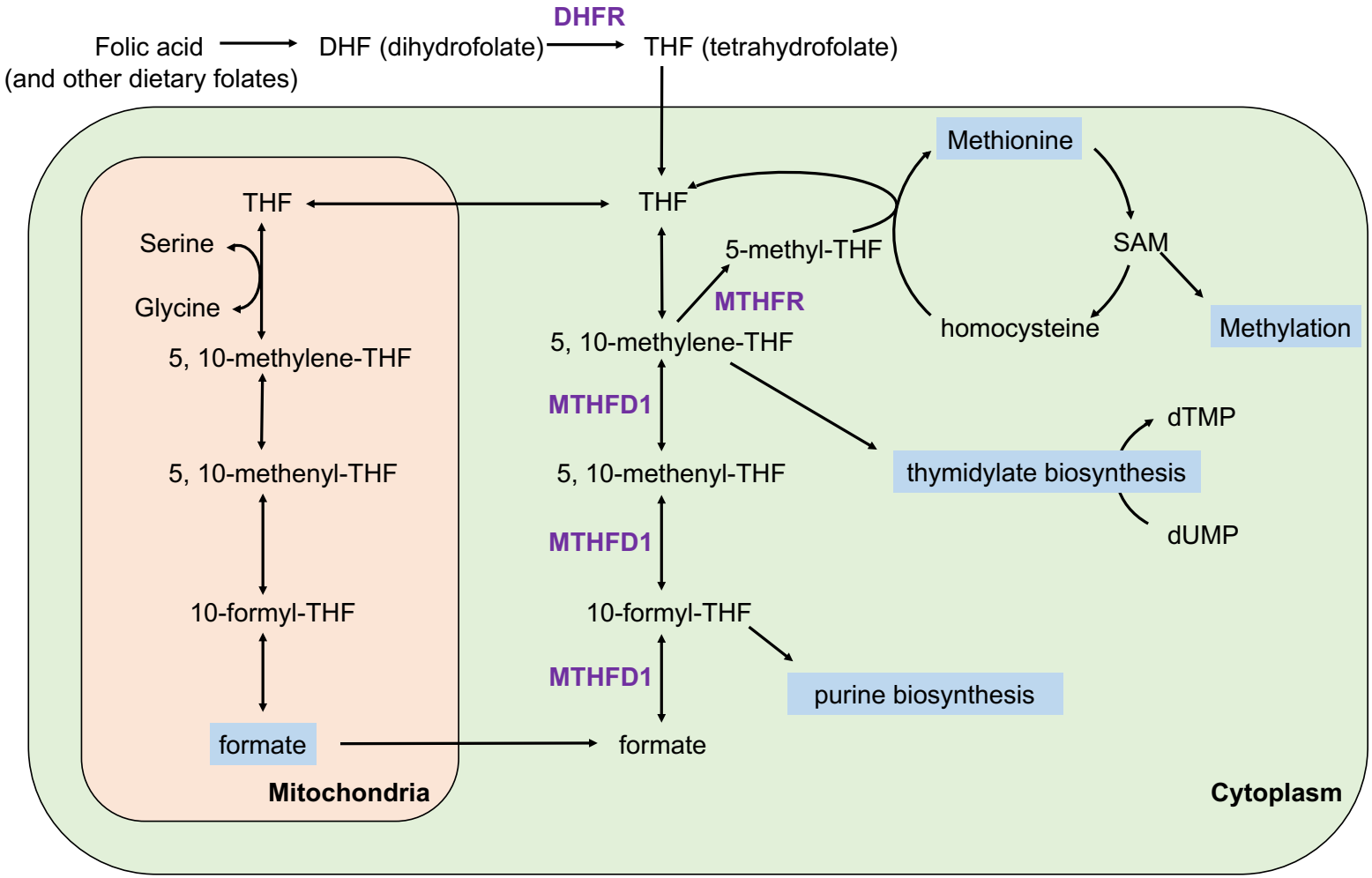

Figure 1.2 Folate-mediated one carbon metabolism cycle in cells

CHAPTER 2

INSULIN SIGNALING AND SCF^{LIN-23} REGULATE MITOCHONDRIAL DYNAMICS IN *CAENORHABDITIS ELEGANS*, AND INCREASED MITOCHONDRIAL FUSION IS BROADLY REQUIRED FOR LONGEVITY

Snehal N. Chaudhari and Edward T. Kipreos E.T. **Accepted by *Nature Communications.* Reprinted here with permission of publisher, July 2017**

Abstract

Mitochondria are dynamic organelles that undergo fusion and fission events. Mitochondrial dynamics are required for mitochondrial viability and for responses to changes in bioenergetic status. Here we describe a pathway that regulates mitochondrial fusion in *Caenorhabditis elegans*. In this pathway, the ubiquitin ligase SCF^{LIN-23} and its exchange factor CAND-1 promote the activating phosphorylation of the kinase AKT-1, which inactivates the FOXO transcription factor DAF-16. DAF-16 represses the expression of the mitochondrial proteases SPG-7 and PPGN-1, which negatively regulate the level of the mitochondrial fusion protein EAT-3. Altering components of this pathway to induce mitochondrial fusion extends lifespan. The pathway is required for the fusion of mitochondria in response to physical exertion, and regimens of daily physical exertion extend lifespan. We further show that diverse pathways that extend lifespan exhibit increased levels of elongated mitochondria that are essential for their longevity. Increased mitochondrial fusion is therefore an underlying mechanism that promotes longevity in diverse pathways.

Introduction

Mitochondria play diverse roles in signaling, physiology, and metabolism [1]. Mitochondrial dynamics regulate the morphology, number, and function of mitochondria to allow adaptation to cellular needs [2]. Mitochondrial fission is required for: mitophagy (mitochondrial autophagy); the mitotic segregation of mitochondria to daughter cells; and the distribution of mitochondria to subcellular locations, such as neuronal axons [3]. Mitochondrial fusion is required for maintaining mitochondrial membrane potential and respiratory capacity, and to protect against apoptosis in mammalian cells [4].

Cells adjust mitochondrial morphologies to coordinate between the cellular demand for energy and the availability of resources [4]. Elongated morphology is associated with increased efficiency of ATP production and reduced generation of reactive oxygen species (ROS); while fragmented morphology is linked to reduced ATP production and mitochondrial uncoupling.

Mitochondrial fusion and fission events are tightly regulated and require the activity of evolutionarily conserved GTPases [5]. Mitochondrial fission in yeast, invertebrates, and mammals requires the dynamin-related protein Drp1 (Dnm1 in budding yeast, and DRP-1 in *C. elegans*). Mitochondrial fusion requires mitofusins for outer membrane fusion (Mfn1 and Mfn2 in mammals, Fzo1p in budding yeast, and FZO-1 in *C. elegans*), and inner membrane fusion (OPA1 in mammals, Mgm1p in budding yeast, and EAT-3 in *C. elegans*) [5-7]. In mammalian cells, overexpression of the outer membrane fusion proteins Mfn1 and Mfn2 can lead to either clustering of spherical mitochondria [8-11] or elongated mitochondria [11, 12]. It is likely that the different outcomes result from

differences in the level of expression, as it was shown that modest overexpression of the inner membrane fusion protein OPA1 induces mitochondrial fusion, while higher levels of expression induces fragmentation [13]. In *C. elegans*, the overexpression of either the outer membrane mitofusin FZO-1 or the inner membrane fusion EAT-3 was reported to induce mitochondrial fragmentation [7]; however, in light of the mammalian results, the failure to generate elongated mitochondria could have resulted from excessive expression levels.

Mitochondrial dysfunction, impaired energy homeostasis, and increased production of ROS are associated with aging in both invertebrates and vertebrates [14]. In large-scale *C. elegans* RNAi screens for genes regulating lifespan, one of the largest classes of genes were those encoding mitochondrial proteins [15]. Of these, the largest proportion of RNAi targets were genes affecting the electron transport chain (ETC). RNAi depletion of genes that encode proteins involved in the ETC can shorten or extend lifespan. Lifespan extension in response to ETC impairment occurs, at least in part, from the activation of the mitochondrial unfolded protein response (UPR^{mt}) [16]. In this study, we present evidence that increased mitochondrial elongation, which occurs independently of UPR^{mt}, is a critical contributor to lifespan extension in diverse longevity pathways.

Insulin/IGF-1 signaling (IIS) is an evolutionarily conserved pathway that controls lifespan [17]. In *C. elegans*, IIS reduces lifespan predominantly by inhibiting the activity of the FOXO transcription factor DAF-16 via inhibitory phosphorylation that blocks its nuclear localization. In the absence of IIS activity, DAF-16 enters the nucleus and regulates gene expression to extend lifespan.

In this study, we describe a pathway for the control of mitochondrial fusion in

C. elegans that is regulated by IIS and a cullin-RING ubiquitin ligase (CRL). CRLs are multisubunit E3 complexes that ubiquitylate substrate proteins to induce proteasome-mediated degradation or post-translational regulation [18, 19]. CRLs include a cullin protein as a scaffold, a RING finger protein, which binds the ubiquitin-conjugating enzyme, a substrate receptor that binds the substrate, and (generally) an adaptor that links the substrate receptor to the core complex. Substrate receptors are variable components, and core CRL complexes function with multiple substrate receptors. The binding of a different substrate receptor to the core CRL complex changes the substrates that are targeted and the cellular function of the complex. The most widely-studied CRL complex contains the cullin CUL1 and is designated SCF for its core components: the Skp1 adaptor; CUL1; and F-box protein substrate receptors.

CRL complexes are regulated by the CAND1 protein, which functions as an exchange factor for substrate receptors [20-22]. CAND1 affects the relative steady-state levels of different substrate receptors with the core CRL components [20-22]. In diverse organisms, the loss of CAND-1 selectively affects a subset of CRL complexes, suggesting that certain substrate receptors are particularly reliant on CAND1 for their inclusion in CRL complexes [19].

Here, we describe a mitochondrial fusion pathway that is regulated by CAND-1 and SCF^{LIN-23}. This pathway defines a new regulatory input for IIS, and describes how IIS directly controls mitochondrial fusion in *C. elegans*. We show that this pathway is responsible for an increase in elongated mitochondria that is observed in response to physical exercise. Increasing mitochondrial fusion through this pathway extends

lifespan. Finally, we show that increased levels of elongated mitochondria are associated with diverse lifespan-extension pathways, and is essential for their longevity.

Results

A gain-of-function mutation in the mitochondrial m-AAA protease gene *spg-7* is a *cand-1* suppressor

Inactivation of *C. elegans cand-1* results in developmental and morphological defects, including impenetrant embryonic and larval arrest, developmental delays, altered cell divisions, and morphological defects [23]. To identify CAND-1 molecular pathways, we isolated a genetic suppressor mutation, *ek25*, that can suppress multiple *cand-1(tm1683)* loss-of-function phenotypes (Table 2.S1; data not shown). *ek25* was identified as an insertion mutation in an intron of the *spg-7* gene and the 3'UTR of the *Y47G6A.15* gene (Figs 2.S1, 2.S2; Supplementary Information). *Y47G6A.15* is not conserved even in closely-related *Caenorhabditis* species (data not shown). *spg-7* is the ortholog of the mammalian mitochondrial m-AAA protease *AFG3L2* [24]. RNAi depletion of *spg-7* in *cand-1* mutants enhanced *cand-1* mutant phenotypes, and abrogated suppression in *cand-1*; *spg-7(ek25)* animals (Table 2.S1). In contrast, RNAi inactivation of *Y47G6A.15* had no obvious effects (Table 2.S1). CAND-1 positively regulates *spg-7* mRNA levels. *cand-1* mutants have lower levels of *spg-7* mRNA than wild type, and the *spg-7(ek25)* mutant allele rescues the decrease in *spg-7* expression in *cand-1* mutants (Figs 2.1a, 2.S3). These results suggest that *spg-7(ek25)* acts as a gain-of-function mutation that suppresses *cand-1* mutant phenotypes by restoring *spg-7* expression.

CAND-1 and LIN-23 inhibit elongated mitochondrial morphology

Since the *spg-7(ek25)* suppressor regulates the expression of a mitochondrial m-AAA protease, we wanted to determine if *cand-1* mutants have a mitochondrial phenotype. To characterize mitochondrial morphology, we used a transgenic strain expressing mitochondria-targeted GFP in muscle cells [25]. Mitochondrial morphology was scored blinded, and the scoring correlates with a quantitative assessment of mitochondrial area (Fig. 2.S4). The majority of wild-type hermaphrodite body wall muscle cells have longitudinally-arrayed tubular mitochondria (Fig. 2.1b,c). Smaller percentages of muscle cells exhibit elongated mitochondria in an interconnected mesh-like network, or fragmented mitochondria (Fig. 2.1b,c). Inactivation of *cand-1* significantly increases the percentage of cells exhibiting elongated mitochondria; and this phenotype is rescued by the *spg-7(ek25)* suppressor mutation in *cand-1, spg-7(ek25)* animals (Figs 2.1c, 2.S5). Inactivation of the COP9/Signalosome component CSN-3, which, like CAND-1, is required for CRL function [18], also increased the proportion of elongated mitochondria (Figs 2.1c, 2.S5). This suggests that the *cand-1* increased mitochondrial elongation phenotype arises from loss of CRL activity. The CRL SCF^{LIN-23}, which contains the substrate receptor LIN-23, is particularly reliant on CAND-1 for activity [23]. We found that inactivation of *lin-23* similarly reduces *spg-7* expression and has increased levels of elongated mitochondria (Fig. 2.1a,c, 2.S5).

CAND-1 and SCF^{LIN-23} regulate mitochondrial morphology through DAF-16-mediated regulation of SPG-7 and its paralog PPGN-1

spg-7(ad2249) loss-of-function and *spg-7(tm2312)* deletion (Δ) mutants exhibit mitochondrial elongation, but the proportion of mitochondria with the elongated morphology is not as large as that observed in *cand-1(RNAi)* or *lin-23(RNAi)* animals (Figs 2.1c, 2.S5). Mammalian m-AAA proteases form hexameric complexes in the inner mitochondrial membrane that exist as hetero-oligomeric complexes of AFG3L2 and SPG7/paraplegin or homo-oligomeric complexes of AFG3L2 [26]. The partial mitochondrial fusion phenotypes of *spg-7* mutants could potentially arise from functional redundancy between SPG-7 and PPGN-1, the *C. elegans* ortholog of mammalian SPG7/paraplegin.

We found that inactivation of *ppgn-1* alone increased mitochondrial fusion, while inactivating both *ppgn-1* and *spg-7* further increased the level of elongated mitochondria, implying that both m-AAA proteases negatively regulate mitochondrial elongation (Fig. 2.1c). CAND-1 and LIN-23 also promote *ppgn-1* expression (Fig. 2.1d), suggesting that the increase in mitochondrial elongation in *cand-1* and *lin-23* mutants arises from the failure to adequately express both *spg-7* and *ppgn-1*.

To determine how the *spg-7(ek25)* mutation increases *spg-7* mRNA levels, we looked for transcription factor binding sites that are affected by the *spg-7(ek25)* mutation. The *spg-7(ek25)* mutation disrupts a consensus DAF-16/FOXO binding site [27] within a region confirmed for DAF-16 binding by ChIP-seq [28] (Fig. 2.S2). DAF-16 was also shown to bind to the *ppgn-1* regulatory region [28]. *daf-16(mu86)* deletion mutants have elevated levels of *spg-7* and *ppgn-1* mRNA, suggesting that DAF-16 is a transcriptional

repressor of both *spg-7* and *ppgn-1* (Fig. 2.1a,d). Interestingly, the reduction of *ppgn-1* mRNA levels observed in *cand-1* mutants is also rescued by the *spg-7(ek25)* suppressor allele, suggesting co-regulation of *spg-7* and *ppgn-1* expression.

We wanted to determine if CAND-1 and SCF^{LIN-23} promote *spg-7* and *ppgn-1* expression by inhibiting DAF-16 activity. One of the primary mechanisms to control DAF-16 activity is by regulating its nuclear localization [17]. We observed that inactivation of *cand-1*, *cul-1*, and *lin-23* significantly increased DAF-16::GFP nuclear localization, suggesting that CAND-1 and SCF^{LIN-23} normally act to inhibit DAF-16 nuclear localization (Fig. 2.2a,b). To determine if the CAND-1-mediated inhibition of mitochondrial fusion is dependent on DAF-16 activity, we combined *daf-16* and *cand-1* loss-of-function mutations. The addition of the *daf-16* mutation rescued the *cand-1* elongated mitochondria phenotype, suggesting that CAND-1 inhibits mitochondrial elongation by negatively regulating DAF-16 activity (Fig. 2.1c).

To determine how SCF^{LIN-23} inhibits DAF-16 nuclear localization, we analyzed the kinase AKT-1, which phosphorylates DAF-16 to prevent its nuclear localization [17, 29]. Inactivating *cand-1* or the SCF^{LIN-23} components *cul-1* and *lin-23* leads to the accumulation of a faster migrating form of AKT-1::GFP without affecting its overall levels (Figs 2.2c, 2.S6). AKT-1 is activated by PDK-1 phosphorylation [17, 29], RNAi depletion of *pdk-1*, or the inhibition of the IIS pathway upstream of PDK-1 and AKT-1, results in the accumulation of a faster migrating form of AKT-1::GFP that is consistent with the unphosphorylated, inactive form (Fig. 2.S6a) [30]. *pdk-1* RNAi does not produce a further shift in the migration of AKT-1::GFP when combined with *lin-23* RNAi (Fig. 2.S6a). This suggests that the lower molecular weight form of AKT-1::GFP

observed upon loss of SCF^{LIN-23} activity reflects the loss of PDK-1-dependent activating-phosphorylation.

To further analyze the activity of AKT-1 in *cand-1(RNAi)*, *cul-1(RNAi)* and *lin-23(RNAi)* animals, we probed whole-animal lysate with an antibody that detects a phospho-epitope on substrates phosphorylated by AKT. The level of the AKT phospho-epitope was significantly reduced in *cand-1*, *cul-1*, and *lin-23* RNAi depletions (Fig. 2.2d,e). These results suggest that SCF^{LIN-23} increases AKT-1 activity by promoting its activating phosphorylation.

SPG-7 and PPGN-1 negatively regulate the mitochondrial fusion protein EAT-3

In yeast and mammals, the inner mitochondrial fusion protein, Mgm1 or OPA1, respectively, is cleaved into long (L) and short (S) isoforms, both of which are required for mitochondrial fusion [31, 32]. In mammals, there are two cleavage sites, S1 and S2. S1 is cleaved by the protease OMA1, and S2 is cleaved by the protease YME1L [31]. *C. elegans* lacks an *OMA1* homolog, and the corresponding S1 cleavage site is not conserved in EAT-3/OPA1 (data not shown). In contrast, *C. elegans* has a *YME1L* ortholog, *ymel-1*, and its target S2 site is conserved in EAT-3. The expected sizes of EAT-3 in *C. elegans* are consistent with an L-isoform (after removal of the mitochondrial targeting sequence) and an S-isoform cleaved at the conserved S2 site (Fig. 2.2f; Supplementary Information).

Mammalian m-AAA components AFG3L2 and SPG7/paraplegin can cleave OPA1 when overexpressed or expressed ectopically in yeast [33, 34]. We tested if inactivating *C. elegans spg-7* and *ppgn-1* affects EAT-3 levels. We observed that co-inactivation of

spg-7 and *ppgn-1* significantly increases the overall level of EAT-3, indicating that both m-AAA proteases negatively regulate EAT-3 levels (Fig. 2.2f,g). *cand-1* mutants, which have reduced expression of *spg-7* and *ppgn-1*, have higher levels of EAT-3 protein compared to wild type (Fig. 2.2f,g). Significantly, the *cand-1*; *spg-7(ek25)* strain, which restores expression of *spg-7* and *ppgn-1* mRNA, does not have elevated EAT-3 levels (Fig. 2.2f,g). The levels of *eat-3* mRNA remain unchanged in the above conditions, indicating that the negative regulation of EAT-3 protein is post-transcriptional (Fig. 2.S7). It is currently not known if the negative regulation of EAT-3 is direct or indirect. EAT-3 appears to function downstream of CAND-1, LIN-23, SPG-7, and PPGN-1, as the *eat-3(RNAi)* mitochondrial fragmentation phenotype is epistatic to the mitochondrial fusion associated with inactivation of these genes (Fig. 2.3a,b).

Levels of FZO-1::GFP (outer mitochondrial membrane fusion protein), and DRP-1::GFP (inner mitochondrial fission protein) are not affected by inactivation of the mitochondrial fusion pathway genes (Fig. 2.S8a,b). We also do not observe a major change in the levels of mitochondria-targeted GFP upon RNAi depletions of the mitochondrial fusion pathway genes (Fig. 2.S8c). This suggests that the mitochondrial fusion pathway does not significantly affect the level of mitophagy, as changes in mitophagy directly affect the level of mitochondria-targeted GFP [35].

Our data supports the model shown in Figure 2.4, in which CAND-1 activates SCF^{LIN-23}; SCF^{LIN-23} activates AKT-1 thereby reducing DAF-16-mediated transcriptional repression of *spg-7* and *ppgn-1*. SPG-7 and PPGN-1 inhibit mitochondrial fusion, at least in part, by negatively regulating the level of EAT-3.

The regulation of mitochondrial fusion in response to physical exertion

Acute physical exertion in mice induces mitochondrial fusion in skeletal muscle cells [36], presumably because fusion increases the efficiency of ATP production [4]. We wanted to determine if physical exertion similarly induces mitochondrial fusion in *C. elegans*, and if the fusion is DAF-16-dependent. To assess the level of mitochondrial fusion in response to physical exertion, we utilized swimming behavior. Animals were kept in a state of constant swimming by gently rocking them in M9 solution that contained OP50 bacteria. Swimming, which manifests as an intense thrashing motion, appears to be vigorous exercise based not only on the motion but also on the observation that ATP levels decrease during swimming (Fig. 2.5a). Wild-type animals and *daf-16(mu86)* mutants expressing mitochondria-targeted GFP swam vigorously at an equivalent swimming rate (Fig. 2.5b). Wild-type animals showed an increase in elongated mitochondria that reached an elevated plateau at 60 min that persisted through the remainder of the five-hour test period (Figs 2.5c, 2.S9a). Significantly, *daf-16* mutants did not exhibit increased levels of elongated mitochondria, implying that DAF-16 is required for this physiological response (Figs 2.5c, 2.S9b). Consistently, we observed a significant increase in DAF-16 nuclear localization in response to swimming in wild-type animals (Figs 2.5d, 2.S10). Notably, *cand-1*; *spg-7(ek25)* mutants, which have stabilized *spg-7* and *ppgn-1* expression, exhibited a lack of mitochondrial fusion in response to physical exertion despite a slightly faster swim rate (Figs 2.5b,c, 2.S9c). Similarly, we did not observe an increase in mitochondrial fusion in *spg-7(ek25)* mutants, which also swam at a rate equivalent to wild-type animals (Fig 2.S11). This suggests that

the DAF-16-mediated inhibition of *spg-7* and *ppgn-1* controls mitochondrial dynamics in response to physical exertion.

Increased mitochondrial fusion is associated with increased lifespan

DAF-16 is required for the extended lifespan of IIS pathway mutants [29]. Because CAND-1 and SCF^{LIN-23} inhibit DAF-16 nuclear localization, we hypothesized that inactivation of these regulators would extend lifespan. As expected, RNAi depletion of *cand-1* and *lin-23* (begun in late L4-stage to ensure normal larval development) extended lifespan (Fig. 2.6a; see Table 2.S2 for statistics on lifespan data). Interestingly, the *cand-1*; *spg-7(ek25)* strain, which rescues the *cand-1* increase in elongated mitochondria, had normal lifespan, suggesting that the extended lifespan of *cand-1* mutants requires increased levels of elongated mitochondria (Fig. 2.6b). Notably, we observed that increasing mitochondrial fusion independently of DAF-16 also extends lifespan. *ppgn-1(RNAi)*, *spg-7(Δ)*, and *spg-7 + ppgn-1* double RNAi animals, all of which exhibit increases in elongated mitochondria (Fig. 2.1c), had extended lifespan (Fig. 2.6c,d). In contrast to *spg-7(Δ)* mutants, *spg-7(RNAi)* animals do not exhibit increased levels of elongated mitochondria (Fig. 2.3b), potentially due to the impenetrant effects of RNAi, and had normal lifespan (Fig. 2.6c).

The mitochondrial fusion pathway includes activating AKT-1 to repress the DAF-16 transcription factor. The IIS pathway has the same downstream pathway, and so mutation of the IIS receptor DAF-2 would also be expected to activate DAF-16-mediated repression of *spg-7* and *ppgn-1* to activate mitochondrial fusion. Consistent with this, *daf-2* mutants exhibit increased levels of elongated mitochondria (Fig. 2.6g). To

determine the extent to which increased levels of elongated mitochondria contribute to the extended *daf-2* mutant lifespan, we inactivated the mitochondrial fusion gene *eat-3* in *daf-2* mutants. Strikingly, *eat-3* RNAi reduced the extended lifespan of *daf-2* mutants to wild-type levels (Fig. 2.6e). To test an alternate method to reduce elongated mitochondria in *daf-2* mutants, we RNAi depleted the outer membrane fusion protein FZO-1; and this also significantly reduced the extended lifespan of *daf-2* mutants (Fig. 2.6f). These results suggest that increased levels of mitochondrial elongation are required for lifespan extension in *daf-2* mutants.

Elongated mitochondria are known to produce ATP more efficiently [4]. We analyzed ATP levels in several key mutants, and found a correlation between increased levels of elongated mitochondria and increased ATP/protein ratios (Fig. 2.S12). The *daf-2* mutant is known to have significantly increased ATP levels [37], and had the highest ATP levels in our assay. Additionally, we observed statistically significant increases in ATP levels in *lin-23(RNAi)*, *cand-1(lf)*, and *ppgn-1(RNAi)* animals, all of have increased levels of elongated mitochondria. *spg-7(RNAi)* animals, which do not exhibit increased levels of elongated mitochondria (Fig. 2.3b), did not have significantly increased ATP levels. The observation that *cand-1(lf),spg-7(ek25)* mutants had significantly lower ATP levels than *cand-1(lf)* mutants suggests that a significant portion of the increase in ATP levels in *cand-1(lf)* mutants can be attributed to the reduction of *spg-7* expression. That ATP levels in *cand-1(lf),spg-7(ek25)* remained higher than in wild type may reflect the impact of the loss of CAND-1 on other CRL-regulated processes, given that CAND-1 potentially regulates hundreds of CRL complexes.

Swimming extends lifespan

We observed that swimming induces mitochondrial fusion through a SCF^{LIN-23}/DAF-16 regulated pathway, which we found to be associated with lifespan extension. We wanted to determine if exercise would also increased median lifespan compared to animals that did not exercise. We observed that making animals swim initially for 30 min per day, followed by consecutive reductions in swim time of 1 min per day, produced significant lifespan extension. However, this swimming regimen (A) caused a rapid drop-off in the viability of older animals (Fig. 2.7a, see Table 2.S3 for statistics). We tried two different swimming regimens (B and C) that reduced the extent of swimming as the animals aged to limit over-exertion in older animals: arbitrary reductions from 30 min/day swimming (B), described in the Figure 2.7 legend; or reductions of two min per day (C). We observed that the two age-moderated swim regimens produced further lifespan extensions relative to regimen A (Fig. 2.7b). Notably, *cand-1; spg-7(ek25)* and *daf-16* mutants, which failed to exhibit increased mitochondrial fusion in response to swimming, did not have lifespan extension in response to swimming (Fig. 2.7c,d). This suggests that the induction of mitochondrial fusion during exercise contributes to the observed lifespan extension associated with exercise.

Due to how the swim experiments were carried out, the lifespans of the control animals are not directly comparable to the lifespans of control animals in other (non-swim) experiments. Control animals in the swim experiments had shorter lifespans than the control animals in non-swim experiments. Presumably, this difference arose because all animals in the swim experiments (including controls) were kept at room temperature during the swim periods (rather than the lower temperature of 20°C) and were transferred

daily to new plates. Notably, the swim regimens B and C produced a significant extension of lifespan even when compared to control animals from the non-swim lifespan experiments (Table 2.S3).

Mitochondrial fusion is required for longevity in diverse lifespan mutants

To determine if mitochondrial fusion is more broadly correlated with longevity, we analyzed the mitochondrial morphologies of animals that exhibit longevity from five distinct mechanisms: *age-1*(*RNAi)* and *pdk-1(RNAi)* animals have extended lifespan from loss of IIS [17]; *eat-1*(*RNAi)* and *eat-6*(*RNAi)* animals have extended lifespan linked to caloric/dietary restriction [38]; *clk-1(RNAi)* extends lifespan because of mitochondrial ETC dysfunction; *glp-1*(*RNAi)* extends lifespan as a result of the loss of the germline [39]; and *vhl-1*, von Hippel Lindau tumor suppressor ortholog, mutants/RNAi animals have lifespan extension due to deregulation of the hypoxia transcriptional program [40].

We analyzed the distribution of mitochondrial morphologies in the seven long-lived strains. Strikingly, six out of the seven long-lived mutants/RNAi animals have increased levels of elongated mitochondria, with *vhl-1(RNAi)* animals the lone exception, with predominantly tubular mitochondria (Figs 2.8a,b, 2.S5). Caloric restricted mutants, such as *eat-6*, have lifespan extension independent of DAF-16 [38]. We found that the increase in elongated mitochondria in *eat-6* mutants was not affected by *daf-16* RNAi, suggesting that mitochondrial morphology in these mutants is regulated through a DAF-16-independent pathway (Fig. 2.8a).

Significantly, the increase in elongated mitochondria in these diverse mutants are essential for their longevity. RNAi depletion of the mitochondrial fusion gene *eat-3*

abolished the extended lifespans of: *glp-1(e2141ts)* (loss of the germline); *eat-2(ad1116)* and *eat-6(ad467)* (caloric restriction); and *clk-1(RNAi)* (ETC dysfunction) (Fig. 2.9a-d). Significantly, *eat-3* RNAi depletion in a wild-type background or in *vhl-1(ok161)* mutants, which do not have significantly elevated elongated mitochondria, did not affect their lifespans (Fig. 2.9e). This suggests that *eat-3* RNAi does not act directly to reduce lifespan, but rather indirectly affects lifespan by reducing the level of elongated mitochondria in those mutants that have increased mitochondrial elongation.

Elongated mitochondria have decreased production of ROS [4]. To determine if a reduction in ROS levels correlated with levels of elongated mitochondria in the long-lived *daf-2*, *glp-1*, and *eat-6* mutants, we measured mitochondrial ROS levels using the dye MitoSOX Red [41]. Each of the long-lived mutants had reduced levels of ROS relative to wild type (Fig. 2.S13, Table 2.S4). ROS levels increased significantly when the long-lived mutants were subjected to *eat-3* RNAi to block mitochondrial fusion, suggesting that the increase in elongated mitochondria contributes to the reduced ROS levels in these mutants (Fig. 2.S13, Table 2.S4).

We considered the possibility that the effect on lifespan by the mitochondrial fusion pathway was primarily due to changes in energy levels that were a secondary consequence of the changes in mitochondrial morphology. We analyzed three energy sensors that impact lifespan: LET-363/TOR; SIR-2.1; and AAK-2/AMPK. LET-363/TOR responds to metabolic inputs to regulate lifespan through inhibition of the transcription factors DAF-16; SKN-1; and PHA-4 [42, 43]. SIR-2.1 is a NAD^+-dependent histone deacetylase whose activity decreases during aging as NAD^+ levels drop [44].

SIR-2.1 overexpression increases lifespan by activating DAF16, UPR^{mt}, and autophagy [44]. Both SIR-2.1 overexpression and let-363/TOR RNAi exhibited increased mitochondrial elongation, as expected for pathways that include the activation of DAF-16 (Figs 2.8b, 2.S5). *eat-3* RNAi reduced the extended lifespan of both SIR-2.1 overexpression and *let-363(RNAi)* animals, suggesting that their elongated mitochondrial morphology contributes to the lifespan extension (Fig. 2.9f,g).

The AMP-activated protein kinase AAK-2 is required for lifespan extension in response to ROS-signals and impaired glycolysis, such as inactivation of GPI-1, glucose phosphate isomerase [37, 45]. The AAK-2 overexpression strain and *gpi-1(RNAi)* animals both exhibit increased levels of elongated mitochondria, and their extended lifespans were significantly reduced by *eat-3* RNAi (Figs 2.8c, 2.9h,i, 2.S5).

The UPR^{mt} links mitochondrial ETC dysfunction during larval stages with lifespan extension in adults [46]. To determine if the mitochondrial fusion pathway that we have described activates the UPR^{mt}, we analyzed the induction of the UPR^{mt} reporters *Phsp-6*::GFP and *Phsp-60*::GFP [47]. RNAi depletion of *spg-7* is known to induce UPRmt [48], and we observed increased expression of *Phsp-6*::GFP and *Phsp-60*::GFP in *spg-7(RNAi)* animals (Fig. 2.10a,b; data not shown). Notably, *ppgn-1* RNAi, which induces substantially more mitochondrial fusion than *spg-7* RNAi (Figs 2.1c and 2.3b) did not induce *Phsp-6*::GFP and *Phsp-60*::GFP expression (Fig. 2.10a,b; data not shown). Additionally, *cand-1*, *lin-23*, and *cul-1* RNAi depletions did not induce *Phsp-6*::GFP or *Phsp-60*::GFP, indicating that the mitochondrial fusion pathway does not induce UPR^{mt}.

The induction of UPR^{mt} is mediated by the transcription factor ATFS-1, which is required for the expression of *hsp-6*, *hsp-60*, and other UPR^{mt}-regulated genes [48]. Counterintuitively, a gain-of-function mutation of ATFS-1, *atfs-1(et17gf)* [49], with constitutively activated UPR^{mt}, exhibits reduced lifespan, not lifespan extension [50]. We used the *atfs-1(et17)* gain-of-function mutant to ask if activation of the mitochondrial fusion pathway reduces lifespan further, as would be expected if the pathway further activated the UPR^{mt}. We found that RNAi depletion of *cand-1*, *lin-23*, *spg-7*, and *ppgn-1* increased the lifespan of *atfs-1(et17)* mutants, suggesting that the lifespan extension operates independently of the UPR^{mt} (Fig. 2.10c,d). Also, induction of UPR^{mt} by loss of *spg-7* is abolished upon loss of *atfs-1* [48], however, we did not observe any significant differences in mitochondrial morphology in *spg-7(Δ)* mutants and *spg-7(Δ)*; *atfs-1(RNAi)* mutants (Fig. 2.10e). The UPR^{mt} is also not induced upon swimming, unlike the mitochondrial fusion pathway (Fig. 2.10f).

Discussion

The regulation of mitochondrial dynamics by SCF^{LIN-23} and IIS

Our study has uncovered the ubiquitin ligase SCF^{LIN-23} as a new regulator of IIS, and revealed a pathway by which SCF^{LIN-23} and IIS control mitochondrial fusion in *C. elegans* (Fig. 4a). We found that the CRL regulator CAND-1 and SCF^{LIN-23} are required to activate AKT-1. Active AKT-1 inhibits the nuclear localization of DAF-16, which inhibits the expression of the mitochondrial m-AAA proteases SPG-7 and PPGN-1 (Fig. 4b). We observed that decreased expression of SPG-7 and PPGN-1 is associated

with increased levels of the mitochondrial fusion protein EAT-3, whose activity is essential for the increased mitochondrial fusion observed upon inactivating the pathway components CAND1, LIN-23, and PPGN-1 (Fig. 4c). Our analysis does not indicate whether SPG-7 and PPGN-1 directly reduce EAT-3 levels or whether the impact on EAT-3 is indirect. Given the additional functions of the yeast and mammalian orthologs of *spg-7* and *ppgn-1* it is likely that reducing their levels affects multiple mitochondrial pathways [31]. Additionally, SCF complexes are known to target multiple substrates [18, 19], and we cannot rule out the possibility that CAND-1 and SCF^{LIN-23} impact mitochondria through other pathways.

The *spg-7(ek25)* allele disrupts a DAF-16 binding element (DBE) in an *spg-7* intron, and increases *spg-7* mRNA expression. DAF-16 is predominantly a transcriptional activator that functions by binding to DBE sites [51]. In contrast, genes that are repressed in a DAF-16-dependent manner are usually repressed by the PQM-1 transcription factor through its binding to DAF-16-associated element (DAE) sites [27]. However, a meta-analysis of DAF-16-responsive genes [27] suggests that DAF-16 can repress genes independently of PQM-1 (see Supplementary Information). Furthermore, since DAF-16, but not PQM-1, was found to bind to the regulatory sequences of *spg-7* and *ppgn-1*, DAF-16 may be a direct transcriptional repressor of these two genes [27].

Our work identifies the CAND-1/SCF^{LIN-23}-mediated activation of AKT-1 as a new regulatory mechanism for IIS, for which AKT-1 is a critical component. Currently, it is unclear how SCF^{LIN-23} promotes AKT-1 phosphorylation. Ubiquitylation has been linked to AKT activation in mammalian cells, wherein K63-linked poly-ubiquitylation of AKT is required for its translocation to the plasma membrane, where it is activated [52, 53]. In

mammalian cells, the K63 linkage is only detectable with anti-K63 ubiquitin antibodies immediately after stimulation of the relevant signaling pathways, but not in unstimulated cells [52, 53]. We have been unable to detect K63 poly-ubiquitin on immunoprecipitated AKT-1::GFP (data not shown). However, the inability to rapidly induce signaling in intact animals limits the implications of this negative result.

The control of mitochondrial fusion in response to exercise and its effect on lifespan

In mouse skeletal muscle cells, physical exercise increases mitochondrial fusion [36]. We have shown a similar result in *C. elegans* using swimming as a source of exercise. *C. elegans* swimming is associated with a reduction in the level of ATP, indicating that the "thrashing" swim strokes involves a greater expenditure of energy than their normal movement on plates. Swimming induces an increase in the level of elongated mitochondria, and this increase appears to be controlled by the IIS/SCF^{LIN-23} regulated pathway, as the increase in elongated mitochondria is blocked in *daf-16* mutants as well as *cand-1*; *spg-7(ek25)* mutants, which are no longer responsive to DAF-16-mediated inhibition of *spg-7* expression.

In rodents, modest physical exercise correlates with increases in mean lifespan and healthspan [54]. and we have found that exercise regimens increase *C. elegans* lifespan. Exercise regimens that limit the time of exercise as animals get older produces longer lifespan extensions. The lifespan extension in response to exercise is not observed in *daf-16* mutants or *cand-1*; *spg-7(ek25)* mutants, which are unable to activate the IIS/SCF^{LIN-23} pathway to increase mitochondrial fusion, suggesting that increased mitochondrial elongation positively contributes to exercise-induced longevity.

Increased levels of elongated mitochondria are observed in diverse longevity pathways, and are required for lifespan extension

We observed an increase in elongated mitochondria in diverse longevity pathways, including: IIS inactivation; caloric restriction; germline depletion; ETC dysfunction leading to UPR^{mt}; TOR inactivation; Sirtuin overexpression; AMPK overexpression; impaired glycolysis; and exercise. An analysis of six genes whose RNAi depletions cause ETC dysfunction leading to extended lifespan, also all showed increased mitochondrial fusion [55]. These observations suggest that increased levels of elongated mitochondria are broadly associated with longevity. In contrast to the other longevity pathways that we analyzed, the inactivation of *vhl-1* was not associated with an increase in elongated mitochondria.

Notably, the extended lifespans for the longevity pathway mutants with increased mitochondrial elongation were significantly reduced by *eat-3* RNAi, which reduces mitochondrial fusion. *eat-3* RNAi does not affect the lifespans of wild-type animals or *vhl-1* mutants, neither of which exhibit increased levels of elongated mitochondria. This suggests that inactivation of the mitochondrial fusion protein EAT-3 does not directly reduce lifespan, but rather indirectly reduces lifespan by countering the beneficial effects of elongated mitochondria. RNAi depletion of the outer membrane mitochondrial fusion protein FZO-1 also reduces *daf-2* mutant extended lifespan. *fzo-1* RNAi has a smaller reduction in mitochondrial elongation than *eat-3* RNAi, and consistently it produces a smaller reduction of the extended lifespan of *daf-2* mutants.

ppgn-1 mutants have a substantial increase in elongated mitochondria, yet have only modestly longer lifespans. This suggests that increasing mitochondrial elongation

does not, by itself, greatly extend lifespan. Rather, increased levels of elongated mitochondria appear to be a requirement for the survival of older animals in diverse longevity pathways. Thus, while an increase in elongated mitochondria is essential for longevity in many pathways, the precise level of the increase would not be expected to be predictive of the extent of lifespan extension.

The lifespan reducing effect of *eat-3* RNAi is larger than what has been observed for other lifespan-extension mechanisms that affect diverse pathways, such as mitophagy and the mitochondrial unfolded protein response (UPR^{mt}) [35, 56]. The breadth of the effect of increased mitochondrial elongation is also greater than that of other pathway components that are linked to mitochondria-associated lifespan extension. The intrinsic apoptosis pathway, which is required for ETC dysfunction-mediated longevity does not affect lifespan extension associated with caloric restriction, IIS, or germline depletion [57]. CEP-1/p53 is required for ETC dysfunction-linked longevity but does not affect caloric restriction or IIS lifespan extension [56]. Finally, the transcription factor CEH-23 contributes to ETC dysfunction-mediated longevity, but not to longevity in response to caloric restriction [58].

DAF-16 has a central role in mediating longevity in both IIS and germline-depleted mutants [15]. The described DAF-16-dependent pathway to regulate mitochondrial fusion is therefore likely to be operating in both IIS and germline-depletion pathways. In contrast, caloric restriction-mediated lifespan extension does not require DAF-16 activity [38, 59]. Caloric restriction mutants do not exhibit increased nuclear localization of DAF-16::GFP [60], and we observed that *daf-16* RNAi did not reduce the increase in elongated mitochondria in caloric-restricted *eat-6* mutants. Therefore, the caloric

restriction pathway does not appear to utilize DAF-16 to increase mitochondrial fusion. In other organisms, nutrient limitation increases mitochondrial fusion, presumably to increase the efficiency of ATP production [4]. Caloric restriction in *Drosophila* has been shown to increase mitochondrial volume and prevent mitochondrial fragmentation associated with aging [61]. It is therefore possible that mitochondrial fusion occurs in response to caloric restriction through a conserved pathway that responds to low nutrient levels.

Aging in many animal species, including *C. elegans*, is associated with a decline in mitochondrial function and an increase in mitochondrial fragmentation [14, 62]. However, mitochondrial fragmentation was not found to reduce lifespan in *C. elegans* [62]. Consistent with this, we observed that the increased mitochondrial fragmentation observed upon *eat-3* RNAi does not reduce lifespan. Therefore, while mitochondrial fragmentation increases as animals age, it does not appear to directly shorten lifespan. Rather, increased fragmentation during aging could indirectly contribute to shorter lifespans by preventing mitochondrial elongation.

Mitochondrial dynamics have been found to be essential for health and viability in many organisms. In mice and humans, inactivation of mitochondrial fusion or fission compromises tissue function and is lethal [5]. In *C. elegans*, it has been reported that blocking fission by inactivating DRP-1 reduces [63] or has no effect on the lifespan of wild-type animals [64], but increases the extended lifespans of IIS pathway mutants [64]. Based on observations from other organisms, it is likely that mitochondrial dynamics are essential for the overall health of *C. elegans*, and that the lifespan extension due to increased fusion occurs within the context of a still-functioning dynamics cycle.

vhl-1 mutants – an exception to the requirement for increased mitochondrial elongation in extended longevity

Elongated mitochondria have increased mitochondrial efficiency [4]; and we have observed increased ATP levels in mitochondrial fusion pathway mutants that have increased mitochondrial elongation. This leads to the suggestion that increased mitochondrial efficiency resulting in sufficient ATP production is required in diverse longevity pathways to allow the survival of long-lived adults.

We observed that *vhl-1* mutants do not have increased levels of elongated mitochondria and that their extended lifespan is not reduced by *eat-3* RNAi. This would on the surface suggest that increased mitochondrial elongation, and any potential benefit from increased energy efficiency, is not required for the longevity of *vhl-1* mutants. However, a large-scale Cas9 inactivation screen in human cells found that inactivation of VHL uniquely allowed a bypass of the complete block on mitochondrial respiration [65]. VHL functions as a substrate receptor for a $CRL2^{VHL}$ ubiquitin ligase complex that degrades the hypoxia-inducible factor HIF1α. During hypoxia, VHL-mediated degradation of HIF1α is blocked, leading to HIF1α inducing the transcriptional hypoxic response. The bypass of mitochondrial function by VHL inactivation is associated with a major reorganization of energy metabolism via deregulation of HIF1α transcription [65]. This suggests that unregulated HIF1α transcriptional activity can functionally replace the requirement for mitochondrial respiration in human cells [65].

C. elegans VHL-1 similarly targets the degradation of the HIF1α ortholog HIF-1 [66]. HIF-1 is required for the lifespan extension of *vhl-1* mutants [40]. If the role of HIF-1 in providing alternate energy sources under hypoxic conditions is conserved, then

vhl-1 mutants would have increased energy capacity via HIF-1-mediated induction of energy metabolism. It is possible that increased energy capacity is a requirement for survival beyond the normal lifespan, and that most longevity mutants increase energy capacity via mitochondrial elongation while *vhl-1* mutants utilize HIF-1-mediated transcriptional activity. We propose that increased energy availability, either through an increase in more efficient, elongated mitochondria or induction of alternate energy pathways is generally a requirement for significant lifespan extension in *C. elegans*.

In conclusion, our results have identified increased mitochondrial elongation as a previously unrecognized mechanism by which mitochondria are linked to longevity in *C. elegans* across diverse lifespan extension mechanisms. We describe a new regulator of *C. elegans* IIS and a pathway through which IIS directly controls mitochondrial fusion to regulate both lifespan and the response to physical exercise. This work implies that insulin-like peptides act systemically to regulate mitochondrial dynamics in order to modulate *C. elegans* lifespan.

Acknowledgements

We thank K.R. Williams, Y. Cao and Z.M. Detwiler for technical help; E.V. Stabb for use of equipment; H.A. Tissenbaum, A.M. van der Bliek, B. Conradt, and G.M. Benian for reagents; J. Gaertig for suggestions; and Z.M. Detwiler and members of the Kipreos lab for critical comments on the manuscript. Some *C. elegans* strains were provided by the CGC, which is funded by NIH Office of Research Infrastructure Programs (P40

OD010440). This work was supported by a grant to ETK from NIH/NIGMS (R01GM074212).

Experimental Procedures

C. elegans strains

The following *C. elegans* strains were used, with strain designations in parentheses: wild type Bristol (N2), wild type Hawaiian (CB4856), *cand-1(tm1683)* (ET327), *cand-1(tm1683)* outcrossed 8x into Hawaiian strain CB4856 (ET335), *cand-1(tm1683)*; *spg-7(ek25)* (ET329), *lin-23(e1883)/mIn-1* (ET351), *daf-16(mu86)* (CF1038), *spg-7(ad2249)* (DA2249) [67], *spg-7(tm2312)* (ET352), *daf-2(e1370)* (CB1370), *muEx248* [*pNL209(Pdaf-16*::DAF-16::GFP) + *Podr-1*::RFP], *Pakt-1*::AKT-1::GFP (SP209) [68], *glp-1(e2141)* (CF1903), *eat-6(ad467)* (DA467), *zcIs14* [*Pmyo-3::*GFP*(mit)*] (SJ4103) [69], *cand-1(tm1683)*; *zcIS14* (ET353), *cand-1(tm1683)*; *spg-7(ek25)*; *zcIS14* (ET354), *spg-7(tm2312)*; *zcIS14* (ET355), *daf-2(e1370)*; *zcIS14* (ET356), *daf-16(mu86)*; *zcIS14* (ET357), *cand-1(tm1683)*; *daf-16(mu86)*; *zcIS14* (ET358), *spg-7(ek25)*; *zcIS14* (ET359) *atfs-1(et17)* (QC117); *vhl-1(ok161)* (CB5602); *eat-2(ad1116)* (DA1116), *uthEx299* [*aak-2* (genomic aa1-aa321)::GFP::*unc-54* 3'UTR + *Pmyo-2::*tdTomato] (AGD731), *lin-15(n765ts)*; *bcEx665* [*Phsp*::FZO-1::GFP; *lin-15(+)*] (MD2642), unc-119(ed3); ekEx37 [pPD96.52/*Pmyo-3*::DRP-1::GFP; *unc-119(+)*] (ET537), *geIs3* [*sir-2.1*(+) + *rol-6(su1006)*] (LG394), *zcIs9* [*hsp-60::*GFP + *lin-15*(+)] (SJ4058), and *zcIs13* [*Phsp-6::*GFP] (SJ4100).

Analysis of mitochondrial morphology

Adult hermaphrodites expressing mitochondrial matrix-targeted GFP [*Pmyo-3*::GFP(mit)] in their body wall muscle cells [69] were imaged for mitochondrial morphology. Cells were categorized as harboring tubular, elongated, or fragmented mitochondria, as described [6]. Mitochondrial morphology was assessed with at least 100 muscle cells analyzed for each condition; and was scored blinded where noted. To quantitatively categorize cells harboring tubular, elongated, or fragmented mitochondria, the two-dimensional areas of mitochondria were measured as previously described [70]. The areas (in pixels) of the five largest mitochondria per cell in ~40 body-wall muscle cells were measured from micrographs using Photoshop software (Adobe).

Analysis of mitochondrial ROS

Eggs were placed on RNAi plates and L4-stage larval stage were used for the analysis of mitochondrial ROS with the dye MitoSOX Red (Life Technologies), which was performed as previously described [41]. Animals were incubated in 10 μM MitoSOX Red in M9 buffer with cholesterol and RNAi bacteria in the dark at 20°C for 24 hours. Animals were washed two times in M9 buffer and incubated in M9 buffer with OP50 bacteria for an hour to clear their intestines of residual dye. ROS levels were analyzed in the posterior pharyngeal bulb by measuring the MitoSOX Red epifluorescence intensity with a 300 ms exposure. Mitochondrial ROS levels were measured in adult hermaphrodites one day-post-L4 stage.

Physical exertion swimming assay

L4-stage larvae and young adults expressing the *Pmyo-3*::GFP(mit) transgene were placed on one 6 cm OP50-seeded NGM plate per timepoint. To induce the swimming behavior, 3ml of M9 buffer was added to each plate, and the plates were placed on a rocking platform to prevent the animals from settling down. At each timepoint, animals were collected by centrifugation, and visualized by epifluorescence microscopy to determine mitochondrial morphology (obtaining data from at least 100 cells). To determine the swim rate, 12 animals were analyzed for the number of swim-strokes per minute for each genotype.

Other methods are described in the Supplementary Information.

References

1. Chan, D.C., *Mitochondria: dynamic organelles in disease, aging, and development.* Cell, 2006. **125**(7): p. 1241-52.
2. Chan, D.C., *Fusion and fission: interlinked processes critical for mitochondrial health.* Annu Rev Genet, 2012. **46**: p. 265-87.
3. Gomes, L.C. and L. Scorrano, *Mitochondrial morphology in mitophagy and macroautophagy.* Biochim Biophys Acta, 2013. **1833**(1): p. 205-12.
4. Liesa, M. and O.S. Shirihai, *Mitochondrial dynamics in the regulation of nutrient utilization and energy expenditure.* Cell Metab, 2013. **17**(4): p. 491-506.

5. Zhao, J., U. Lendahl, and M. Nister, *Regulation of mitochondrial dynamics: convergences and divergences between yeast and vertebrates.* Cell Mol Life Sci, 2013. **70**(6): p. 951-76.

6. Kanazawa, T., et al., *The C. elegans Opa1 homologue EAT-3 is essential for resistance to free radicals.* PLoS Genet, 2008. **4**(2): p. e1000022.

7. Rolland, S.G., et al., *The BCL-2-like protein CED-9 of C. elegans promotes FZO-1/Mfn1,2- and EAT-3/Opa1-dependent mitochondrial fusion.* J Cell Biol, 2009. **186**(4): p. 525-40.

8. Santel, A. and M.T. Fuller, *Control of mitochondrial morphology by a human mitofusin.* J Cell Sci, 2001. **114**(Pt 5): p. 867-74.

9. Rojo, M., et al., *Membrane topology and mitochondrial targeting of mitofusins, ubiquitous mammalian homologs of the transmembrane GTPase Fzo.* J Cell Sci, 2002. **115**(Pt 8): p. 1663-74.

10. Bach, D., et al., *Mitofusin-2 determines mitochondrial network architecture and mitochondrial metabolism. A novel regulatory mechanism altered in obesity.* J Biol Chem, 2003. **278**(19): p. 17190-7.

11. Santel, A., et al., *Mitofusin-1 protein is a generally expressed mediator of mitochondrial fusion in mammalian cells.* J Cell Sci, 2003. **116**(Pt 13): p. 2763-74.

12. Shen, T., et al., *Mitofusin-2 is a major determinant of oxidative stress-mediated heart muscle cell apoptosis.* J Biol Chem, 2007. **282**(32): p. 23354-61.

13. Liu, X., et al., *Mitochondrial 'kiss-and-run': interplay between mitochondrial motility and fusion-fission dynamics.* EMBO J, 2009. **28**(20): p. 3074-89.

14. Bratic, A. and N.G. Larsson, *The role of mitochondria in aging.* J Clin Invest, 2013. **123**(3): p. 951-7.

15. Yanos, M.E., C.F. Bennett, and M. Kaeberlein, *Genome-Wide RNAi Longevity Screens in Caenorhabditis elegans.* Curr Genomics, 2012. **13**(7): p. 508-18.

16. Tatar, M. and J.M. Sedivy, *Mitochondria: Masters of Epigenetics.* Cell, 2016. **165**(5): p. 1052-4.

17. Murphy, C.T. and P.J. Hu, *Insulin/insulin-like growth factor signaling in C. elegans.* WormBook, 2013: p. 1-43.

18. Bosu, D.R. and E.T. Kipreos, *Cullin-RING ubiquitin ligases: global regulation and activation cycles.* Cell Div, 2008. **3**: p. 7.

19. Lydeard, J.R., B.A. Schulman, and J.W. Harper, *Building and remodelling Cullin-RING E3 ubiquitin ligases.* EMBO Rep, 2013. **14**(12): p. 1050-61.

20. Zemla, A., et al., *CSN- and CAND1-dependent remodelling of the budding yeast SCF complex.* Nat Commun, 2013. **4**: p. 1641.

21. Pierce, N.W., et al., *Cand1 promotes assembly of new SCF complexes through dynamic exchange of F box proteins.* Cell, 2013. **153**(1): p. 206-15.

22. Wu, S., et al., *CAND1 controls in vivo dynamics of the cullin 1-RING ubiquitin ligase repertoire.* Nat Commun, 2013. **4**: p. 1642.

23. Bosu, D.R., et al., *C. elegans CAND-1 regulates cullin neddylation, cell proliferation and morphogenesis in specific tissues.* Dev Biol, 2010. **346**(1): p. 113-26.

24. Juhola, M.K., et al., *The mitochondrial inner membrane AAA metalloprotease family in metazoans.* FEBS Lett, 2000. **481**(2): p. 91-5.

25. Labrousse, A.M., et al., *C. elegans dynamin-related protein DRP-1 controls severing of the mitochondrial outer membrane.* Mol Cell, 1999. **4**(5): p. 815-26.

26. Koppen, M., et al., *Variable and tissue-specific subunit composition of mitochondrial m-AAA protease complexes linked to hereditary spastic paraplegia.* Mol Cell Biol, 2007. **27**(2): p. 758-67.

27. Tepper, R.G., et al., *PQM-1 complements DAF-16 as a key transcriptional regulator of DAF-2-mediated development and longevity.* Cell, 2013. **154**(3): p. 676-90.

28. Gerstein, M.B., et al., *Integrative analysis of the Caenorhabditis elegans genome by the modENCODE project.* Science, 2010. **330**(6012): p. 1775-87.

29. Lin, K., et al., *Regulation of the Caenorhabditis elegans longevity protein DAF-16 by insulin/IGF-1 and germline signaling.* Nat Genet, 2001. **28**(2): p. 139-45.

30. Yung, H.W., D.S. Charnock-Jones, and G.J. Burton, *Regulation of AKT phosphorylation at Ser473 and Thr308 by endoplasmic reticulum stress modulates substrate specificity in a severity dependent manner.* PLoS One, 2011. **6**(3): p. e17894.

31. Anand, R., T. Langer, and M.J. Baker, *Proteolytic control of mitochondrial function and morphogenesis.* Biochim Biophys Acta, 2013. **1833**(1): p. 195-204.

32. Escobar-Henriques, M. and F. Anton, *Mechanistic perspective of mitochondrial fusion: tubulation vs. fragmentation.* Biochim Biophys Acta, 2013. **1833**(1): p. 162-75.

33. Ishihara, N., et al., *Regulation of mitochondrial morphology through proteolytic cleavage of OPA1.* EMBO J, 2006. **25**(13): p. 2966-77.

34. Duvezin-Caubet, S., et al., *OPA1 processing reconstituted in yeast depends on the subunit composition of the m-AAA protease in mitochondria.* Mol Biol Cell, 2007. **18**(9): p. 3582-90.

35. Palikaras, K., E. Lionaki, and N. Tavernarakis, *Coordination of mitophagy and mitochondrial biogenesis during ageing in C. elegans.* Nature, 2015. **521**(7553): p. 525-8.

36. Picard, M., et al., *Acute exercise remodels mitochondrial membrane interactions in mouse skeletal muscle.* J Appl Physiol (1985), 2013. **115**(10): p. 1562-71.

37. Zarse, K., et al., *Impaired insulin/IGF1 signaling extends life span by promoting mitochondrial L-proline catabolism to induce a transient ROS signal.* Cell Metab, 2012. **15**(4): p. 451-65.

38. Lakowski, B. and S. Hekimi, *The genetics of caloric restriction in Caenorhabditis elegans.* Proc Natl Acad Sci U S A, 1998. **95**(22): p. 13091-6.

39. Berman, J.R. and C. Kenyon, *Germ-cell loss extends C. elegans life span through regulation of DAF-16 by kri-1 and lipophilic-hormone signaling.* Cell, 2006. **124**(5): p. 1055-68.

40. Mehta, R., et al., *Proteasomal regulation of the hypoxic response modulates aging in C. elegans.* Science, 2009. **324**(5931): p. 1196-8.

41. Dingley, S., et al., *Mitochondrial respiratory chain dysfunction variably increases oxidant stress in Caenorhabditis elegans.* Mitochondrion, 2010. **10**(2): p. 125-36.

42. Robida-Stubbs, S., et al., *TOR signaling and rapamycin influence longevity by regulating SKN-1/Nrf and DAF-16/FoxO.* Cell Metab, 2012. **15**(5): p. 713-24.

43. Sheaffer, K.L., D.L. Updike, and S.E. Mango, *The Target of Rapamycin pathway antagonizes pha-4/FoxA to control development and aging.* Curr Biol, 2008. **18**(18): p. 1355-64.

44. Mouchiroud, L., et al., *The NAD(+)/Sirtuin Pathway Modulates Longevity through Activation of Mitochondrial UPR and FOXO Signaling.* Cell, 2013. **154**(2): p. 430-41.

45. Schulz, T.J., et al., *Glucose restriction extends Caenorhabditis elegans life span by inducing mitochondrial respiration and increasing oxidative stress.* Cell Metab, 2007. **6**(4): p. 280-93.

46. Dillin, A., et al., *Rates of behavior and aging specified by mitochondrial function during development.* Science, 2002. **298**(5602): p. 2398-401.

47. Haynes, C.M. and D. Ron, *The mitochondrial UPR - protecting organelle protein homeostasis.* J Cell Sci, 2010. **123**(Pt 22): p. 3849-55.

48. Nargund, A.M., et al., *Mitochondrial import efficiency of ATFS-1 regulates mitochondrial UPR activation.* Science, 2012. **337**(6094): p. 587-90.

49. Rauthan, M., et al., *The mitochondrial unfolded protein response activator ATFS-1 protects cells from inhibition of the mevalonate pathway.* Proc Natl Acad Sci U S A, 2013. **110**(15): p. 5981-6.

50. Bennett, C.F., et al., *Activation of the mitochondrial unfolded protein response does not predict longevity in Caenorhabditis elegans.* Nat Commun, 2014. **5**: p. 3483.

51. Schuster, E., et al., *DamID in C. elegans reveals longevity-associated targets of DAF-16/FoxO.* Mol Syst Biol, 2010. **6**: p. 399.

52. Yang, W.L., et al., *The E3 ligase TRAF6 regulates Akt ubiquitination and activation.* Science, 2009. **325**(5944): p. 1134-8.

53. Chan, C.H., et al., *The Skp2-SCF E3 ligase regulates Akt ubiquitination, glycolysis, herceptin sensitivity, and tumorigenesis.* Cell, 2012. **149**(5): p. 1098-111.

54. Mercken, E.M., et al., *Of mice and men: the benefits of caloric restriction, exercise, and mimetics.* Ageing Res Rev, 2012. **11**(3): p. 390-8.

55. Lee, S.S., et al., *A systematic RNAi screen identifies a critical role for mitochondria in C. elegans longevity.* Nat Genet, 2003. **33**(1): p. 40-8.

56. Durieux, J., S. Wolff, and A. Dillin, *The cell-non-autonomous nature of electron transport chain-mediated longevity.* Cell, 2011. **144**(1): p. 79-91.

57. Yee, C., W. Yang, and S. Hekimi, *The intrinsic apoptosis pathway mediates the pro-longevity response to mitochondrial ROS in C. elegans.* Cell, 2014. **157**(4): p. 897-909.

58. Walter, L., et al., *The homeobox protein CEH-23 mediates prolonged longevity in response to impaired mitochondrial electron transport chain in C. elegans.* PLoS Biol, 2011. **9**(6): p. e1001084.

59. Houthoofd, K., T.E. Johnson, and J.R. Vanfleteren, *Dietary restriction in the nematode Caenorhabditis elegans.* J Gerontol A Biol Sci Med Sci, 2005. **60**(9): p. 1125-31.

60. Henderson, S.T. and T.E. Johnson, *daf-16 integrates developmental and environmental inputs to mediate aging in the nematode Caenorhabditis elegans.* Curr Biol, 2001. **11**(24): p. 1975-80.

61. Magwere, T., et al., *The effect of dietary restriction on mitochondrial protein density and flight muscle mitochondrial morphology in Drosophila.* J Gerontol A Biol Sci Med Sci, 2006. **61**(1): p. 36-47.

62. Regmi, S.G., S.G. Rolland, and B. Conradt, *Age-dependent changes in mitochondrial morphology and volume are not predictors of lifespan.* Aging (Albany NY), 2014.

63. Kim, H., et al., *Fine-tuning of Drp1/Fis1 availability by AKAP121/Siah2 regulates mitochondrial adaptation to hypoxia.* Mol Cell, 2011. **44**(4): p. 532-44.

64. Yang, C.C., et al., *The dynamin-related protein DRP-1 and the insulin signaling pathway cooperate to modulate Caenorhabditis elegans longevity.* Aging Cell, 2011. **10**(4): p. 724-8.

65. Jain, I.H., et al., *Hypoxia as a therapy for mitochondrial disease.* Science, 2016. **352**(6281): p. 54-61.

66. Epstein, A.C., et al., *C. elegans EGL-9 and mammalian homologs define a family of dioxygenases that regulate HIF by prolyl hydroxylation.* Cell, 2001. **107**(1): p. 43-54.

67. Zubovych, I.O., S. Straud, and M.G. Roth, *Mitochondrial dysfunction confers resistance to multiple drugs in Caenorhabditis elegans.* Mol Biol Cell, 2010. **21**(6): p. 956-69.

68. Padmanabhan, S., et al., *A PP2A regulatory subunit regulates C. elegans insulin/IGF-1 signaling by modulating AKT-1 phosphorylation.* Cell, 2009. **136**(5): p. 939-51.

69. Benedetti, C., et al., *Ubiquitin-like protein 5 positively regulates chaperone gene expression in the mitochondrial unfolded protein response.* Genetics, 2006. **174**(1): p. 229-39.

70. Westrate, L.M., et al., *Mitochondrial morphological features are associated with fission and fusion events.* PLoS One, 2014. **9**(4): p. e95265.

Supplementary Information

The isolation of the *ek25 cand-1*-suppressor mutation

cand-1(tm1683) mutants were synchronized as L1-stage larvae by isolating eggs by hypochlorite treatment [1] and allowing the eggs to hatch overnight in M9 buffer [1] supplemented with 5 µg/ml cholesterol. The synchronized L1-stage larvae were grown on NGM plates with OP50 bacteria until the L4/young-adult stage, when they were mutagenized with 0.5 mM N-nitroso-N-ethylurea (ENU) for 4 hours as described [2]. The mutagenized animals were cultured on NGM plates with OP50 for one day, at which time F1 mutant eggs were isolated from the gravid adults and synchronized as L1 larvae. The F1 mutant animals were cultured on NGM plates with OP50 bacteria until they became gravid adults. F2 mutant eggs were isolated from the F1 gravid adults and synchronized as L1 larvae. 10,000 F2 mutant L1 larvae were grown in a 500 ml liquid culture [1] supplemented with OP50 bacteria for 11 days, and then collected by centrifugation and regrown in fresh liquid culture for 3 days. Propagation in liquid culture is a hardship for *C. elegans*, and this culturing condition selects for healthier *cand-1* suppressors, as *cand-1(tm1683)* mutants have lower brood sizes, impenetrant

embryonic lethality, and impenetrant larval arrest [3]. Animals from the liquid culture were placed on 3xNGM plates. Twelve healthy L4 larvae that did not exhibit *cand-1* mutant phenotypes (e.g., no bobtail phenotype) were cloned onto separate NGM plates with OP50 bacteria. One of these cloned animals (*cand-1(tm1683)*; *ek25*) had 100% healthy progeny without visible *cand-1* mutant phenotypes.

SNP Mapping

SNP mapping was performed as described [4]. The *cand-1(tm1683)*; *ek25* strain was outcrossed 10 times into the Hawaiianized *cand-1(tm1683)* strain ET335. The resulting Hawaiianized *cand-1*; *ek25* strain appears to be largely Hawaiian throughout the genome with the exception of the +7.5 to +11.5 region of chromosome V, which contains the *cand-1* gene and remains N2 Bristol. *cand-1(tm1683)* was crossed with the Hawaiianized *cand-1(tm1683)*; *ek25*, and confirmed F1s were allowed to lay eggs. 273 L1 larvae from the F2 generation were transferred onto separate *csn-3* RNAi plates. *cand-1* mutants subjected to *csn-3* RNAi have an enhanced phenotype of 100% arrested embryos; in contrast, *cand-1*; *ek25* is highly resistant to *csn-3* RNAi (Table 2.S1). Using the resistance to *csn-3* RNAi as a measure of *cand-1* suppression, we identified 40 'suppressed' and 40 'non-suppressed' plates from the 273 F2 cross progeny. Using whole-genome SNP mapping of pooled DNA from the suppressed and non-suppressed progeny respectively, we found an enrichment of Hawaiian regions in the Chromosome I region -4 to -2 in the 'suppressed' population (Fig. 2.S1a). We then looked at the distribution of Hawaiian vs. N2 regions in the each of the 40 'suppressed' clones (Fig. 2.S1b). Most clones were Hawaiian in the -4 to -2 chromosome I region, but 12 clones

were heterozygous in parts of this region. The only SNP that was Hawaiian in all clones was -3.18, which narrowed the location of the suppressor to the -3.96 to -2.07 interval. By sequencing SNPs in this region, we narrowed the region containing the suppressor to -3.48 to -3.18 and found a 26 bp insertion mutation in the major intron of *spg-7* (located at -3.22 on chromosome I). The insertion mutation segregated completely with the rescue of the *cand-1(tm1683)* mutant phenotypes through additional outcrossings, suggesting that it is the *cand-1* suppressor mutation (data not shown).

DAF-16 and PQM-1 meta-analysis data

DAF-16 has been found to predominantly function as a transcriptional activator via binding regulatory regions through DBE (DAF-16-binding element) sites [5]. In contrast, genes that are repressed in a DAF-16-dependent manner are predominantly repressed by the PQM-1 transcription factor via binding to DAE (DAF-16-associated element) sites [6]. However, an analysis of DAF-16-reponsive genes shows that of 2196 genes repressed in a DAF-16-dependent manner at $p< 0.01$ significance, 563 (26%) were shown to be bound by DAF-16 but not by PQM-1, and 131 of the genes have PSAM affinity scores of 0 for DAE sites but positive scores for DBE sites [6] (analysis not shown). This suggests that DAF-16 can represses gene expression independently of PQM-1. The activating *spg-7(ek25)* mutation disrupts a DBE site, and both *spg-7* and *ppgn-1* regulatory regions have been found to be bound by DAF-16 but not by PQM-1 [6]. This suggests that *spg-7* and *ppgn-1* are repressed by DAF-16 in a PQM-1-independent manner.

Supplementary Materials and Methods

RNA interference

Feeding RNAi was performed as described [7]. Feeding-RNAi constructs (expressed in HT115 bacteria) were obtained from the Ahringer library [7]. RNAi-feeding bacteria were induced in 1 mM IPTG in liquid 2xYT media plus 100 μg/ml carbenicillin (Gold Biotechnology) for 5 to 7 hours with the exception of *lin-23*, *let363*, and *atfs-1* RNAi bacteria, which was induced by plating overnight cultures of the *lin-23* RNAi bacteria on 1 mM IPTG plus 100 μg/ml carbenicillin plates. Double RNAi treatments were performed by combining RNAi bacteria at a 1:1 ratio (unless otherwise indicated) using OD_{600} optical densities to quantify the bacteria prior to seeding plates. Unless otherwise indicated, eggs were placed on the RNAi plates and adults from the next generation were analyzed.

Epifluorescence microscopy

RNAi-treated and mutant animals were maintained at 20°C, and L4- to young adult-stage animals were used for imaging. FZO-1::GFP expressing L4-stage animals were subjected to heat-shock treatment at 33.5°C for 10 hours to ensure stable expression prior to imaging. Animals were mounted on slides with 0.5 mM levamisole (Sigma) to induce muscle paralysis. Animals were visualized with a Zeiss Axioskop microscope, and images were taken with a Hamamatsu ORCA-ER digital camera using Openlab 4.0.2 software (Agilent Technologies). Images were processed and analyzed with Adobe Photoshop CS6 or CC software. Matched images were taken with the same exposure and were processed and analyzed identically. Images from 20 animals were analyzed for

AKT::GFP (Fig. 2.S6b), FZO-1::GFP (Fig. 2.S7a), DRP-1::GFP (Fig. 2.S7b), and mitochondrial GFP (Fig. 2.S7c) levels.

Real-time quantitative RT-PCR

Total RNA was isolated from whole-animal lysate using TRIzol reagent (Life Technologies) according to the manufacturer's instructions. RNA was reverse transcribed into cDNA using the SuperScript III First-Strand Synthesis for RT-PCR kit from Life Technologies, according to the manufacturer's instructions. The first-strand cDNA was used for PCR amplification of *spg-7* and *ppgn-1*. *rpl-19*, which encodes the large ribosomal subunit L-19, was used as a normalization control. RT-PCR was performed using SYBR Green Supermix (Bio-Rad) and analyzed using the CFX Connect Real-Time PCR Detection System (Bio-Rad). The primers used were: *spg-7*, forward: 5'-CCGTTGTCGTTTGAGACACC-3', reverse: 5'- CGGCGAAGTGCGTTCATTAC-3'; *ppgn-1*, forward: 5'-ATGCTTCTACACCGCTCCAC-3', reverse: 5'-GTGGAAATCTGCGAGCACT-3'; *eat-3*, forward: 5'-AGAGCATCGAAACCGGATGG-3', reverse: 5'- GCGTCAGCATAGCTTCTTCG-3'; and *rpl-19*, forward: 5'- CGCGCAAAGGGAAACAACTT-3', reverse: 5'-CTTGCGGCTCTCCTTGTTCT-3'. mRNA levels were normalized using *rpl-19* mRNA and the relative fold change was calculated using the ΔΔCt method. The normalized mRNA levels are reported in arbitrary units with the wild-type level set to 1.0.

Western blot analysis

Mixed-stage animals were lysed in SDS sample buffer and used for Western blot analysis. The following mouse primary antibodies were used: anti-GFP (GF28R, Roche, 1:2000); and anti-α-tubulin (DM1A, Sigma; 1:4000). The following rabbit primary antibodies were used: anti-EAT-3 (1:1000) [8]; anti-AKT phospho-substrate (9611S, Cell Signaling, 1:1000); and anti-histone H4 (Upstate Biotechnology, Inc.; 1:1000). Anti-rabbit-HRP (Pierce, 1:5000) and anti-mouse-HRP (Pierce; 1:10,000) were used as secondary antibodies. Chemiluminescence was performed with the Advanced ECL chemiluminescence system (GE Healthcare). Western Blot images were obtained using the Bio-Rad ChemiDoc MP Imaging System**.** Western blots were analyzed and quantified with Adobe Photoshop CS6 or CC software using non-saturated images with background level subtracted. Signals of the bands of interest were normalized with α-tubulin or histone H4, and are reported in arbitrary units.

The expected molecular weight of EAT-3 isoforms was determined as follows. The mitochondrial targeting sequence (MTS), which is cleaved from the precursor protein to form the L-isoform, was identified using the MitoProt program [9]. The predicted MTS in EAT-3 (NP495986) encompasses residues 1-59. The predicted L-isoform therefore encompasses amino acids 60-964 of EAT-3. The mammalian S2 cleavage site has been identified between amino acids 217-223 of human OPA1 (NP_570849) [10]. The human S2 cleavage site corresponds to residues 215-221 in EAT-3; cleavage of which would produce an S-isoform of between 216-964 and 222-964 amino acids.

Lifespan analysis

Survival assays were performed at 20°C, as described [11]. Eggs were isolated from gravid adults by hypochlorite treatment and allowed to hatch on RNAi-feeding bacteria plates, with the exception of *cand-1*, *cul-1*, *lin-23*, *clk-1*, and *let-363* RNAi, where wild-type hermaphrodites were transferred to RNAi-feeding bacteria plates as late-L4 stage larvae to ensure that prior larval development was normal. Animals were transferred to fresh plates every alternate day throughout the lifespan study. For all lifespan studies, animals in the L4 larval stage were picked at day 0. Lifespan analysis of wild-type adult hermaphrodites subjected to a swimming regimen was performed by adding 3 ml of M9 buffer to plates, and the plates were placed on a rocking platform at room temperature to prevent the animals from settling down. The daily swim regimens are described in the main text. After swimming, animals were transferred to fresh agar plates with OP50 bacteria. The non-swim control animals were placed at room temperature for the duration of the swim period, and also transferred to new OP50-seeded NGM plates at the same time as swim animals. Animals that crawled off the plate or had ruptured vulvae were censored. Immobile adults were counted as dead when they failed to respond to prodding. *P*-values were calculated by the Log-rank (Mantel-Cox) and Wilcoxon tests using GraphPad Prism software (version 6.0).

ATP Quantification

ATP levels were measured using the EnzyLight^{TM} ADP/ATP Ratio Assay Kit (ELDT-100) from BioAssay Systems per manufacturer's protocol with the following modifications. Eggs were isolated from gravid adults by hypochlorite treatment and

allowed to hatch on RNAi-feeding bacteria plates, or OP50 plates for mutant animals, and maintained at 20°C. L4-stage animals were collected by centrifugation and washed 3 times in M9 buffer + 5mg/ml Cholesterol, flash-frozen in liquid nitrogen, and stored at -80°C. Frozen samples were boiled for 15min to release ATP, and centrifuged at 15,000 x g to pellet debris. The supernatant was diluted 2-fold in RNase/DNase-free water, and used for ATP measurement. Protein concentration was measured using the Bradford reagent (Sigma). ATP levels were normalized to protein concentration.

Statistical Analysis

The Student's t-test (two-tailed, unpaired) was used to determine statistical significance for: quantification of RT-qPCR (Figs 2.1a,d, 2.S3, 2.S7); epifluorescence signal intensity (Figs 2.2b, 2.10b,f, 2.S4, 2.S6b, 2.S8, 2.S10); ATP levels (Figs 2.5a, 2.S12); western blot quantification (Fig. 2.2e,g); swimming rate (Figs 2.5b, 2.S9c, 2.S11b); and MitoSOX Red staining (Fig. 2.S12). The chi-square test was used to determine statistical significance for the percentages of mitochondrial morphologies (Figs 2.1c, 2.3, 2.8, 2.10e, 2.6g, 2.S5c, 2.S9).

References

1. Sulston, J. and J. Hodgkin, *Methods*, in *The Nematode Caenorhabditis elegans*, W.B. Wood, Editor. 1988, Cold Spring Harbor Laboratory: Cold Spring Harbor, New York. p. 587-606.

2. De Stasio, E.A. and S. Dorman, *Optimization of ENU mutagenesis of Caenorhabditis elegans.* Mutat Res, 2001. **495**(1-2): p. 81-8.

3. Bosu, D.R., et al., *C. elegans CAND-1 regulates cullin neddylation, cell proliferation and morphogenesis in specific tissues.* Dev Biol, 2010. **346**(1): p. 113-26.

4. Davis, M.W., et al., *Rapid single nucleotide polymorphism mapping in C. elegans.* BMC Genomics, 2005. **6**: p. 118.

5. Schuster, E., et al., *DamID in C. elegans reveals longevity-associated targets of DAF-16/FoxO.* Mol Syst Biol, 2010. **6**: p. 399.

6. Tepper, R.G., et al., *PQM-1 complements DAF-16 as a key transcriptional regulator of DAF-2-mediated development and longevity.* Cell, 2013. **154**(3): p. 676-90.

7. Kamath, R.S., et al., *Systematic functional analysis of the Caenorhabditis elegans genome using RNAi.* Nature, 2003. **421**(6920): p. 231-7.

8. Kanazawa, T., et al., *The C. elegans Opa1 homologue EAT-3 is essential for resistance to free radicals.* PLoS Genet, 2008. **4**(2): p. e1000022.

9. Claros, M.G. and P. Vincens, *Computational method to predict mitochondrially imported proteins and their targeting sequences.* Eur J Biochem, 1996. **241**(3): p. 779-86.

10. Alavi, M.V. and N. Fuhrmann, *Dominant optic atrophy, OPA1, and mitochondrial quality control: understanding mitochondrial network dynamics.* Mol Neurodegener, 2013. **8**: p. 32.

11. Kenyon, C., et al., *A C. elegans mutant that lives twice as long as wild type.* Nature, 1993. **366**(6454): p. 461-4.

12. Furuyama, T., et al., *Identification of the differential distribution patterns of mRNAs and consensus binding sequences for mouse DAF-16 homologues.* Biochem J, 2000. **349**(Pt 2): p. 629-34.

13. Gerstein, M.B., et al., *Integrative analysis of the Caenorhabditis elegans genome by the modENCODE project.* Science, 2010. **330**(6012): p. 1775-87.

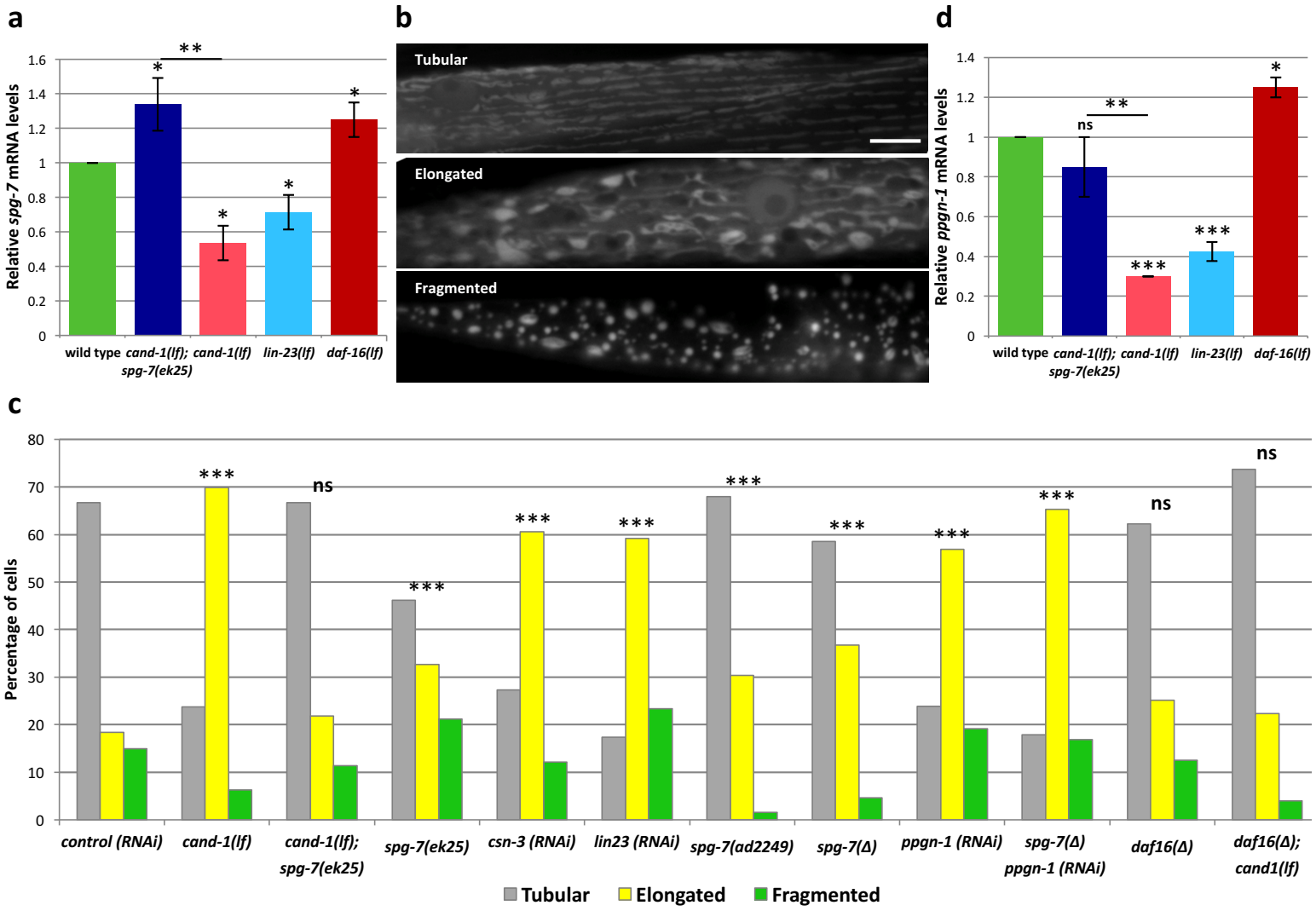
a
Relative spg-7 mRNA levels
wild type
cand-1(lf); spg-7(ek25)
cand-1(lf)
lin-23(lf)
daf-16(lf)
b
Tubular
Elongated
Fragmented
d
Relative ppgn-1 mRNA levels
ns
c
Percentage of cells
control (RNAi)
cand-1(lf)
cand-1(lf); spg-7(ek25)
spg-7(ek25)
csn-3 (RNAi)
lin23 (RNAi)
spg-7(ad2249)
spg-7(Δ)
ppgn-1 (RNAi)
spg-7(Δ) ppgn-1 (RNAi)
daf16(Δ)
daf16(Δ); cand1(lf)
Tubular
Elongated
Fragmented

Figure 2.1. CAND-1 and SCF^{LIN-23} promote the expression of the m-AAA protease genes *spg-7* and *ppgn-1* to regulate mitochondrial morphology.

(**a**) Real-time PCR quantification of *spg-7* mRNA levels in adults of the indicated genotypes, normalized to control *rpl-19* (ribosomal protein L19) mRNA. Error bars denote standard error of the mean (SEM). (**b**) Images of tubular, elongated, and fragmented mitochondria visualized by mitochondria-targeted GFP expressed in body wall muscle cells. Scale bar, 10 µm. (**c**) The percentages of muscle cells with tubular, elongated, and fragmented mitochondria for the indicated genotypes and RNAi treatments. Mitochondrial morphology was scored blinded. (**d**) Real-time PCR quantification of *ppgn-1* mRNA levels normalized to control *rpl-19* mRNA in adults of the indicated genotypes. Error bars denote standard error of the mean (SEM). For all figures, asterisks above bars denote *P*-value comparisons to wild type/controls; asterisks above lines denote comparisons under the lines: **P*<0.05; ***P*<0.01; ****P*<0.001; ns = not significant. Statistical tests are described in the Supplemental Methods.

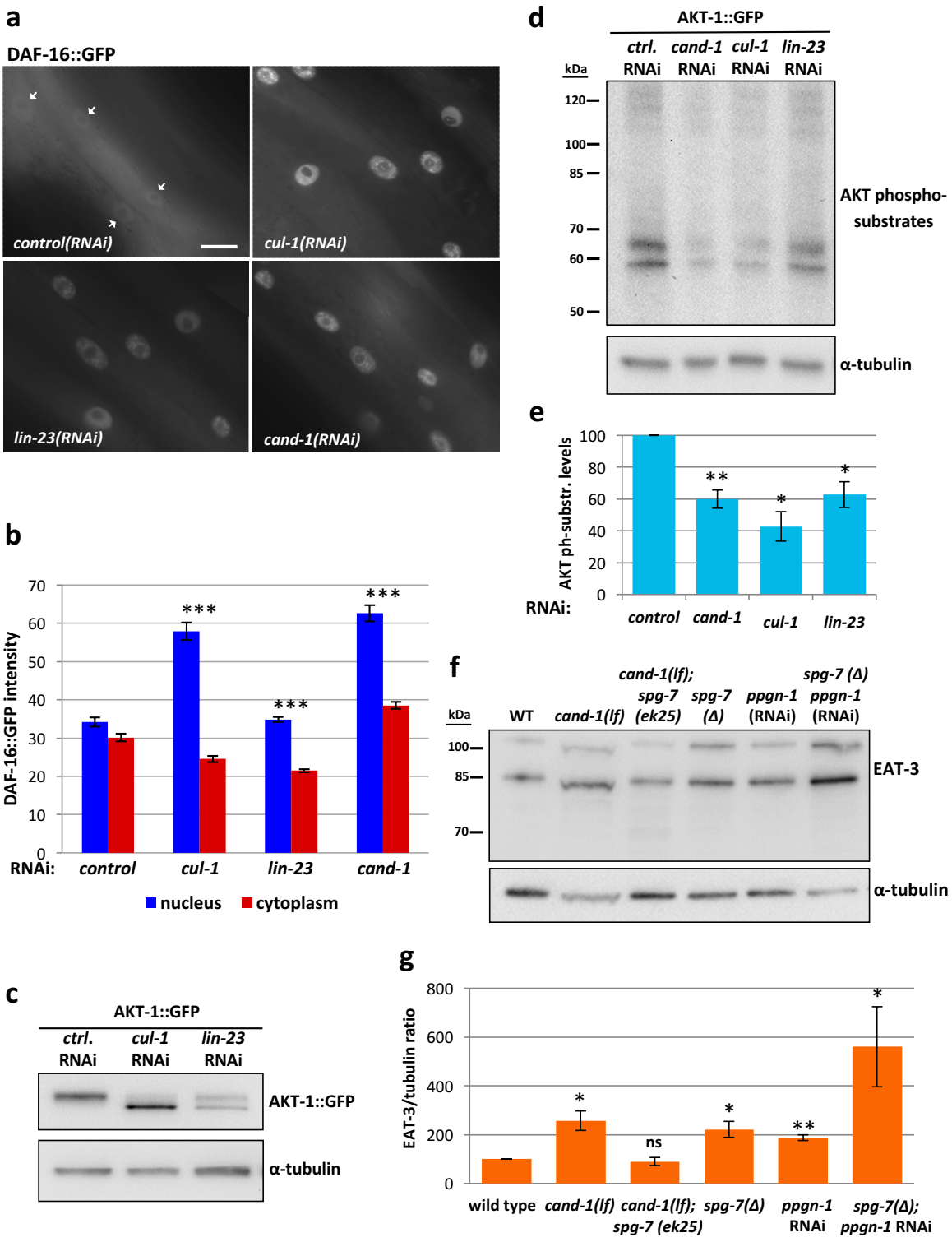
a
DAF-16::GFP
control(RNAi)
cul-1(RNAi)
lin-23(RNAi)
cand-1(RNAi)
b
DAF-16::GFP intensity
RNAi: control cul-1 lin-23 cand-1
nucleus
cytoplasm
c
AKT-1::GFP
ctrl. RNAi
cul-1 RNAi
lin-23 RNAi
AKT-1::GFP
α-tubulin
d
AKT-1::GFP
ctrl. RNAi
cand-1 RNAi
cul-1 RNAi
lin-23 RNAi
kDa
AKT phospho-substrates
α-tubulin
e
AKT ph-substr. levels
RNAi: control cand-1 cul-1 lin-23
f
WT
cand-1(lf)
cand-1(lf); spg-7 (ek25)
spg-7 (Δ)
ppgn-1 (RNAi)
spg-7 (Δ) ppgn-1 (RNAi)
kDa
EAT-3
α-tubulin
g
EAT-3/tubulin ratio
wild type
cand-1(lf)
cand-1(lf); spg-7 (ek25)
spg-7(Δ)
ppgn-1 RNAi
spg-7(Δ); ppgn-1 RNAi
ns

Figure 2.2. CAND-1 and SCF^{LIN-23} activate AKT-1 to inhibit DAF-16 nuclear localization and inhibit EAT-3 levels.

(**a**) DAF-16::GFP nuclear localization in body wall muscle cells for animals with the indicated RNAi treatments. White arrows indicate nuclei in the control RNAi image. Scale bar, 10 μm. (**b**) Quantification of the mean level of nuclear and cytoplasmic DAF-16::GFP intensity in body wall muscle cells. Error bars denote SEM. (**c**) Western blot with anti-GFP antibody showing the altered mobility of AKT-1::GFP on SDS-PAGE in animals treated with *cul-1* and *lin-23* RNAi. (**d**) Western blot showing staining for an antibody that recognizes AKT phospho-substrates in animals expressing AKT-1::GFP and subjected to the indicated RNAi treatments. (**e**) Graph showing the levels of AKT phospho-substrate signal relative to α-tubulin from three to four biological replicates. (**f**) Western blot showing EAT-3 protein levels in the indicated genotypes and RNAi treatments. The expected molecular weights of the L- and S-isoforms of EAT-3 are 110.1 and 85.5-86.4 kDa, respectively (see Supplementary Information). (**g**) Quantification of EAT-3 levels normalized to α-tubulin from two to four biological replicates; error bars denote SEM.

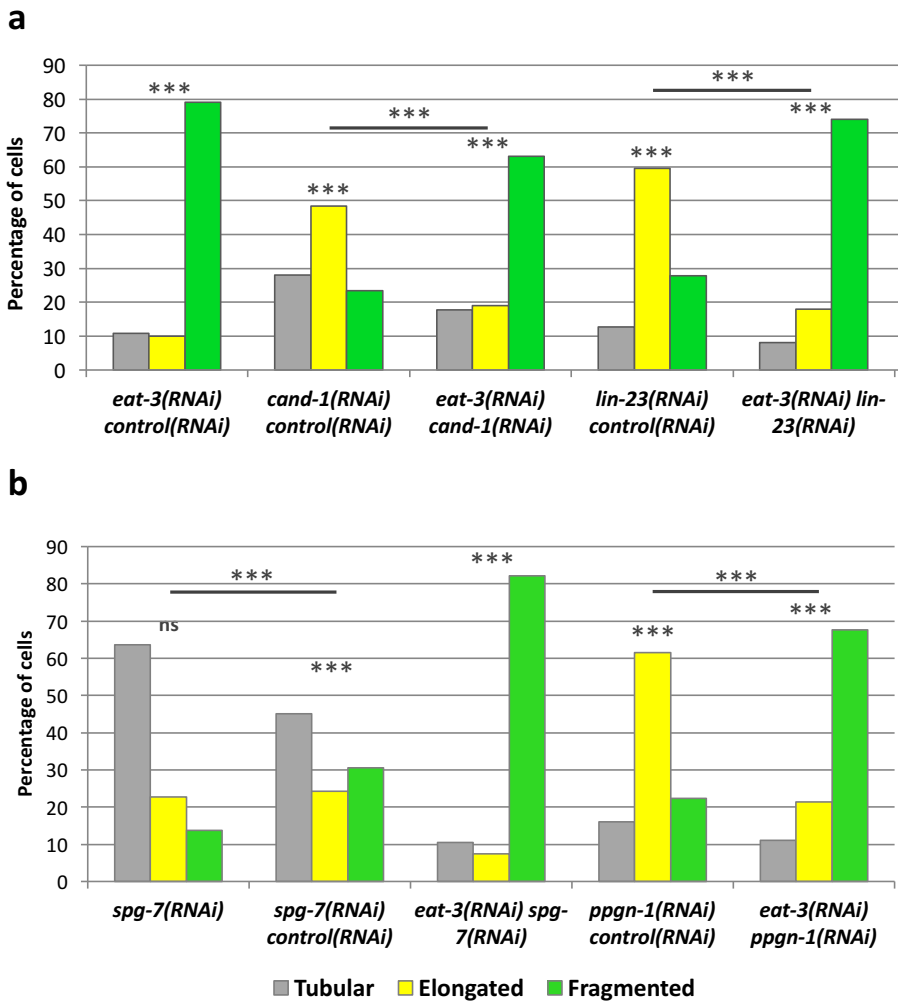

Figure 2.3. Mitochondrial morphology in *C. elegans* body wall muscles.

(**a**, **b**) The percentages of muscle cells with predominantly tubular, elongated, or fragmented mitochondria in adult hermaphrodites of the indicated RNAi treatments visualized by mitochondria-targeted GFP expressed in body wall muscle cells. Mitochondrial morphology was scored blinded. Statistical significance was determined with the chi-square test.

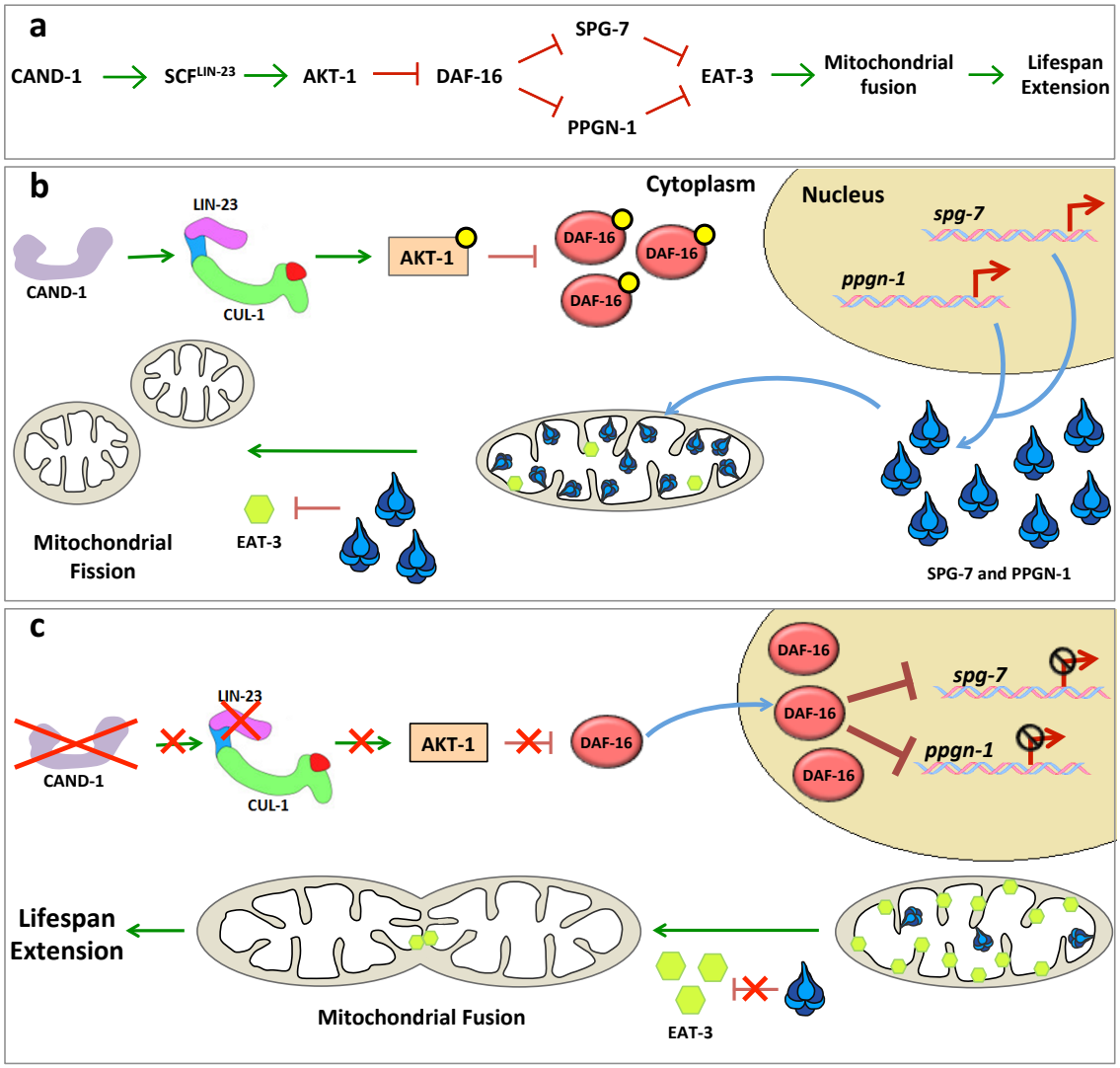

Figure 2.4. Model for regulation of mitochondrial fusion.

(**a**), Proposed linear pathway for CAND-1 and SCF^{LIN-23} regulation of mitochondrial fusion; see text for description. (**b**) and (**c**), Schematic of the proposed intracellular pathway regulating mitochondrial fusion and lifespan extension in the presence (**b**) or absence (**c**) of CAND-1.

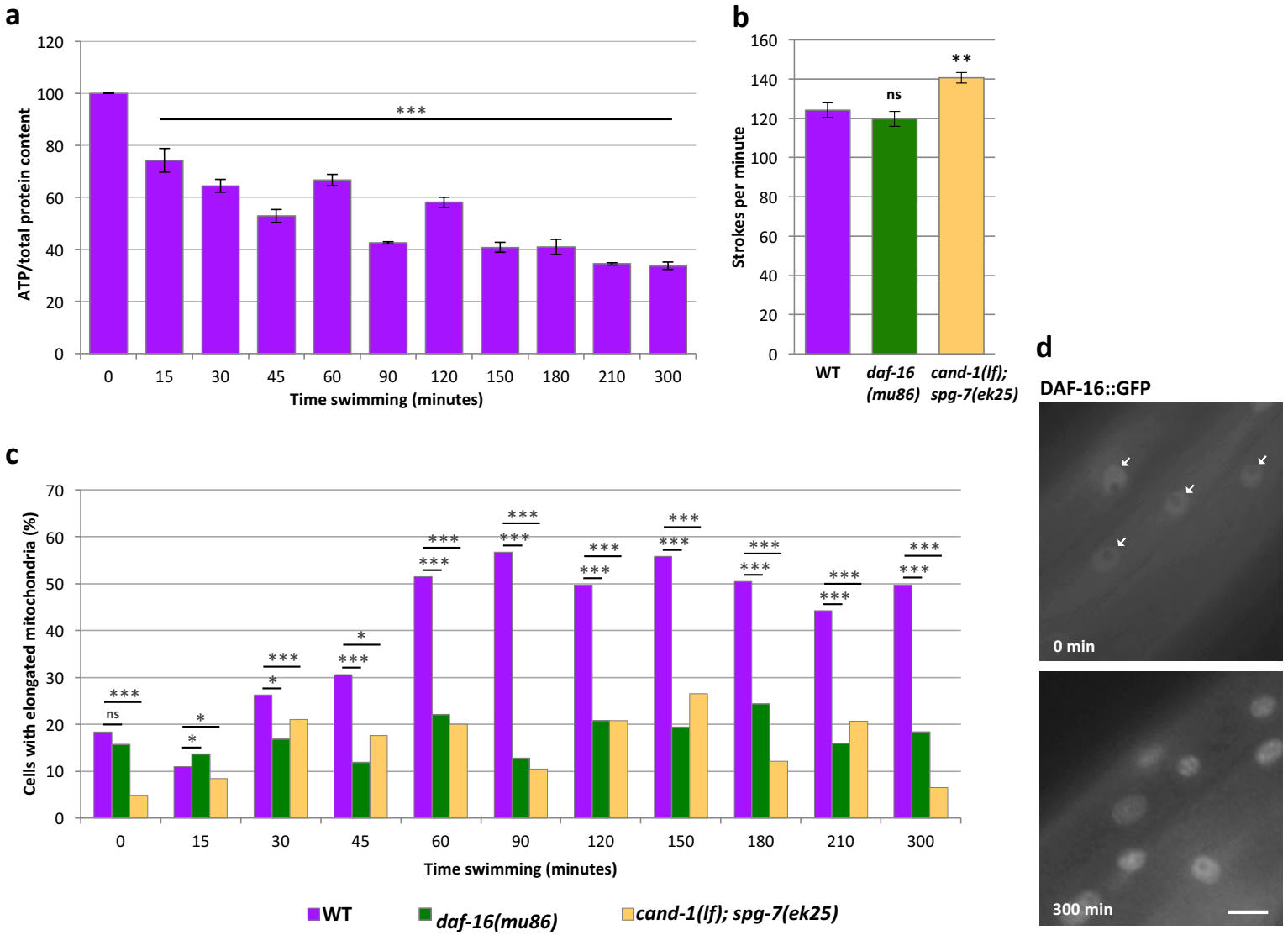
a
ATP/total protein content
Time swimming (minutes)
***
b
Strokes per minute
WT
daf-16 (mu86)
cand-1(lf); spg-7(ek25)
ns
**
c
Cells with elongated mitochondria (%)
Time swimming (minutes)
WT
daf-16(mu86)
cand-1(lf); spg-7(ek25)
d
DAF-16::GFP
0 min
300 min

Figure 2.5. DAF-16 is required for physical exertion-induced mitochondrial fusion.

(**a**) ATP levels decrease during swimming. Graph of ATP levels (normalized to whole-animal protein levels) at the indicated times of continuous swimming. (**b**) Average swim strokes-per-minute for the indicated genotypes upon induction of swimming behavior. (**c**) The percentages of muscle cells with elongated mitochondria in wild type, *daf-16(mu86)*, and *cand-1(tm1683); spg-7(ek25)* animals for the indicated times post-induction of swimming behavior. Full distributions of mitochondrial morphology are shown in Fig. S9. (**d**) DAF-16::GFP nuclear localization in body wall muscle cells for animals at 0 min and 300 min post-induction of swimming behavior. White arrows indicate nuclei in the 0 min image. Scale bar, 10 μm.

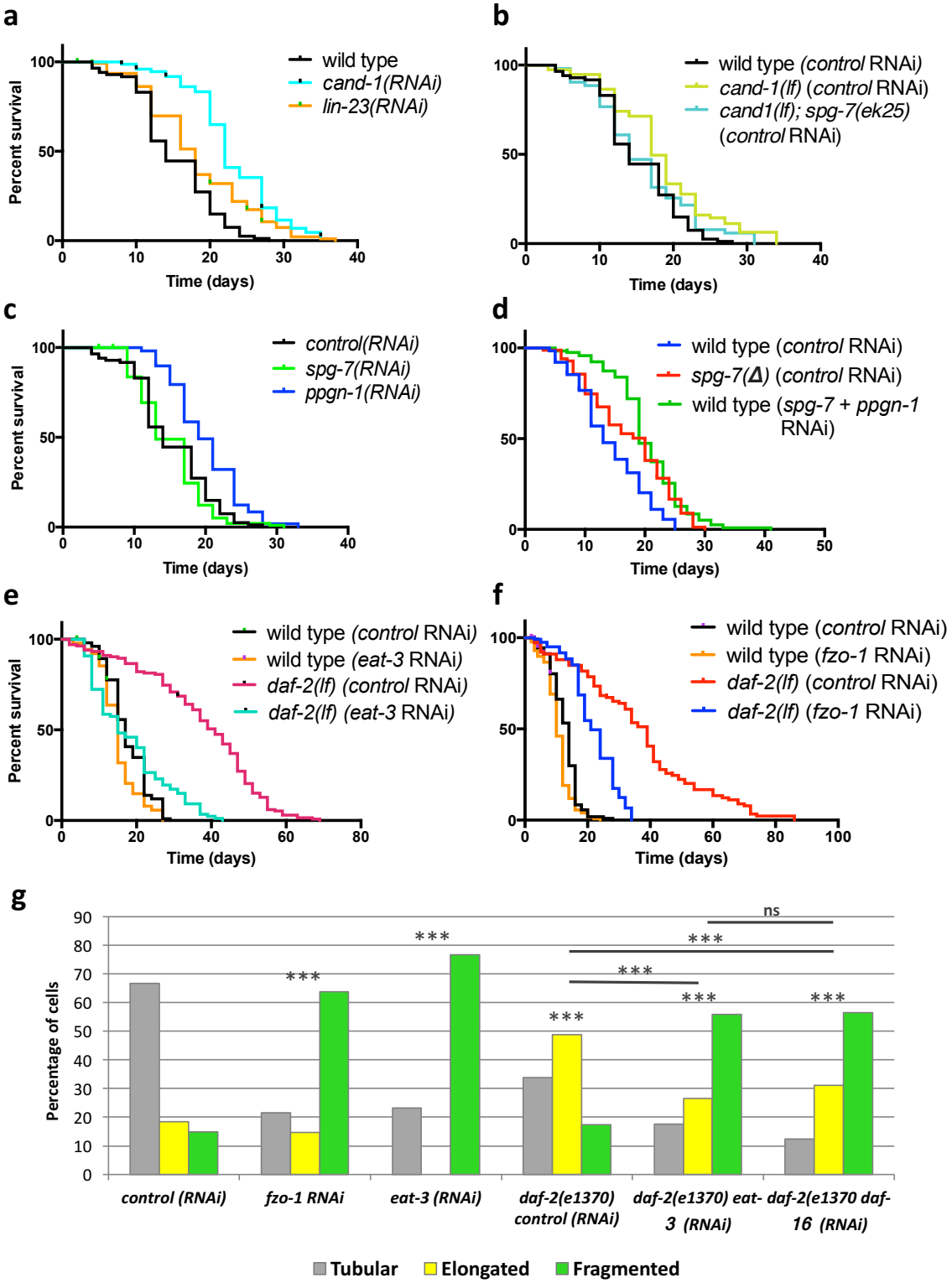
a
Percent survival
Time (days)
wild type
cand-1(RNAi)
lin-23(RNAi)
b
Time (days)
wild type (control RNAi)
cand-1(lf) (control RNAi)
cand1(lf); spg-7(ek25) (control RNAi)
c
Percent survival
Time (days)
control(RNAi)
spg-7(RNAi)
ppgn-1(RNAi)
d
Time (days)
wild type (control RNAi)
spg-7(Δ) (control RNAi)
wild type (spg-7 + ppgn-1 RNAi)
e
Percent survival
Time (days)
wild type (control RNAi)
wild type (eat-3 RNAi)
daf-2(lf) (control RNAi)
daf-2(lf) (eat-3 RNAi)
f
Time (days)
wild type (control RNAi)
wild type (fzo-1 RNAi)
daf-2(lf) (control RNAi)
daf-2(lf) (fzo-1 RNAi)
g
Percentage of cells
ns
***
control (RNAi)
fzo-1 RNAi
eat-3 (RNAi)
daf-2(e1370) control (RNAi)
daf-2(e1370) eat-3 (RNAi)
daf-2(e1370 daf-16 (RNAi)
Tubular
Elongated
Fragmented

Figure 2.6. Inactivating mitochondrial fusion pathway components that increase mitochondrial elongation extends lifespans.

(**a**-**e**) Survival curves for adults of the indicated RNAi treatments. The wild-type survival curves for (**a**-**c**) were analyzed at the same time and are shown in each panel for comparison. RNAi depletions of *lin-23* (**a**), *cand-1* (**a**), *ppgn-1* (**c**) and *spg-7* + *ppgn-1* (**d**) significantly increased mean lifespan. (**b**) *cand-1* mutants and *spg-7(tm2312)* mutants (**d**) had increased mean lifespan relative to wild type, while *cand-1*; *spg-7(ek25)* (**c**) animals had lifespan comparable to wild type. (**e, f**) *eat-3* RNAi (**e**) and *fzo-1* RNAi (f) depletions significantly decreased the mean lifespan of *daf-2(e1370)* mutants. See Table 2.S2 for statistics. (**g**) The percentages of muscle cells with predominantly tubular, elongated, or fragmented mitochondria in adult hermaphrodites of the indicated genotypes/RNAi treatments visualized by mitochondria-targeted GFP expression in body wall muscle cells. Mitochondrial morphology was scored blinded. The wild-type control from Fig. 1c was analyzed at the same time and is shown here for comparison. Statistical significance was determined with the chi-square test.

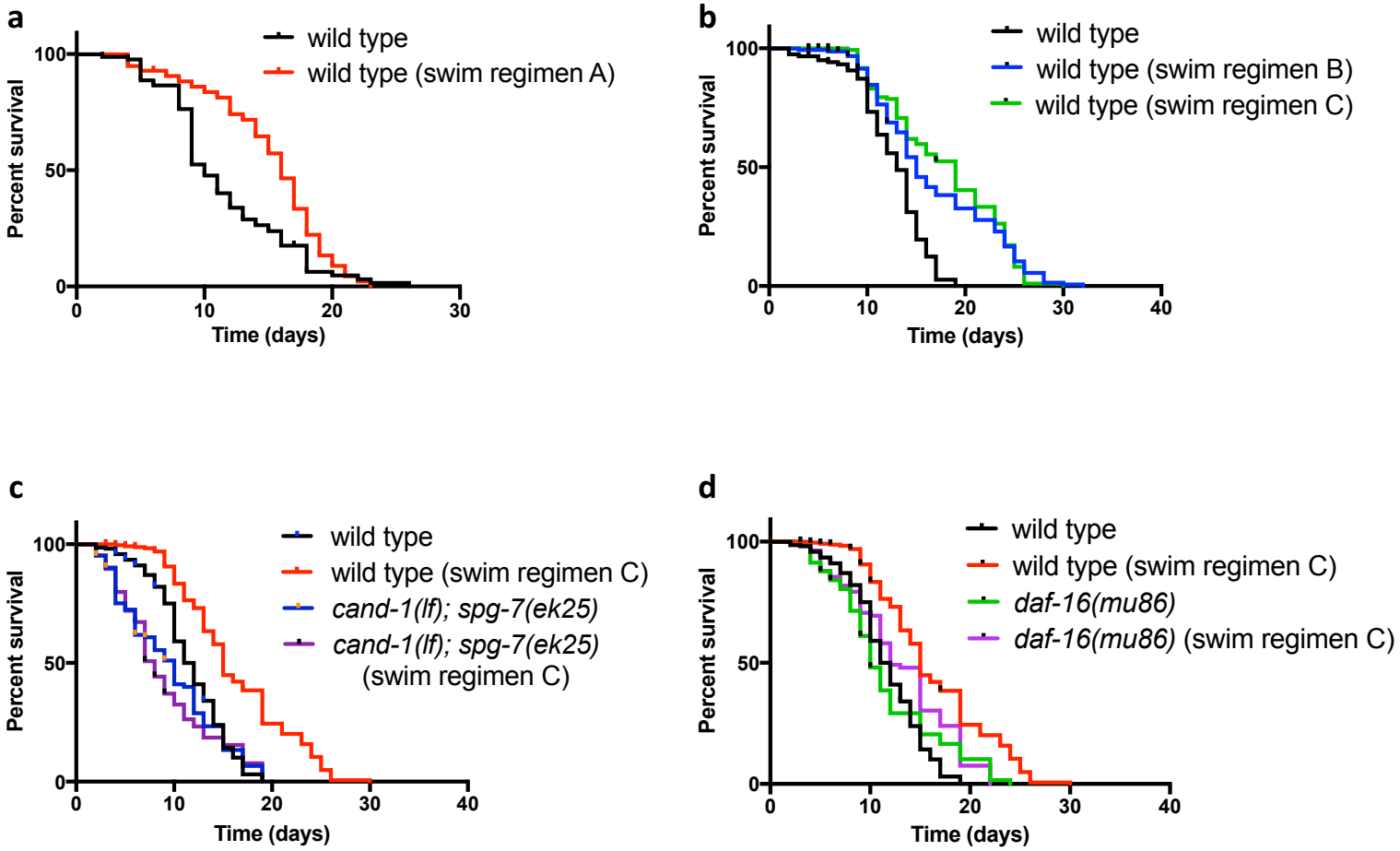
a
wild type
wild type (swim regimen A)
Percent survival
Time (days)
b
wild type
wild type (swim regimen B)
wild type (swim regimen C)
Percent survival
Time (days)
c
wild type
wild type (swim regimen C)
cand-1(lf); spg-7(ek25)
cand-1(lf); spg-7(ek25)
(swim regimen C)
Percent survival
Time (days)
d
wild type
wild type (swim regimen C)
daf-16(mu86)
daf-16(mu86) (swim regimen C)
Percent survival
Time (days)

Figure 2.7. Physical exercise in *C. elegans* extends lifespan in a process that is dependent on components of the mitochondrial fusion pathway.

(**a-d**) Survival curves for adults that were kept continuously on agar plates or removed from the plates for brief periods for the described swim regimens. (**a**) Comparison of wild type kept on agar plates continuously or subject to swim regimen A (30 min of swimming per day). (**b**) Test of swim regimens B and C. Swim regimen B was the following swimming times/day on the listed days: 30 min on days 1-5; 25 min on days 6 and 7; 20 min on days 8 and 9; 15 min on day 10; 10 min on day 11; and 5 min on day 12. Swim regimen C was 30 min of swimming on day 1, followed by a reduction in swim time of 2 min/day on subsequent days. (**c**, **d**) Test of swim regimen C with wild type, *cand-1(tm1683)*; *ek25* (**c**), or *daf-16(mu86)* (**d**). The wild-type control and wild-type swim regimen C survival curves were analyzed at the same time and are shown in (**c**) and (**d**) for comparison. All swimming regimens significantly increased the mean lifespan of wild type (**a-d**). Swim regimen C did not increase the mean lifespan of *cand-1(tm1683); ek25* (**c**) or *daf-16(mu86)* mutants (**d**) relative to the control, non-swimming condition. See Table 2.S3 for statistics.

a

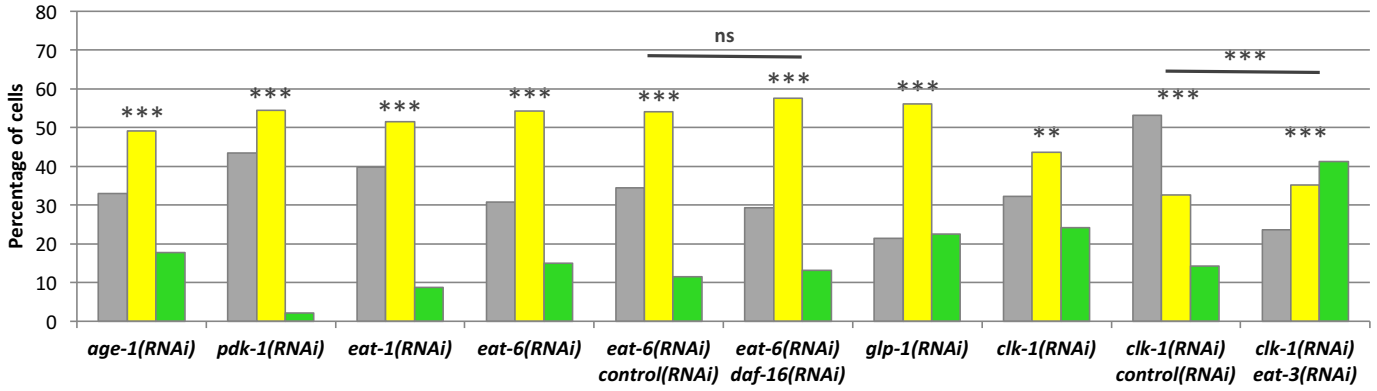
Percentage of cells
80
70
60
50
40
30
20
10
0
ns
***
**
age-1(RNAi)
pdk-1(RNAi)
eat-1(RNAi)
eat-6(RNAi)
eat-6(RNAi) control(RNAi)
eat-6(RNAi) daf-16(RNAi)
glp-1(RNAi)
clk-1(RNAi)
clk-1(RNAi) control(RNAi)
clk-1(RNAi) eat-3(RNAi)

b

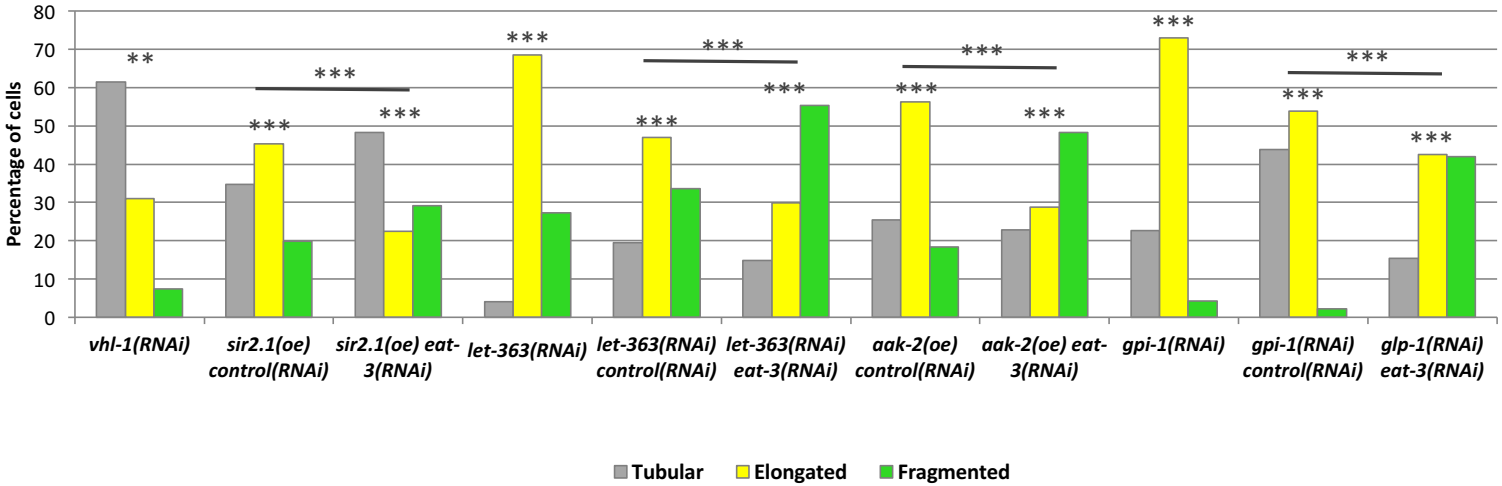
Percentage of cells
80
70
60
50
40
30
20
10
0
**
***
vhl-1(RNAi)
sir2.1(oe) control(RNAi)
sir2.1(oe) eat-3(RNAi)
let-363(RNAi)
let-363(RNAi) control(RNAi)
let-363(RNAi) eat-3(RNAi)
aak-2(oe) control(RNAi)
aak-2(oe) eat-3(RNAi)
gpi-1(RNAi)
gpi-1(RNAi) control(RNAi)
glp-1(RNAi) eat-3(RNAi)
Tubular
Elongated
Fragmented

Figure 2.8. Diverse life extension pathways have increased levels of elongated mitochondria.

(**a-c**) The percentages of body wall muscle cells with tubular, elongated, and fragmented mitochondria in the indicated genotypes, over-expression (oe), and RNAi-treatments.

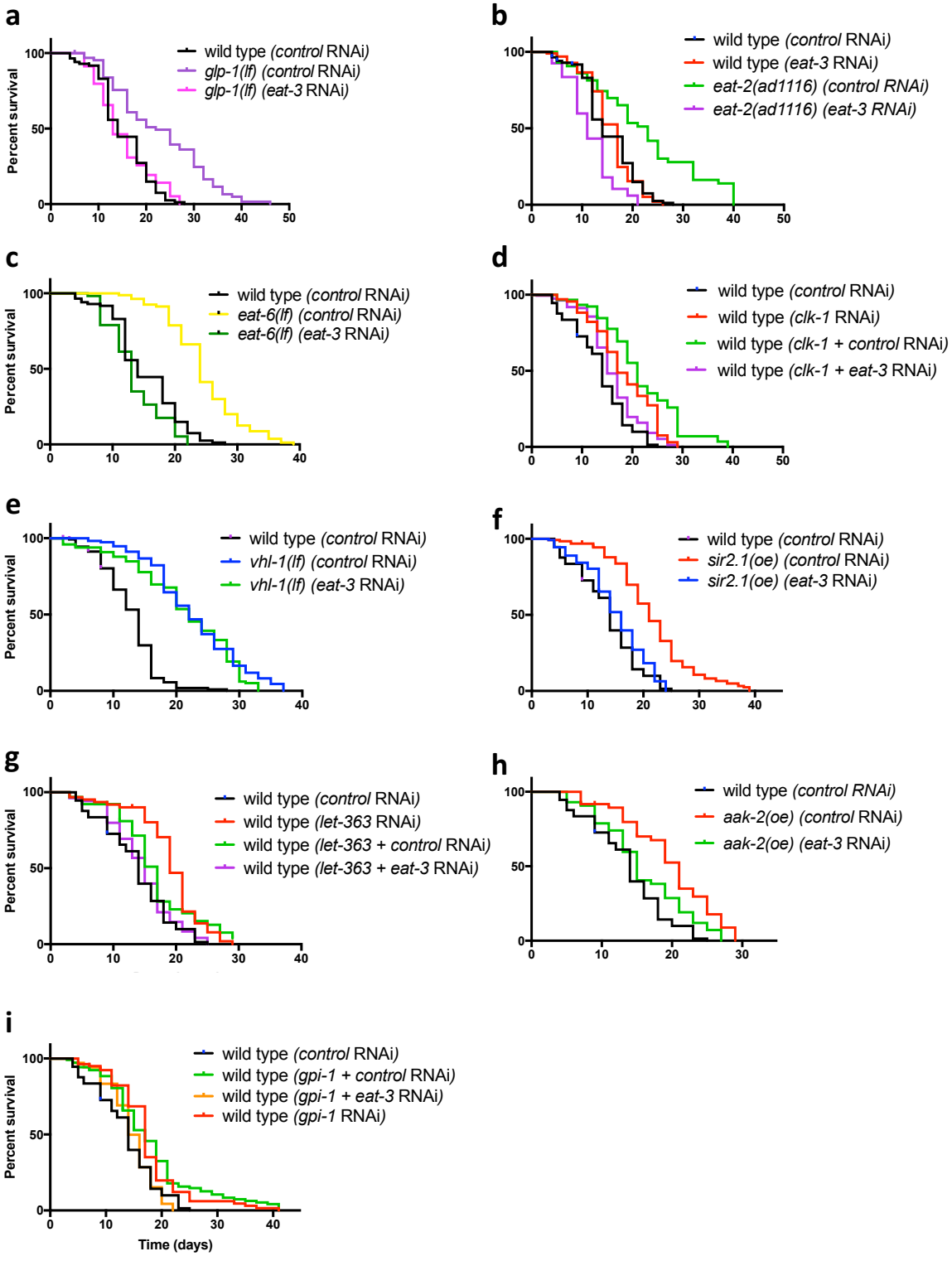
a
Percent survival
wild type (control RNAi)
glp-1(lf) (control RNAi)
glp-1(lf) (eat-3 RNAi)
b
wild type (control RNAi)
wild type (eat-3 RNAi)
eat-2(ad1116) (control RNAi)
eat-2(ad1116) (eat-3 RNAi)
c
Percent survival
wild type (control RNAi)
eat-6(lf) (control RNAi)
eat-6(lf) (eat-3 RNAi)
d
wild type (control RNAi)
wild type (clk-1 RNAi)
wild type (clk-1 + control RNAi)
wild type (clk-1 + eat-3 RNAi)
e
Percent survival
wild type (control RNAi)
vhl-1(lf) (control RNAi)
vhl-1(lf) (eat-3 RNAi)
f
wild type (control RNAi)
sir2.1(oe) (control RNAi)
sir2.1(oe) (eat-3 RNAi)
g
Percent survival
wild type (control RNAi)
wild type (let-363 RNAi)
wild type (let-363 + control RNAi)
wild type (let-363 + eat-3 RNAi)
h
wild type (control RNAi)
aak-2(oe) (control RNAi)
aak-2(oe) (eat-3 RNAi)
i
Percent survival
wild type (control RNAi)
wild type (gpi-1 + control RNAi)
wild type (gpi-1 + eat-3 RNAi)
wild type (gpi-1 RNAi)
Time (days)

Figure 2.9. Increased mitochondrial elongation is required for longevity in diverse lifespan extension mutants.

(**a**-**i**) Survival curves for adults of the indicated genotypes, over-expressions (oe), and RNAi treatments. The wild-type and *eat-3(RNAi)* survival curves are shown in graphs for comparison. *eat-3* RNAi significantly reduced the extended lifespans relative to control RNAi for all tested genotypes, overexpression, and RNAi treatments except for *vhl-1* mutants (**e**). See Table 2.S2 for statistics

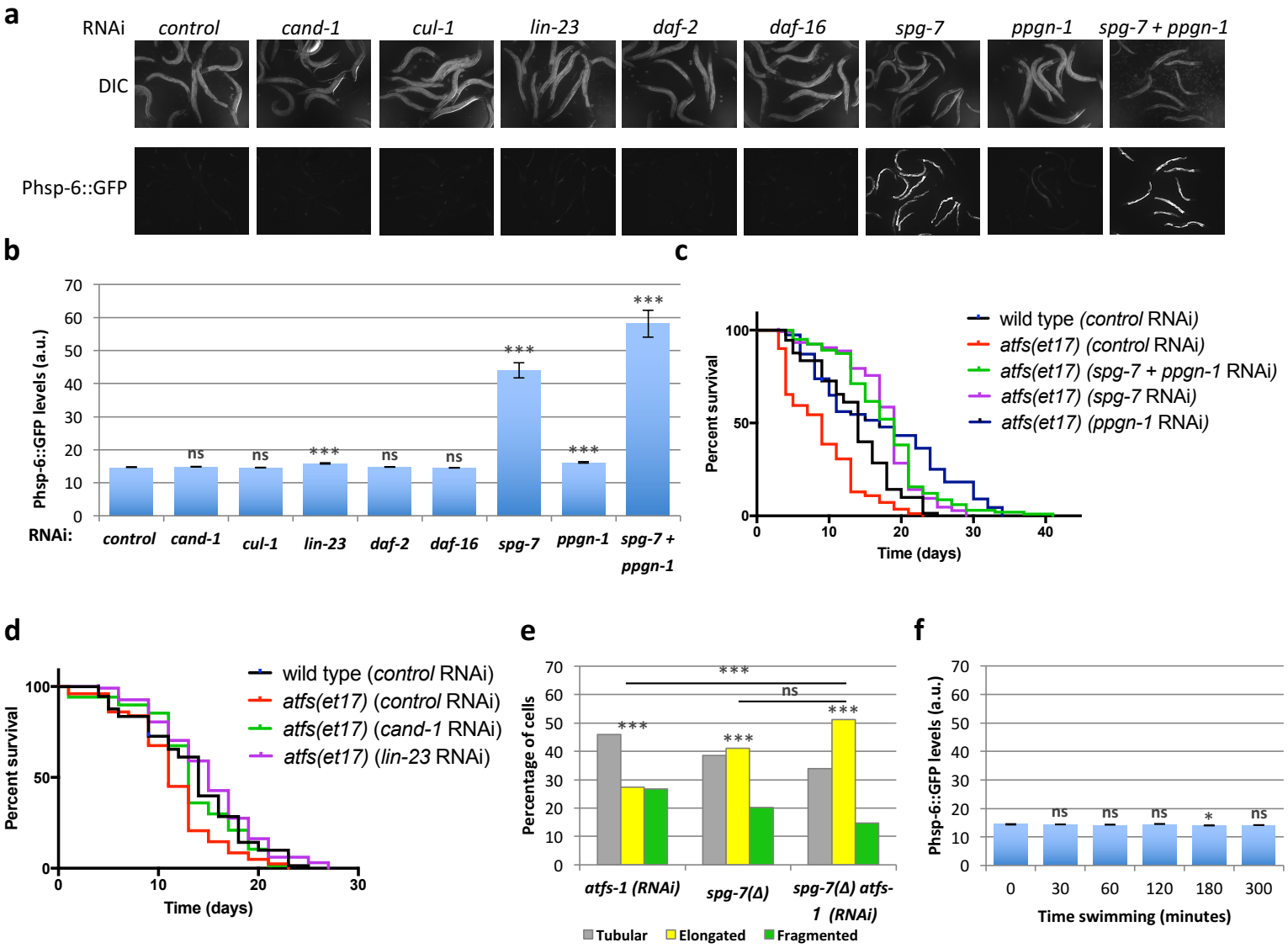
a
RNAi
control
cand-1
cul-1
lin-23
daf-2
daf-16
spg-7
ppgn-1
spg-7 + ppgn-1
DIC
Phsp-6::GFP
b
Phsp-6::GFP levels (a.u.)
RNAi:
control
cand-1
cul-1
lin-23
daf-2
daf-16
spg-7
ppgn-1
spg-7 + ppgn-1
c
Percent survival
Time (days)
wild type (control RNAi)
atfs(et17) (control RNAi)
atfs(et17) (spg-7 + ppgn-1 RNAi)
atfs(et17) (spg-7 RNAi)
atfs(et17) (ppgn-1 RNAi)
d
Percent survival
Time (days)
wild type (control RNAi)
atfs(et17) (control RNAi)
atfs(et17) (cand-1 RNAi)
atfs(et17) (lin-23 RNAi)
e
Percentage of cells
atfs-1 (RNAi)
spg-7(Δ)
spg-7(Δ) atfs-1 (RNAi)
Tubular
Elongated
Fragmented
f
Phsp-6::GFP levels (a.u.)
Time swimming (minutes)

Figure 2.10. The UPR^{mt} is not involved in the mitochondrial fusion pathway.

(**a**) Representative images of the UPR^{mt} marker *Phsp-6*::GFP in L4/young-adult stage animals for the indicated RNAi treatments. (**b**) Quantitation of *Phsp-6*::GFP signal for the RNAi treatments shown in (**a**). (**c**, **d**) Survival curves for *atfs-1(et17)* gain-of-function mutants with the indicated RNAi treatments; the wild-type survival curve is shown in both graphs for comparison. (**e**) The percentages of body wall muscle cells with tubular, elongated, and fragmented mitochondria in the indicated genotypes and RNAi-treatments. (**f**) Quantification of *Phsp-6*::GFP signal for animals swimming for the indicated times. The quantification was performed as for (**b**) and the two graphs can be compared directly. No significant differences in *Phsp-6*::GFP were observed relative to 0 min control animals

a

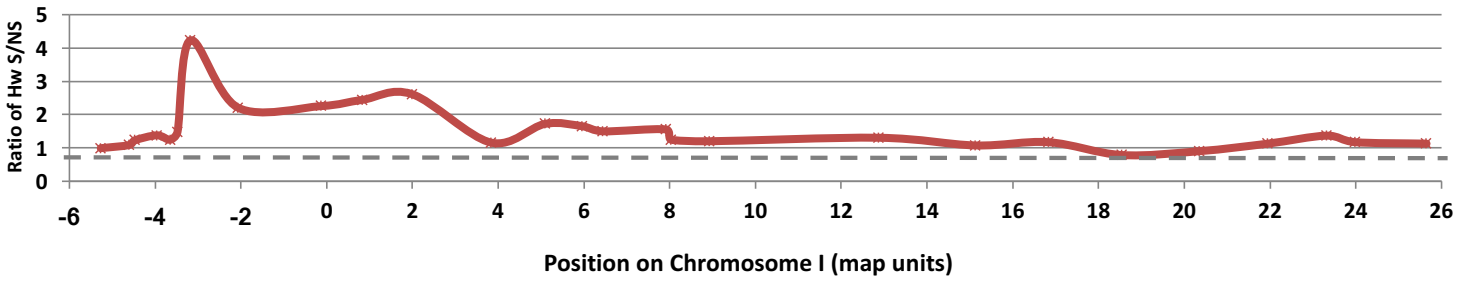

b

Suppressed clones	Characterization of SNPs (listed by genetic map position on Chromosome I)							
	-5.27	-4.61	-4.47	-3.96	-3.18	-2.07	-0.13	+0.83
7	het	Hw	Hw	Hw	Hw	Hw	het	het
9	het	Hw	Hw	Hw	Hw	het	het	het
15	het	Hw	Hw	Hw	Hw	het	het	het
18	het	het	Hw	Hw	Hw	Hw	Hw	Hw
20	het	Hw	Hw	Hw	Hw	Hw	Hw	het
21	het	Hw	Hw	Hw	Hw	Hw	Hw	het
22	het	het	Hw	Hw	Hw	Hw	Hw	het
25	het	het	Hw	Hw	Hw	Hw	Hw	Hw
33	Hw	Hw	Hw	Hw	Hw	het	het	het
35	het	het	het	het	Hw	Hw	Hw	Hw
37	het	het	Hw	Hw	Hw	het	het	het
38	het	het	het	Hw	Hw	het	het	het

Figure 2.S1. Identification of the suppressor region in *cand-1*; *ek25*.

(**a**) Ratio of Hawaiian to Bristol (N2) SNPs in the 'suppressed' (S) vs. 'not-suppressed' (NS) progeny for chromosome I from a cross of Hawaiianized *cand-1*; *ek25* mutant and *cand-1* mutant (N2 background). Note that the Hawaiianized *cand-1*; *ek25* mutation was previously outcrossed 10 times to a Hawaiianized *cand-1* mutant strain. This effectively replaced N2 SNPs in the original *cand-1*; *ek25* mutant strain with Hawaiian SNPs. There is a peak of suppression between SNPs at -3.96 and -2.07, suggesting that the *ek25* suppressor mutation is in this region. (**b**) Clonal analysis of individual 'suppressed' cross progeny for region -5.27 to +0.83 on chromosome I. SNPs for each progeny clone are marked as heterozygous for Hawaiian and N2 SNPs (het, yellow) or homozygous for Hawaiian SNPs (Hw, green).

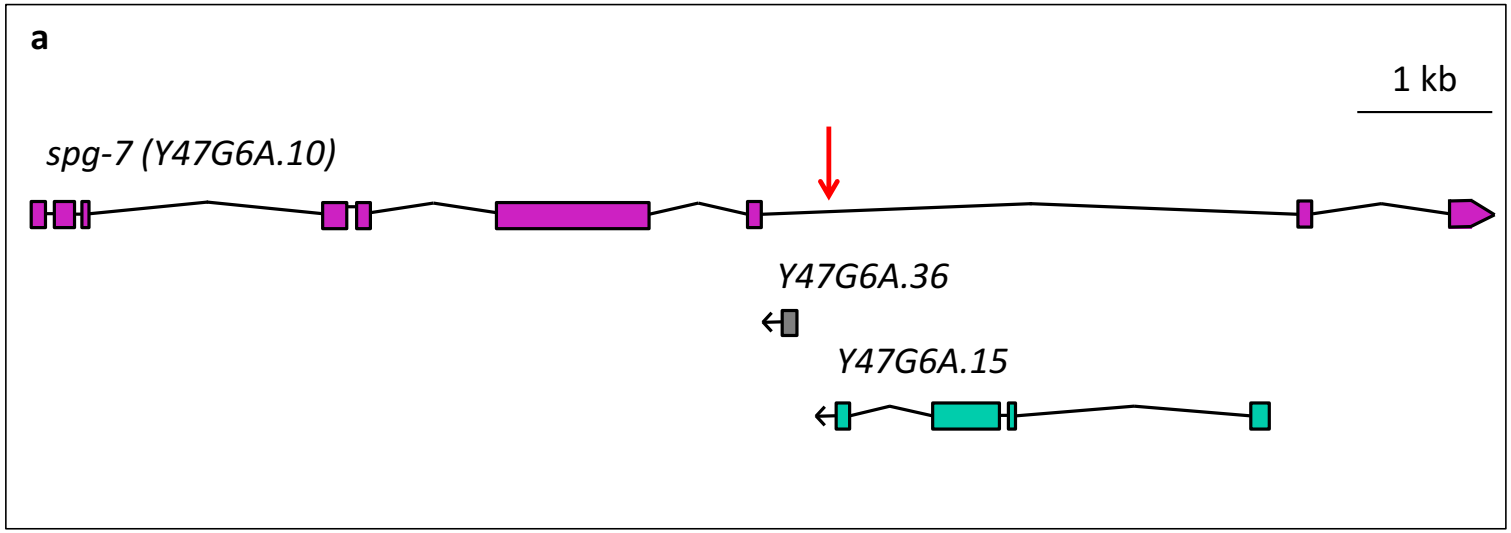

b

Chromosome I: 3,472,973 – 3,473,104

```
                  TaTTTAg  GaAAACA                                    aTAAAtt
ek25    GAAACCATTTATTTAGAAGAAAACAGAAAAAGAATAAGATGAAAAGAATAGGACAAATAAATTAGA
-       ||||||||||||||||||||||||||||||||||||||||||||||||||||||||||||||||||
wild type -GAAACCATTTATTTAGAAGAAAACAGAAAAAGAATAAGATGAAAAGAATAGGACAAATAAATTAGA

            aaAAACA       G                                 AxgCA      aTAAAta
ek25    TTGAAAAACAAAGAATGTAGGCATGCCTACCTAGGCAGGCAGGCAGGCACTCGAATAAATAGCTTA
-       ||||||||||||||||||||||||||||||||||||||||||||||||||||||||||||||||||
wild type -TTGAAAAACAAAGAATGT                                AGGCACTCGAATAAATAGCTTA
```

Figure 2.S2. The location of the *cand-1*; *ek25* suppressor mutation.

(**a**) Schematic of the region of chromosome I containing the genes *spg-7* (encoding an m-AAA protease), *Y47G6A.15* (encoding a non-conserved protein), and the non-conserved, non-coding RNA *Y47G6A.36*. The location of the *ek25* mutation is marked by a red arrow. (**b**) The *ek-25* allele is a 26 bp insertion (shown in red lettering) that disrupts a predicted DAF-16-binding element (DBE) (highlighted in yellow). This region contains six sequences that differ from the DBE consensus (GTAAACA and TGTTTAC) by one or more nucleotides, with the alternate nucleotide generally the second most abundant nucleotide for the consensus position[6,12]. The DBE matches are highlighted in yellow and listed above the sequence with the dominant nucleotide for a consensus position in upper case, the second most abundant nucleotide in lower case, and nucleotides that do not match the consensus marked by an 'x'. The sequence highlighted in blue was identified as a DAF-16::GFP-bound sequence by ChIP[13].

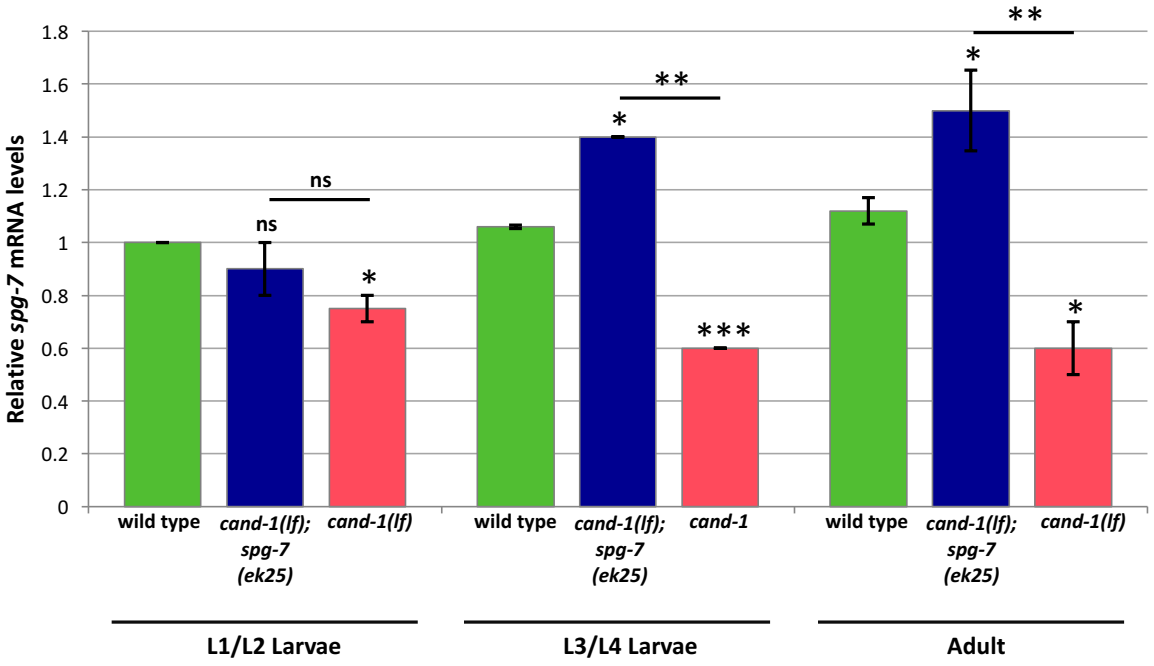

Figure 2.S3. Real-time quantitative PCR of *spg-7* mRNA levels in larval and adult stages.

RT-qPCR quantification of *spg-7* mRNA levels normalized to *rpl-19* control mRNA for L1/L2-stage larvae, L3/L4-stage larvae, and adults of the indicated genotypes. The mRNA levels are reported in arbitrary units with the wild-type level for L1/L2 larvae set to 1.0. For all supplementary figures, asterisks above bars denote *P*-values for comparisons to wild type/controls; asterisks above lines denote comparisons under the lines: **P*<0.05; ***P*<0.01; ****P*<0.001; ns = not significant. The type of statistical test (Student's t-test or chi-square) used for each experimental approach is described in the Supplemental Methods section. Error bars denote SEM.

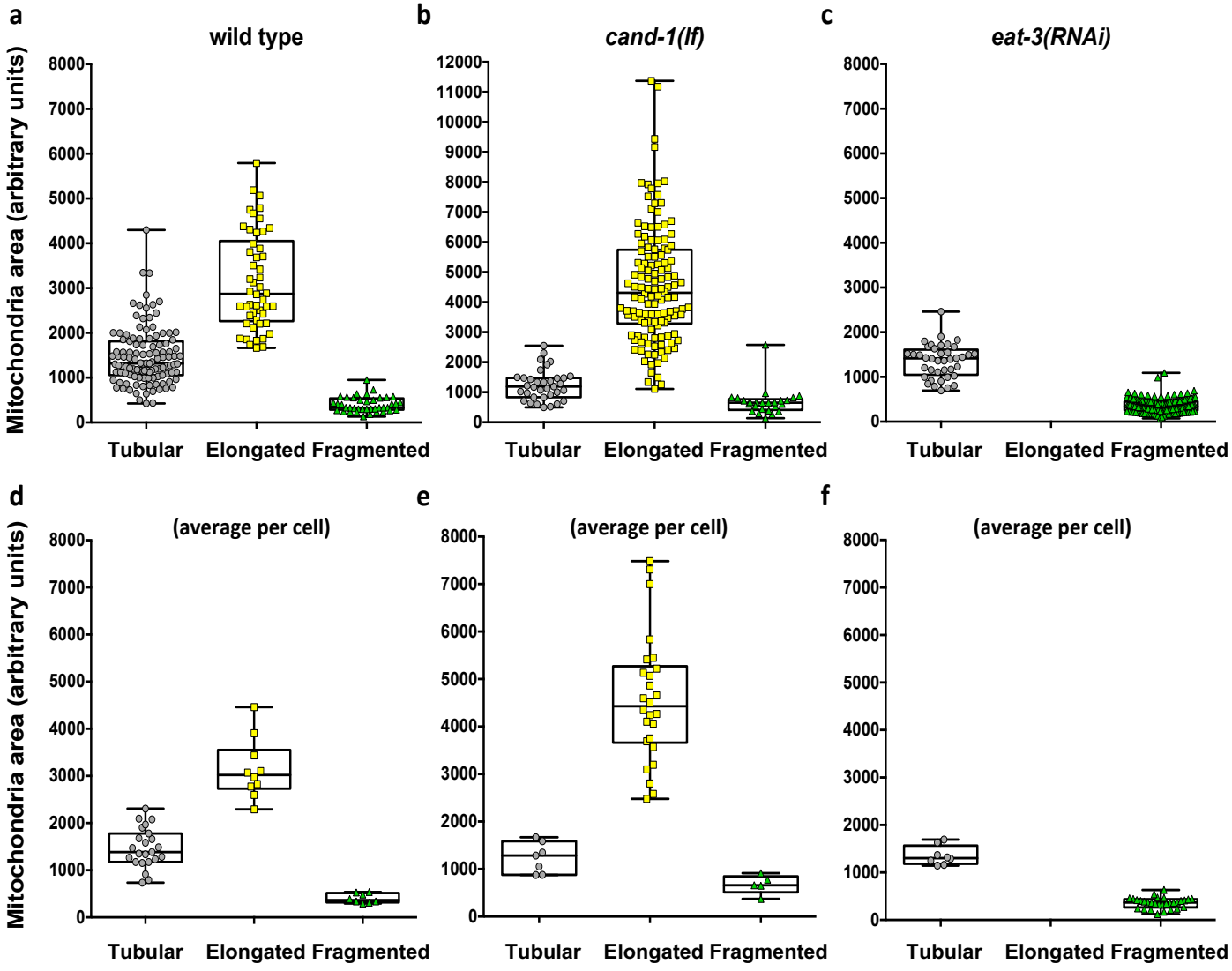
a
wild type
b
cand-1(lf)
c
eat-3(RNAi)
Mitochondria area (arbitrary units)
Tubular
Elongated
Fragmented
d
(average per cell)
e
(average per cell)
f
(average per cell)

Figure 2.S4. Quantification of mitochondrial areas in tubular, elongated, and fragmented mitochondria.

(**a**-**c**) Scatter plot of the areas of the five largest mitochondria per cell in micrographs of ~40 body wall muscle cells per genotype visualized by mitochondria-targeted GFP expression for wild type (**a**), *cand-1(lf)* (**b**), and *eat-3(RNAi)* (**c**). Note that the categorization of cell mitochondria as tubular, elongated, or fragmented correlates with the areas of the mitochondria in these cells. (**d**-**f**) Scatter plot of the averages of the areas of the five largest mitochondria per body wall muscle cell for wild type (**d**), *cand-1(lf)* (**e**), and *eat-3(RNAi)* (**f**). Boxes represent the SEM range with the mean denoted by a central horizontal line; vertical lines extending above and below the box denote the range. Within each genotype, the tubular, elongated, and fragmented distributions are statistically different; $P < 0.0001$ using Student's t-test.

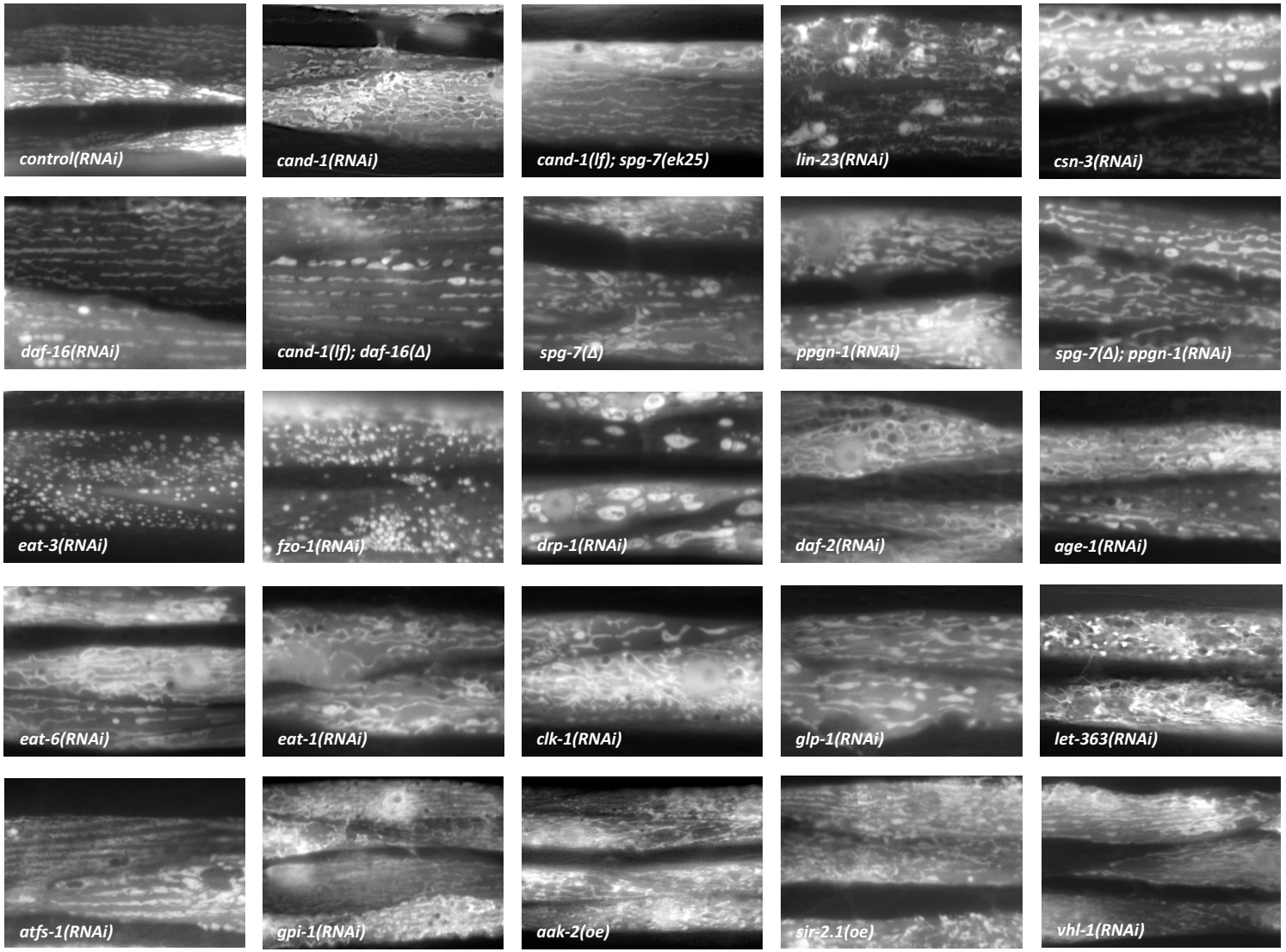
control(RNAi)
cand-1(RNAi)
cand-1(lf); spg-7(ek25)
lin-23(RNAi)
csn-3(RNAi)
daf-16(RNAi)
cand-1(lf); daf-16(Δ)
spg-7(Δ)
ppgn-1(RNAi)
spg-7(Δ); ppgn-1(RNAi)
eat-3(RNAi)
fzo-1(RNAi)
drp-1(RNAi)
daf-2(RNAi)
age-1(RNAi)
eat-6(RNAi)
eat-1(RNAi)
clk-1(RNAi)
glp-1(RNAi)
let-363(RNAi)
atfs-1(RNAi)
gpi-1(RNAi)
aak-2(oe)
sir-2.1(oe)
vhl-1(RNAi)

Figure 2.S5. Images of mitochondrial morphologies.

Representative images of mitochondria-targeted GFP in body wall muscles of the indicated mutants, overexpression strains, or RNAi-treated animals. Scale bar, 10 μm.

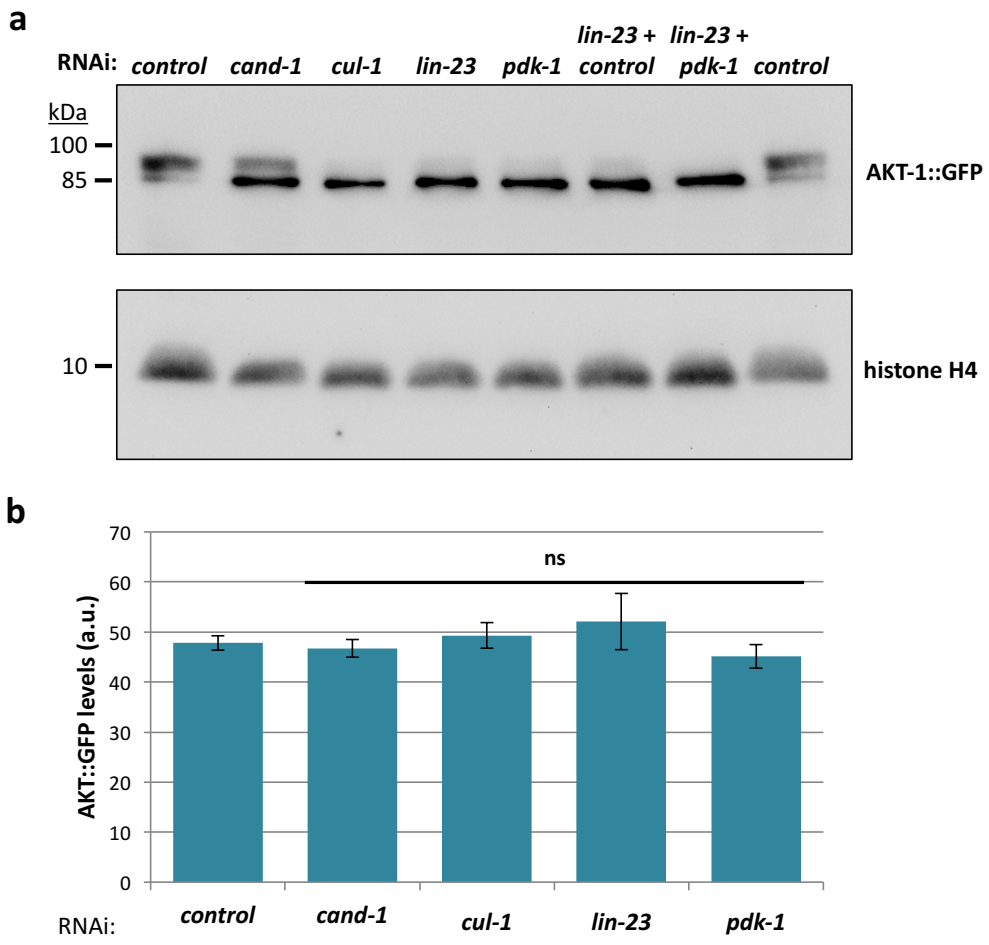

Figure 2.S6. The mobility of AKT-1::GFP on SDS-PAGE is regulated by PDK-1, CAND-1, CUL-1, and LIN-23.

(**a**) Anti-GFP western blot of AKT-1::GFP from whole-animal lysate of L4/young adult-stage animals treated with the indicated RNAi; anti-histone H4 staining is used as a loading control. (**b**) The level of *Pakt-1*::AKT-1::GFP epifluorescence signal in the whole bodies of L4/young-adult stage animals treated with the indicated RNAi.

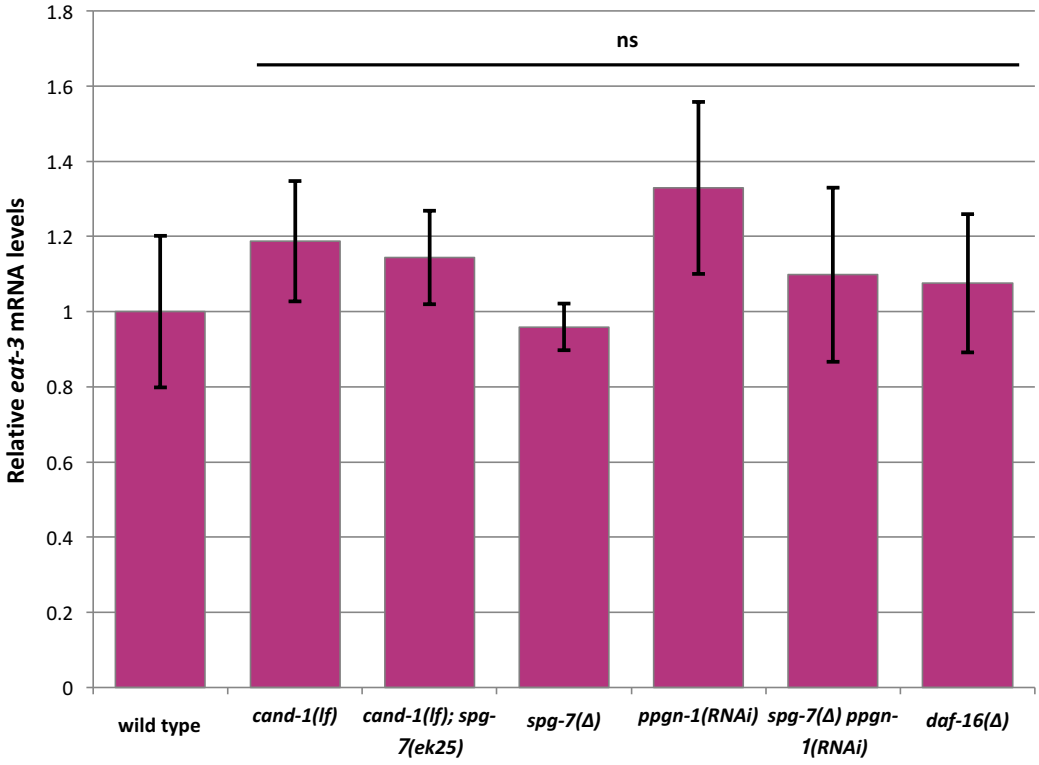

Figure 2.S7. *eat-3* mRNA levels are not altered in mitochondrial fusion pathway mutants.

RT-qPCR quantification of *eat-3* mRNA levels normalized to *rpl-19* control mRNA for young adults of the indicated genotypes/RNAi treatments. Error bars denote SEM.

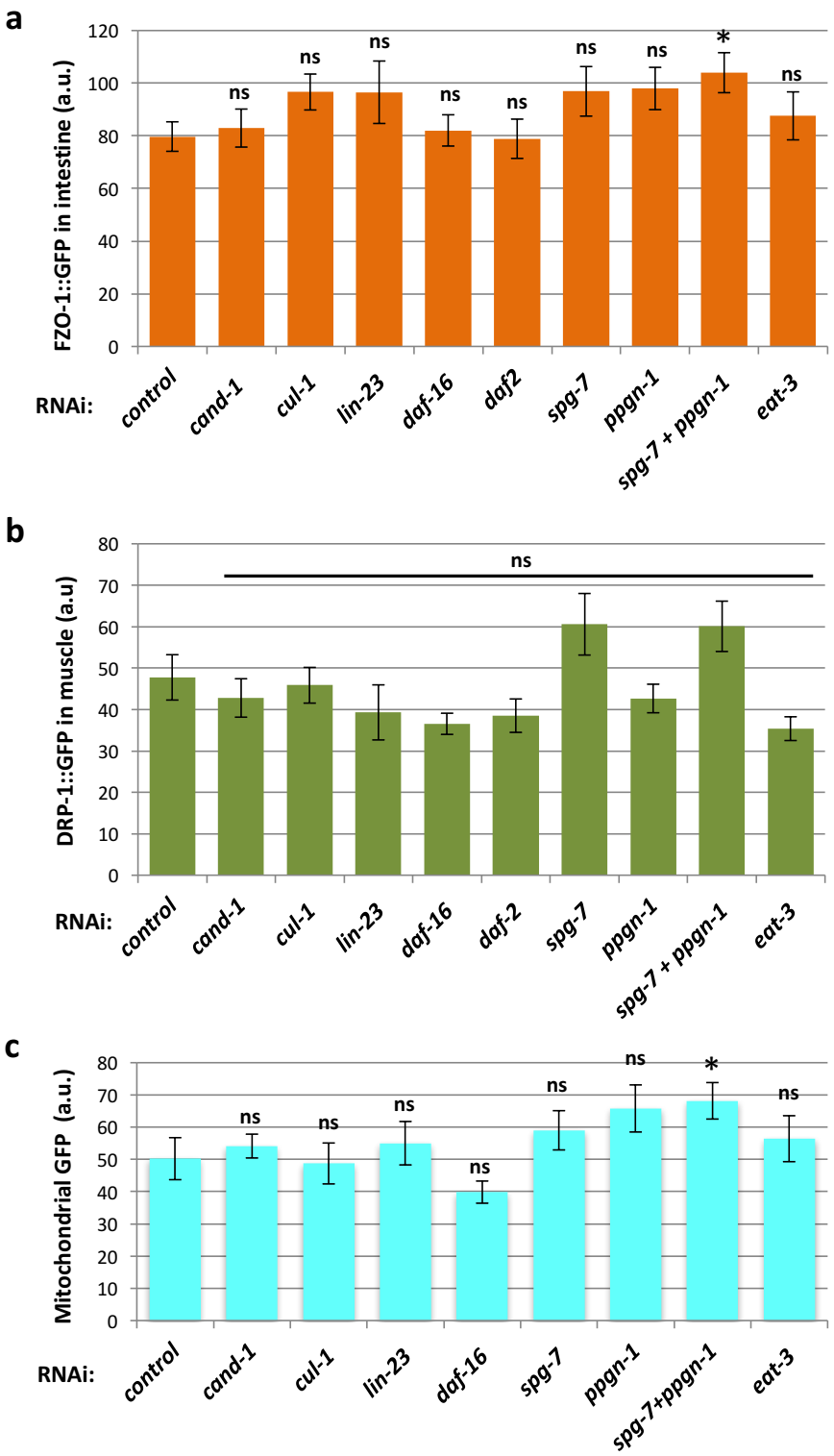
a
FZO-1::GFP in intestine (a.u.)
120
100
80
60
40
20
0
ns
ns
ns
ns
ns
ns
ns
ns
*
ns
RNAi:
control
cand-1
cul-1
lin-23
daf-16
daf2
spg-7
ppgn-1
spg-7 + ppgn-1
eat-3
b
DRP-1::GFP in muscle (a.u)
80
70
60
50
40
30
20
10
0
ns
RNAi:
control
cand-1
cul-1
lin-23
daf-16
daf-2
spg-7
ppgn-1
spg-7 + ppgn-1
eat-3
c
Mitochondrial GFP (a.u.)
80
70
60
50
40
30
20
10
0
ns
ns
ns
ns
ns
ns
*
ns
RNAi:
control
cand-1
cul-1
lin-23
daf-16
spg-7
ppgn-1
spg-7+ppgn-1
eat-3

Figure 2.S8. DRP-1::GFP, FZO-1::GFP, and *Pmyo-3*::GFP(mit) protein levels in mitochondrial fusion pathway RNAi depletions.

(**a**) The level of *Pmyo-3*::DRP-1::GFP signal was quantified in the body wall muscle cells of L4/young-adult stage animals with the indicated RNAi treatments quantified from epifluorescence images. (**b**) The level of *Phsp*::FZO-1::GFP signal was quantified in intestine cells of L4/young-adult stage animals with the indicated RNAi treatments quantified from epifluorescence images. (**c**) The level of *Pmyo-3*::GFP(mit) signal was quantified in the body wall muscle cells of L4/young-adult stage animals with the indicated RNAi treatments quantified from epifluorescence images.

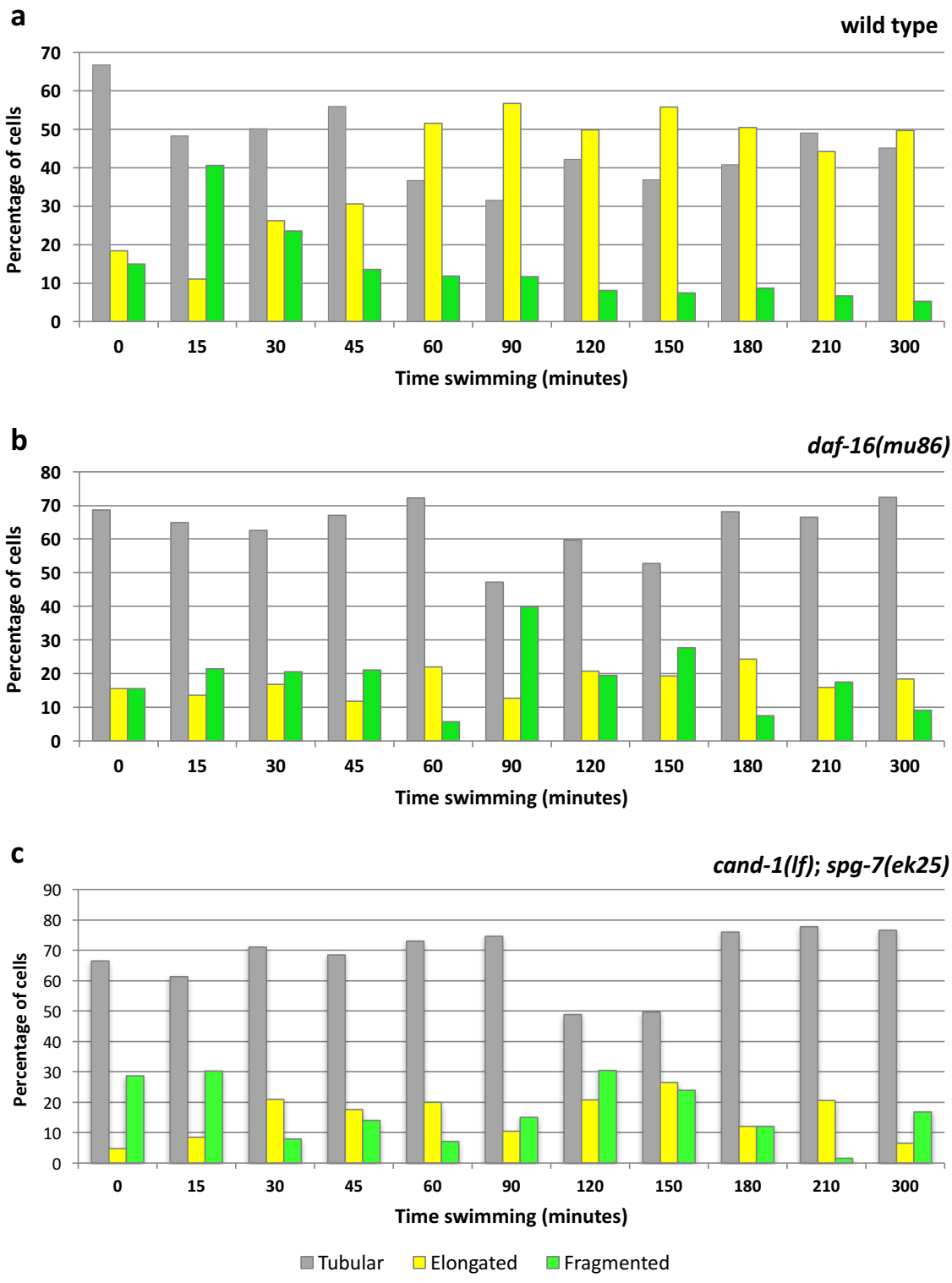
a
wild type
Percentage of cells
70
60
50
40
30
20
10
0
0
15
30
45
60
90
120
150
180
210
300
Time swimming (minutes)
b
daf-16(mu86)
Percentage of cells
80
70
60
50
40
30
20
10
0
0
15
30
45
60
90
120
150
180
210
300
Time swimming (minutes)
c
cand-1(lf); spg-7(ek25)
Percentage of cells
90
80
70
60
50
40
30
20
10
0
0
15
30
45
60
90
120
150
180
210
300
Time swimming (minutes)
Tubular
Elongated
Fragmented

Figure 2.S9. Mitochondrial morphology in *C. elegans* body wall muscles during swimming.

(**a-c**) The percentages of muscle cells with predominantly tubular, elongated, or fragmented mitochondria in wild type (a), *daf-16(mu86)* (b), and *cand-1*; *spg-7(ek25)* (c) animals upon induction of swimming behavior. Mitochondrial morphology was scored blinded.

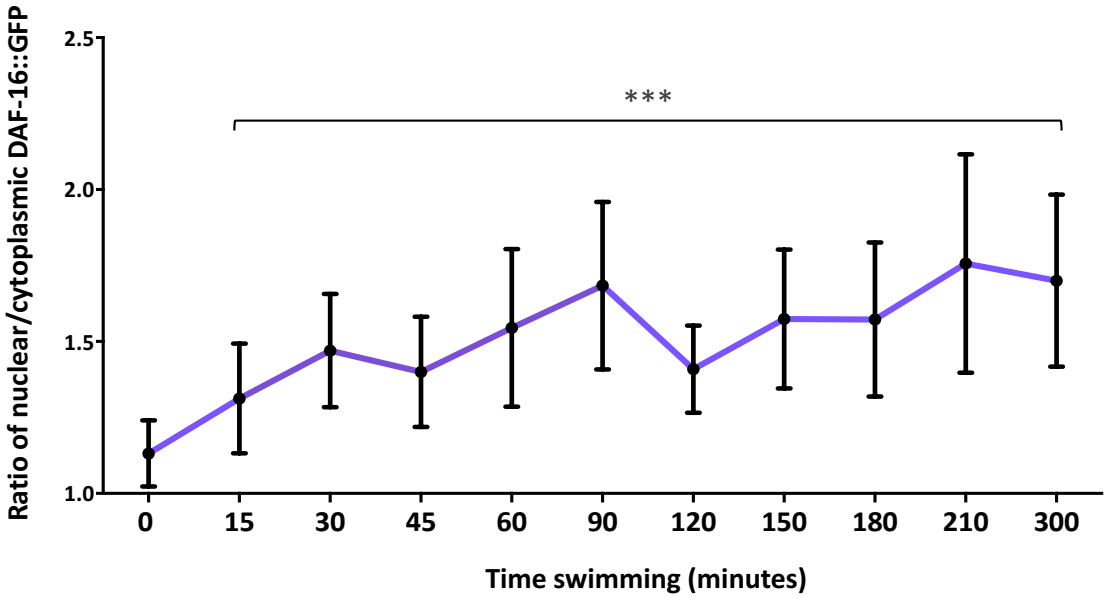

Figure 2.S10. DAF-16::GFP becomes nuclear localized during swimming. Quantification of the ratio of nuclear to cytoplasmic DAF-16::GFP intensity in body wall muscle cells upon induction of swimming behavior. Error bars denote standard deviation.

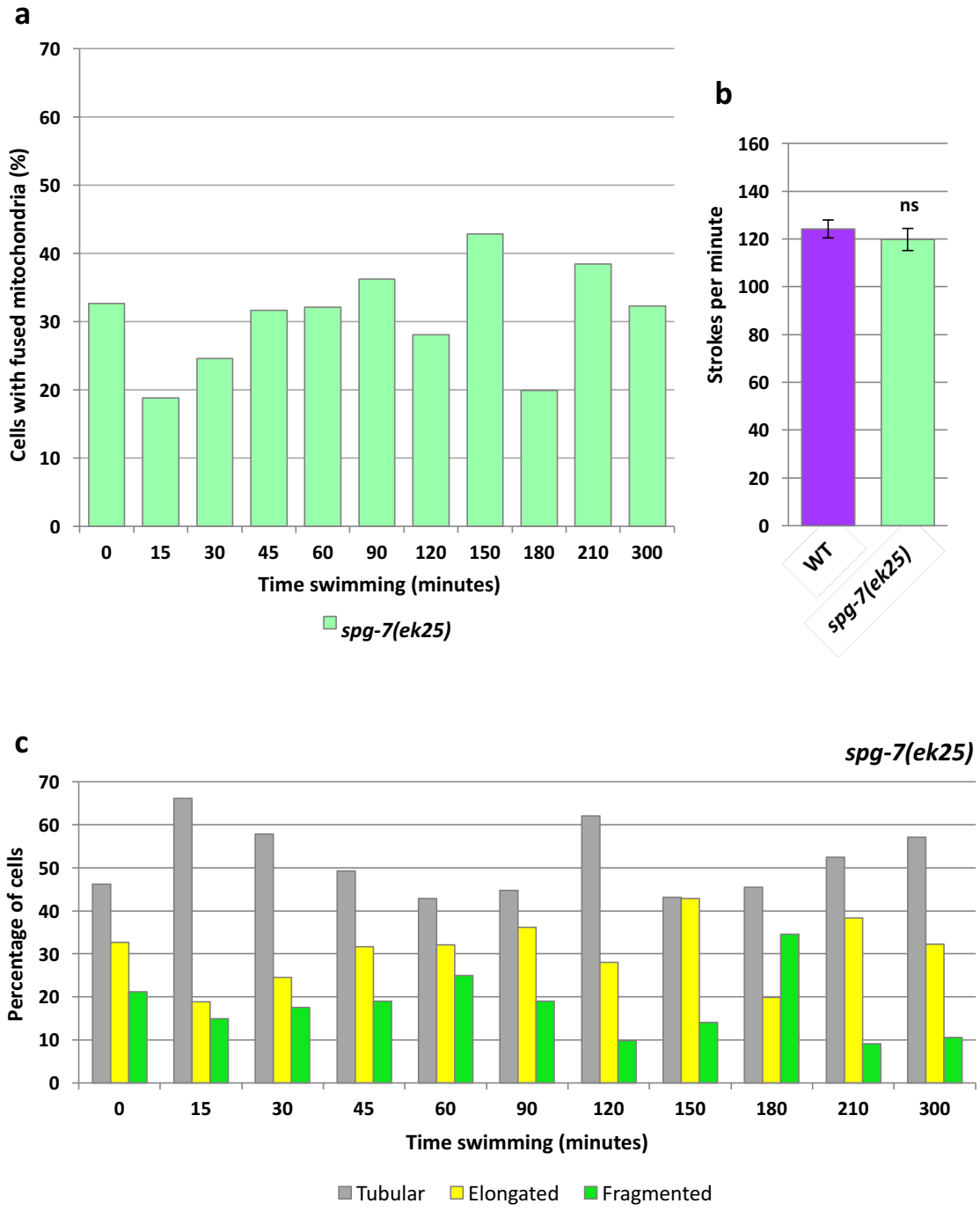
a
Cells with fused mitochondria (%)
70
60
50
40
30
20
10
0
0 15 30 45 60 90 120 150 180 210 300
Time swimming (minutes)
spg-7(ek25)
b
Strokes per minute
160
140
120
100
80
60
40
20
0
ns
WT
spg-7(ek25)
c
spg-7(ek25)
Percentage of cells
70
60
50
40
30
20
10
0
0 15 30 45 60 90 120 150 180 210 300
Time swimming (minutes)
Tubular
Elongated
Fragmented

Figure 2.S11. *spg-7(ek25)* mutants do not exhibit increased mitochondrial elongation during swimming.

(**a**) The percentages of muscle cells with elongated mitochondria in *spg-7(ek25)* mutants for the indicated times post-induction of swimming behavior. (**b**) Average swim strokes-per-minute for *spg-7(ek25)* upon induction of swimming behavior. The wild-type strokes-per-minute is from Fig. 5b, and is shown here for comparison. (**c**) The percentages of muscle cells with predominantly tubular, elongated, or fragmented mitochondria in *spg-7(ek25)* animals upon induction of swimming behavior. Mitochondria were scored blinded.

a

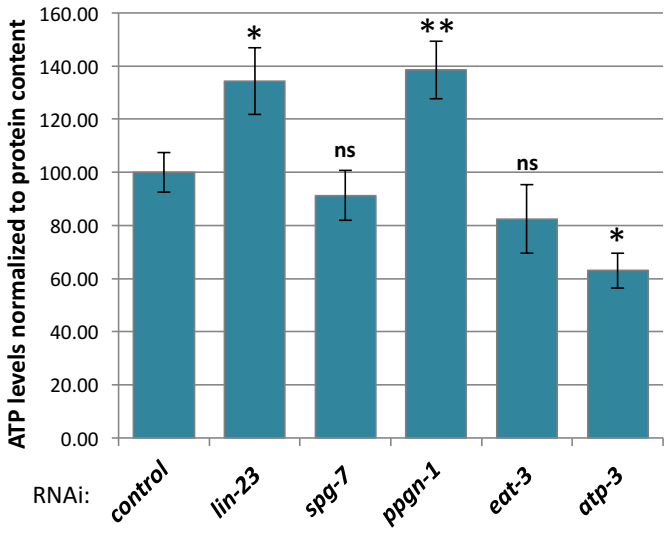
ATP levels normalized to protein content
160.00
140.00
120.00
100.00
80.00
60.00
40.00
20.00
0.00
*
**
ns
ns
*
RNAi:
control
lin-23
spg-7
ppgn-1
eat-3
atp-3

b

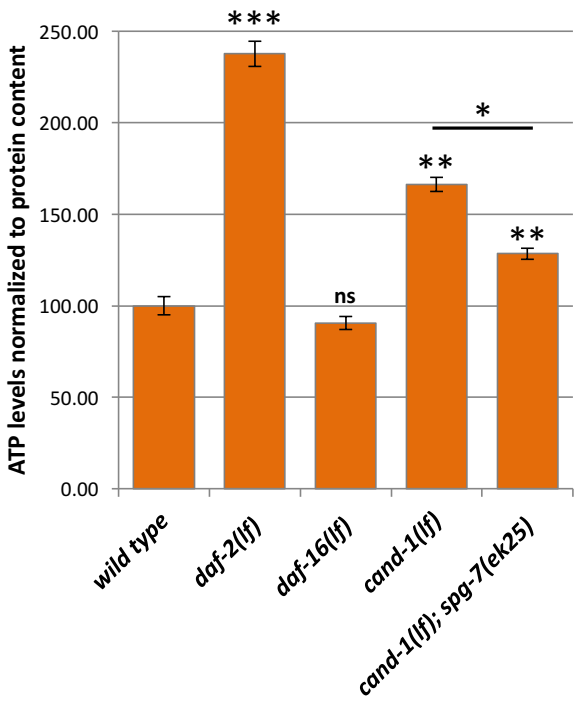
ATP levels normalized to protein content
250.00
200.00
150.00
100.00
50.00
0.00
***
*
**
ns
**
wild type
daf-2(lf)
daf-16(lf)
cand-1(lf)
cand-1(lf); spg-7(ek25)

Figure 2.S12. ATP levels are elevated in mitochondrial fusion pathway mutants that have increased elongated mitochondria.

(**a**, **b**) The ratio of ATP to whole-animal protein level is shown for the indicated RNAi treatments (**a**) or mutant genotypes (**b**) for L4/young-adult stage animals. Levels are standardized to control RNAi or wild type (set to 100). *atp-3* RNAi is a negative control that depletes a component of the ATP synthase complex V.

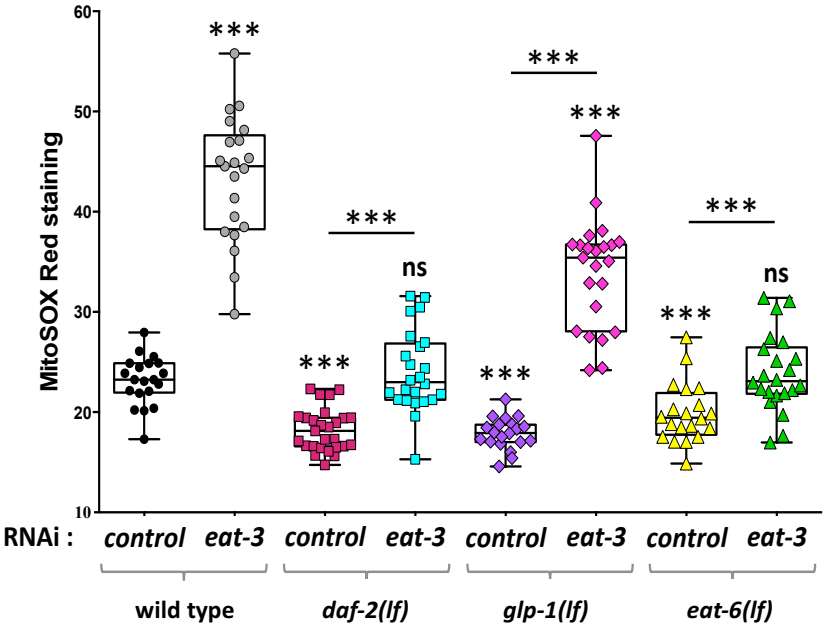

Figure 2.S13. Mitochondrial ROS levels in *C. elegans* longevity mutants upon *eat-3* RNAi

Mean intensity of the posterior pharyngeal bulb stained with the ROS-indicator MitoSOX Red in young adults of wild type, *daf-2(e1370)*, *glp-1(e2141)*, and *eat-6(ad467)* genotypes subjected to control or *eat-3* RNAi. See Table 2.S4 for statistics. Boxes represent the SEM range with the mean denoted by a central horizontal line; vertical lines extending above and below the box denote the range.

Table 2.S1. Analysis of RNAi inactivations of *ek25*-candidate genes for *cand-1* mutant phenotypes

RNAi	bobtail phenotype (%)			egg hatch (%)		
	cand-1	***cand-1*; *ek25***	**wild type**	***cand-1***	***cand-1*; *ek25***	**wild type**
control[b]	11.0	1.2	0	94.6	100.0	100.0
cand-1[a]	29.0	2.0	0	58.0	91.0	97.0
csn-3[a,c]	dead eggs	4.0	0	0.0	96.0	56.0
spg-7[a]	40.7	11.4	0	sterile	sterile	sterile
spg-7:ctrl 1:1[a]	48.0	6.0	0	sterile	45.4	sterile
spg-7:ctrl 1:2[a]	23.0	4.0	0	sterile	77.7	81.8
spg-7:ctrl 1:5[a]	11.0	5.0	0	75.6	95.2	91.0
Y47G6A.15[a]	12.0	1.0	0	92.7	98.0	100.0

[a]n = ~100 animals; [b]n = ~250 animals;

[c]*csn-3* RNAi acts as an enhancer for *cand-1* mutants that results in 100% dead eggs.

Table 2.S2. Lifespan analysis

Genotype/(RNAi Treatment)	n (censored)	median life span	mean life span ± STDEV	*P*-value vs. wild type		*P*-value vs. control	
				Log-rank	Wilcoxon	Log-rank	Wilcoxon
N2 wild type (*control* RNAi)	86 (5)	14±0.2	15.5±0.2	–	–	–	–
N2 (*eat-3* RNAi)	89 (1)	15±0.1	15.4	0.8660	0.9684	–	–
N2 (*cand-1* RNAi)	75 (10)	22±0.3	25.4	< 0.0001	< 0.0001	–	–
N2 (*lin-23* RNAi)	129 (14)	18±0.3	19.2	0.0002	0.0090	–	–
N2 (*spg-7* RNAi)	103 (5)	13±0.2	15.3	0.3153	0.4344	–	–
N2 (*ppgn-1* RNAi)	108 (2)	19±0.1	20.2	< 0.0001	< 0.0001	–	–

cand-1(tm1683) (*control* RNAi)	76 (9)	17±0.3	19.7	0.0015	0.0109	–	–
cand-1(tm1683); *spg-7(ek25)* (*control* RNAi)	52 (1)	14±0.1	16.0	0.3879	0.8882	–	–
N2 wild type (*control* RNAi)	56 (8)	13±0.3	15.0	–	–	–	–
spg-7(tm2312) (*control* RNAi)	81(2)	20±0.2	17.7	0.0003	0.0076		
N2 (*spg-7* + *ppgn-1* RNAi)	118(1)	19±0.1	20.4	< 0.0001	< 0.0001		
N2 wild type (*control* RNAi)	101 (8)	17±0.3	18.0	–	–	–	–
N2 (*eat-3* RNAi)	97 (0)	15±0.1	15.2	0.8184	0.6745	–	–
daf-2(e1370) (*control* RNAi)	109 (8)	41±0.1	37.8	< 0.0001	< 0.0001	< 0.0001	< 0.0001
daf-2(e1370) (*eat-3* RNAi)	87 (0)	15±0.0	18.3	0.1265	0.3773		

eat-2(ad116) (*control* RNAi)	43 (0)	23±0.0	22.3	< 0.0001	< 0.0001	< 0.0001	< 0.0001
eat-2(ad116) (*eat-3* RNAi)	67 (0)	11±0.0	11.6	< 0.0001	< 0.0001		
eat-6(ad467) (*control* RNAi)	80 (0)	24±0.2	24.6	< 0.0001	< 0.0001	< 0.0001	< 0.0001
eat-6(ad467) (*eat-3* RNAi)	57 (0)	13±0.0	13.4	0.0112	0.0490		
glp-1(e2141) (*control* RNAi)	65 (4)	22±0.2	23.4	< 0.0001	< 0.0001	< 0.0001	< 0.0001
glp-1(e2141) (*eat-3* RNAi)	80 (2)	13±0.2	15.3	0.7682	0.6498		
N2 (*clk-1* RNAi)	66 (2)	17±0.1	18.5	< 0.0001	< 0.0001	–	–
N2 (*clk-1* + *control* RNAi)	86 (5)	21±0.2	22.2	< 0.0001	< 0.0001	< 0.0001	< 0.0001
N2 (*clk-1* + *eat-3* RNAi)	157 (5)	15±0.1	16.5	0.0008	0.0017		
sir-2.1(oe) (*control* RNAi)	122 (4)	21±0.1	21.9	< 0.0001	< 0.0001	< 0.0001	< 0.0001

sir-2.1(oe) (*eat-3* RNAi)	126 (1)	16±0.1	15.2	0.0815	0.0681		
N2 (*let-363* RNAi)	52 (10)	19±0.3	20.6	< 0.0001	< 0.0001	–	–
N2 (*let-363* + *control* RNAi)	40 (24)	17±0.4	21.5	0.0081	0.0109	0.0322	0.1002
N2 (*let-363* + *eat-3* RNAi)	48 (4)	15±0.2	15.0	0.5964	0.4065		
aak-2(oe) (*control* RNAi)	33 (15)	21±0.4	25.0	< 0.0001	< 0.0001	0.0081	0.0091
aak-2(oe) (*eat-3* RNAi)	42 (1)	15±0.1	16.0	0.0367	0.1029		
N2 (*gpi-1* RNAi)	67 (14)	17±0.3	18.0	0.0004	0.0003	–	–
N2 (*gpi-1* + *control* RNAi)	99 (7)	17±0.2	18.5	< 0.0001	0.0008	< 0.0001	0.0082
N2 (*gpi-1* + *eat-3* RNAi)	98 (5)	14±0.2	15.0	0.9975	0.1816		
N2 wild type (*control* RNAi)	109 (22)	14±0.3	13.6	–	–	–	–
vhl-1(ok161) (*control* RNAi)	112 (2)	22±0.1	23.0	< 0.0001	< 0.0001	0.1691	0.4245

vhl-1(ok161) (*eat-3* RNAi)	99 (0)	22±0.0	21.2	< 0.0001	< 0.0001		
N2 (*fzo-1* RNAi)	126 (2)	10±0.1	10.6	< 0.0001	< 0.0001	–	–
daf-2(e1370) (*control* RNAi)	94 (13)	39±0.3	37.7	< 0.0001	< 0.0001	< 0.0001	< 0.0001
daf-2(e1370) (*fzo-1* RNAi)	121(0)	21±0.0	22.0	< 0.0001	< 0.0001		
N2 wild type (*control* RNAi)	71 (2)	14±0.1	13.8	–	–	–	–
atfs-1(et17) (*control* RNAi)	87 (13)	11±0.3	12.3	0.0015	0.0085	–	–
atfs-1(et17) (*cand-1* RNAi)	67 (2)	13±0.1	13.6	0.4160	0.7258	0.0083	0.0036
atfs-1(et17) (*lin-23* RNAi)	97 (15)	15±0.3	16.0	0.1044	0.1027	< 0.0001	< 0.0001
atfs-1(et17) (*control* RNAi)	99 (2)	9±0.1	9.0	< 0.0001	< 0.0001	–	–
atfs-1(et17) (*spg-7* RNAi)	107 (14)	19±0.3	18.5	< 0.0001	< 0.0001	–	–
atfs-1(et17) (*ppgn-1* RNAi)	56 (23)	17±0.4	18.3	< 0.0001	< 0.0001	–	–
atfs-1(et17) (*spg-7* + *ppgn-1* RNAi)	115 (7)	19±0.2	19.8	< 0.0001	< 0.0001	–	–

n = number of animals scored for lifespan experiment (censored animals were included in the Log-rank and Wilcoxon statistical analysis)

Table 2.S3. Lifespan analysis- Swim assay

Genotype/(RNAi Treatment)	n (censored)	median life span ± STDEV	mean life span ± STDEV	*P*-value vs. wild type		*P*-value vs. control	
				Log-rank	Wilcoxon	Log-rank	Wilcoxon
N2 wild type (crawl)	91 (11)	10±0.3	12.4	–	–	–	–
N2 wild type (swim regimen A)	99 (29)	16±0.4	18.8	–	–	< 0.0001[a]	< 0.0001[b]
N2 wild type (crawl)	114 (7)	13±0.2	13.0	–	–	–	–
N2 wild type (swim regimen B)	145 (12)	15±0.2	17.4	–	–	< 0.0001[c]	< 0.0001[d]
N2 wild type (swim regimen C)	118 (32)	19±0.4	20.6	–	–	< 0.0001[c]	< 0.0001[c]
N2 wild type (crawl)	200 (16)	12±0.2	12.0	–	–	–	–
N2 wild type (swim regimen C)	197 (46)	15±0.3	16.3	–	–	< 0.0001[c]	< 0.0001[c]

cand-1(tm1683); *spg-7(ek25)* (crawl)	100 (24)	10±0.3	10.2	0.0370	< 0.0001	–	–
cand-1(tm1683); *spg-7(ek25)* (swim regimen C)	80 (26)	8±0.4	10.0	0.0008	< 0.0001	0.5631	0.6764
daf-16(mu86) (crawl)	131 (8)	10±0.2	11.9	0.2448	0.1217	–	–
daf-16(mu86) (swim regimen C)	80 (3)	12±0.1	13.2	< 0.0001	0.0368	0.1228	0.0307

n = number of animals scored for lifespan experiment (censored animals were included in the Log-rank and Wilcoxon statistical analysis)

[a,b]Compared to N2 wild-type lifespan (combined from all non-swim experiments, the *P*-values are 0.6288 and 0.1138 for Log-Rank and Wilcoxon tests, respectively.

[c]Compared to N2 wild-type lifespan (combined from all non-swim experiments), the *P*-values are <0.0001 for Log-Rank and Wilcoxon tests.

[d]Compared to N2 wild-type lifespan (combined from all non-swim experiments), the *P*-value is 0.0041 for Wilcoxon test.

Table 2.S4. MitoSOX Red staining analysis.

Genotype/(RNAi Treatment)	**n**	**mean** ± SEM	***P*-value vs. wild type**	***P*-value vs. control RNAi**
N2 wild type (control RNAi)	20	23.15±0.5	–	–
N2 (*eat-3* RNAi)	21	43.32±1.3	< 0.0001	–
daf-2(e1370) (control RNAi)	27	18.25±0.4	< 0.0001	< 0.0001
daf-2(e1370) (*eat-3* RNAi)	24	24.06±0.8	0.3855	
glp-1(e2141) (control RNAi)	20	17.85±0.3	< 0.0001	< 0.0001
glp-1(e2141) (*eat-3* RNAi)	23	33.94±1.1	< 0.0001	
eat-6(ad467) (control RNAi)	20	19.91±0.6	0.0006	0.0006
eat-6(ad467) (*eat-3* RNAi)	22	23.92±0.8	0.4513	

n = number of animals imaged for MitoSOX Red staining.

CHAPTER 3

BACTERIAL FOLATES PROVIDE AN EXOGENOUS SIGNAL FOR *C. ELAGANS* GERMLINE STEM CELL PROLIFERATION

Snehal N. Chaudhari*, Madhumati Mukherjee*, Alexandra S. Vagasi, Gaofeng Bi, Mohammad M. Rahman, Christine Nguyen, Ligi Paul, Jacob Selhub, and Edward T. Kipreos. **Reprinted here with permission of publisher**

*These authors contributed equally.

Abstract

Here we describe an in vitro primary culture system for *C. elegans* germline stem cells. This culture system was used to identify a bacterial folate as a positive regulator of germ cell proliferation. Folates are a family of B-complex vitamins that function in one-carbon metabolism to allow the *de novo* synthesis of amino acids and nucleosides. We show that germ cell proliferation is stimulated by the folate 10-formyl-tetrahydrofolate-Glu_n both in vitro and in animals. Other folates that can act as vitamins to rescue folate deficiency lack this germ cell stimulatory activity. The bacterial folate precursor dihydropteroate also promotes germ cell proliferation in vitro and in vivo, despite its inability to promote one-carbon metabolism. The folate receptor homolog FOLR-1 is required for the stimulation of germ cells by 10-formyl-tetrahydrofolate-Glu_n and dihydropteroate. This work defines a folate and folate-related compound as exogenous signals to modulate germ cell proliferation.

Introduction

Animal germ stem cells (GSCs) are adult stem cell populations that provide reproductive cells to allow species propagation. *C. elegans* hermaphrodite GSCs proliferate in adult stem cell niches located in the distal regions of the two gonad arms [1]. Primary cultures of *C. elegans* germ cells have not been previously reported. *C. elegans* embryonic cells can be cultured, but not propagated, in an L-15-based culture medium [2]. In this study, we describe a primary culture system for *C. elegans* germ cells that utilizes a culture medium with substantially different characteristics than L-15 medium. The in vitro culture system allows the analysis of relatively pure populations of germ cells that are isolated from germline tumorous mutant strains. Two external signals, Notch and Insulin/IGF-like, are known to promote the proliferation of GSCs [1, 3]. We used the in vitro culture system to identify bacterial folate as a new signal that promotes GSC proliferation.

Folates are a group of B vitamins whose canonical role is in one carbon transfer for the *de novo* synthesis of: thymidine; purines; methionine, and the methyl donor S-adenosylmethionine [4] (Fig. 3.1A). Folates comprise moieties of a pteridine ring, para-aminobenzoic acid (PABA), and one or more glutamate residues (Glu_n) in γ-linkages to the terminal glutamate (Fig. 3.1B). Folates differ from each other by: 1) the states of oxidation of the pteridine ring, i.e. dihydrofolate, DHF, or tetrahydrofolate, THF; 2) modification of the 5- and 10- position of the pteridine ring by substitution with formate (5-formyl-, 10-formyl-, and 5,10-methenyl-THF), formaldehyde (5,10-methylene-THF), or methanol (5-methyl-THF); and 3) the number of glutamate residues (Fig. 3.1B,C). The three forms of formylated THF are interconvertible: 5,10-methenyl-THF, which is stable at acid pH (1.5-

2.6), is converted to 5-formyl-THF at pH 4.0-5.5 and to 10-formyl-THF at neutral and higher pH, and vice versa [5].

In mammals, there are three types of folate transporters. The reduced folate carrier, RFC, is a low-affinity, high-capacity transporter that brings folates into all cells of the body [6]. The proton-coupled folate transporter, PCFT, functions at low pH to transport folates from acidic pH environments, such as the mammalian small intestine [7]. Folate receptors, FRs, are high-affinity, low-capacity transporters that have been shown to function in the transcytosis of folates across polarized cell barriers [8-10].

Folates are synthesized by bacteria, plants, fungi, and certain protozoa and archaea [11]. Folates cannot be synthesized *de novo* by animals, and hence are classified as vitamins that must be obtained from the animal's diet or microbiota. As is true for other animals, *C. elegans* requires folates for one-carbon metabolism. Inactivation of the *C. elegans* RFC homolog FOLT-1/RFC results in severely reduced germ cell numbers and sterility [12].

Our work demonstrates that a specific bacterial folate and pteroate (a folate-related compound) stimulate germ cell proliferation in a manner that can be distinguished from the canonical role of folates in one-carbon metabolism.

Results

Cellularization of tumorous germ cells

In an effort to understand the regulation of GSC survival and proliferation, we sought to create a primary culture system for *C. elegans* germ cells. Wild-type germ cells are syncytial [1] and therefore cannot be isolated as viable cells. We found that germ cells can be isolated from the tumorous germline mutant strain *glp-1(ar202)*; *cki-2(ok2105)*; *daf-16(mu86)* (hereafter *glp-1(gf)*; *cki-2*; *daf-16*) (Fig. 3.2A). Staining with the dye calcein-AM shows that the cells have intact plasma membranes, as calcein-AM is converted by cellular esterases to a fluorescent form that is unable to cross intact plasma membranes (Fig. 3.2A).

To determine the percentage of germ cells among the isolated cells, we compared the number of germ cells isolated from *glp-1(gf)*; *cki-2*; *daf-16* mutants and wild-type adult hermaphrodites. Wild-type germ cells are not cellularized and therefore would not survive in culture. *glp-1(gf)*; *cki-2*; *daf-16* mutants have increased numbers of germ cells, but appear to have approximately the same number of somatic cells as wild type. Therefore, any significant increase in the number of isolated cells from *glp-1(gf)*; *cki-2*; *daf-16* mutants can be attributed to germ cells. *glp-1(gf)*; *cki-2*; *daf-16* mutants released an average of 6023 ± 196 live cells per adult hermaphrodite, while wild type released an average of 37 ± 10 live cells per adult hermaphrodite (n = 3 and n = 6 sets of 25 animals, respectively). These results suggest that over 99% of the *glp-1(gf)*; *cki-2*; *daf-16* isolated cells are germ cells.

The *glp-1(gf)*; *cki-2*; *daf-16* strain contains: a temperature-sensitive, gain-of-function (gf) allele of the Notch receptor GLP-1, which promotes germ cell proliferation at the non-permissive temperature [13]; and loss-of-function mutations of the CDK-inhibitor CKI-2 and the FOXO transcription factor DAF-16, both of which inhibit GSC proliferation [3, 14]. In *glp-1(gf)*; *cki-2*; *daf-16* mutants, germ cell proliferation is not constrained to the distal stem cell niche but occurs throughout the gonad. This is demonstrated by the presence of cells in mitosis throughout the gonad, as shown by immunofluorescence staining with the mitotic marker anti-phosphohistone H3 (Ser10) antibody [15] (Fig. 3.S1). The addition of *cki-2(lf)* and *daf-16(lf)* mutations to the *glp-1(ar202)* mutation produced more mitotic proliferation, as demonstrated by the significantly decreased region of the gonad in which the meiotic marker HIM-3 is present relative to *glp-1(ar202)* mutants alone [16] (Fig. 3.S1).

Development of an in vitro culture medium for *C. elegans* germ cells

Embryonic *C. elegans* cells can be maintained, but not propagated, in L-15-based cell culture medium [2]. We observed that isolated germ cells die rapidly in the L-15 medium (Fig. 3.2B). After carrying out a systematic analysis of culture medium components, we prepared a medium optimized for germ cell culture called CeM1 (*C. elegans* medium 1) (Table 3.S1). Cell survival in CeM1 was extended relative to L-15 medium by altering: the base medium (3:1 Schneider's insect:L-15 medium); fetal bovine serum (FBS) concentration (8%); heat-inactivation of FBS at 65°C for 30 min; osmolality (390 mOsm/kg); and pH (6.5) (Fig. 3.S2). Additionally, the following CeM1 components contribute to germ cell survival: reduced L-glutathione; RPMI vitamins; the sugar

trehalose; and cholesterol and heme, for which *C. elegans* are auxotrophic [17, 18] (Fig. 3.2C).

We tested different FBS lots and observed a partial negative correlation between the levels of thyroxine (Atlanta Biologicals data sheets) and the ability of the FBS to support germ cell viability (data not shown). Steroid hormones, such as thyroxine, can be removed by exposing FBS to the anion-exchange resin Amberlite IRA 400-CL and charcoal-dextran [19, 20]. Treatment of FBS with both reagents significantly increased germ cell survival (Fig. 3.2D). The full CeM1 medium can maintain the viability of a majority of isolated germ cells for a period of one month (Fig. 3.2).

Bacteria can differentially stimulate *C. elegans* germ cell proliferation

We considered the possibility that *C. elegans*' major dietary component, bacteria, could regulate germ cell proliferation. To test this, we created a bacterial extract of the *Escherichia coli* K-12 strain HT115(DE3) (hereafter HT115), which is used for feeding RNAi [21]. Addition of HT115 bacterial extract to CeM1 medium increased the number of germ cells over the first three days in culture, suggesting that bacterial component(s) induce germ cell proliferation (Fig. 3.2E). Heat-inactivation of the bacterial extract (60°C for 30 min) did not affect its ability to induce transient proliferation, suggesting that the active compound(s) are not particularly heat-sensitive (Fig. 3.2E).

In laboratory settings, *C. elegans* is propagated on a monoxenic diet of a single bacterial species. To assess the effects of extracts from different bacteria, we created extracts from two additional bacteria: *E. coli* B strain OP50, which is the standard laboratory diet; and *Comamonas aquatica* DA1877, which accelerates *C. elegans* growth

[22]. Bacterial extracts from the three strains were added to germ cells isolated from the tumorous mutant strain *glp-1(gf)*; *cki-2*; *daf-16* (hereafter referred to as "isolated germ cells"). Incorporation of the thymidine-analog EdU was used to follow DNA replication 24 to 48 hr post-isolation. Typically, 3-10% of the isolated germ cells incorporate EdU in the absence of bacterial extract. The addition of the bacterial extracts increased the percentage of cells incorporating EdU, with HT115 and DA1877 extracts having more activity than OP50 extract (Fig. 3.3A).

We tested the effect of diets of the three bacteria on germ cell proliferation in vivo by analyzing the frequency of germline tumor formation in the *glp-1(gf)*; *cki-2*; *daf-16* mutant strain grown at a semi-permissive temperature (Fig. 3.S3A). Hereafter, references to "tumor frequency" will imply that the assay was performed with *glp-1(gf)*; *cki-2*; *daf-16* mutants. Similar results were obtained whether tumor frequency was scored blinded or non-blinded (see Experimental Procedures). Consistent with the EdU incorporation data, the frequency of visible tumors at the semi-permissive temperature of 18°C was higher with a diet of DA1877 or HT115 than with OP50 (Fig. 3.3B). Diets of the three bacteria appear to stimulate germ cell proliferation through a common pathway, as mixed diets of the different bacteria did not synergistically increase tumor formation (Fig. 3.S3B).

Bacterial folates stimulate germ cell proliferation

Several bacteria-derived compounds have been implicated in modulating *C. elegans* biological processes, including: folates, which reduce lifespan [23]; tryptophan metabolite(s), which alter the expression of detoxification genes [24]; and vitamin B12, which accelerates growth [25]. Supplementing bacteria with tryptophan or vitamin B12 did

not stimulate germ cell proliferation (Fig. 3.S4). In contrast, our analysis of folates found that they are linked to the stimulation of germ cell proliferation.

Most bacteria are capable of the *de novo* synthesis of folate through a pathway that includes the condensation of the dihydropteridine ring with PABA, followed by the addition of one or more glutamates (Glu) (Fig. 3.1B). PABA can be rate-limiting for folate synthesis in bacteria [26]. To test if increasing the level of bacterial folates increases germ cell proliferation, we supplemented bacteria with PABA. Diets of the three bacteria supplemented with PABA produced an increase in tumor frequencies (Fig. 3.3B). Similarly, adding extracts from bacteria supplemented with PABA to isolated germ cells increased the percentage of cells incorporating EdU (Fig. 3.3A). As expected, based on the inability of animals to use PABA to create folates, adding PABA directly to isolated germ cells had no affect on EdU incorporation (Fig. 3.3A). Similarly, adding PABA to a diet of heat-killed bacteria, which cannot metabolize the PABA, had no stimulatory effect (Fig. 3.3C).

To further address the contribution of bacterial folates or folate-related compounds to germ cell proliferation, we used the antibiotic trimethoprim (TRI), which inhibits dihydrofolate reductase (DHFR) in bacteria to block the generation of THF. TRI reduces overall THF folate levels in *E. coli*; however, while the levels of poly-Glu_3 or higher THF folates become undetectable upon TRI exposure, the levels of mono- and di-Glu THF folates modestly increase [27]. We observed that incubating HT115 and DA1877 bacteria with 2.5 μg/ml TRI prior to creating extract reduced the extract's ability to stimulate EdU incorporation in isolated germ cells (Fig. 3.3D). Pretreatment of OP50 with TRI did not have an obvious effect on the extract's (normally lower) level of stimulating DNA

replication (Fig. 3.3D). Similarly, feeding *glp-1(gf)*; *cki-2*; *daf-16* mutants a diet of HT115 or DA1877 grown on TRI reduced tumor frequency, while a diet of OP50 grown on TRI did not significantly reduce tumor frequency (Fig. 3.3E). The lack of effect of TRI on an OP50 diet or OP50 bacterial extract indicates that TRI by itself has no appreciable effect on germ cell proliferation, but rather mediates its effects via its action on specific bacteria.

We wanted to determine if the choice of bacterial diet and increasing bacterial folate production affects GSC proliferation in wild-type animals. Increases or decreases in mitotic proliferation of GSCs expand or contract the proliferative zone of the gonad to alter the number of germ cell nuclei in the zone [3]. When wild-type hermaphrodites were fed a diet of HT115 or DA1877 bacteria, the number of germ cell nuclei in the proliferative zone was higher compared to an OP50 diet (Fig. 3.3F). Supplementing the bacteria with PABA increased the number of germ cell nuclei in the proliferative zone for OP50 and HT115 diets, with a higher mitotic index for the HT115 diet, suggesting that a diet with increased levels of folates increases proliferative germ cell numbers (Figs 3.3F, 3.S5A). Incubation of the three bacteria with TRI reduced the numbers of mitotic germ cells per gonad arm in wild-type hermaphrodites fed a diet of DA1877, but had less effect on OP50 and HT115 diets (Fig. 3.S5B). Overall, these results suggest that increased levels of bacterial folates can increase mitotic germ cell proliferation in wild-type hermaphrodites.

To confirm that folates are the active bacterial component, folates were purified from bacteria and tested for their ability to induce germ cell proliferation. Total bacterial extract, purified folates, and folate-free, flow-through extract were tested on isolated germ cells for their effect on DNA replication. Total extract and purified folates increased the number of cells incorporating EdU when added to isolated germ cells (Fig. 3.4A; Table 3.S2). In

contrast, the addition of the folate-free flow-through extract reduced EdU incorporation, suggesting that in the absence of folates, bacterial extract negatively impacts germ cell cultures. The addition of purified folates to a diet of heat-killed OP50 bacteria also increased tumor frequency (Fig. 3.4B).

To determine if purified folates increase the number of mitotic cells in wild-type animals, we added purified folates from OP50, DA1877, or HT115 to heat-killed OP50 bacteria and allowed wild-type animals to develop from eggs on these plates. The addition of purified folates from HT115 and DA1877 increased the number of nuclei in the proliferative zone, with the mitotic index statistically higher for DA1877 folates (Figs 3.4C, 3.S5C). These results indicate that bacterial folates promote GSC proliferation in wild-type hermaphrodites.

Our previous analysis used equal volumes of isolated purified folates. To compare the relative activity of the purified folates among the three bacteria, we added equal concentrations of purified folates (0.06 μM) to isolated germ cells. The purified folates from HT115 induced a higher percentage of cells incorporating EdU than purified folates from OP50 and DA1877 (Fig. 3.4D). Folates purified from the mouse microbiota also have potent activity in stimulating EdU incorporation in isolated germ cells, suggesting that the active folate(s) are present in diverse microbial settings (Fig. 3.S5D).

10-formyl-THF-Glu$_n$ stimulates germ cell proliferation

CeM1 medium contains the synthetic folate folic acid at 2.8 μM, which is 40-fold higher than the concentration of purified folates that stimulate increased EdU incorporation in

isolated germ cells. Therefore, bacterial folates provide a signal that is not provided by folic acid.

We tested the germ cell stimulatory activity of the reduced monoglutamyl forms of folates, including racemic (S,R) THF, 5-formyl-THF (folinic acid), and 5-methyl-THF, as well as the biologically active (S) isomer for the latter two folates. We found that these basic folates, which can promote one-carbon metabolism when added to other animal cells, were unable to stimulate germ cell DNA replication even at concentrations significantly higher than the purified bacterial folates (Fig. 3.4D). The addition of 5-methyl-THF and THF to a diet of heat-killed bacteria also did not have a major effect on tumor frequency (Fig. 3.4B).

In an effort to identify the active germ cell-stimulatory folate(s), we analyzed the folates from OP50, HT115, and DA1877 bacteria grown under normal or PABA-supplemented conditions. Ion-pair high performance liquid chromatography (HPLC) was used to separate the affinity-purified folates, which were then identified by their stereotypical UV absorbance spectra [28]. Four folate species were detected in the bacterial extracts: 10-formyl-THF-Glu_n; THF-Glu_n; 5-formyl-THF-Glu_n; and 5-methyl-THF-Glu_n (Fig. 3.S6). The folates from DA1877 consisted predominantly of folates with three Glu residues, the most abundant of which was 5-methyl-THF-Glu_3 (Fig. 3.S6C). In contrast, OP50 and HT115 had primarily formylated folates with 3-7 Glu residues (Fig. 3.S6A,B). Notably, the only folate species that increased upon growth with PABA in all three bacterial species was 10-formyl-THF-Glu_n.

We isolated individual DA1877 folate fractions using HPLC (Fig. 3.5A). The 5-methyl-THF-$Glu_{1,3}$ fractions lacked stimulatory activity, consistent with our analysis of

pure folates. In contrast, the 10-formyl-THF-Glu_3 and 5,10-methenyl-THF-Glu_3 fractions stimulated EdU incorporation in isolated germ cells and increased tumor frequency assays when added to a diet of heat-killed bacteria (Fig. 3.5B,C). The activity of 5,10-methenyl-THF-Glu_3 is likely to be due to its conversion to 10-formyl-THF-Glu_3, which would occur because the assays were performed at neutral pH. The first peak from the chromatogram, whose molecular identity we could not determine, also exhibited stimulatory activity (data not shown). Overall, our results suggest that 10-formyl-THF-Glu_n can stimulate germ cell proliferation.

To clarify the importance of the number of glutamate residues, we converted purified OP50 bacterial folates from poly-$Glu_{3\text{-}7}$ to mono-Glu by treatment with tri-enzyme (a mixture of chicken pancreas conjugase, alpha amylase, and pronase) [29]. The conversion to mono-Glu folates abolished the stimulatory activity in EdU incorporation assays with isolated germ cells and tumor frequency assays (Fig. 3.6A,B). The stimulation of tumor frequency was also abolished when purified DA1877 bacterial folates were converted to mono-Glu using conjugase enzyme alone (Fig. 3.S5E).

To further confirm that poly-Glu contributes to germ cell stimulatory activity, we synthesized folates with 1, 3, or 6 Glu from folic acid-$Glu_{1,3,6}$: THF-$Glu_{1,3,6}$; 5-methyl-THF-$Glu_{1,3,6}$; 5,10-methenyl-THF-$Glu_{1,3,6}$; and 10-formyl-THF-$Glu_{1,3,6}$. We observed that folic acid, 5-methyl-THF, and THF were not active in stimulating increased tumor frequencies irrespective of the number of Glu residues (Figs 3.6D; 3.S5F). In contrast, 10-formyl-THF and 5,10-methenyl-THF increased tumor frequency in vivo and EdU incorporation in isolated germ cells in vitro, with greater activity with higher numbers of poly-glutamates (Figs 3.6C,D; 3.S5F). Significantly, 10-formyl-THF-$Glu_{3,6}$ and 5,10-

methenyl-THF-$Glu_{3,6}$ had activity even at the lowest concentration tested: 1 nM (Fig. 3.6C,D). The addition of 5,10-methenyl-THF-Glu_6 stimulated the transient proliferation of germ cells in vitro, similar to what we had observed with HT115 bacterial extract (Fig. 3.S5G). The ability of the synthetic folates 10-formyl-THF-Glu_n and 5,10-methenyl-THF-Glu_n to match the stimulatory activity of the folates isolated from bacteria confirms the identity of the bacterial stimulatory folates.

Folates stimulate germ cell proliferation independently of one-carbon metabolism

In other animals, multiple folates can act as single vitamin sources to reconstitute all of the folates required for one-carbon metabolism [30]. One potential model to explain the specificity of germ cell stimulation is that perhaps, unlike other animals, *C. elegans* can only utilize a single folate as a vitamin source. To address the role of folates as vitamins, we used the *folt-1* mutant as a means to deplete folate levels. *folt-1* is the *C. elegans* homolog of the mammalian RFC.

In mammals, the ubiquitously-expressed RFC transports the bulk of systemic folates into tissues [30]. In *C. elegans*, FOLT-1/RFC is required for ~80% of folate uptake into animals [31]. *folt-1(ok1467)* deletion mutants, when grown on a diet of OP50 bacteria, have severe defects in germ cell proliferation, with few germ cells per gonad arm [12]. Strikingly, we found that providing *folt-1*/RFC mutants a diet of OP50 supplemented with PABA rescued the germ cell number defect, and allowed 100% of the *folt-1*/RFC mutant adult hermaphrodites to become gravid (Fig. 3.7A). Therefore, the *folt-1*/RFC mutant is responsive to increased folate levels.

To further reduce the levels of folates, *folt-1*/RFC mutants were fed a diet of heat-killed, folate-depleted *pabC* mutant bacteria, which are unable to produce PABA [32]. To deplete folates in *pabC* mutants, the bacteria were incubated 24 hr in PABA-free minimal media. The resulting folate-depleted *pabC* bacteria had only 2.3% of the folate level of the parental *E. coli* K-12 strain (data not shown).

To test the ability of folates to rescue folate deficiency, heat-killed, folate-depleted *pabC* bacteria were supplemented with 10 μM of either the non-stimulatory folate S-5-formyl-THF-Glu_1 or the stimulatory folate 5,10-methenyl-THF-Glu_1. Both folates were able to rescue germ cell proliferation in the folate-depleted *folt-1*/RFC mutants, with the non-stimulatory S-5-formyl-THF-Glu_1 exhibiting more activity (Fig. 3.7B). Racemic 5-formyl-THF-Glu_1 (folinic acid) also rescues *C. elegans* sterility due to folate deficiency [33]. These results suggest that the effectiveness of a folate to function as a vitamin does not correlate with its ability to stimulate germ cell proliferation under normal growth conditions.

To directly test if a folate-related compound can stimulate germ cell proliferation independently of one-carbon metabolism, we analyzed dihydropteroate. Pteroates are comprised of a pteridine ring and PABA moieties, but lack glutamates (Fig. 3.1B). Dihydropteroate is a precursor to all folate synthesis in bacteria. Animals are unable to convert pteroates to folates because they lack the enzyme (dihydrofolate synthase) that is required to add glutamate to pteroates (Fig. 3.1B). Animals therefore cannot utilize pteroates for one-carbon metabolism. As expected for a compound that cannot support one-carbon metabolism, dihydropteroate was unable to rescue the folate deficiency of *folt-1*/RFC mutants grown on folate-depleted bacteria (Fig. 3.7B).

Significantly, dihydropteroate stimulated increased EdU incorporation in isolated germ cells and tumor frequency, although it was less active than 5,10-methenyl-THF-Glu_6 in inducing the proliferation of isolated germ cells (Figs 3.7C,D; 3.S5G). The ability of dihydropteroate to stimulate germ cell proliferation implies that the stimulation occurs independently of one-carbon metabolism.

The folate receptor homolog FOLR-1 is required for the stimulation of germ cell proliferation

The mammalian FRs, α, β, and γ, transport folates, but have more restricted tissue expression than RFC [30]. Notably, mammalian FR can bind both folates and pteroates [34]. *C. elegans* contains an apparent ortholog of FR, *folr-1* (C17G1.1). Although FOLR-1/FR and human FRγ proteins only share 12% identity and 25.5% similarity, they are the top scores in the two respective species using reciprocal psi-BLAST searches [35]. FOLR-1/FR has a predicted signal peptide and transmembrane domain that is compatible with cell surface localization [36, 37].

In contrast to *folt-1*/RFC mutants, RNAi depletion of *folr-1*/FR does not appear to affect the basal number of germ cells, and *folr-1(RNAi)* hermaphrodites lay the same number of eggs as wild type (Fig. 3.S7A). This suggests that unlike FOLT-1/RFC, FOLR-1/FR is not essential for the uptake of folates to function as vitamins. Strikingly, RNAi depletion of *folr-1*/FR abolishes the stimulatory effect of purified bacterial folates, 10-formyl-THF-Glu_6, 5,10-methenyl-THF-$Glu_{1,6}$, and dihydropteroate both in vivo (for tumor frequency) and in vitro (for EdU incorporation) (Figs 3.7E,F, 3.S7B). At the fully non-permissive temperature of 25°C, *folr-1*/FR RNAi only modestly suppresses tumor

formation in *glp-1(gf)*; *cki-2*; *daf-16* mutants, but blocks the response to PABA supplementation, indicating that it still blocks the stimulatory effect of folates (Fig. 3.S7C). These results suggest that both 10-formyl-THF-Glu_n and dihydropteroate stimulate germ cell proliferation through a FOLR-1-dependent pathway.

A folate-enriched diet increases cell number in somatic hyperplasia

We wanted to determine if bacterial folates could stimulate somatic cell division using the *cul-1* mutant, which exhibits hyperplasia of larval somatic cell lineages [38]. *cul-1(e1756)* mutants expressing a hypodermal seam cell GFP marker were fed diets of OP50 or OP50 supplemented with 10 μM PABA. Both *cul-1* homozygous and heterozygous mutants exhibited increased seam cell numbers when on the diet supplemented with PABA (Fig. 3.3G). Notably, the hyperplasia in *cul-1* heterozygotes is a synthetic phenotype, as *cul-1* heterozygotes do not exhibit hyperplasia under normal growth conditions [38] and wild-type animals do not exhibit seam cell hyperplasia on a diet of OP50 supplemented with PABA (Fig. 3.3G).

We were unable to use heat-killed bacteria to assess the effect of pure folates or pteroates because *cul-1* homozygotes arrest development on heat-killed bacteria, and *cul-1* heterozygotes do not exhibit hyperplasia on heat-killed bacteria with added folates, potentially due to the sub-optimal diet (data not shown). Nevertheless, these results suggest that a diet with increased bacterial folates can stimulate the proliferation of a somatic cell lineage.

Discussion

In this study, we describe the first primary culture system for *C. elegans* germ cells. The CeM1 medium that we created differs markedly from the L-15-based medium used for *C. elegans* embryonic and larval cell cultures. CeM1 medium can maintain the viability of germ cells for up to one month, thereby providing an experimental platform for the study of nearly homogeneous populations of germ cells.

10-formyl-THF-Glu_n is a germ cell-stimulatory folate

Our results show that bacterial folates act as an exogenous signal to stimulate an adult stem cell population. Surprisingly, many folate species (folic acid, THF, 5-formyl-THF, and 5-methyl-THF) are unable to stimulate germ cells under normal growth conditions, despite the fact that these folates are readily taken up by animals, including *C. elegans* [31]. Instead, we observed germ cell stimulatory activity only with the folates 10-formyl-THF-Glu_n and 5,10-methenyl-THF-Glu_n, with increasing activity with larger numbers of poly-Glu. The ability of 5,10-methenyl-THF-Glu_n to stimulate germ cells is unlikely to reflect its own activity, as it converts to 10-formyl-THF-Glu_n within minutes at the neutral pH used in our experiments.

Bacterial folates and related compounds can stimulate *C. elegans* germ cells independently of one-carbon metabolism

We observed that the non-stimulatory folate S-5-formyl-THF-Glu_1 rescued the folate deficiency of folate-depleted *folt-1*/RFC mutant germ cells more effectively than the

stimulatory folate 5,10-methenyl-THF-Glu_1. This suggests that the ability of a folate to act as a vitamin does not correlate with its ability to stimulate germ cell proliferation under normal growth conditions. Additionally, 10-formyl-THF-Glu_n can stimulate *C. elegans* germ cell proliferation at a concentration of 1 nM, which is lower than the levels required for one-carbon metabolism in mammals [39, 40].

Dihydropteroate can also stimulate germ cell proliferation. Dihydropteroate is unable to function in one-carbon metabolism in animal cells, and consistently, its addition was unable to rescue folate deficiency in *C. elegans*. Significantly, the stimulation of germ cell proliferation by both dihydropteroate and 10-formyl-THF-Glu_n requires the presence of FOLR-1/FR. The mammalian homolog of FOLR-1/FR can bind both folates and pteroates [34]. These results suggest that dihydropteroate and 10-formyl-THF-Glu_n stimulate germ cell proliferation through a FOLR-1/FR-dependent pathway that is independent of one-carbon metabolism.

Dihydropteroate is present in all bacteria that are capable of *de novo* folate biosynthesis. However, we did not observe detectable levels of dihydropteroate by chromatography in extracts from the three bacteria (data not shown). This suggests that in these three bacteria, dihydropteroate is not the predominant germ cell stimulatory signal, with 10-formyl-THF-Glu_n and 5,10-methenyl-THF-Glu_n present at much higher levels. It is possible that in the wild, other bacteria produce higher levels of dihydropteroate that contribute to the stimulation of *C. elegans* germ cell proliferation.

One obvious question is why 10-formyl-THF and dihydropteroate, but not other folates, were selected during evolution to regulate germ cell proliferation. In this regard, it is notable that 10-formyl-THF and dihydropteroate are particularly unstable relative to

other folates and folate-related compounds ([41] Schircks Laboratories data sheets). Potentially, the labile nature of these folate and folate-related compounds allows a tighter linkage between the presence of live bacteria and germ cell proliferation.

The folate receptor and signaling

The finding that FOLR-1/FR is required for the stimulation of *C. elegans* germ cell proliferation is interesting in light of recent mammalian cancer research. In many cancers, FRs are overexpressed, and this is associated with neoplastic progression and poor prognosis [42]. FRα promotes proliferation, migration, and invasiveness of SKOV-3 ovarian cancer cells, which have high-level FRα expression; while surprisingly, RFC acts oppositely to reduce cell proliferation, migration, and invasiveness [43]. Notably, FRα only contributes 20-30% of the uptake of folate in SKOV-3 and four other ovarian cancer cell lines, while RFC is responsible for ~70% of their folate uptake [44]. Similarly, in *C. elegans*, FOLT-1/RFC is required for the majority of folate uptake to allow basal germ cell proliferation and fertility, while FOLR-1/FR is required for stimulatory folate signaling but is not essential for providing folates for basal germ cell proliferation.

Recent emerging evidence suggests the potential for human FR to function in cell signaling independently of one-carbon metabolism. The addition of folates to cells activates intracellular signaling pathways in a FR-dependent manner in time periods that are shorter than would be expected from changes in one-carbon metabolism. The addition of folic acid to mammalian cells has been reported to induce the phospho-activation of c-src tyrosine kinase, ERK kinase, and STAT transcription factor in a FRα-dependent manner within 2-5 minutes of stimulation [45-47]. Additionally, FRα itself has been

reported to translocate to the nucleus and function as a transcription factor in human tissue culture cells after stimulation with 453 μM of folic acid [48]. These studies used folic acid, a non-natural, synthetic folate, at elevated, non-physiological levels of 10 to 600 μM. These concentrations are orders of magnitude higher than the concentration of folates in human serum, which are 8.6 to 29.7 nM for the 5^{th}-95^{th} percentiles of an unsupplemented population [49]. This raises the question of the physiological relevance of the observations. In contrast, our results show biological effects with 1 nM of a specific, naturally-available folate.

Our work provides a direct link between microbial factors and the regulation of an adult stem cell population. The importance of the microbiota for animal health has recently been recognized [50]. Microbiota-derived folates are readily absorbed by the human host [51]. In diverse human populations, the initial colonization of the gut is enriched for microbes capable of *de novo* folate synthesis, indicating that humans harbor folate-synthesizing bacteria throughout their lifespan [52]. We observed that folates isolated from mouse microbiota are potent stimulators of *C. elegans* germ cells, indicating that the active folates are present at high levels in the mammalian microbiota. Our work therefore suggests the possibility that microbiota-derived folates can act as signaling molecules, potentially to the host or to other organisms that may reside within the host, such as parasitic nematodes.

Experimental Procedures

CeM1 medium preparation

CeM1 medium was prepared with the ingredients listed in Table 3.S1. CeM1 was sterile filtered through 0.22 μm 150 ml filter units (Millipore). Three sequential treatments were performed on the FBS prior to its inclusion in CeM1: heat inactivation; and treatments with Amberlite IRA 400-CL and charcoal-dextran (see Supplemental Experimental Procedures).

Germ cell isolation and primary culture

To obtain synchronous adult germline tumorous mutants, eggs were isolated by sodium hypochlorite treatment [53]. The eggs were transferred to a 3xNGM plate (an NGM agar plate [53] with 3x peptone concentration) with a lawn of OP50 bacteria and grown at 25°C for four days to ensure that all animals became adults with germline tumors. The animals were washed four times with M9 salt solution [53] in 15 ml polystyrene tubes (Falcon) to remove live bacteria and transferred to a 12.5 cm^2 cell culture flask (Corning) containing 2.5 ml of M9 solution supplemented with: heat-killed OP50 bacteria; 200 units penicillin and 0.2 mg streptomycin per ml); 25 μg/ml tetracycline (Sigma-Aldrich, 87128); 34 μg/ml chloramphenicol (Research Products International); 50 μg/ml kanamycin; 0.02% normocin; and 5 μg/ml cholesterol. Animals were incubated overnight in the antibiotic-supplemented M9 solution. The next day, animals were washed four times with phosphate buffered saline (PBS) in 15 ml polystyrene tubes, washed one time with CeM1, and then resuspended in 2 ml of CeM1 in a 35 mm tissue culture dish (Falcon). Animals were

transferred with a platinum wire to a 120 µl spot of CeM1 in another 35 mm culture dish. Germ cells were released by cutting animals into quarters using 31 gauge needles (Becton Dickinson). Cells were collected with three sequential washes with 1 ml of CeM1, collected into a 15ml polypropylene tube and spun at 300-1000 rpm for 1 min to pellet body parts and large cell aggregates. The supernatant was transferred to a new 15 ml tube and spun at 2000 rpm for 5 min to pellet individual cells. The cells were resuspended in full CeM1 (unless otherwise stated) and transferred to a tissue culture dish. If multi-well tissue culture dishes were used, the outer wells were filled with PBS to keep the inner wells humidified, then sealed with parafilm to prevent loss of moisture, and incubated at 25°C.

Bacterial Extract

Bacteria were grown overnight in 2xYT medium that was either unsupplemented for OP50, or supplemented with 25 µg/ml tetracycline for HT115, or 100 µg/ml streptomycin for DA1877. The bacteria were collected by centrifugation at 4000 rpm for 30 min at 4°C, washed two times with sterile 0.9% NaCl, and the bacterial pellet was frozen at -80°C. Bacterial pellets were lyophilized under vacuum at room temperature. Crushed bacterial pellet was added at 0.08 g/ml to folate-extraction buffer (1% Na ascorbate, 20 mM phosphate buffer, pH 6.5), vortexed, and rotated at room temperature in the dark for 1 hr. The bacteria were spun out in a microcentrifuge at 13,300 rpm for 15 min. The supernatant was transferred to a new microcentrifuge tube and extracted once with 1:1 phenol:choloroform and three times with chloroform to remove proteins; spun out and transferred to a new tube to remove any residual chloroform, and then sterile filtered using

a 0.2 μm syringe filter. The bacterial extract used in Fig. 3.2E was prepared with water instead of folate-extraction buffer and was used immediately after preparation.

Tumor frequency assay

Eggs isolated by sodium hypochlorite treatment were placed on 1x NGM plates seeded with live bacteria or heat-killed OP50 bacteria with the indicated experimental additives. Assays with live bacteria were performed at the semi-permissive temperature of 18°C; assays with heat-killed bacteria were performed at 20°C. L4-stage animals were transferred onto fresh plates, and the percentages of adult animals with tumors were scored two days later by observation with a dissecting microscope. Tumor frequency assays were performed in triplicate with ~100 animals per replicate. Several tumor frequency assays were performed blind, including Figs 3.6B, 3.7D, 3.S5E, and 3.S5F. The supplements trimethoprim (cat. no. 92131) and PABA (100536) were from Sigma-Aldrich; vitamin B12 (103278) was from MP Biomedicals.

Counts of live isolated germ cells

Counts of live isolated germ cells were performed with the live-cell stain calcein-AM and dead-cell stain ethidium homodimer [54]. The numbers of live cells were obtained by counting cells stained with 1 μM calcein-AM (Sigma-Aldrich, C1359), 0.1 μM Ethidium homodimer (Sigma-Aldrich, E1903), and with or without 2 μg/ml Hoechst 33342 (Sigma-Aldrich, B2261). A minimum of three counts were made for each sample using a cellometer counting grid (CP2, Nexcelom Bioscience LLC) analyzed with an inverted fluorescence microscope (Zeiss Axio Observer.A1); cell count variation is presented as

SEM. Typically, germ cells were isolated from 25 adult hermaphrodites for 0.5 ml/well of a 24-well plate.

Counts of germ cells in mid-L4-stage larvae

Counts of germ cells in mid-L4-stage larvae were performed with animals fixed with 95% ethanol for 10 min as described [55], and then stained with 2 µg/ml Hoechst 33342 in PBS. Germ cell counts were performed blind, with the identity of the treatment masked. The germ cells in one gonad arm per animal were counted. Mid-L4-stage larvae were identified based on vulva morphology. Larvae selected for germ cell counts had vulva morphologies categorized as L4.1 to L4.3 on the L4.0–L4.9 vulval morphology scale that has been previously defined [56]. For Fig. 3.7B, between 9 and 17 animals were analyzed per condition.

EdU-incorporation assay

Isolated germ cells from *glp-1(gf)*; *cki-2*; *daf-16* mutant adults were incubated in 80 µl of CeM1 in a 96-well plate, with the germ cells from approximately eight adults per well. 24 hr post-isolation, EdU was added to a concentration of 20 µM. At 48 hr post-isolation, cells were harvested and processed with the Click-iT Alexa Fluor 488 Imaging kit (Life Technologies), according to the manufacturer's instructions. Cells were subsequently stained with 2 µg/ml Hoechst 33342 DNA stain and analyzed by fluorescence microscopy for EdU staining of DNA, with images of EdU Alexa Fluor 488 staining taken initially, and then images of Hoechst staining taken subsequently. Typically, 150-200 cells were counted for each condition.

Folate analysis

Folates for chromatography analysis were prepared as follows. Lyophilized bacteria were resuspended at a concentration of 0.09-0.1 mg/ml in folate-extraction buffer (2% sodium ascorbate, 0.05 M 2-mercaptoethanol), boiled for 15 min, then spun in a centrifuge at 30,000xg for 30 min to remove insoluble components. Aliquots (2 ml) of the supernatants were mixed with 18 ml of potassium phosphate buffer containing 1% sodium ascorbate. Purified folates were isolated by passage through affinity columns (2.4 ml bed volume) containing purified milk folate-binding protein which was immobilized to a Sepharose matrix [28].

For HPLC detection of folate species, 250 µl of the purified folate was mixed with 1% sodium ascorbate, 0.01 M potassium phosphate pH 7.5. A 0.9 ml aliquot was injected into a 4.6x250 mm Betasil Phenyl analytic column and eluted under acid conditions using acetonitrile gradient and detection by UV, fluorescence, and electrochemical signals [57] (data not shown). The use of multisignaling allowed better identification of the various peaks that were eluted from the column.

The microbial assay was used to determine folate concentration. Purified extract was treated with conjugase using the tri-enzyme system, as described [58], and folate was then analyzed using 96 well plates, as described [59].

Statistical analysis

Two-tailed Student's t-test was used to analyze the three replicates of tumor frequencies, the data for mitotic index, numbers of germ cell nuclei per proliferative zone, egg numbers per animal, and the number of germ cells per gonad arm. The chi-squares test was used to

analyze the percentages of EdU positive cells. The nonparametric Mann-Whitney test was used to analyze the number of phosphohistone H3 positive cells per gonad arm. All error bars reflect standard error of the mean (SEM).

Additional methods are provided in the Supplemental Information.

Author Contributions

Conceptualization, E.T.K. and J.S.; Methodology, E.T.K. and J.S.; Investigation, S.N.C., M.M., A.S.V., G.B., M.M.R., C.N., and E.T.K.; Resources, J.S.; Writing – Original Draft, E.T.K. and J.S.; Writing – Review and Editing, S.N.C., M.M., E.T.K., J.S., M.M.R., and L.P.; Visualization, M.M. and S.N.C.; Supervision, E.T.K., J.S., and L.P.; Funding Acquisition, E.T.K. and J.S.

Acknowledgements

We thank M.J. McEachern and members of the Kipreos lab for critical comments on the manuscript, M.C. Zetka, D.B. Hausman, and S. Dougan for reagents or resources. Some *C. elegans* strains were provided by the CGC, which is funded by NIH Office of Research Infrastructure Programs (P40 OD010440). This work was supported by grants from NSF (MCB-1138454) and NIH/NIGMS (1R01GM074212) (ETK), and support from United States Department of Agriculture cooperative agreement 51520-008-04S (JS). Any opinions, findings, conclusion, or recommendations expressed in this publication are those

of the authors and do not necessarily reflect the view of the United States Department of Agriculture.

References

1. Hansen, D. and T. Schedl, *Stem cell proliferation versus meiotic fate decision in Caenorhabditis elegans.* Adv Exp Med Biol, 2013. **757**: p. 71-99.
2. Christensen, M., et al., *A primary culture system for functional analysis of C. elegans neurons and muscle cells.* Neuron, 2002. **33**(4): p. 503-14.
3. Michaelson, D., et al., *Insulin signaling promotes germline proliferation in C. elegans.* Development, 2010. **137**(4): p. 671-80.
4. Selhub, J., *Folate, vitamin B12 and vitamin B6 and one carbon metabolism.* J Nutr Health Aging, 2002. **6**(1): p. 39-42.
5. Stover, P. and V. Schirch, *Synthesis of (6S)-5-formyltetrahydropteroyl-polyglutamates and interconversion to other reduced pteroylpolyglutamate derivatives.* Anal Biochem, 1992. **202**(1): p. 82-8.
6. Matherly, L.H., Z. Hou, and Y. Deng, *Human reduced folate carrier: translation of basic biology to cancer etiology and therapy.* Cancer Metastasis Rev, 2007. **26**(1): p. 111-28.
7. Desmoulin, S.K., et al., *The human proton-coupled folate transporter: Biology and therapeutic applications to cancer.* Cancer Biol Ther, 2012. **13**(14): p. 1355-73.
8. Grapp, M., et al., *Choroid plexus transcytosis and exosome shuttling deliver folate into brain parenchyma.* Nat Commun, 2013. **4**: p. 2123.
9. Henderson, G.I., et al., *Maternal-to-fetal transfer of 5-methyltetrahydrofolate by the perfused human placental cotyledon: evidence for a concentrative role by*

placental folate receptors in fetal folate delivery. J Lab Clin Med, 1995. **126**(2): p. 184-203.

10. Selhub, J., et al., *Renal folate absorption and the kidney folate binding protein. I. Urinary clearance studies.* Am J Physiol, 1987. **252**(4 Pt 2): p. F750-6.
11. Rossi, M., A. Amaretti, and S. Raimondi, *Folate production by probiotic bacteria.* Nutrients, 2011. **3**(1): p. 118-34.
12. Austin, M.U., et al., *Knockout of the folate transporter folt-1 causes germline and somatic defects in C. elegans.* BMC Dev Biol, 2010. **10**: p. 46.
13. Pepper, A.S., D.J. Killian, and E.J. Hubbard, *Genetic analysis of Caenorhabditis elegans glp-1 mutants suggests receptor interaction or competition.* Genetics, 2003. **163**(1): p. 115-32.
14. Kalchhauser, I., et al., *FBF represses the Cip/Kip cell-cycle inhibitor CKI-2 to promote self-renewal of germline stem cells in C. elegans.* EMBO J, 2011. **30**(18): p. 3823-9.
15. Hendzel, M.J., et al., *Mitosis-specific phosphorylation of histone H3 initiates primarily within pericentromeric heterochromatin during G2 and spreads in an ordered fashion coincident with mitotic chromosome condensation.* Chromosoma, 1997. **106**: p. 348-360.
16. Hansen, D., E.J. Hubbard, and T. Schedl, *Multi-pathway control of the proliferation versus meiotic development decision in the Caenorhabditis elegans germline.* Dev Biol, 2004. **268**(2): p. 342-57.
17. Shim, Y.H., et al., *Role of cholesterol in germ-line development of Caenorhabditis elegans.* Mol Reprod Dev, 2002. **61**(3): p. 358-66.

18. Rao, A.U., et al., *Lack of heme synthesis in a free-living eukaryote.* Proc Natl Acad Sci U S A, 2005. **102**(12): p. 4270-5.

19. Wiedemann, M., et al., *Trennung von freien und proteingebundenen Steroiden mit Amberlite.* Fresenius' Zeitschrift für analytische Chemie, 1972. **261**(4-5): p. 382-385.

20. Leake, R.E., R.I. Freshney, and I. Munir, *Steroid response in vivo and in vitro*, in *Steroid hormones: a practical approach*, B. Green and R.E. Leake, Editors. 1987, IRL Press Limited: Oxford, England. p. 205-218.

21. Timmons, L. and A. Fire, *Specific interference by ingested dsRNA.* Nature, 1998. **395**(6705): p. 854.

22. MacNeil, L.T., et al., *Diet-induced developmental acceleration independent of TOR and insulin in C. elegans.* Cell, 2013. **153**(1): p. 240-52.

23. Virk, B., et al., *Excessive folate synthesis limits lifespan in the C. elegans: E. coli aging model.* BMC Biol, 2012. **10**: p. 67.

24. Gracida, X. and C.R. Eckmann, *Fertility and germline stem cell maintenance under different diets requires nhr-114/HNF4 in C. elegans.* Curr Biol, 2013. **23**(7): p. 607-13.

25. Watson, E., et al., *Interspecies systems biology uncovers metabolites affecting C. elegans gene expression and life history traits.* Cell, 2014. **156**(4): p. 759-70.

26. Sybesma, W., et al., *Effects of cultivation conditions on folate production by lactic acid bacteria.* Appl Environ Microbiol, 2003. **69**(8): p. 4542-8.

27. Kwon, Y.K., et al., *A domino effect in antifolate drug action in Escherichia coli.* Nat Chem Biol, 2008. **4**(10): p. 602-8.

28. Selhub, J., O. Ahmad, and I.H. Rosenberg, *Preparation and use of affinity columns with bovine milk folate-binding protein (FBP) covalently linked to Sepharose 4B.* Methods Enzymol, 1980. **66**: p. 686-90.

29. Martin, J.I., et al., *Application of a tri-enzyme extraction for total folate determination in foods.* J Assoc Off Anal Chem, 1990. **73**(5): p. 805-8.

30. Zhao, R., L.H. Matherly, and I.D. Goldman, *Membrane transporters and folate homeostasis: intestinal absorption and transport into systemic compartments and tissues.* Expert Rev Mol Med, 2009. **11**: p. e4.

31. Balamurugan, K., et al., *Cloning and functional characterization of a folate transporter from the nematode Caenorhabditis elegans.* Am J Physiol Cell Physiol, 2007. **293**(2): p. C670-81.

32. Roux, B. and C.T. Walsh, *p-Aminobenzoate synthesis in Escherichia coli: mutational analysis of three conserved amino acid residues of the amidotransferase PabA.* Biochemistry, 1993. **32**(14): p. 3763-8.

33. Virk, B., et al., *Folate Acts in E. coli to Accelerate C. elegans Aging Independently of Bacterial Biosynthesis.* Cell Rep, 2016. **14**(7): p. 1611-20.

34. Sodji, Q.H., et al., *Design and structure activity relationship of tumor-homing histone deacetylase inhibitors conjugated to folic and pteroic acids.* Eur J Med Chem, 2015. **96**: p. 340-59.

35. Altschul, S.F., et al., *Gapped BLAST and PSI-BLAST: a new generation of protein database search programs.* Nucleic Acids Res., 1997. **25**: p. 3389-3402.

36. Petersen, T.N., et al., *SignalP 4.0: discriminating signal peptides from transmembrane regions.* Nat Methods, 2011. **8**(10): p. 785-6.

37. Cserzo, M., et al., *On filtering false positive transmembrane protein predictions.* Protein Eng, 2002. **15**(9): p. 745-52.

38. Kipreos, E.T., et al., *cul-1 is required for cell cycle exit in C. elegans and identifies a novel gene family.* Cell, 1996. **85**(6): p. 829-39.

39. Neuhouser, M.L., et al., *Mathematical modeling predicts the effect of folate deficiency and excess on cancer-related biomarkers.* Cancer Epidemiol Biomarkers Prev, 2011. **20**(9): p. 1912-7.

40. Geng, Y., et al., *Folate deficiency impairs decidualization and alters methylation patterns of the genome in mice.* Mol Hum Reprod, 2015. **21**(11): p. 844-56.

41. Blakley, R.L., *The Biochemistry of Folic Acid and Related Pteridines*. Frontiers of Biology, ed. A. Neuberger and E.L. Tatum. 1969, Amsterdam, Netherlands: North-Holland Publishing Company. 569.

42. Kelemen, L.E., *The role of folate receptor alpha in cancer development, progression and treatment: cause, consequence or innocent bystander?* Int J Cancer, 2006. **119**(2): p. 243-50.

43. Siu, M.K., et al., *Paradoxical impact of two folate receptors, FRalpha and RFC, in ovarian cancer: effect on cell proliferation, invasion and clinical outcome.* PLoS One, 2012. **7**(11): p. e47201.

44. Corona, G., et al., *Role of folate receptor and reduced folate carrier in the transport of 5-methyltetrahydrofolic acid in human ovarian carcinoma cells.* Int J Cancer, 1998. **75**(1): p. 125-33.

45. Lin, S.Y., et al., *Folic acid inhibits endothelial cell proliferation through activating the cSrc/ERK 2/NF-kappaB/p53 pathway mediated by folic acid receptor.* Angiogenesis, 2012. **15**(4): p. 671-83.

46. Zhang, X.M., et al., *Folate stimulates ERK1/2 phosphorylation and cell proliferation in fetal neural stem cells.* Nutr Neurosci, 2009. **12**(5): p. 226-32.

47. Hansen, M.F., et al., *Folic acid mediates activation of the pro-oncogene STAT3 via the Folate Receptor alpha.* Cell Signal, 2015. **27**(7): p. 1356-68.

48. Boshnjaku, V., et al., *Nuclear localization of folate receptor alpha: a new role as a transcription factor.* Sci Rep, 2012. **2**: p. 980.

49. Hustad, S., et al., *Riboflavin as a determinant of plasma total homocysteine: effect modification by the methylenetetrahydrofolate reductase C677T polymorphism.* Clin Chem, 2000. **46**(8 Pt 1): p. 1065-71.

50. Clemente, J.C., et al., *The impact of the gut microbiota on human health: an integrative view.* Cell, 2012. **148**(6): p. 1258-70.

51. Camilo, E., et al., *Folate synthesized by bacteria in the human upper small intestine is assimilated by the host.* Gastroenterology, 1996. **110**(4): p. 991-8.

52. Yatsunenko, T., et al., *Human gut microbiome viewed across age and geography.* Nature, 2012. **486**(7402): p. 222-7.

53. Sulston, J. and J. Hodgkin, *Methods*, in *The Nematode Caenorhabditis elegans*, W.B. Wood, Editor. 1988, Cold Spring Harbor Laboratory: Cold Spring Harbor, New York. p. 587-606.

54. Zhang, S., D. Banerjee, and J.R. Kuhn, *Isolation and culture of larval cells from C. elegans.* PLoS One, 2011. **6**(4): p. e19505.

55. Killian, D.J. and E.J. Hubbard, *Caenorhabditis elegans germline patterning requires coordinated development of the somatic gonadal sheath and the germ line.* Dev Biol, 2005. **279**(2): p. 322-35.

56. Mok, D.Z., P.W. Sternberg, and T. Inoue, *Morphologically defined sub-stages of C. elegans vulval development in the fourth larval stage.* BMC Dev Biol, 2015. **15**: p. 26.

57. Bagley, P.J. and J. Selhub, *Analysis of folate form distribution by affinity followed by reversed- phase chromatography with electrical detection.* Clin Chem, 2000. **46**(3): p. 404-11.

58. Poo-Prieto, R., et al., *Use of the affinity/HPLC method for quantitative estimation of folic acid in enriched cereal-grain products.* J Nutr, 2006. **136**(12): p. 3079-83.

59. Tamura, T., L.E. Freeberg, and P.E. Cornwell, *Inhibition of EDTA of growth of Lactobacillus casei in the folate microbiological assay and its reversal by added manganese or iron.* Clin Chem, 1990. **36**(11): p. 1993.

60. Zhao, R. and I.D. Goldman, *Resistance to antifolates.* Oncogene, 2003. **22**(47): p. 7431-57.

Supplemental Experimental Procedures

Treatment of FBS prior to inclusion in CeM1 medium

Three sequential treatments were performed on FBS prior to its inclusion in CeM1 medium. FBS was heat inactivated by incubation at 56°C or 65°C for 30 minutes. The FBS was then incubated with 50 mg/ml of the strongly basic resin Amberlite IRA 400-CL (Sigma-Aldrich, 247669) that had been prewashed in water, on a rotator for 4-6 hours at room temperature. The FBS was separated from the beads by centrifugation, transferred to a fresh tube, and incubated with a second round of 50 mg/ml Amberlite IRA 400-CL beads overnight at 4°C. After separating the FBS from the Amberlite IRA 400-CL beads, the FBS was rotated with 100 mg/ml charcoal-dextran (Sigma-Aldrich, C6241) overnight at 4°C. The charcoal-dextran was removed by two sequential centrifugations at 3500 rpm for 30 min, 4°C. For all experiments, unless otherwise specified, FBS was heat-inactivated and treated with Amberlite IRA 400-CL and charcoal-dextran. We have observed differences in the performance of FBS lots, similar to what is observed in the cell culture of many other species (data not shown).

C. elegans and bacterial strains

The following *C. elegans* strains were used: wild type (N2), *glp-1(ar202)* (GC143); *glp-1(ar202)*; *cki-2(ok2105)*; *daf-16(mu86)* (ET507); *unc-119(e2498::Tc1)*; *wIs51*[scm::GFP; *unc-119(+)*] (JR667); *cul-1(e1756)*/*unc-69(e587)*; *him-5(e1490)*; *wIs51* (ET350); and *folt-1(ok1460)*/nT1 [*qIs51*] (VC959). Strains with *glp-1(ar202)* mutants were maintained at 16°C; wild-type animals were maintained at 20°C, using established methods [1].

Unless otherwise stated, eggs for experiments came from hermaphrodites grown on live OP50 bacteria.

The following bacteria were acquired from the *Caenorhabditis* Genetics Center: *E. coli* OP50; *E. coli* HT115(DE3) [*F-, mcrA, mcrB, IN(rrnD-rrnE)1, rnc14::Tn10(DE3 lysogen: lavUV5 promoter -T7 polymerase*]; and *Comamonas aquatica* DA1877. HT115(DE3) is tetracycline resistant. DA1877 is streptomycin resistant. The following bacteria strains were obtained from the *Coli* Genetics Stock Center: JW1082-7 [F-, *Δ(araD-araB)567, ΔlacZ4787(::rrnB-3), λ⁻, ΔpabC760::kan, rph-1, Δ(rhaD-rhaB)568, hsdR514*]; and BW25113 [F-, *Δ(araD-araB)567*, *ΔlacZ4787*(::rrnB-3), *λ⁻*, *rph-1*, *Δ(rhaD-rhaB)568*, *hsdR514*]. Growth of *pabC* mutants (JW1082-7) under folate-deficient conditions utilized glucose minimal medium [2].

Preparation of animals for germ cell isolation

To obtain synchronous adult germline tumorous mutants, eggs were isolated by sodium hypochlorite treatment [1]. The eggs were transferred to a 3xNGM plate (an NGM agar plate [1] with 3x peptone concentration) with a lawn of OP50 bacteria and grown at 25°C for four days to ensure that all animals became adults with germline tumors. The animals were washed four times with M9 salt solution [1] in 15 ml polystyrene tubes (Falcon) to remove live bacteria and transferred to heat-killed OP50 bacteria plates, which were created by placing OP50-seeded 3xNGM plates at 62-67°C for 24 hr. After two (or more) hours on the heat-killed bacteria plate, the animals were transferred to a 12.5 cm^2 cell culture flask (Corning) containing 2.5 ml of M9 solution supplemented with: heat-

killed OP50 bacteria; 200 units penicillin and 0.2 mg streptomycin per ml); 25 µg/ml tetracycline (Sigma-Aldrich, 87128); 34 µg/ml chloramphenicol (Research Products International); 50 µg/ml kanamycin; 0.02% normocin; and 5 µg/ml cholesterol. Animals were incubated overnight in the antibiotic-supplemented M9 solution.

Folate analysis

After passage of bacterial extract onto the folate-binding protein affinity column (described in Methods), effluents were collected separately and the column was subsequently washed with one volume of 0.1 M potassium phosphate buffer pH 7.4, and the effluent was added to the first effluent. The column was subsequently washed with 10 volumes of the same buffer, then with 5 volumes of 2 mM potassium phosphate buffer pH 7.4 to rid the column of the high salt buffer. Folate bound to the columns was then eluted with 20 mM trifluoroacetic acid into tubes that contained 10 µl of 10 mM dithiothreitol (DTT) and 1 M dipotassium phosphate to neutralize the acid and protect the eluted folate from oxidation.

The affinity chromatography utilizes the high affinity (Kd = 10^{-9} - 10^{-11} M) folate binding protein, which was purified to almost homogeneity [3-5] to purify and concentrate biological folate. The affinity column has been used to purify folates from: diverse tissues from different animals (liver, kidney, brain, blood, etc.) that were exposed to different conditions; more than 100 food products; and blood and plasma (for examples, see [6-8]. When sufficient concentration permitted, subsequent fractionation of these affinity-purified extracts was accompanied by detection of peak activities by UV

absorption, which revealed spectra that were specific for folate; there were no other peaks. When the concentration did not permit the use of UV absorption, we used an ESA CoulArray electrochemical detector consisting of four flow-through, porous-carbon graphite coulometric electrodes, each set at incrementally higher potentials. The different potentials allowed us to distinguish between different forms of folates, and at the same time increase the sensitivity of detection by more than one order of magnitude. We used this method to analyze thousands of human plasma samples to detect unmetabolized folic acid and other folates. In these analyses, only two activity peaks were detected, 5-methyl-THF and folic acid, no other peaks were detected by the electrochemical detector, UV absorbance, fluorescence, or other means [9, 10]. These results suggest that it is highly unlikely that other compounds coelute with folate at significant levels from the affinity column.

The following basic folates and pteroates were used: 5-formyl-5,6,7,8-tetrahydrofolic acid (Sigma); (6S)-5-formyl-5,6,7,8-tetrahydrofolic acid (Schircks Laboratories); 5-methyl-5,6,7,8-tetrahydrofolic acid (Merck); (6S)-5-methyl-5,6,7,8-tetrahydrofolic acid (Schircks Laboratories); 5,6,7,8-tetrahydrofolic acid (Merck); and 7,8-dihydropteroic acid (Schircks Laboratories). 5,10-methenyl-5,6,7,8-tetrahydrofolic acid and 10-formyl-5,6,7,8-tetrahydrofolic acid were synthesized from 5-formyl-5,6,7,8-tetrahydrofolic acid as described [11]. The creation of Glu1, 3, and 6 folate derivatives is described in the section below. For consistency, we will refer to the number of Glu in all folates by a subscript number, so for example, folic acid-Glu_3 contains three Glu residues. For tumor

frequency assays, the folates and other compounds were added to the agar plates when the plates were poured, after allowing the agar to cool to ~47°C prior to addition.

Interconversion of folates during analysis

In the analysis of bacterial folate species shown in Fig. 3.S6, the folates were isolated from bacteria at pH 7.0 and separated by ion-pair chromatography, also at pH 7.0. At this neutral pH, 5,10-methenyl-THF will convert predominantly to 10-formyl-THF, and to some extent 5-formyl-THF. For the separation (and subsequent purification) of folates from DA1877 (Fig. 3.5A), folates were isolated from bacteria at neutral pH and then purified by ion-pair chromatography at neutral pH. This isolated mixture of folates was then separated by reverse-phase chromatography at acid pH to allow the isolation of individual folates. In the initial purification with ion-pair chromatography, 5,10-methenyl-THF would convert predominantly to 10-formyl-THF (with potential conversion to 5-formyl-THF). In the subsequent reverse-phase chromatography at acid pH, 10-formyl-THF and 5-formyl-THF would convert to 5,10-methenyl-THF. In all chromatographic analyses undertaken, 5,10-methylene-THF, if present in the bacterial extract, may have converted to THF as a result of the chromatography process [12].

Synthesis of reduced monoglutamyl and polyglutamyl folates

Reduced folates were prepared as described previously [13]. Aliquots of 50 nmoles in 800 µl water of pteroylglutamates (folic acids) with 1, 3, and 6 glutamate residues ($PteGlu_1$, $PteGlu_3$, and $PteGlu_6$, Schircks Laboratories, Switzerland), were reduced to the corresponding tetrahydro-pteroylglutamates ($H_4PteGlu_n$) by potassium borohydride in

presence of PtO as a catalyst. 0.3 ml aliquots from these solutions were used to synthesize the corresponding 5-methylH_4PteGlu$_n$ after incubation with formaldehyde and reduction with potassium borohydride for 1 hr at 37°C. Second 0.3 ml aliquots were used for the synthesis of the corresponding 10-formylH_4PteGlu$_n$. These were mixed with 2 ml formic acid (88%) in the presence of 0.1 M DTE and incubated under nitrogen for 1 hr at 37°C. Excess formic acid was removed by vacuum evaporation, and an aliquot of the remaining solution was brought to pH 8.3 for converting the 5,10-methenylH_4PteGlu$_n$ to the corresponding 10-formyl- derivatives. The purity of the products was determined by ion-pair HPLC and spectral analysis with a diode array detector [13].

Isolation of individual folate species from bacteria

Lyophilized DA1877 bacteria were heat extracted by boiling for 15 min in 2% sodium ascorbate. After centrifugation, folates in the supernatant were purified by affinity chromatography using highly-purified milk folate binding protein bound to Sepharose [14]. The affinity purified folate was then fractionated by ion-pair chromatography, which separates folates into clusters each with the same number of glutamate residues [13]. Fractions from same cluster were combined, vacuum evaporated to remove acetonitrile, and passed through a C18 Sep Pack cartridge, which retains all folates in the combined fractions. The cartridge was then washed with 5 ml of acid (pH 3.0) solution, and then eluted from the cartridge with 1 ml of methanol containing 10 mM dithioerythritol (DTE). The eluate was evaporated to dryness, reconstituted with a pH 7.0 buffer solution containing 10 mM DTE, and fractionated with HPLC using an acetonitrile gradient elution at acid pH (2.6) [15]. In this method, folates are separated on the basis of

their pteridine ring structure (Fig. 3.5A) thus allowing the collection of separate forms of folate.

In the procedure used to collect folate fractions, 5,10-methenyl-THF (if present in bacteria) would be converted (due to the neutral pH used) predominantly to 10-formyl-THF and, to some extent, 5-formyl-THF. Additionally chromatography causes 5,10-methylene-THF to convert to THF [12].

RNA interference

Feeding RNAi was performed as described [16]. Feeding-RNAi constructs, expressed in HT115(DE3) bacteria, were obtained from the Ahringer library [17]. Overnight cultures of RNAi-feeding bacteria in LB medium were induced the next day on NGM agar plates containing 1mM IPTG and 100 μg/ml carbenicillin. Eggs or synchronized L1 larvae were placed on the RNAi plates and adults were scored for tumor frequency assay or harvested for analysis of mitotic germ cell numbers, or EdU incorporation assays with isolated germ cells.

Immunofluorescence and analysis of mitotic germ cell numbers

For the analysis of mitotic germ cell numbers, eggs were isolated by sodium hypochlorite treatment [1] of gravid adults. Synchronized L1-stage larvae were isolated by placing the eggs in M9 solution with 0.5 μg/ml cholesterol and incubating overnight at 25°C. The L1 larvae were placed on NGM agar plates with the indicated additives and live or heat-killed bacteria at 20°C. Plates seeded with heat-killed OP50 bacteria contained 100

µg/ml carbenicillin and 25 µg/ml tetracycline to prevent growth of any possible bacterial contaminants. After development to the young adult stage, hermaphrodites (without eggs) were segregated onto new plates and cultured for 36 hr. Gonads were dissected from animals 36 hr-post adulthood. To harvest gonads, adults were placed in 20 µl of PBS containing 0.875 mM tetramisole (Sigma). Animals were cut behind the pharynx using 21g syringe needles to extract the gonad. Using a glass Pasteur pipette, extracted gonads were collected in 1.5 ml pre-lubricated micro-centrifuge tubes and fixed by incubation with 3% formaldehyde in 0.1 M K_2HPO_4 (pH 7.2) buffer for 1 hr at room temperature. Following fixation, the gonads were permeabilized by incubation with -20°C 100% methanol for 5 min. Gonads were blocked in PBT (PBS + 0.1% Tween-20) with 0.5% bovine serum albumin (BSA, Fisher) for 30 min at room temperature, and then incubated with anti-phosphohistone H3 (Ser10) antibody (Cell Signaling; 1:200 dilution) in PBT + 0.5% BSA overnight at 4°C. Samples were washed 3 times in PBT; incubated with Dylight 488 Goat anti-rabbit secondary antibody (Thermo Scientific Pierce; 1:500) in PBT + 0.5% BSA for 2 hr at room temperature; then washed 3 times with PBT. DNA was stained with 1 µg/ml Hoechst 33342. Extracted gonads were mounted on slides with 90% glycerol and 1 mg/ml p-phenylenediamine (Sigma) and visualized using a Zeiss Axioskop microscope. The number of nuclei in the proliferative zone was determined by counting mitotic nuclei based on morphology [18], using image stacks of dissected gonads stained with Hoechst 33342. The Image J plugin program Point Picker was used to assist in germ cell counts (http://bigwww.epfl.ch/thevenaz/pointpicker/).

For Figure 3.1B, wild-type and *glp-1(gf)*; *cki-2*; *daf-16* mutant animals were harvested by hypochlorite treatment and eggs were placed on 1X NGM plates and grown at 25°C for 3 days. Gonads were dissected and fixed as described above. Gonads were incubated with anti-phosphohistone H3 (Ser-10) antibody (Cell Signaling; 1:200) and anti-HIM-3 antibody [19] (the kind gift of Monika C. Zetka; 1:200) in PBT + 0.5% BSA overnight at 4°C and processed as described above.

Analysis of seam cell numbers

Eggs from the strains JR667 and ET350 were isolated by sodium hypochlorite treatment and placed on live bacteria with 10 μM PABA or ethanol control. After 4 days at 20°C, adult hermaphrodites were analyzed for seam cell numbers. *cul-1(e1756)* homozygotes (strain ET350) do not become adults and were also analyzed as 4-day old larvae. Seam cell numbers were determined based on GFP epifluorescence on one lateral side of each of 10 animals per condition.

Supplemental References

1. Sulston, J. and J. Hodgkin, *Methods*, in *The Nematode Caenorhabditis elegans*, W.B. Wood, Editor. 1988, Cold Spring Harbor Laboratory: Cold Spring Harbor, New York. p. 587-606.
2. Shehata, T.E. and A.G. Marr, *Synchronous growth of enteric bacteria.* J Bacteriol, 1970. **103**(3): p. 789-92.
3. Selhub, J. and N. Grossowicz, *Chemical fixation of folate binding protein to activated sepharose.* FEBS Lett, 1973. **35**(1): p. 76-8.
4. Selhub, J., O. Ahmad, and I.H. Rosenberg, *Preparation and use of affinity columns with bovine milk folate-binding protein (FBP) covalently linked to Sepharose 4B.* Methods Enzymol, 1980. **66**: p. 686-90.
5. Selhub, J. and W.A. Franklin, *The folate-binding protein of rat kidney. Purification, properties, and cellular distribution.* J Biol Chem, 1984. **259**(10): p. 6601-6.
6. Poo-Prieto, R., et al., *Use of the affinity/HPLC method for quantitative estimation of folic acid in enriched cereal-grain products.* J Nutr, 2006. **136**(12): p. 3079-83.
7. Rong, N., et al., *Bacterially synthesized folate in rat large intestine is incorporated into host tissue folyl polyglutamates.* J Nutr, 1991. **121**(12): p. 1955-9.
8. Selhub, J., et al., *Effects of choline deficiency and methotrexate treatment upon liver folate content and distribution.* Cancer Res, 1991. **51**(1): p. 16-21.

9. Kalmbach, R., L. Paul, and J. Selhub, *Determination of unmetabolized folic acid in human plasma using affinity HPLC.* Am J Clin Nutr, 2011. **94**(1): p. 343S-347S.

10. Morris, M.S., et al., *Circulating unmetabolized folic acid and 5-methyltetrahydrofolate in relation to anemia, macrocytosis, and cognitive test performance in American seniors.* Am J Clin Nutr, 2010. **91**(6): p. 1733-44.

11. Stover, P. and V. Schirch, *Synthesis of (6S)-5-formyltetrahydropteroyl-polyglutamates and interconversion to other reduced pteroylpolyglutamate derivatives.* Anal Biochem, 1992. **202**(1): p. 82-8.

12. Horne, D.W., *High-performance liquid chromatographic measurement of 5,10-methylenetetrahydrofolate in liver.* Anal Biochem, 2001. **297**(2): p. 154-9.

13. Selhub, J., *Determination of tissue folate composition by affinity chromatography followed by high-pressure ion pair liquid chromatography.* Anal Biochem, 1989. **182**(1): p. 84-93.

14. Selhub, J., B. Darcy-Vrillon, and D. Fell, *Affinity chromatography of naturally occurring folate derivatives.* Anal Biochem, 1988. **168**(2): p. 247-51.

15. Bagley, P.J. and J. Selhub, *Analysis of folate form distribution by affinity followed by reversed- phase chromatography with electrical detection.* Clin Chem, 2000. **46**(3): p. 404-11.

16. Kamath, R.S. and J. Ahringer, *Genome-wide RNAi screening in Caenorhabditis elegans.* Methods, 2003. **30**(4): p. 313-21.

17. Kamath, R.S., et al., *Systematic functional analysis of the Caenorhabditis elegans genome using RNAi.* Nature, 2003. **421**(6920): p. 231-7.

18. Michaelson, D., et al., *Insulin signaling promotes germline proliferation in C. elegans.* Development, 2010. **137**(4): p. 671-80.

19. Zetka, M.C., et al., *Synapsis and chiasma formation in Caenorhabditis elegans require HIM-3, a meiotic chromosome core component that functions in chromosome segregation.* Genes Dev, 1999. **13**(17): p. 2258-70.

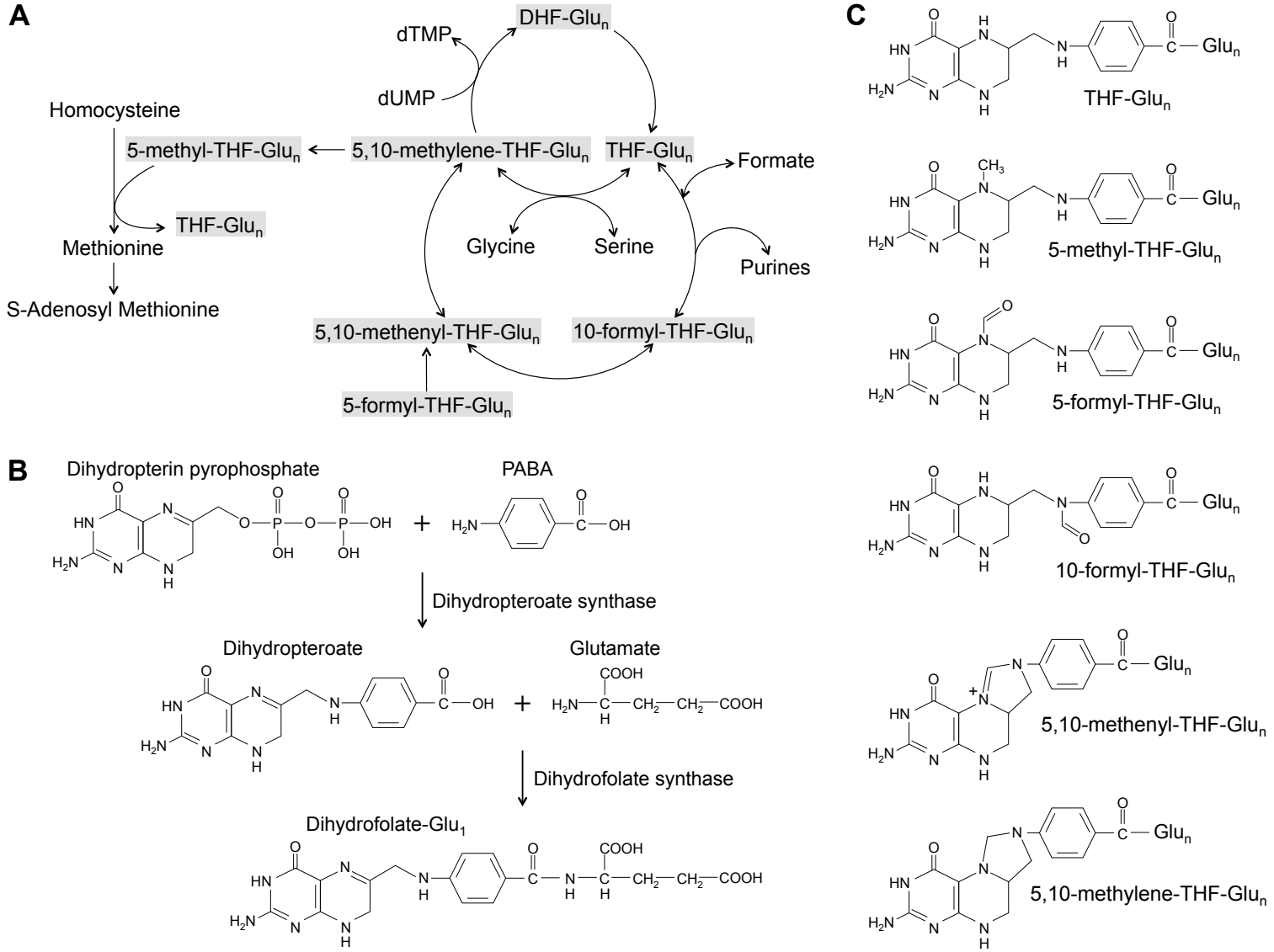
A
DHF-Glu$_n$
dTMP
dUMP
Homocysteine
5-methyl-THF-Glu$_n$
5,10-methylene-THF-Glu$_n$
THF-Glu$_n$
Formate
THF-Glu$_n$
Methionine
Glycine
Serine
Purines
S-Adenosyl Methionine
5,10-methenyl-THF-Glu$_n$
10-formyl-THF-Glu$_n$
5-formyl-THF-Glu$_n$
B
Dihydropterin pyrophosphate
PABA
Dihydropteroate synthase
Dihydropteroate
Glutamate
Dihydrofolate synthase
Dihydrofolate-Glu$_1$
C
THF-Glu$_n$
5-methyl-THF-Glu$_n$
5-formyl-THF-Glu$_n$
10-formyl-THF-Glu$_n$
5,10-methenyl-THF-Glu$_n$
5,10-methylene-THF-Glu$_n$

Figure 3.1. Partial one-carbon metabolism cycle and folate structures.

(A) Diagram of partial one-carbon metabolism cycle; modified from (Zhao and Goldman, 2003).

(B) Schematic of the last stages of folate biosynthesis in bacteria. The enzymatic reactions to create dihydrofolate (DHF) only occur in organisms that are capable of *de novo* folate synthesis.

(C) Structures of one-carbon metabolism folates. The bonds linking the PABA and Glu are shown in-line.

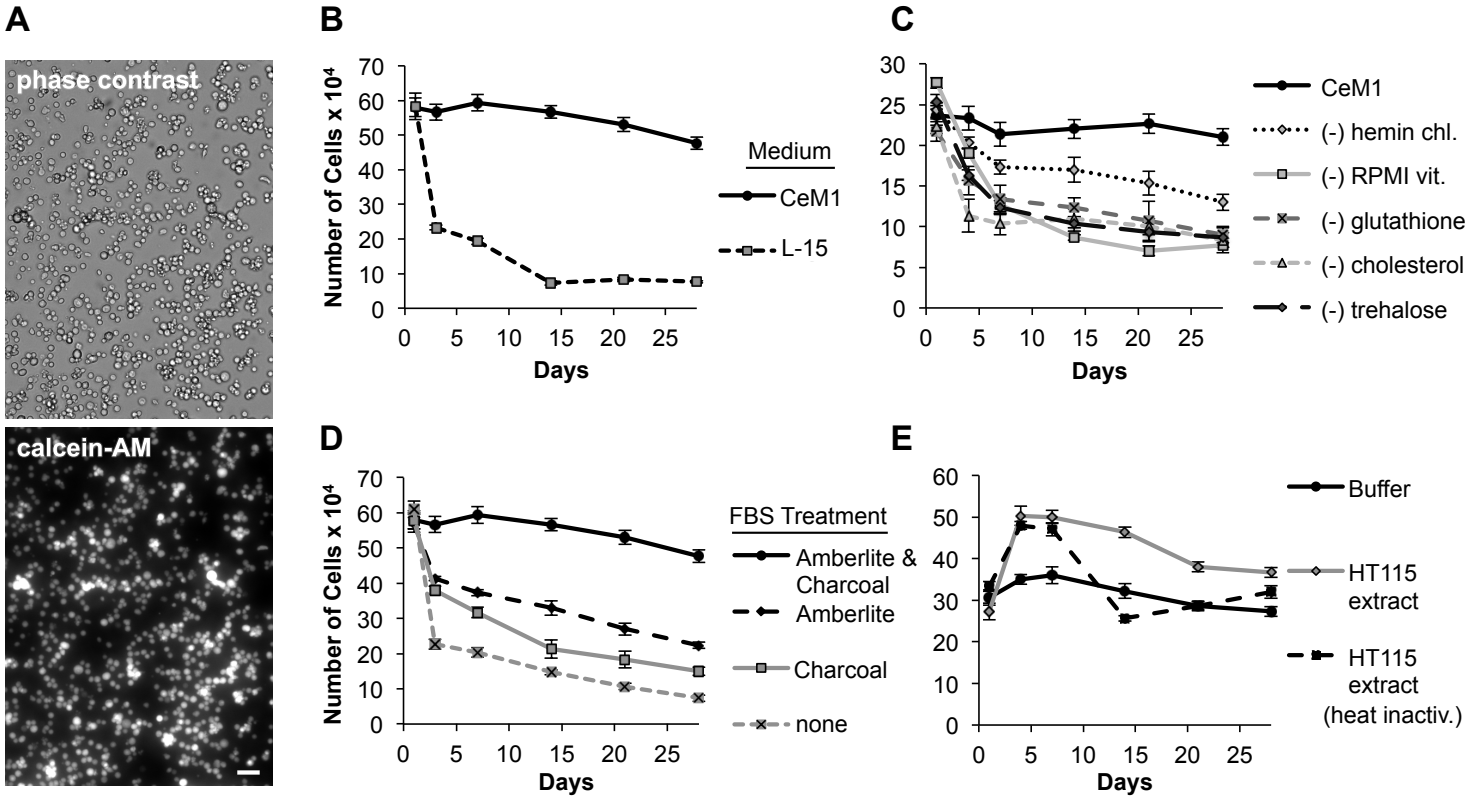
A
phase contrast
calcein-AM
B
Number of Cells x 10⁴
Days
Medium
CeM1
L-15
C
Days
CeM1
(-) hemin chl.
(-) RPMI vit.
(-) glutathione
(-) cholesterol
(-) trehalose
D
Number of Cells x 10⁴
Days
FBS Treatment
Amberlite & Charcoal
Amberlite
Charcoal
none
E
Days
Buffer
HT115 extract
HT115 extract (heat inactiv.)

Figure 3.2. Optimization of *C. elegans* germ cell culture conditions.

(A) Images of *glp-1(gf)*; *cki-2*; *daf-16* germ cells one-day post-isolation in CeM1 medium: phase contrast; and calcein-AM live-cell stain. Scale bar, 20 μm.

(B-E) Live cell counts for *glp-1(gf)*; *cki-2*; *daf-16* germ cells are shown for all panels. (B) CeM1 maintains germ cell viability more effectively than L-15 medium. (C) Germ cell viability decreases when CeM1 lacks the specified components. (D) Pretreatment of FBS with Amberlite IRA 400-CL and charcoal-dextran increases germ cell viability. (E) Bacterial extract (with or without heat inactivation at 60°C for 30 min) promotes initial germ cell proliferation. The same full CeM1 control was analyzed in (B) and (D), and is shown in each panel for comparison.

For all figures, error bars reflect standard error of the mean, SEM. See also Figures 3.S1 and 3.S2, and Table 3.S1.

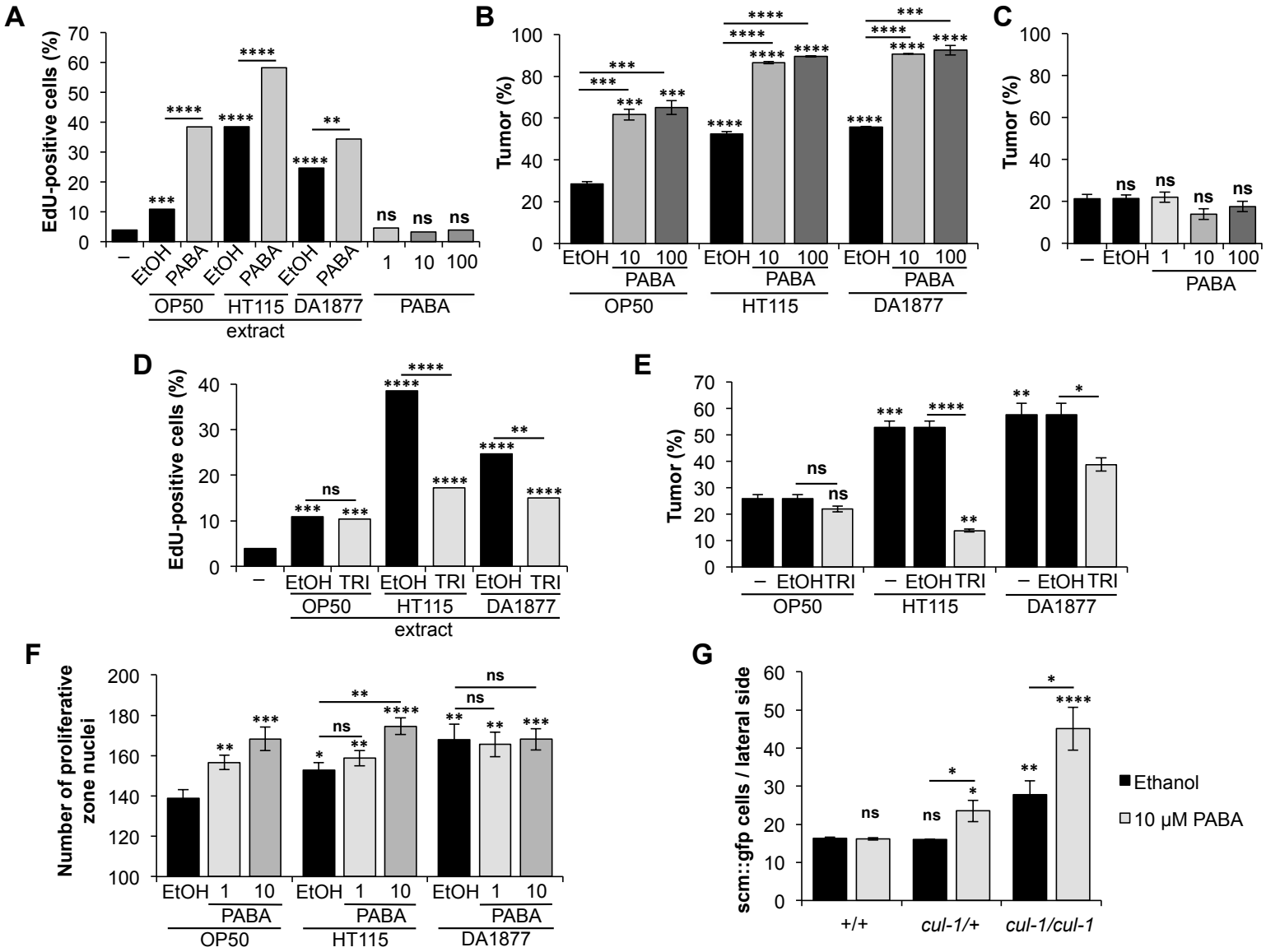
A
EdU-positive cells (%)
–
EtOH
PABA
EtOH
PABA
EtOH
PABA
1
10
100
OP50
HT115
DA1877
PABA
extract
B
Tumor (%)
EtOH
10
100
PABA
OP50
HT115
DA1877
C
Tumor (%)
–
EtOH
1
10
100
PABA
D
EdU-positive cells (%)
–
EtOH
TRI
OP50
HT115
DA1877
extract
E
Tumor (%)
–
EtOH
TRI
OP50
HT115
DA1877
F
Number of proliferative zone nuclei
EtOH
1
10
PABA
OP50
HT115
DA1877
G
scm::gfp cells / lateral side
+/+
cul-1/+
cul-1/cul-1
Ethanol
10 µM PABA

Figure 3.3. Bacterial folates stimulate germ cell proliferation in vitro and in vivo.

(A) EdU incorporation in isolated germ cells increases when CeM1 is supplemented with extract from bacteria grown with 2.5 mM PABA, but not from adding PABA alone at the indicated concentrations (in μM). Dash indicates buffer control.

(B) The percentages of germline tumors in *glp-1(gf)*; *cki-2*; *daf-16* mutants at 18°C increase on diets of live bacteria grown with PABA compared to ethanol carrier control (EtOH). The concentrations of PABA are in μM (for panels B, C, F).

(C) Tumor frequency with a diet of heat-killed OP50 bacteria supplemented with PABA at 20°C (the higher temperature compensates for the suboptimal diet of heat-killed bacteria). Dash indicates no addition.

(D) EdU incorporation in isolated germ cells using extracts from bacteria treated with the DHFR-inhibitor trimethoprim (TRI). Dash indicates buffer control. The concentration of TRI was 2.5 μg/ml (for panels D and E).

(E) Tumor frequency at 18°C with diets of bacteria treated with TRI. Dash indicates no addition.

(F) The number of germ cell nuclei in the proliferative zone of wild-type hermaphrodite gonads (analyzed 36 hr post-adulthood) when animals were fed diets of the indicated bacteria supplemented with PABA.

(G) The number of cells expressing seam cell marker scm::GFP per lateral side in *cul-1* homozygous and heterozygous mutants fed a diet of OP50 bacteria with or without PABA supplementation.

The same buffer and control bacterial extract samples were analyzed in (A) and (D), and are shown in each panel for comparison. For all figures, asterisks above bars denote statistical significance relative to the control, and asterisks above lines are for comparisons below

the lines: *P<0.05; **P<0.01; ***P<0.001; ****P<0.0001; ns = not significant. Statistics are described in the Experimental Procedures section. See also Figures 3.S3–3.S5.

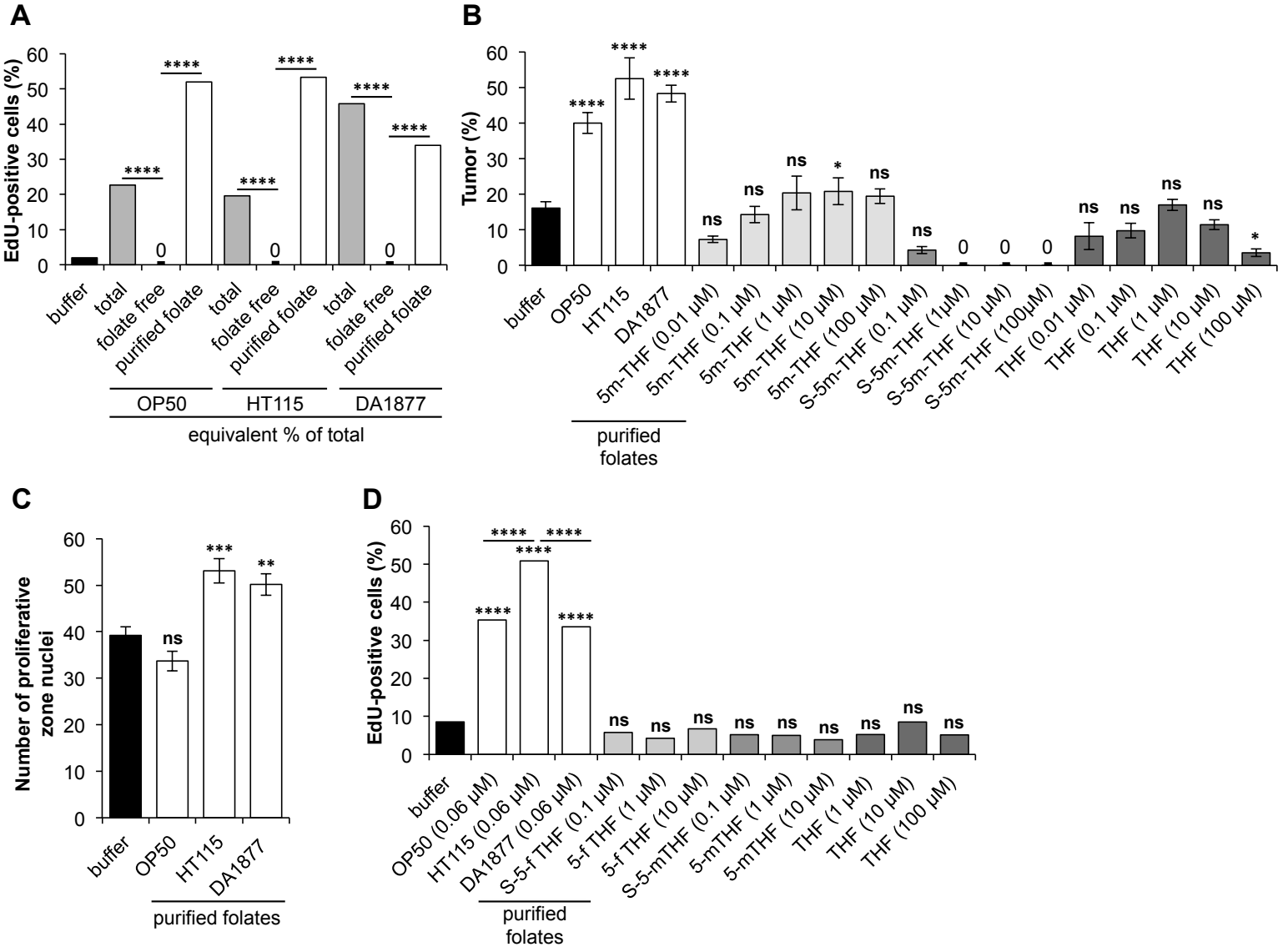
A
EdU-positive cells (%)
buffer
total
folate free
purified folate
OP50
HT115
DA1877
equivalent % of total
B
Tumor (%)
purified folates
5m-THF (0.01 µM)
5m-THF (0.1 µM)
5m-THF (1 µM)
5m-THF (10 µM)
5m-THF (100 µM)
S-5m-THF (0.1 µM)
S-5m-THF (1µM)
S-5m-THF (10 µM)
S-5m-THF (100µM)
THF (0.01 µM)
THF (0.1 µM)
THF (1 µM)
THF (10 µM)
THF (100 µM)
C
Number of proliferative zone nuclei
D
EdU-positive cells (%)
OP50 (0.06 µM)
HT115 (0.06 µM)
DA1877 (0.06 µM)
S-5-f THF (0.1 µM)
5-f THF (1 µM)
5-f THF (10 µM)
S-5-mTHF (0.1 µM)
5-mTHF (1 µM)
5-mTHF (10 µM)

Figure 3.4. Purified folates stimulate germ cell proliferation.

(A) Germ cell stimulatory activity segregates with purified folates during affinity purification. Equal percentages of total bacterial extract; folate-free extract (post-folate purification); or folates purified from the extract were added to isolated germ cells and EdU incorporation was assessed. The concentrations of the purified folates were: 0.063 μM (OP50); 0.038 μM (HT115); and 0.055 μM (DA1877).

(B) The effect of purified folates and the reduced folates shown on tumor frequency at 20°C when added to heat-killed bacteria. Equal volumes of purified folates were used; the concentrations of purified folates for experiments (B) and (C) were: 0.21 μM (OP50); 0.13 μM (HT115); and 0.18 μM (DA1877).

(C) The number of germ cell nuclei in the proliferative zone of wild-type hermaphrodite gonads for animals fed a diet of heat-killed OP50 supplemented with purified folates from the indicated bacteria.

(D) Purified folates from the indicated bacteria stimulate EdU incorporation at 0.06 μM, while the basic reduced folates, 5-methyl-THF (5m-THF), 5-formyl-THF (5f-THF), and THF, are not active at concentrations of 0.1 to 100 μM.

See also Figure 3.S5 and Table 3.S2.

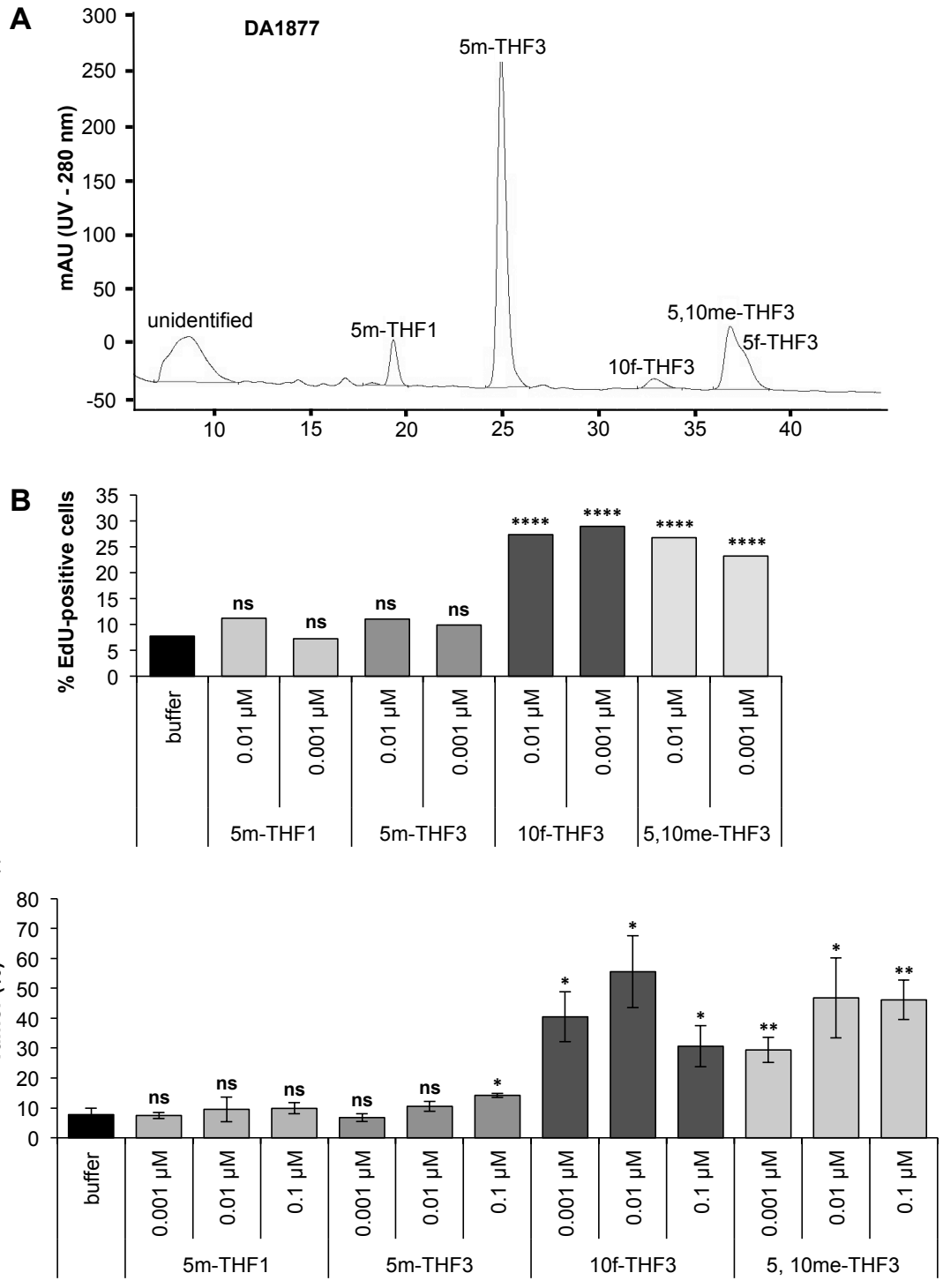
A
DA1877
5m-THF3
mAU (UV - 280 nm)
unidentified
5m-THF1
10f-THF3
5,10me-THF3
5f-THF3
B
% EdU-positive cells
ns
****
buffer
0.01 µM
0.001 µM
5m-THF1
5m-THF3
10f-THF3
5,10me-THF3
C
Tumor (%)
ns
*
**
buffer
0.001 µM
0.01 µM
0.1 µM
5m-THF1
5m-THF3
10f-THF3
5, 10me-THF3

Figure 3.5. 10-formyl-THF and 5,10-methenyl-THF isolated from bacteria stimulate germ cells.

(A) Chromatogram showing UV absorbance (milli-absorbance units) of affinity-purified DA1877 folates separated by ion-pair chromatography. Folate species identified by UV spectra are labeled.

(B and C) Affinity-purified folate fractions, containing the indicated folates, were isolated from DA1877 bacteria grown with PABA supplementation and tested for their ability to induce DNA replication (EdU incorporation) in isolated germ cells (B) or increase tumor frequency at 20°C with a diet of heat-killed bacteria (C). 10-formyl-THF (10f-THF); 5,10-methenyl-THF (5,10me-THF).

See also Figure 3.S6.

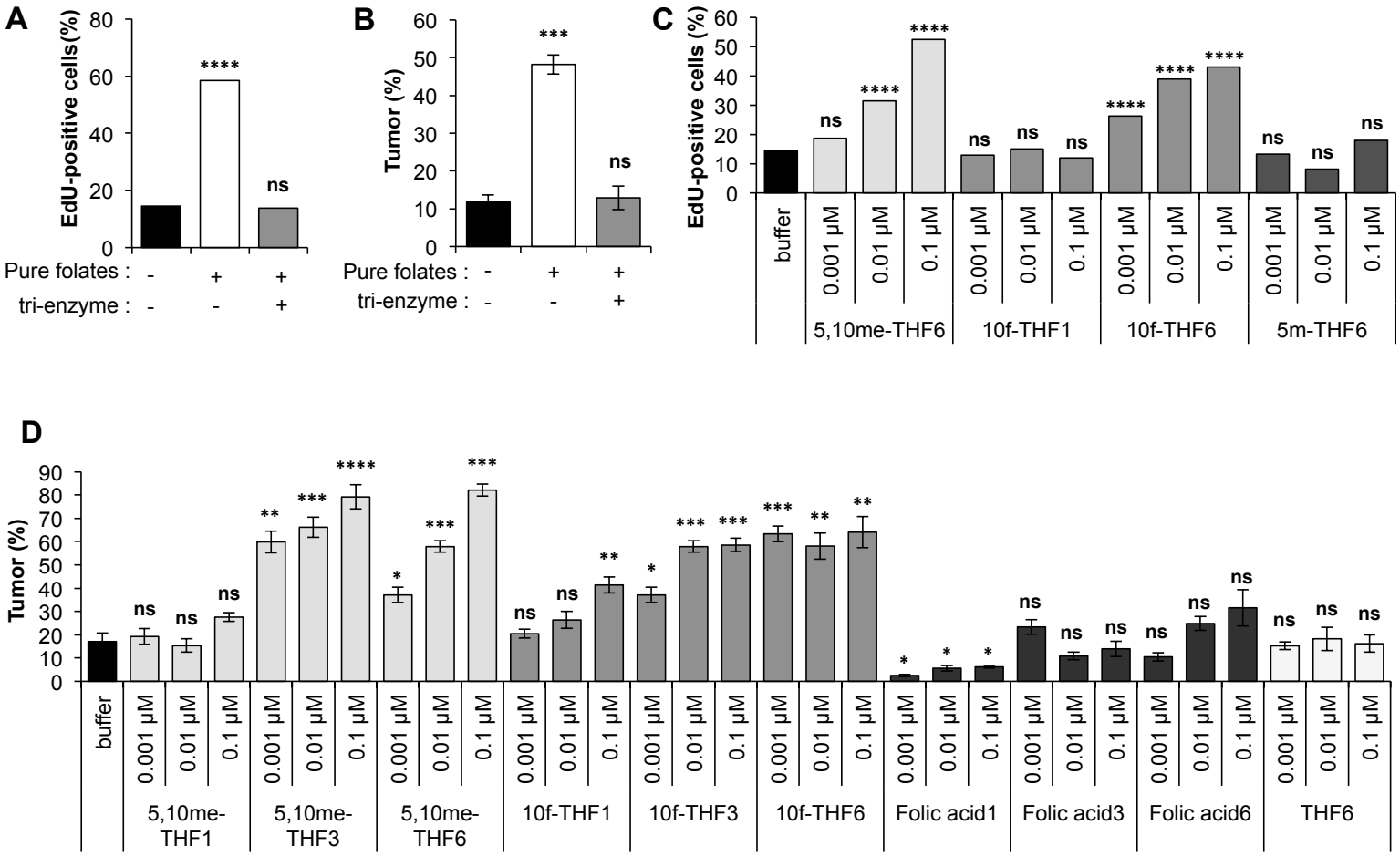
A
EdU-positive cells(%)
Pure folates :
tri-enzyme :
B
Tumor (%)
Pure folates :
tri-enzyme :
C
EdU-positive cells (%)
buffer
5,10me-THF6
10f-THF1
10f-THF6
5m-THF6
D
Tumor (%)
buffer
5,10me-THF1
5,10me-THF3
5,10me-THF6
10f-THF1
10f-THF3
10f-THF6
Folic acid1
Folic acid3
Folic acid6
THF6

Figure 3.6. Poly-glutamate increases 10-formyl-THF-Glu$_n$ germ cell stimulatory activity.

(A and B) Purified folates from OP50 were treated with tri-enzyme to convert poly-Glu folates to mono-Glu folates. Germ cell stimulatory activity was assessed by analyzing EdU incorporation in isolated germ cells (A) and tumor frequency at 20°C with a diet of heat-killed bacteria (B). The concentration of purified folates was 0.06 μM for (A) and 0.12 μM for (B).

(C and D) Comparison of the activity of synthetic folates with 1, 3, 6 Glu residues in the EdU incorporation assay with isolated germ cells (C) and tumor frequency assay at 18°C (D).

See also Figure 3.S5.

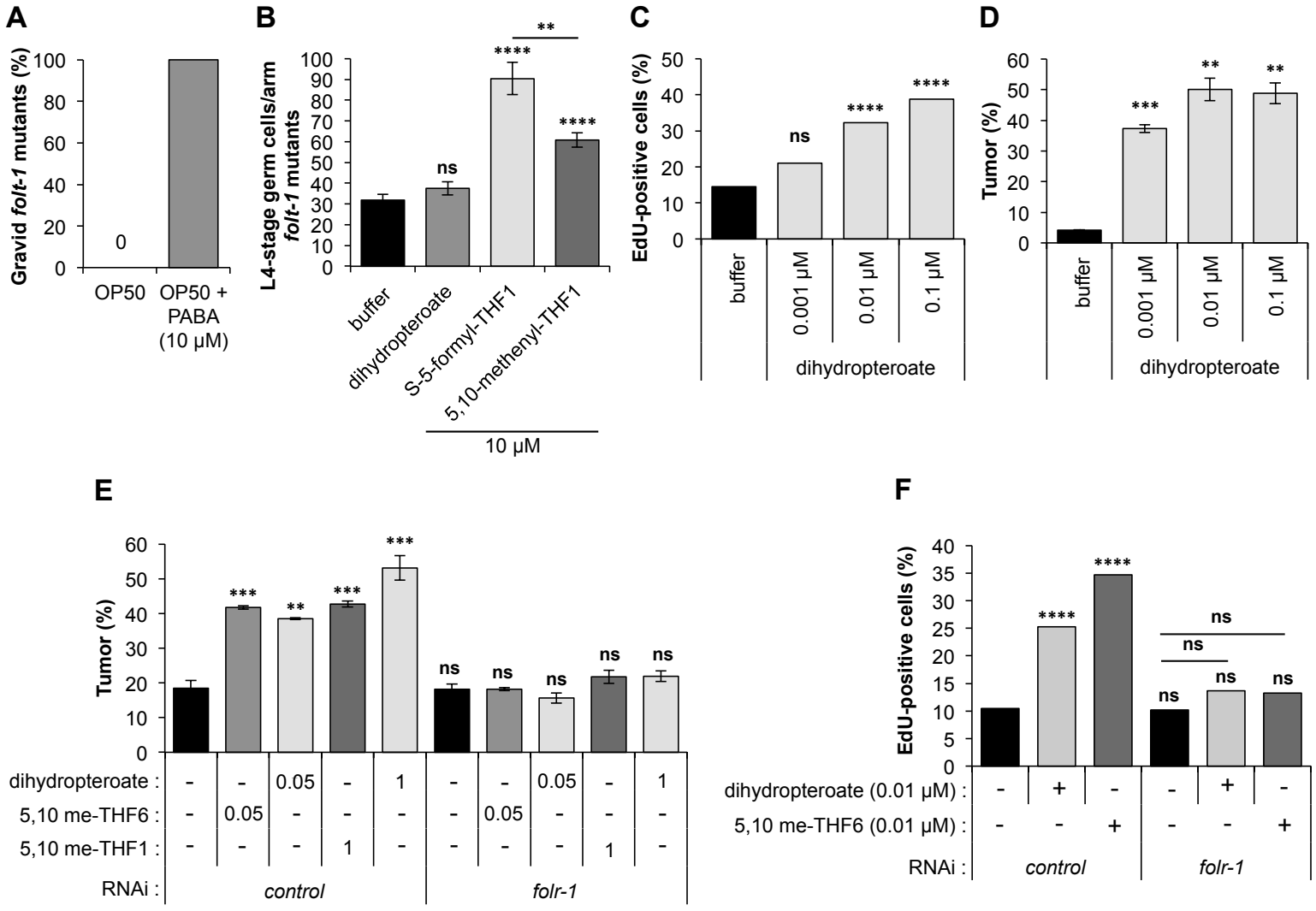
A
Gravid folt-1 mutants (%)
100
80
60
40
20
0
0
OP50
OP50 + PABA (10 µM)
B
L4-stage germ cells/arm folt-1 mutants
100
90
80
70
60
50
40
30
20
10
0
**
****
****
ns
buffer
dihydropteroate
S-5-formyl-THF1
5,10-methenyl-THF1
10 µM
C
EdU-positive cells (%)
50
40
30
20
10
0
ns
****
****
buffer
0.001 µM
0.01 µM
0.1 µM
dihydropteroate
D
Tumor (%)
60
50
40
30
20
10
0
***
**
**
buffer
0.001 µM
0.01 µM
0.1 µM
dihydropteroate
E
Tumor (%)
60
50
40
30
20
10
0
***
**
***
***
ns
ns
ns
ns
ns
dihydropteroate :
5,10 me-THF6 :
5,10 me-THF1 :
RNAi :
control
folr-1
F
EdU-positive cells (%)
40
35
30
25
20
15
10
5
0
****
****
ns
ns
ns
ns
ns
dihydropteroate (0.01 µM) :
5,10 me-THF6 (0.01 µM) :
RNAi :
control
folr-1

Figure 3.7. Folates and pteroates stimulate germ cell proliferation independently of a role as vitamins.

(A) *folt-1(ok1467)* mutant sterility is rescued by growth on OP50 supplemented with PABA. The percentage of gravid animals is shown (n = 20 each).

(B) Stimulatory and non-stimulatory folates can rescue folate deficiency, but dihydropteroate cannot. *folt-1(ok1467)* mutants were fed heat-killed, folate-depleted *pabC* mutant bacteria with the indicated folates or folate-related compounds (10 μM). Germ cell numbers per gonad arm from mid/late L4-stage larvae were scored blindly.

(C and D) Dihydropteroate stimulates EdU incorporation in isolated germ cells (C) and tumor frequency at 18°C (D). For (C), the experiment was performed at the same time as Fig. 3.6C, and the same control is shown for comparison.

(E) *folr-1*/FR RNAi blocks the stimulatory effect of dihydropteroate, 5,10-methenyl-THF_6, and 5,10-methenyl-THF_1 on tumor frequency at 18°C. The concentrations are in μM.

(F) *folr-1*/FR RNAi blocks the stimulatory effect of dihydropteroate and 5,10-methenyl-THF-Glu_6 on EdU incorporation in isolated germ cells.

See also Figure 3.S7.

Supplemental Figures

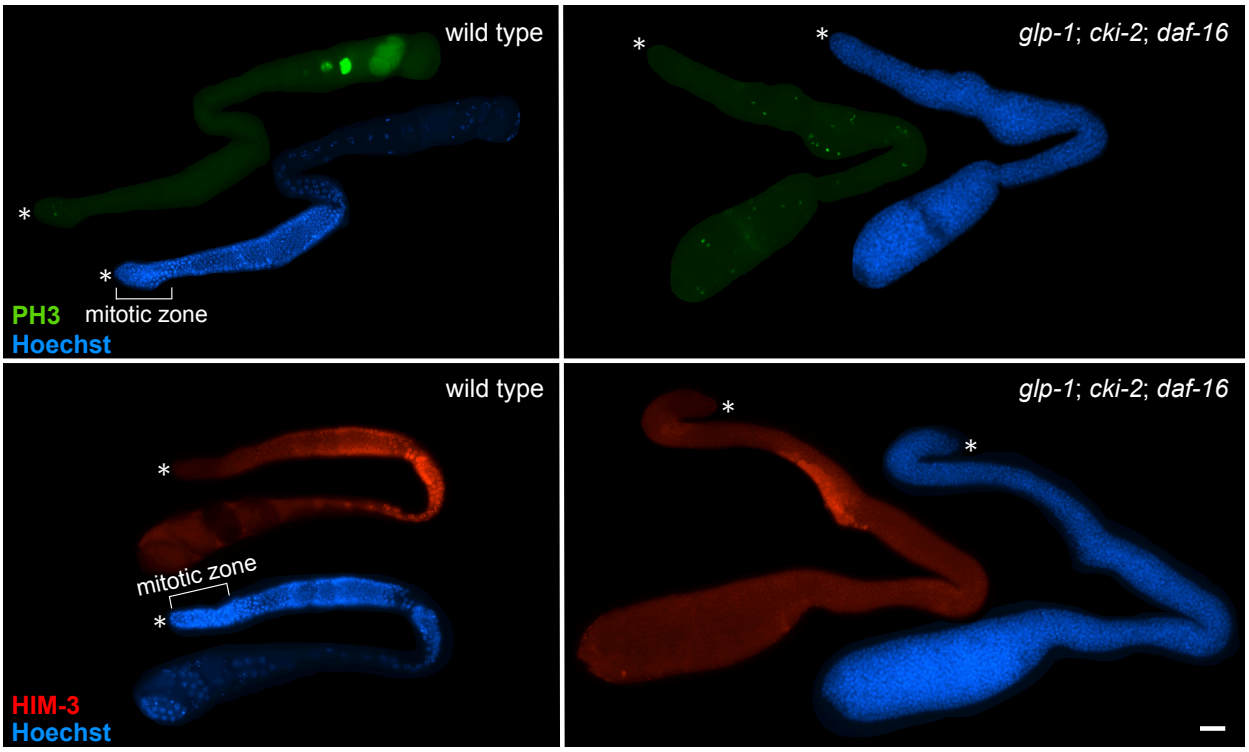

Figure 3.S1, related to Figure 3.2A. Tumorous gonads from *glp-1(gf)*; *cki-2*; *daf-16* mutants.

Images of *glp-1(gf)*; *cki-2*; *daf-16* and wild-type dissected gonads stained with the mitotic marker anti-phosphohistone H3 (Ser10) antibody (green, top), the meiotic marker anti-HIM-3 antibody (red, bottom), and Hoechst 33342 DNA stain (blue). Image z-sections were merged for the anti-phosphohistone H3 staining to show mitotic cells throughout the gonad. Asterisks mark the distal end of the gonad. Scale bar, 20 µm.

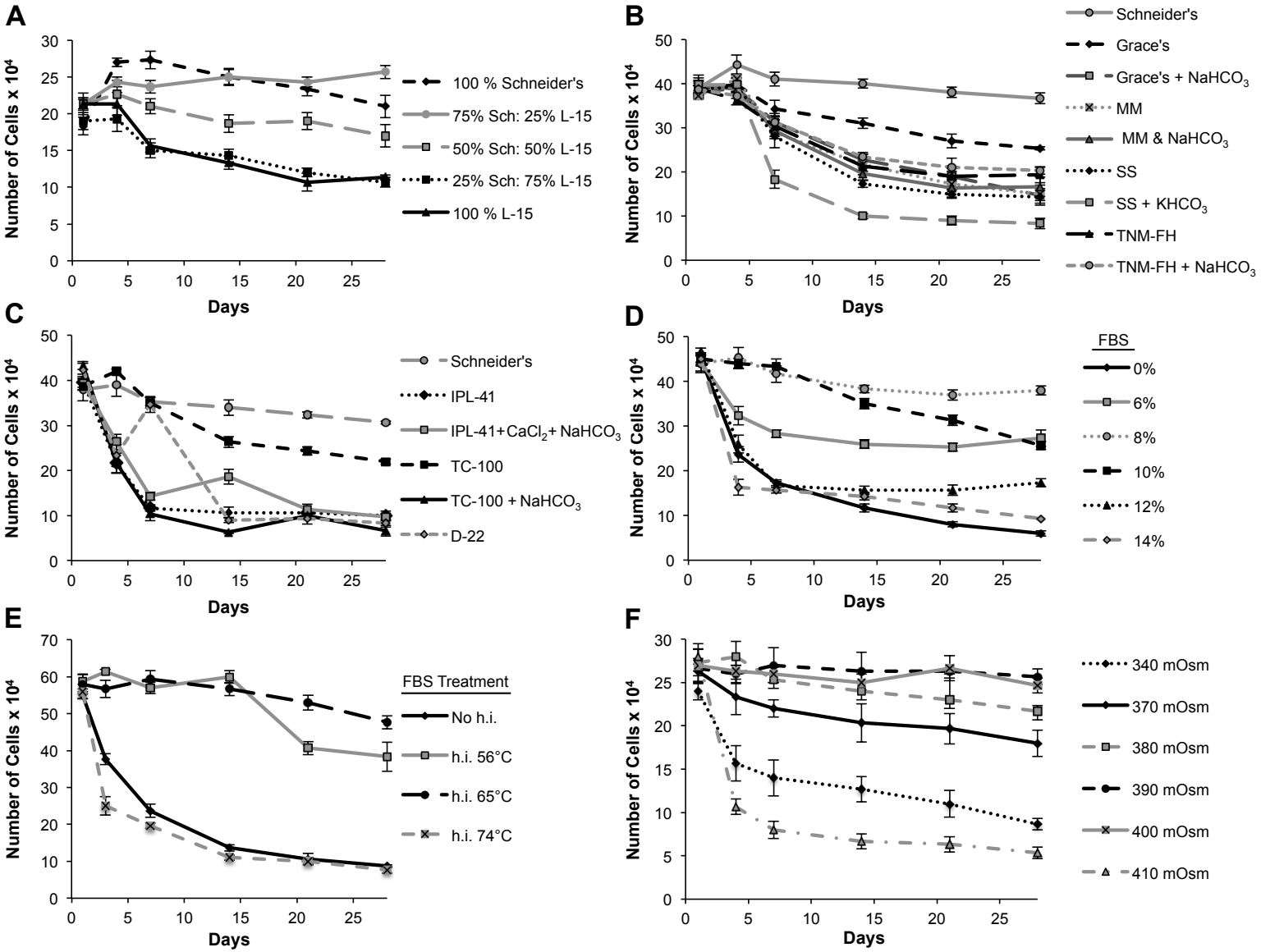
A
Number of Cells x 10⁴
Days
100 % Schneider's
75% Sch: 25% L-15
50% Sch: 50% L-15
25% Sch: 75% L-15
100 % L-15
B
Number of Cells x 10⁴
Days
Schneider's
Grace's
Grace's + NaHCO3
MM
MM & NaHCO3
SS
SS + KHCO3
TNM-FH
TNM-FH + NaHCO3
C
Number of Cells x 10⁴
Days
Schneider's
IPL-41
IPL-41+CaCl2+ NaHCO3
TC-100
TC-100 + NaHCO3
D-22
D
Number of Cells x 10⁴
Days
FBS
0%
6%
8%
10%
12%
14%
E
Number of Cells x 10⁴
Days
FBS Treatment
No h.i.
h.i. 56°C
h.i. 65°C
h.i. 74°C
F
Number of Cells x 10⁴
Days
340 mOsm
370 mOsm
380 mOsm
390 mOsm
400 mOsm
410 mOsm

Figure 3.S2, related to Figure 3.2B-E. Comparison of media components for germ cell culture.

(A-F) Live germ cell counts for cultures with: (A) different ratios of Schneider's insect medium and L-15 medium; (B and C) different base insect media (MM, Mitsuhashi and Maramorosch medium; SS, Shields and Sang medium); (D) CeM1 prepared with different FBS concentrations; (E) CeM1 prepared with FBS that was heat inactivated at different temperatures for 30 min, or no heat inactivation. The 65°C heat-inactivated FBS sample is the complete CeM1 medium, and this sample was analyzed at the same time as the experiments shown in Fig. 3.2B and 3.2D; the curve is shown here for comparison. (F) CeM1 media adjusted to different osmolalities.

A


wild-type
glp-1(gf); cki-2; daf-16

B

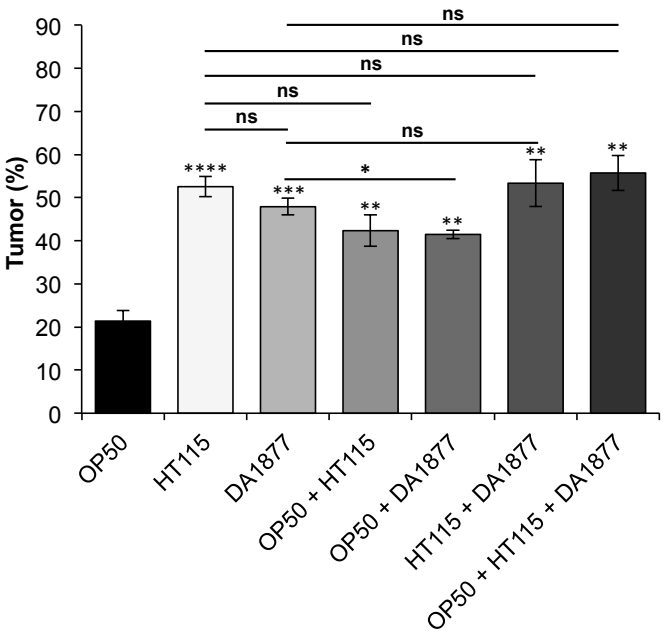
Tumor (%)
90
80
70
60
50
40
30
20
10
0
ns
ns
ns
ns
ns
ns
*
****
***
**
**
**
**
OP50
HT115
DA1877
OP50 + HT115
OP50 + DA1877
HT115 + DA1877
OP50 + HT115 + DA1877

Figure 3.S3, related to Figure 3.3. Images of germline tumors and the lack of synergistic effects from mixing bacterial diets on tumor frequency. (A) Bottom-illuminated stereomicroscope images of three wild-type adult hermaphrodites with no tumors and three *glp-1(gf)*; *cki-2*; *daf-16* adult hermaphrodite mutants exhibiting tumors that are visible as white regions within the body. Scale bar, 100 μm. (B) Tumor frequency of *glp-1(gf)*; *cki-2*; *daf-16* mutants grown at 18°C and fed diets of the indicated live bacteria, or 1:1 or 1:1:1 mixtures of live bacteria.

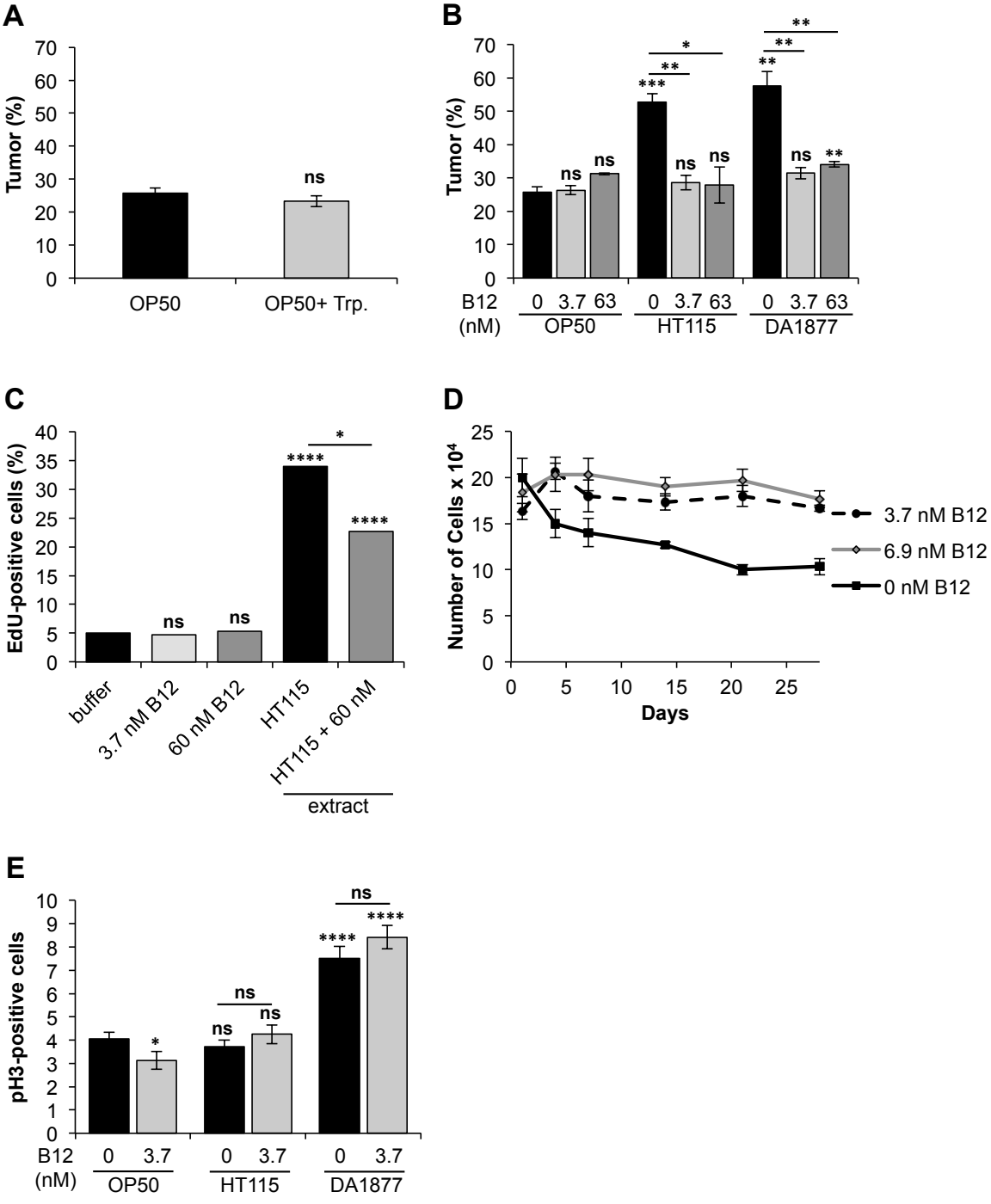
A
Tumor (%)
70
60
50
40
30
20
10
0
ns
OP50
OP50+ Trp.
B
Tumor (%)
***
**
*
**
**
**
ns
ns
ns
ns
ns
**
B12
(nM)
0 3.7 63
0 3.7 63
0 3.7 63
OP50
HT115
DA1877
C
EdU-positive cells (%)
40
35
30
25
20
15
10
5
0
****
****
*
ns
ns
buffer
3.7 nM B12
60 nM B12
HT115
HT115 + 60 nM
extract
D
Number of Cells x 10⁴
25
20
15
10
5
0
0
5
10
15
20
25
Days
3.7 nM B12
6.9 nM B12
0 nM B12
E
pH3-positive cells
10
9
8
7
6
5
4
3
2
1
0
*
ns
ns
ns
ns
****
****
B12
(nM)
0 3.7
0 3.7
0 3.7
OP50
HT115
DA1877

Figure 3.S4, related to Figure 3.3. Increased supplementation with tryptophan or vitamin B12 does not increase germ cell proliferation.

(A and B) Tumor frequencies for *glp-1(gf)*; *cki-2*; *daf-16* mutants grown at 18°C on a diet of OP50 with or without 0.15 mM tryptophan (A); or in different concentrations of vitamin B12 with the indicated bacteria (B). (C) The percentage of isolated germ cells that incorporated EdU into genomic DNA 24-48 hr post-isolation when supplemented with the indicated amount of vitamin B12 and HT115 bacterial extract. (D) Counts of live germ cells cultured with CeM1 containing the following concentrations of vitamin B12: 3.7 nM (the normal CeM1 medium); 6.9 nM; or 0 nM. (E) The number of mitotic phosphohistone H3 Ser10-positive cells per gonad arm for wild-type adults grown on a diet of the bacterial strains listed with the indicated concentrations of vitamin B12. These results suggest that the concentration of vitamin B12 in CeM1 medium is sufficient to maintain cell viability, and that increased levels of vitamin B12 or tryptophan metabolites do not stimulate germ cell pro

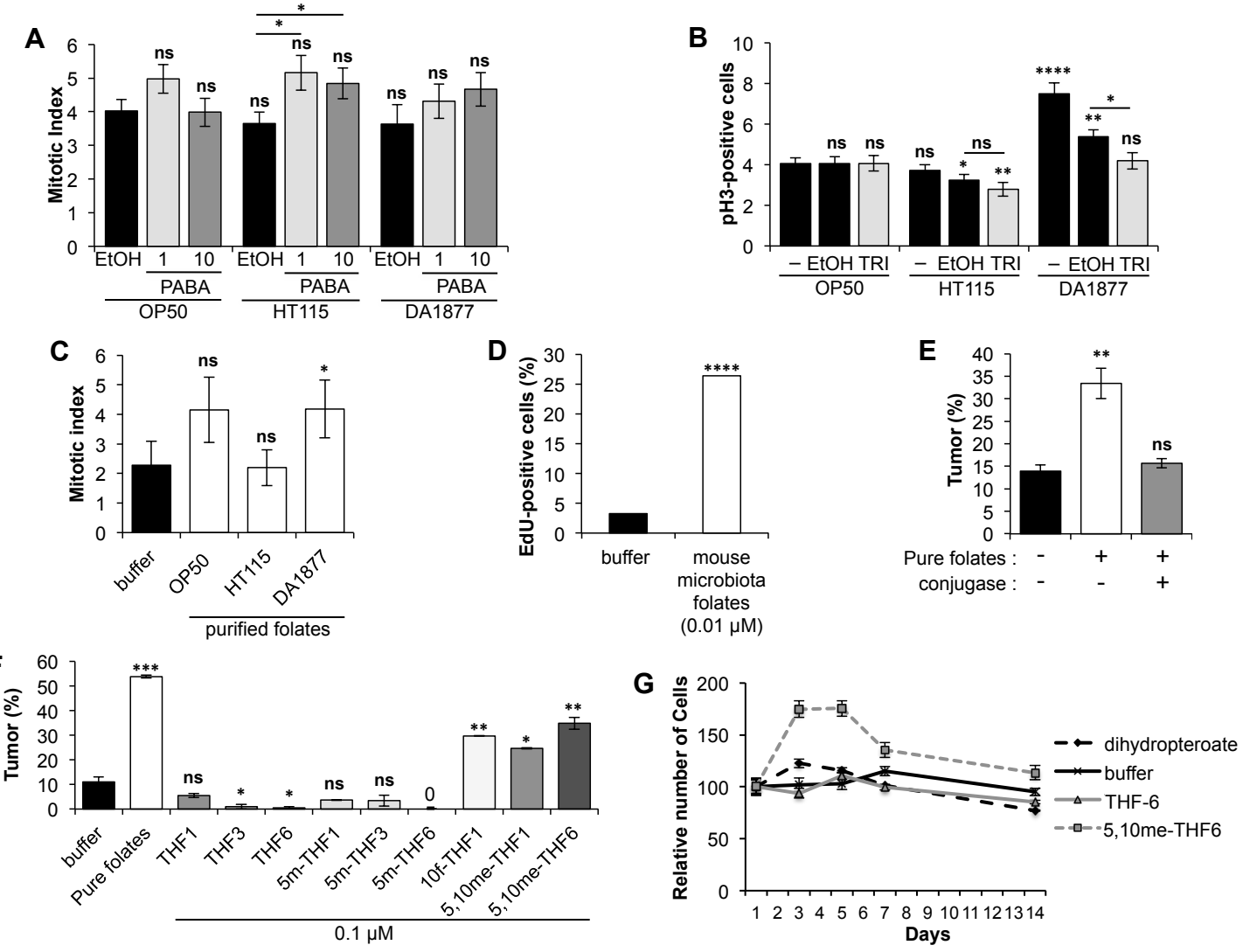
A
Mitotic Index
EtOH 1 10 EtOH 1 10 EtOH 1 10
PABA PABA PABA
OP50 HT115 DA1877
B
pH3-positive cells
– EtOH TRI – EtOH TRI – EtOH TRI
OP50 HT115 DA1877
C
Mitotic index
buffer OP50 HT115 DA1877
purified folates
D
EdU-positive cells (%)
buffer
mouse microbiota folates (0.01 µM)
E
Tumor (%)
Pure folates : - + +
conjugase : - - +
F
Tumor (%)
buffer Pure folates THF1 THF3 THF6 5m-THF1 5m-THF3 5m-THF6 10f-THF1 5,10me-THF1 5,10me-THF6
0.1 µM
G
Relative number of Cells
Days
dihydropteroate
buffer
THF-6
5,10me-THF6

Figure 3.S5, related to Figures 3.3, 3.4, and 3.6. Wild-type germ cell proliferation is increased by bacterial folates; poly-Glu increases folate stimulatory activity; and 5,10-methenyl-THF-Glu_n stimulates germ cell proliferation. (A,C) Mitotic index of wild-type hermaphrodite proliferative zone germ cells fed a diet of the indicated bacteria supplemented with PABA at the indicated concentrations in μM or ethanol control (EtOH) (A), or purified folates at 0.21 μM (OP50), 0.13 μM (HT115), and 0.18 μM (DA1877) (C). (B) The number of mitotic, phosphohistone H3-positive germ cells per gonad arm in wild-type adult hermaphrodites fed a diet of live bacteria supplemented with 2.5 μg/ml TRI or ethanol control. (D) Purified folates (0.01 μM) from a mouse microbiota increase EdU incorporation in isolated germ cells. (E) Tumor frequencies at 20°C on heat-killed bacteria supplemented with DA1877 purified folates (0.043 μM) treated with or without conjugase. (F) Tumor frequencies with the indicated synthetic folates (0.1 μM) or purified folates from OP50 bacteria (0.21 μM) on a diet of heat-killed bacteria at 20°C. (G) 5,10-methenyl-THF-Glu_6 supports initial germ cell proliferation in vitro. Numbers of live isolated germ cells supplemented with 0.1 μM of the indicated supplements. The graph is the average of two experiments; cell numbers are set to 100 on day 1.

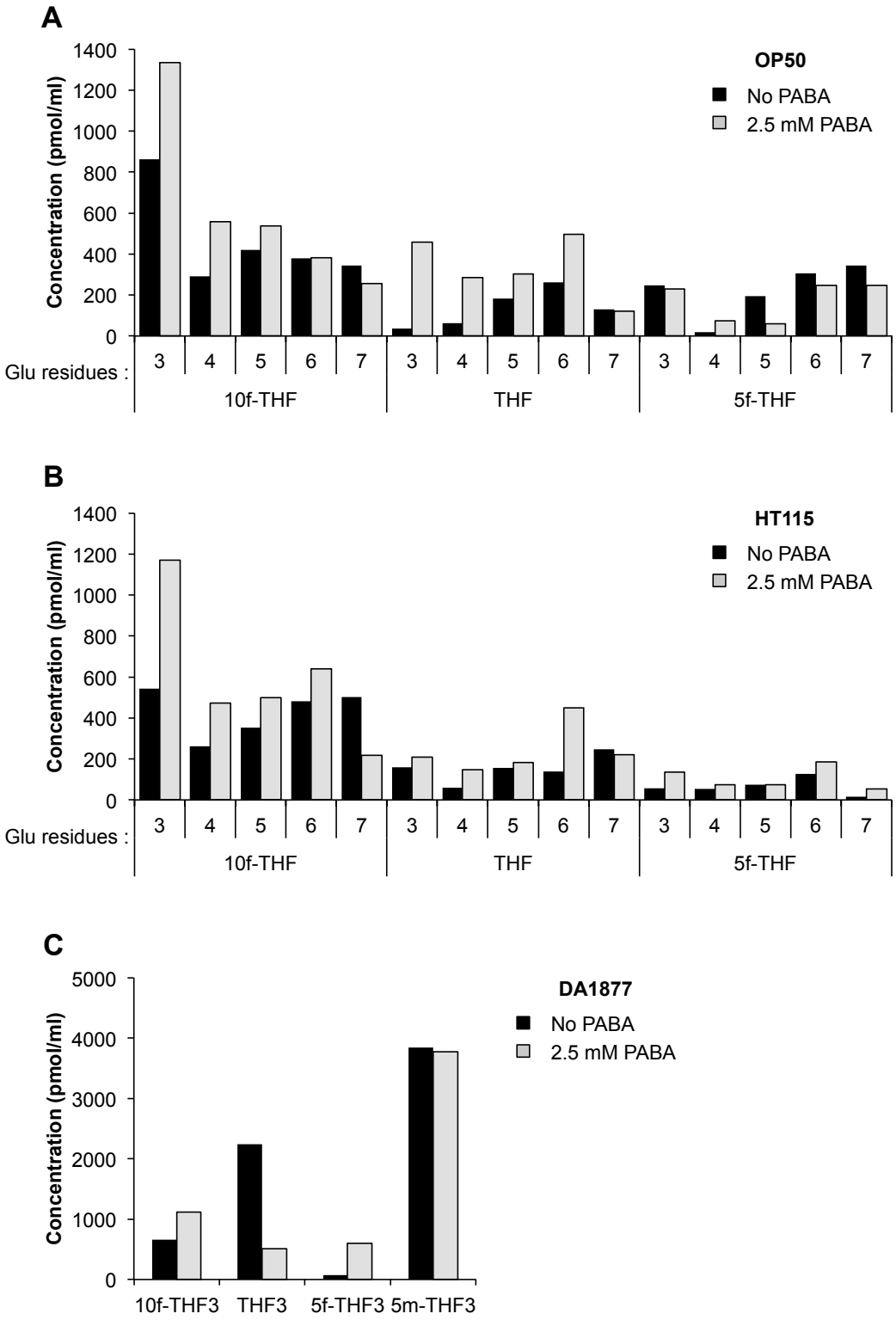
A
OP50
No PABA
2.5 mM PABA
Concentration (pmol/ml)
1400
1200
1000
800
600
400
200
0
Glu residues :
3 4 5 6 7 3 4 5 6 7 3 4 5 6 7
10f-THF
THF
5f-THF
B
HT115
No PABA
2.5 mM PABA
Concentration (pmol/ml)
1400
1200
1000
800
600
400
200
0
Glu residues :
3 4 5 6 7 3 4 5 6 7 3 4 5 6 7
10f-THF
THF
5f-THF
C
DA1877
No PABA
2.5 mM PABA
Concentration (pmol/ml)
5000
4000
3000
2000
1000
0
10f-THF3
THF3
5f-THF3
5m-THF3

Figure 3.S6, related to Figure 3.5. 10-formyl-THF-Glu$_n$ is increased upon supplementing bacteria with PABA.

(A-C) Graph of folate species identified by affinity chromatography with detection by UV absorption spectra for OP50 (A), HT115 (B), and DA1877 (C) bacterial strains grown with or without PABA supplementation.

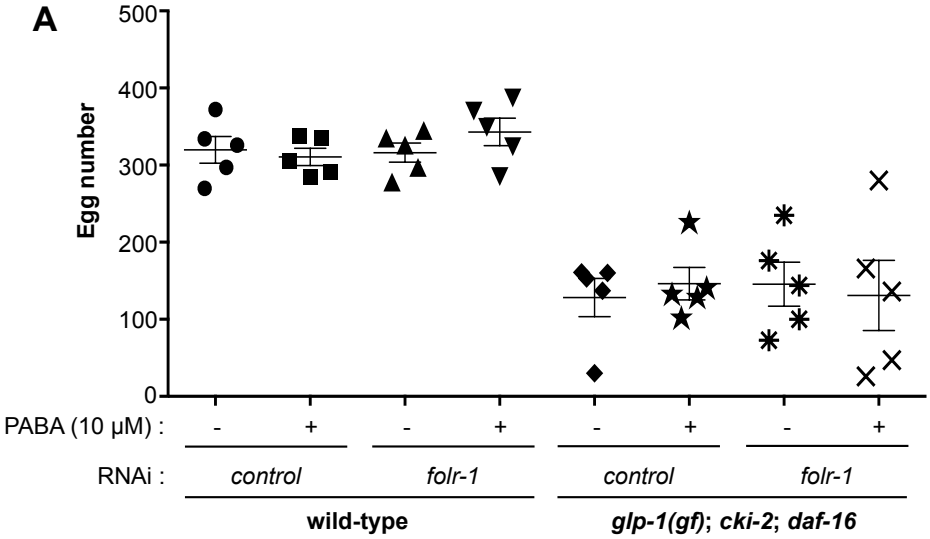
A
Egg number
500
400
300
200
100
0
PABA (10 μM) :
- + - + - + - +
RNAi :
control
folr-1
control
folr-1
wild-type
glp-1(gf); cki-2; daf-16

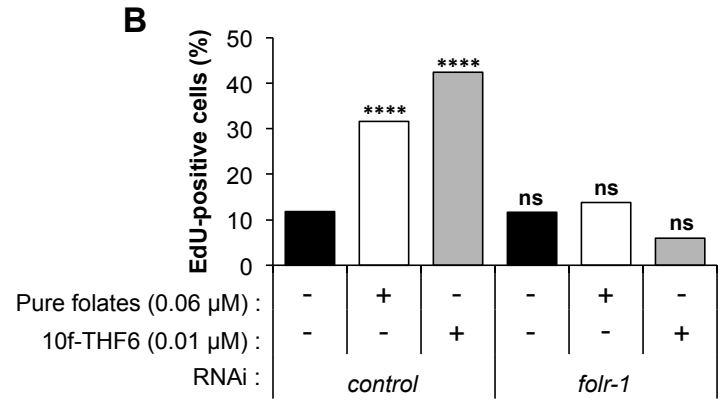
B
EdU-positive cells (%)
50
40
30
20
10
0
****
****
ns
ns
ns
Pure folates (0.06 μM) :
10f-THF6 (0.01 μM) :
RNAi :
control
folr-1

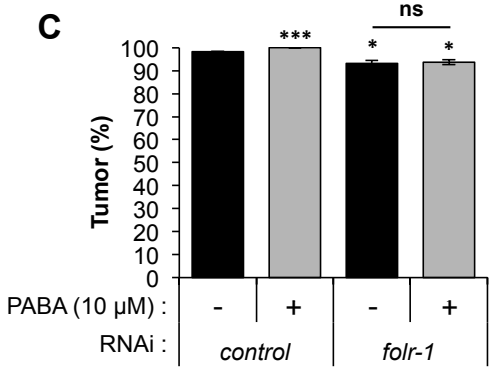
C
Tumor (%)
100
90
80
70
60
50
40
30
20
10
0
***
ns
*
*
PABA (10 μM) :
- + - +
RNAi :
control
folr-1

Figure 3.S7, related to Figure 3.7. *folr-1*/FR RNAi does not affect egg number but blocks the stimulatory effect of folates or PABA supplementation.

(A) *folr-1*/FR RNAi and control RNAi gives comparable numbers of eggs for wild type and *glp-1(gf)*; *cki-2*; *daf-16* mutants grown at 18°C. Note that *glp-1(gf)*; *cki-2*; *daf-16* mutants have lower egg numbers due to the inhibition of egg formation by tumors at the semi-permissive temperature. Within each genotype, no pairwise comparison is statistically significant. (B) *folr-1*/FR RNAi blocks the stimulatory effect of 10-formyl-THF-Glu_6 and purified bacterial folates on EdU incorporation in isolated germ cells. (C) Tumor frequency of *glp-1(gf)*; *cki-2*; *daf-16* mutants grown on live HT115 bacteria expressing control RNAi or *folr-1*/FR RNAi constructs with or without 10 μM PABA supplementation at 25°C.

Table 3.S1, related to Figure 3.2. CeM1 medium components.

Component (attribute)	CeM1 medium	L-15 medium
Schneider's Insect medium (Life Technologies, 21720-024)	67.2%	–
Leibovitz's L-15 medium without phenol red (Life Technologies, 21083-027)	22.4%	90%
Fetal Bovine Serum (lot G11012, Atlanta Biologicals, Inc.)	8% (heat-inactivated; treat Amberlite IRA-400 & charcoal dextran)	10%
penicillin–streptomycin (Sigma-Aldrich, P4333)	1% (100 units penicillin; 0.1 mg/ml streptomycin)	1%
hemin chloride[a] (MP Biomedicals, 0219402501)	4 μM	–
RPMI vitamins (Sigma-Aldrich, R7256)	1%	–
L-glutathione, reduced (Sigma-Aldrich, G4251)	0.6 mg/ml	–
normocin (InvivoGen)	0.1%	–
cholesterol[b] (J.T. Baker, 1580-01)	10 μg/ml	–

trehalose[c] (Sigma-Aldrich, T0167)	to 390 mOsm/kg	–
(pH)[d]	NaOH added to pH 6.5	~pH 7.2
sucrose	–	to 340 mOsm/kg

[a]Hemin chloride was added from a 2 mM stock solution freshly prepared in 0.1 N NaOH.

[b]Cholesterol was added from a 10 mg/ml stock solution in ethanol.

[c]The medium was adjusted to 390 mOsm/kg by adding trehalose using a freezing point osmometer for osmolality measurements (Advanced Digimatic Osmometer 3DII from Advanced Instruments Inc.).

[d]The medium was adjusted to pH 6.5, using NaOH.

Table 3.S2, related to Figure 3.4A. Affinity purification and quantification of bacterial folates.

Sample	Total folate (no conjugase) (µg folate/g lyoph. bact.)	Total folate (post conjugase) (µg folate/g lyoph. bact.)	Percent recovery of purified folates (post conjugase)[a]
OP50 bacterial extract	19.9	49.8	
HT115 bacterial extract	5.9	19.6	
DA1877 bacterial extract	42.2	98.7	
OP50 purified folates	12.4	55.5	111%
HT115 purified folates	2.9	33.2	169%
DA1877 purified folates	29.7	54.6	55%
OP50 folate-free extract	undetectable	undetectable	
HT115 folate-free extract	undetectable	undetectable	

DA1877 folate-free extract	undetectable	undetectable	

[a]The percent recovery can be over-estimated if the post-purification folates are better able to stimulate growth in the microbial folate assay that is used to determine concentration.

CHAPTER 4

DAFACHRONIC ACID INHIBITS *C. ELEGANS* GERM CELL PROLIFERATION CELL-AUTONOUSLY IN A DAF-12-DEPENDENT MANNER

Snehal N. Chaudhari*, Madhumati M. Mukherjee*, Alexandra S. Vagasi, and Edward T. Kipreos. **Submitted to *Developmental Biology*, 2017**

*These authors contributed equally.

Abstract

Dafachronic acid (DA) is a bile acid-like steroid hormone that regulates dauer formation, heterochrony, and lifespan in *C. elegans*. Here, we describe that DA is an inhibitor of *C. elegans* germ stem cell proliferation. Using a *C. elegans* germ cell primary culture system, we show that DA cell-autonomously inhibits proliferation of germ cells *in vitro*. DA also inhibits tumor formation in a tumorous germline mutant and decreases the proliferation of wild-type GSCs *in vivo*. The inhibition of germ cell proliferation by DA requires its canonical receptor DAF-12. Blocking DA production by inactivating the cytochrome P450 DAF-9 increases germ cell proliferation in germline tumorous mutants and wild-type animals, suggesting that under normal growth conditions, DA acts to inhibit the rate of germ cell proliferation.

Introduction

C. elegans germline stem cells (GSCs) encompass a population of adult stem cells that generate sperm and ooctyes in hermaphrodites. In adult hermaphrodites, GSCs reside in the most distal regions of the two gonad arms in an adult stem cell niche formed by the somatic distal tip cell (DTC) [1, 2]. Mitotic germ cells are present within a "proliferative zone" that is located in the first ~20 cell diameters of the distal end of the gonad. Proximal to the proliferative zone, germ cells are in meiotic prophase. The GSCs, which are a subset of the germ cells that exhibit mitosis, reside within a smaller region at the distal end of the gonad (~6-8 cell diameters from the distal end) that contains more extensive contacts between the DTC and germ cells [3]. Here we report that germ cell proliferation is negatively regulated by the bile acid-like steroid hormone dafachronic acid (DA).

DA, which includes Δ^4-dafachronic acid and Δ^7-dafachronic acid, regulates multiple processes in *C. elegans*, including heterochrony, longevity in the absence of germ cells, and the dauer diapause [4]. DA mediates many of these cellular functions by binding and activating the steroid hormone receptor DAF-12. In the decision to enter the long-lived dauer larval state, the activity of DAF-12 acts as a switch. DAF-12 bound to DA acts as a transcriptional activator to promote the non-dauer L3 stage and prevent dauer entry, while unliganded DAF-12 acts as a transcriptional repressor to inhibit the non-dauer pathway to promote dauer entry [5]. DA-activated DAF-12 also promotes proper heterochrony of the L2-to-L3 larval transition by increasing the expression of the

let-7 family miRNAs *mir-84* and *mir-241* [4]. And animals that lack germ cells have extended lifespans that depend on the presence of DA and DAF-12 [6].

Adult hermaphrodites that are subject to starvation have extended lifespans [7]. Under starvation, the levels of DA and *daf-9* mRNA increase significantly [7]. The cytochrome P450 DAF-9 mediates the last step in DA synthesis [8]. Inactivation of *daf-9* blocks the starvation-induced lifespan extension, but the addition of exogenous DA can restore the lifespan extension in starved *daf-9* mutants [7]. This suggests that the increased DA levels are required for lifespan extension during starvation.

Unlike the previously discussed DA-regulated processes, starvation-induced lifespan extension still occurs in *daf-12* mutants, and therefore is DAF-12 independent. Mutation of the ligand-binding domain of the NHR-8 steroid hormone receptor prevents starvation-induced lifespan extension [7]. NHR-8 regulates cholesterol and bile acid homeostasis, and complete loss of NHR-8 results in a deficiency of DA [9]. The addition of exogenous DA fails to extend the lifespan of starved *nhr-8(ok186)* mutants, which implies that DA-induced starvation lifespan extension is NHR-8 dependent. One possibile mechanism is that NHR-8 acts as a DA steroid hormone receptor under starvation conditions. However, direct biochemical evidence that NHR-8 can bind DA is lacking; and DA failed to activate NHR-8 that was expressed in mammalian cells [7].

Starvation produces a dramatic reorganization of the germline with a significant reduction in germ cell numbers and shrinkage of gonad size [10]. Upon starvation, the number of germ cells in the proliferative zone of wild-type adult hermaphrodites are reduced by more than half in one to two days [7]. The reduction in germ cell number does not occur in *daf-9* mutants, but can be reinstated if exogenous DA is added to *daf-9*

mutants, suggesting that DA is responsible for the inhibitory effect. Similar to what was observed for starvation-induced lifespan extension, *nhr-8(ok186)* mutants are resistant to the reduction in germ cell number upon starvation irrespective of whether exogenous DA is added [7]. Notably, the role of DAF-12 in the starvation-induced reduction in germ cell numbers was not analyzed. It is also not known whether DA functions cell autonomously in germ cells or non-cell autonomously, and whether it acts to inhibit germ cell proliferation, induce meiosis, or is required more broadly to initiate a general starvation response.

Results

Dafachronic acid inhibits germ cell proliferation in a cell-autonomous manner

To test the effect of DA on an essentially pure population of germ cells, we utilized an *in vitro* primary culture system with germ cells isolated from the tumorous mutant *glp-1(ar202)*; *cki-2(ok2105)*; *daf-16(mu86)*, referred to hereafter as *glp-1(gf)*; *cki-2*; *daf-16* [11]. We observed that the addition of physiological concentrations of Δ^7-DA [8] had deleterious effects on the isolated germ cells, causing them to die more rapidly over time with increasing concentration (Fig. 4.1A).

We wanted to determine whether the addition of DA reduced DNA replication in isolated *glp-1(gf)*; *cki-2*; *daf-16* germ cells. As a measure of DNA replication, we determined the percentage of cells incorporating the thymidine analog EdU. Bacterial extract or purified stimulatory folate (5,10-methenyl-tetrahydrofolate-Glu_6) were added to increase the rate of EdU incorporation in the isolated germ cells, and the effect of DA

was assessed [11]. The addition of 1 μM Δ^4-DA significantly reduced EdU incorporation in the isolated germ cells, indicating that DA inhibits DNA replication in a cell-autonomous manner (Fig. 4.1B,C).

Dafachronic acid inhibits germ cell proliferation in a DAF-12-dependent manner

To determine the role of the canonical DA receptor DAF-12 in the DA-mediated inhibition of DNA replication, we combined a *daf-12(rh61rh411)* null allele [12] with the *glp-1(gf)*; *cki-2*; *daf-16* mutant alleles. Significantly, germ cells isolated from the *glp-1(gf)*; *cki-2*; *daf-16*; *daf-12(rh61rh411)* mutant strain were not affected by the addition of 1 μM Δ^4-DA (Fig 4.1B). This indicates that the cell-autonomous DA-mediated inhibition of germ cell DNA replication requires the DAF-12 steroid hormone receptor.

To determine if DA inhibits the proliferation of germline tumors *in vivo*, we added 1 μM Δ^4-DA to *glp-1(gf)*; *cki-2*; *daf-16* mutants that were grown from eggs at 18°C, a semi-permissive temperature for the gain-of-function (gf) temperature-sensitive *glp-1(gf)* allele, and analyzed the tumor frequency. Significantly, the addition of Δ^4-DA reduced the percentage of animals displaying tumors (Fig. 4.2A,B). The strain *glp-1(gf)*; *cki-2*; *daf-16; daf-12(rh61rh411)*, which includes the *daf-12* null allele, had higher percentages of tumors at multiple semi-permissive temperatures than the corresponding strain without the *daf-12* null allele (Fig. 4.2C). This suggests that physiological DAF-12 activity normally acts to limit germline tumor proliferation. The addition of Δ^4-DA did not inhibit tumor formation in *glp-1(gf)*; *cki-2*; *daf-16*; *daf-12* mutants, indicating that DAF-12 is required to mediate the inhibition of germline tumors in response to DA (Fig. 4.2A,B).

To determine if DA negatively regulates the proliferation of GSCs in wild-type animals, we measured the number of mitotic cells per gonad arm and the number of germ cells in the proliferative zone. The addition of 1 μM Δ^4-DA significantly reduced the number of phospho-histone H3-positive cells per gonad arm and the number of mitotic germ cells in the proliferative zone of wild-type hermaphrodites (Fig. 4.3A-C). The *daf-12(rh61rh412)* null mutant was resistant to the inhibitory effects of 1 μM Δ^4-DA on the number of mitotic germ cells and the size of the proliferative zone (Fig. 4.3A-C). These results indicate that DA inhibits the proliferation of wild-type mitotic germ cells in a DAF-12-dependent manner.

***daf-9* RNAi increases germ cell proliferation**

RNAi depletion of *daf-9*, which inhibits DA biosynthesis, increased the frequency of tumors in *glp-1(gf)*; *cki-2*; *daf-16* mutants at semi-permissive temperature, and increased the number of mitotic phospho-histone H3-positive cells in wild-type gonads (Figs 4.2D and 4.3D). This suggests that physiological levels of DA normally limit the extent of germ cell proliferation in both tumorous germline mutants and wild-type animals.

Dafachronic acid inhibits germ cell proliferation independently of *nhr-8*

The steroid hormone receptor NHR-8 has been implicated in mediating the effect of DA on reducing germ cell proliferation under starvation conditions [7]. We wanted to determine if NHR-8 was required for the inhibition of germ cell proliferation in response to DA under normal well-fed (*ad libitum*) conditions. Because of defects in development associated with full loss of NHR-8, we utilized the *nhr-8(ok186)* allele, which disrupts

the ligand-binding domain, and was previously shown to block the effect of DA during starvation [7]. We wanted to assess the effect of *nhr-8(ok186)* on germline tumor formation. We were unable to obtain a tumorous germline mutant strain that contained *glp-1(gf)*, *cki-2*, *daf-16*, and *nhr-8(ok186)* alleles, and instead used the strain *glp-1(gf)*; *cki-2*; *nhr-8(ok186)* in combination with *daf-16* RNAi. The addition of 1 μM Δ^4-DA inhibited tumor formation in this strain comparably to the inhibition of tumor formation in *glp-1(gf)*; *cki-2*; *daf-16* mutants at 18ºC, indicating that the DA inhibitory activity does not require NHR-8 (Fig. 4.2E).

Discussion

Using a primary germ cell culture system, we identified DA as a signal that cell-autonomously inhibits DNA replication in isolated germ cells in a DAF-12-dependent manner. DAF-12 activity is also required for DA to inhibit the proliferation of germ cells within the proliferative zone of wild-type hermaphrodites. The proliferation of germ cells in tumorous germline mutants is also inhibited by DA in a DAF-12-dependent and NHR-8-independent manner.

RNAi depletion of *daf-9*, which is required for DA synthesis, increased the formation of germline tumors and the number of mitotic germ cells in wild-type animals. This suggests that the normal physiological levels of DA inhibit the extent of germ cell proliferation.

DA is the first example of a *C. elegans* signaling molecule, generated extrinsically of the germline, that inhibits germ cell proliferation. Dietary restriction in the adult leads

to an increase in the levels of the DA-synthesizing enzyme DAF-9 and DA [7]. This suggests that in adults, DA synthesis is regulated by the availability of food. The observation that DA cell-autonomously inhibits germ cell proliferation provides a mechanism for the observation that upon starvation, DA is required for the initial reduction in size of the proliferative zone. It is known that the mitotic index is drastically reduced upon starvation, implying a cell cycle arrest prior to mitosis [13]. It is also known that inhibiting the germ cell cycle causes more proximal mitotic germ cells to enter meiosis, thereby reducing the size of the proliferative zone [14]. The increase in the DA inhibitory signal upon starvation would therefore be expected to contribute to germ cell cycle arrest, leading to meiotic entry that reduces the size of the proliferative zone.

An important question is what is the physiological rationale of DA-mediated germ cell inhibition. The answer is likely to arise in the context of the *C. elegans* physiology and life cycle. In the wild, *C. elegans* has a "boom and bust" life cycle. Wild *C. elegans* seek bacteria growing on rotting plant matter. When in such favorable conditions, the animals reproduce exponentially, with 250–300 progeny per generation, and rapidly exhaust the bacterial food supply; this is then followed by the dispersal of progeny in search of other high-concentrations of bacteria [15]. Reproduction in *C. elegans* constitutes one of the largest expenditures of energy in the adult. The adult germ line contains twice as many cells as the soma, and unlike the post-mitotic soma, germ stem cells can continuously divide during adulthood [2]. Because of this large metabolic load, the proliferation of germ cells must be tightly coordinated with the availability of food.

Four signals, generated extrinsically from the germline, have been identified that increase the rate of germ cell proliferation and/or size of the proliferative zone, in

response to the availability of food. Bacterial folates derived from ingested bacteria cell-autonomously stimulate germ cell proliferation [11]. Insulin-like peptides and TGF-β levels are increased in response to food availability. Insulin signaling increases germ cell proliferation cell autonomously [16], while TGF-β acts on the DTC to increase the size of the proliferative zone [17]. Volatile odors from certain bacteria induce the release of neuropeptides that increase the rate of reproduction [18]. Notably, while these signals increase the proliferation rate of germ cells, proliferation continues in the absence of each of these signals. Our results indicate that DA is a physiologically important inhibitor of germ cell proliferation. Such a negative regulator would be expected to be an important complement to the modulation positive regulators, in the inhibition of germ cell proliferation.

Materials and methods

C. elegans strains

C. elegans strains used for this study were: wild-type (N2), *glp-1(ar202)* (GC143), *glp-1(ar202)*; *cki-2(ok2105)*; *daf-16(mu86)* (ET507), *daf-12(rh61rh412)* (AA18), *glp-1(ar202)*; *cki-2(ok2105)*; *daf-16(mu86)*; *daf-12(rh61rh411)* (ET526), and *glp-1(ar202)*; *cki-2(ok2105)*; *nhr-8(ok186)* (ET539). Strains with *glp-1(ar202)* mutants were maintained at 16°C; other strains were maintained at 20°C, using established methods [19].

Culture of *C. elegans* germ cells, cell counts, and EdU incorporation

The *in vitro* culture of isolated *glp-1(gf); cki-2; daf-16* germ cells in CeM1 medium with stimulatory bacterial extract and folates was as described [11]. Δ^7-DA or Δ^4-DA (both from Cayman Chemical Co.) or DMSO or ethanol carrier controls, respectively, were included in the CeM1 medium. For live cell counts, aliquots of cells from 0.5 ml 24-well plate cultures were incubated with the live-cell stain calcein-AM (Biotium; 1 μM) and the dead-cell stain ethidium homodimer (Biotium; 0.1 μM) [11]. Three counts were made for each sample using a cellometer counting grid (CP2, Nexcelom Bioscience LLC) that was analyzed using an inverted fluorescence microscope (Zeiss Axio Observer.A1); cell count variation is presented as SEM.

The analysis of EdU incorporation was carried out as described [11]. Briefly, isolated germ cells were incubated for 24 hrs in CeM1 medium, then EdU was added to 20 μM. 24 hrs after the addition of EdU, cells were harvested and processed with the Click-iT Alexa Fluor 488 Imaging kit (Life Technologies) according to the manufacturer's instructions. Hoechst 33342 (2 μg/ml) was used to stain DNA, and cells were analyzed by epifluorescence microscopy with a Zeiss Axioskop microscope equipped with a Hamamatsu ORCA-ER digital camera run by Openlab 5.0.2 software (Improvision). EdU Alexa Fluor 488 staining was analyzed initially, and Hoechst staining was analyzed subsequently. At least 150 cells were counted for each condition.

RNA Interference

RNAi was performed as described [20]. Feeding-RNAi constructs for *daf-9*, *daf-16*, and empty vector, expressed in HT115(DE3) bacteria, were obtained from the Ahringer

library [20]. Eggs or synchronized L1 larvae were placed on RNAi plates and adults were collected for the analysis of tumor frequency or mitotic germ cell numbers (36 hrs post adulthood).

Tumor frequency assay

Eggs isolated by sodium hypochlorite treatment were placed on NGM agar plates [19] seeded with either OP50 bacteria or HT115 bacteria containing RNAi vector or empty vector, and with or without DA supplementation, and incubated at the indicated temperatures. L4-stage larvae were transferred to fresh plates with the indicated conditions (~100 larvae/plate; 3 plates per condition). On the second day after transfer, the percentages of adult animals with tumors were scored using a stereomicroscope. Average tumor frequencies were derived from triplicate measurements.

Analysis of mitotic germ cells and proliferative zone germ cell numbers

Immunofluourescence of dissected gonads with rabbit anti-phosphohistone H3 (Ser10) antibody (Cell Signaling) and Dylight 488 Goat anti-rabbit secondary antibody (Thermo Scientific Pierce) was performed as described [11]. DNA was stained by incubation with 2 μg/ml Hoechst 33342. The proliferative zone was defined based on Hoechst staining as described [16]. The number of mitotic germ cells in the proliferative zone was determined based on phosphohistone H3 (Ser10) staining [21]. z-stacks of dissected gonads were obtained at 0.5 μm intervals using a Ludl hardware controller and shutters controlled with Openlab Automation software. Image z-stacks were analyzed with Image

J software [22] using the Point Picker plugin (http://bigwww.epfl.ch/thevenaz/pointpicker/).

Statistical Analysis

The two-tailed Student's t-test was used to analyze data for tumor frequencies, mitotic cells per gonad arm, and the number of germ cells in the proliferative zone. The chi-squares test was used to analyze the percentages of EdU positive cells. Error bars reflect standard error of the mean (SEM).

Acknowledgements

Some *C. elegans* strains were provided by the *Caenorhabditis* Genetics Center, which is funded by NIH Office of Research Infrastructure Programs (P40 OD010440). This work was supported by a grant from NIH/NIGMS (R01-GM074212) to ETK.

References

1. Hansen, D. and T. Schedl, *Stem cell proliferation versus meiotic fate decision in Caenorhabditis elegans.* Adv Exp Med Biol, 2013. **757**: p. 71-99.
2. Kimble, J. and H. Seidel, *C. elegans germline stem cells and their niche*, in *StemBook*, T.S.C.R. Community, Editor. 2013, StemBook: doi/10.3824/stembook.1.95.1. p. 1-12.

3. Byrd, D.T., et al., *A DTC niche plexus surrounds the germline stem cell pool in Caenorhabditis elegans.* PLoS One, 2014. **9**(2): p. e88372.

4. Antebi, A., *Steroid regulation of C. elegans diapause, developmental timing, and longevity.* Curr Top Dev Biol, 2013. **105**: p. 181-212.

5. Ludewig, A.H., et al., *A novel nuclear receptor/coregulator complex controls C. elegans lipid metabolism, larval development, and aging.* Genes Dev, 2004. **18**(17): p. 2120-33.

6. Gerisch, B., et al., *A bile acid-like steroid modulates Caenorhabditis elegans lifespan through nuclear receptor signaling.* Proc Natl Acad Sci U S A, 2007. **104**(12): p. 5014-9.

7. Thondamal, M., et al., *Steroid hormone signalling links reproduction to lifespan in dietary-restricted Caenorhabditis elegans.* Nat Commun, 2014. **5**: p. 4879.

8. Motola, D.L., et al., *Identification of ligands for DAF-12 that govern dauer formation and reproduction in C. elegans.* Cell, 2006. **124**(6): p. 1209-23.

9. Magner, D.B., et al., *The NHR-8 nuclear receptor regulates cholesterol and bile acid homeostasis in C. elegans.* Cell Metab, 2013. **18**(2): p. 212-24.

10. Angelo, G. and M.R. Van Gilst, *Starvation protects germline stem cells and extends reproductive longevity in C. elegans.* Science, 2009. **326**(5955): p. 954-8.

11. Chaudhari, S.N., et al., *Bacterial Folates Provide an Exogenous Signal for C. elegans Germline Stem Cell Proliferation.* Dev Cell, 2016. **38**(1): p. 33-46.

12. Antebi, A., et al., *daf-12 encodes a nuclear receptor that regulates the dauer diapause and developmental age in C. elegans.* Genes Dev, 2000. **14**(12): p. 1512-27.

13. Roy, D., et al., *Cell cycle features of C. elegans germline stem/progenitor cells vary temporally and spatially.* Dev Biol, 2016. **409**(1): p. 261-71.

14. Cinquin, O., et al., *Progression from a stem cell-like state to early differentiation in the C. elegans germ line.* Proc Natl Acad Sci U S A, 2010. **107**(5): p. 2048-53.

15. Frezal, L. and M.A. Felix, *C. elegans outside the Petri dish.* Elife, 2015. **4**.

16. Michaelson, D., et al., *Insulin signaling promotes germline proliferation in C. elegans.* Development, 2010. **137**(4): p. 671-80.

17. Dalfo, D., D. Michaelson, and E.J. Hubbard, *Sensory regulation of the C. elegans germline through TGF-beta-dependent signaling in the niche.* Curr Biol, 2012. **22**(8): p. 712-9.

18. Sowa, J.N., et al., *Olfaction Modulates Reproductive Plasticity through Neuroendocrine Signaling in Caenorhabditis elegans.* Curr Biol, 2015. **25**(17): p. 2284-9.

19. Sulston, J. and J. Hodgkin, *Methods*, in *The Nematode Caenorhabditis elegans*, W.B. Wood, Editor. 1988, Cold Spring Harbor Laboratory: Cold Spring Harbor, New York. p. 587-606.

20. Kamath, R.S., et al., *Systematic functional analysis of the Caenorhabditis elegans genome using RNAi.* Nature, 2003. **421**(6920): p. 231-7.

21. Hendzel, M.J., et al., *Mitosis-specific phosphorylation of histone H3 initiates primarily within pericentromeric heterochromatin during G2 and spreads in an ordered fashion coincident with mitotic chromosome condensation.* Chromosoma, 1997. **106**: p. 348-360.

22. Schindelin, J., et al., *The ImageJ ecosystem: An open platform for biomedical image analysis.* Mol Reprod Dev, 2015. **82**(7-8): p. 518-29.

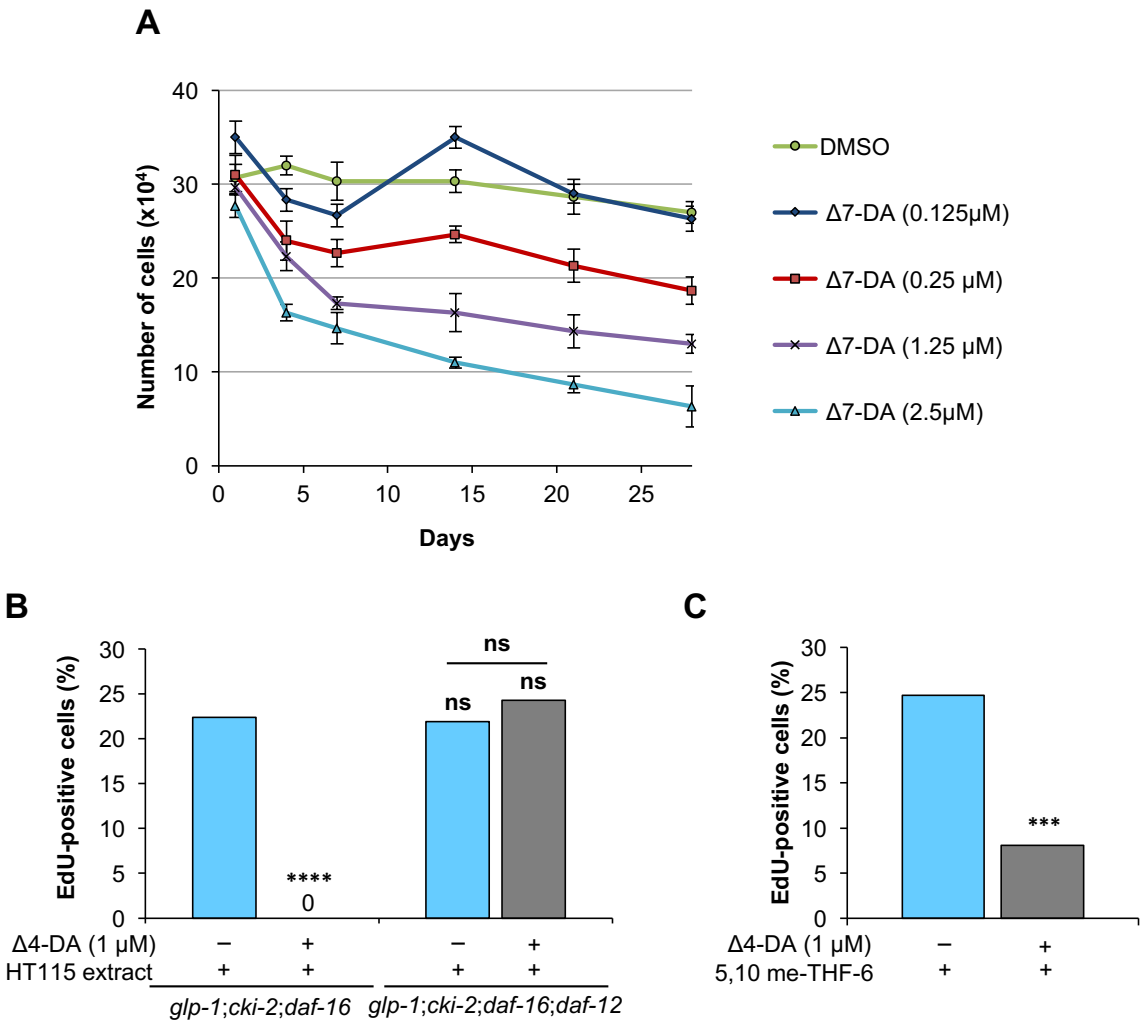
A
Number of cells (x10⁴)
Days
DMSO
Δ7-DA (0.125μM)
Δ7-DA (0.25 μM)
Δ7-DA (1.25 μM)
Δ7-DA (2.5μM)
B
EdU-positive cells (%)
****
0
ns
ns
ns
Δ4-DA (1 μM)
HT115 extract
glp-1;cki-2;daf-16
glp-1;cki-2;daf-16;daf-12
C
EdU-positive cells (%)
***
Δ4-DA (1 μM)
5,10 me-THF-6

Figure 4.1. Dafachronic acid inhibits germ cell survival and proliferation *in vitro*.

(A) DA decreases germ cell survival *in vitro*. Live cell counts of germ cells isolated from *glp-1(gf)*; *cki-2*; *daf-16* mutants and maintained in culture in the indicated concentrations of Δ^7-DA or DMSO control. (B) The percentage of germ cells incorporating EdU is reduced by treatment with DA in a DAF-12-dependent manner. Germ cells isolated from the indicated genotypes were supplemented with HT115 bacterial extract to stimulate DNA replication, and with or without 1 μM Δ^4-DA or ethanol control. (C) 1 μM Δ^4-DA reduces the incorporation of EdU in *glp-1(gf)*; *cki-2*; *daf-16* germ cells supplemented with the stimulatory folate 5,10-methenyl-THF-Glu_6. For all figures, asterisks above bars denote statistical significance relative to the control, and asterisks above lines are for comparisons below the lines: *P<0.05; **P<0.01; ***P<0.001; ****P<0.0001; ns = not significant.

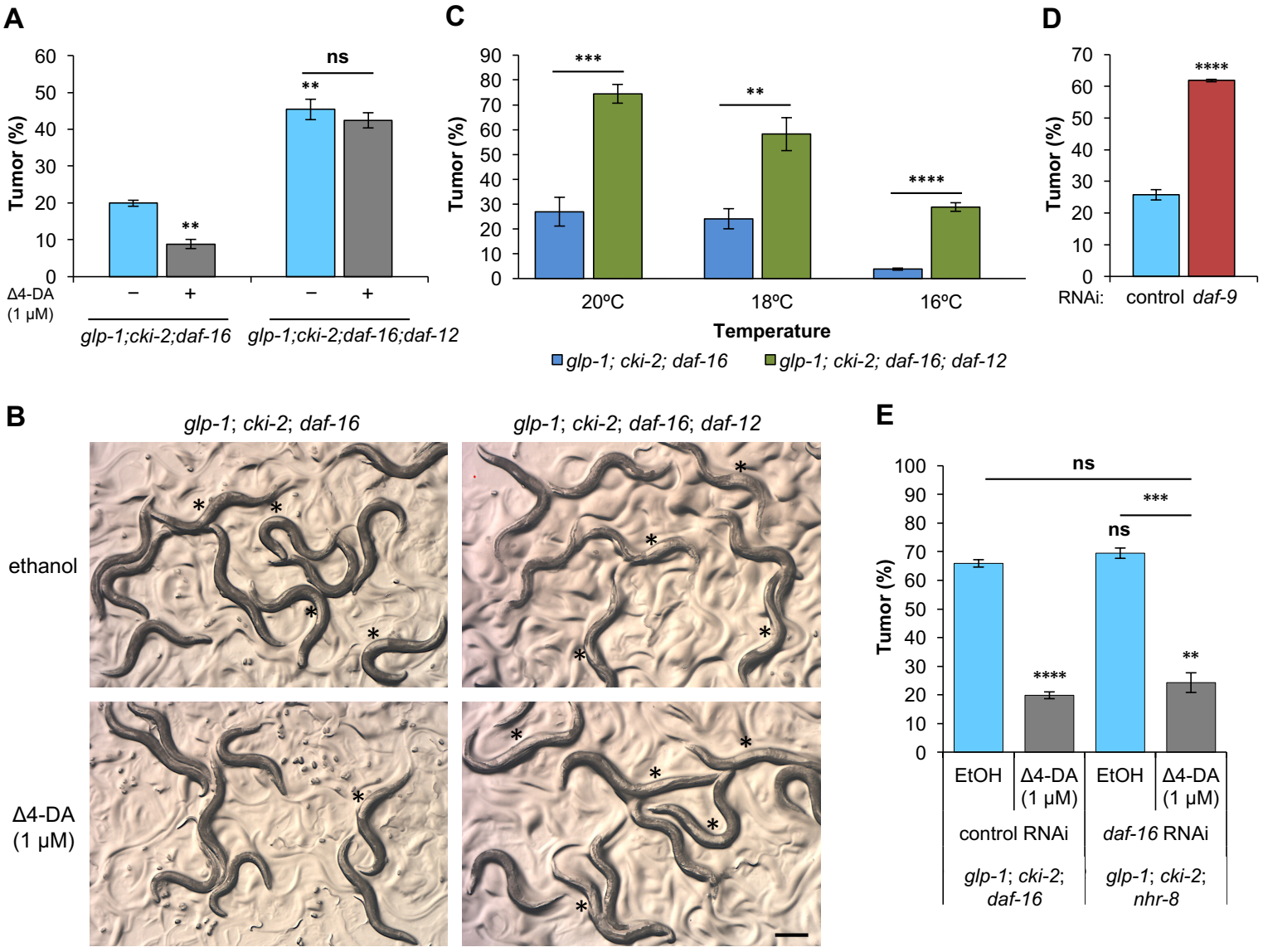
A
Tumor (%)
ns
**
**
Δ4-DA (1 μM)
glp-1;cki-2;daf-16
glp-1;cki-2;daf-16;daf-12
C
Tumor (%)
***
**
****
20ºC
18ºC
16ºC
Temperature
glp-1; cki-2; daf-16
glp-1; cki-2; daf-16; daf-12
D
Tumor (%)
****
RNAi: control daf-9
B
glp-1; cki-2; daf-16
glp-1; cki-2; daf-16; daf-12
ethanol
Δ4-DA (1 μM)
E
Tumor (%)
ns
***
ns
****
**
EtOH
Δ4-DA (1 μM)
EtOH
Δ4-DA (1 μM)
control RNAi
daf-16 RNAi
glp-1; cki-2; daf-16
glp-1; cki-2; nhr-8

Figure 4.2. Dafachronic acid inhibits the proliferation of germline tumors.

(A) The *daf-12(rh61rh411)* mutation makes germline tumors resistant to the inhibitory effects of DA. The percentage of tumors for the indicated strains treated with 1 μM Δ^4-DA or ethanol control. (B) Representative images of adult hermaphrodites from the experiment in (A). Asterisks mark tumors, which are visible as white areas in the body. Scale bar is 200 μm. (C) The *daf-12(rh61rh411)* increases germline tumor frequency. The percentage of tumors for the indicated genotypes and semi-permissive temperatures. (D) *daf-9* RNAi increases the percentage of tumors in the *glp-1(gf)*; *cki-2*; *daf-16* mutant at 18°C. (E) The *nhr-8(ok186)* mutation does not prevent the inhibitory effects of DA on germline tumors. The percentages of tumors are shown for the indicated genotypes and treatments at 18°C.

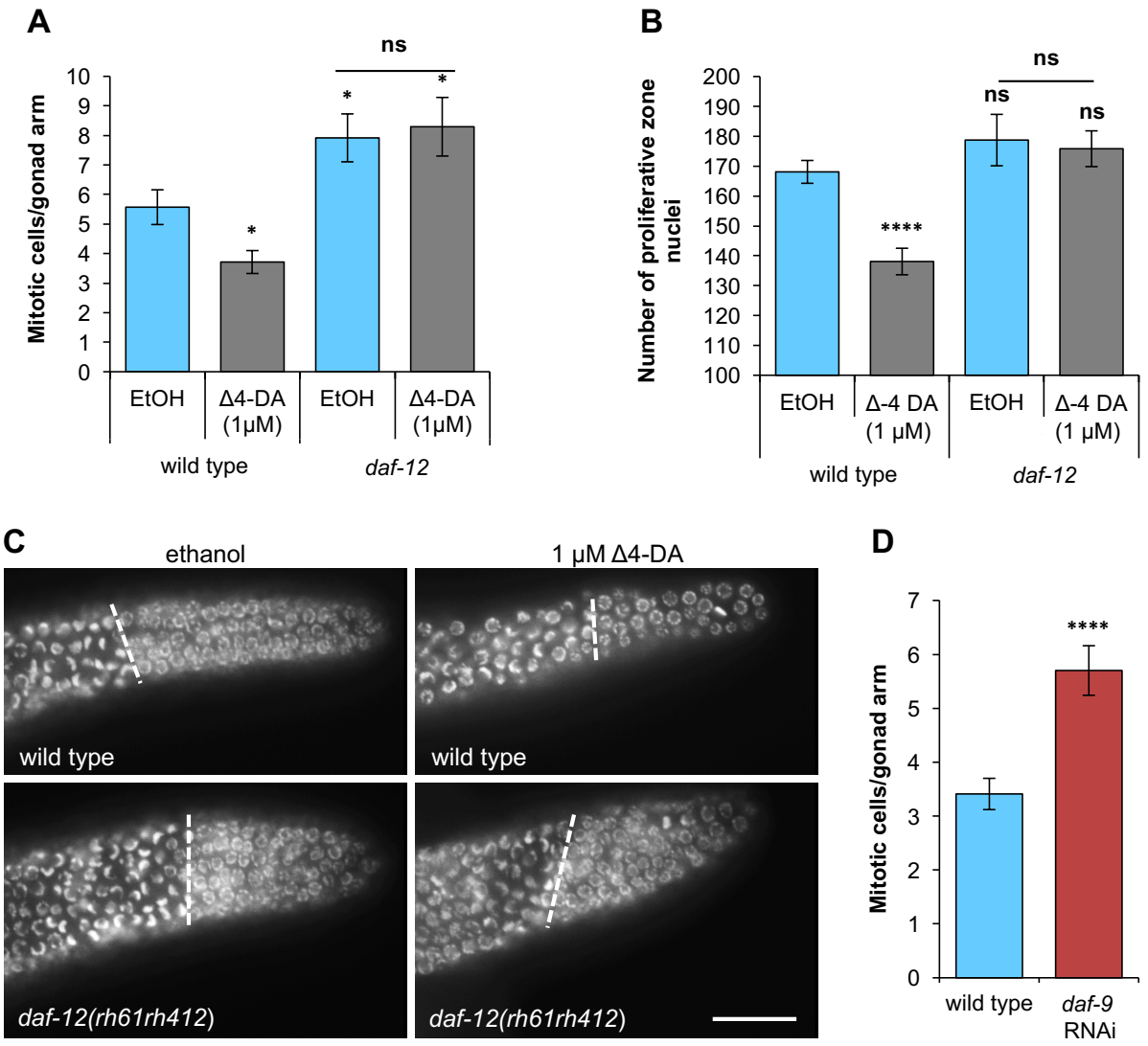
A
Mitotic cells/gonad arm
10
9
8
7
6
5
4
3
2
1
0
ns
*
*
*
EtOH
Δ4-DA (1μM)
EtOH
Δ4-DA (1μM)
wild type
daf-12
B
Number of proliferative zone nuclei
200
190
180
170
160
150
140
130
120
110
100
ns
ns
ns
****
EtOH
Δ-4 DA (1 μM)
EtOH
Δ-4 DA (1 μM)
wild type
daf-12
C
ethanol
1 μM Δ4-DA
wild type
wild type
daf-12(rh61rh412)
daf-12(rh61rh412)
D
Mitotic cells/gonad arm
7
6
5
4
3
2
1
0
****
wild type
daf-9 RNAi

Figure 4.3. Dafachronic acid inhibits mitotic germ cell proliferation in wild type

(A, B) *daf-12(rh61rh411)* mutants are resistant to the inhibitory effects of DA. The number of mitotic, phosphohistone H3 (Ser10)-positive cells per gonad arm (A) or the number of germ cells in the proliferative zone (B) for wild-type and *daf-12(rh61rh411)* adult hermaphrodites grown with 1 μM Δ^4-DA or ethanol control. (C) Representative images of the proliferative zone (to the right of the dashed line) in distal gonads stained with Hoechst 33342 for the the experiment in (B). Scale bar is 20 μm. (D) *daf-9* RNAi increases the number of mitotic germ cells per gonad arm in a wild-type background.

CHAPTER 5

CONCLUSIONS AND DISCUSSION

Mitochondrial dynamics regulation

In Chapter 2, we described a new pathway that regulates a key component of insulin-signaling to control mitochondrial fusion in *C. elegans*. We found that the CRL-regulator CAND-1 and the ubiquitin ligase SCF^{LIN-23} are required to activate the AKT-1 kinase, which inhibits the nuclear localization of DAF-16. DAF-16 transcriptionally represses the expression of the mitochondrial proteases SPG-7 and PPGN-1. In the absence of DAF-16-mediated transcriptional repression, SPG-7 and PPGN-1 reduce the level of the mitochondrial fusion protein EAT-3 to inhibit fusion of mitochondria. IIS activity controls DAF-16 through AKT-1 and therefore, this work directly links IIS to the control of mitochondrial dynamics, and identifies CAND-1 and SCF^{LIN-23}-mediated activation of AKT-1 as a new IIS regulatory mechanism.

The insulin pathway is the most significant regulator of lifespan in *C. elegans* and regulates lifespan in diverse animals [1]. Our work indicates that IIS directly controls mitochondrial fusion through the DAF-16-mediated transcriptional repression of SPG-7 and PPGN-1. DAF-16 has a central role in mediating longevity in IIS mutant and germline-depleted mutants [2]. The molecular pathway by which DAF-16 regulates mitochondrial fusion that we have described is therefore likely to be operating in both IIS and germline depletion mutants, in addition to other longevity mechanisms that rely on

DAF-16 activity. Additionally, we have shown that physical exercise also utilizes the same DAF-16-regulated mitochondrial fusion pathway, and induces longevity.

Exercise and aging

Sarcopenia is the age-dependent loss of muscle function [3]. Currently, the best intervention to slow age-related decline in muscle function is physical exercise [4]. Accumulating evidence from epidemiological studies and randomized clinical trials suggests that regular physical activity and endurance exercises reduce the occurrence of age-related pathologies, including sarcopenia, decline in cardiovascular and cognitive function, telomere length, stem cell exhaustion, and senescence [4, 5]. However, the exact mechanism by which exercise induces longevity was largely unknown. Perhaps the most illuminative study that demonstrated the mechanistic link between exercise and aging was using mitochondrial mutator mice. These mice have a proofreading-deficient mtDNA polymerase, thus accumulating mtDNA mutations at much higher rate than normal, and these mice have accelerated aging [6]. Interestingly, exercise decreased the mortality rate, and increased lifespan in the mitochondrial mutator mice [4]. Therefore, since mitochondria is the central cellular player in aging, especially in muscle cells, the most important age-related pathology overcome by physical exercise is likely to be mitochondrial dysfunction.

Insulin signaling, diabetes, and aging

Exercise also induces longevity in diabetic patients by inducing glucose uptake, thus improving insulin sensitivity [7]. As I discussed in Chapter 1, the link between insulin-

signaling and aging in mammals is counterintuitive, because reduced insulin signaling increases lifespan, but also leads to type 2 diabetes, which significantly reduces lifespan. One possible explanation for this could be that reduced insulin signaling increases lifespan if counterbalanced by efficient glucose uptake. Incidentally, metformin, which is the most widely prescribed drug to treat diabetes, increases lifespan in diabetic and non-diabetic patients by inhibiting the mitochondrial respiratory chain complex 1 [8, 9]. Also, our study shows that inhibition of respiration in *C. elegans* induces mitochondrial fusion, which has been shown to increase lifespan [10]. Therefore, mitochondrial fusion may increase lifespan despite reduced insulin signaling in diabetic patients. Mitochondrial fragmentation on the other hand has been linked to hyperglycemia-induced apoptosis in mice, and yeasts, and high levels of glucose has been shown to reduce lifespan in *C. elegans* [11-13]. Therefore, there appears to be a protective, lifespan-inducing role of mitochondrial fusion under conditions of reduced insulin-signaling, while mitochondrial fragmentation associates with hyperglycemia, apoptosis, and reduced lifespan. Incidentally, the only *C. elegans* ETC mutant that does not increase lifespan is a respiratory chain complex II mutant, which is the only respiratory complex that is nuclear encoded, therefore unaffected by age-related accumulation of mtDNA mutations [9]. Therefore, mitochondrial morphology is the central player that is a common link between insulin signaling, exercise, and aging.

Mitochondrial fusion and aging

Our work demonstrated that an increase in mitochondrial fusion causes an increase in ATP production in *C. elegans*. Reduction in ATP production is a hallmark of aging, and

mtDNA mutations that accumulate in an aging cell directly affect ATP production. Mitochondrial fusion has been shown to mechanistically increase ATP production in response to stress [14]. Since mtDNA mutations cause aging, and mitochondrial fusion prevents mtDNA mutations from spreading and enables their repair, mitochondrial fusion could influence aging by directly curbing mtDNA mutations. [15, 16]. Fusion also inhibits apoptosis, another important hallmark of aging, while mitochondrial fragmentation, which increases with age, induces apoptosis [17, 18]. Lastly, exercise has been shown to clear mutant mtDNA by activating mitophagy, and inducing mitochondrial biogenesis, both of which decline as mammals age [19]. Therefore, increased mitochondrial fusion appears to be a protective, unifying mechanism that links diverse longevity pathways, and could be an important therapeutic intervention to increase lifespan, and healthspan if conserved in humans.

Folates and FR in signaling

In Chapter 3 we described the first primary culture system for *C. elegans* germ cells. The triple mutant *glp-1(gf); cki-2; daf-16* allows cellularization and overproliferation of germ cells in vivo. This allows a homogenous population of germ cells to be isolated and cultured in CeM1 media, with survival of the cells for up to a month. This culture system was used to identify a new role of folates in signaling the proliferation of *C. elegans* germ cells. Our results show that bacterial folates arising from the *C. elegans* diet acts as an exogenous signal to stimulate the adult germ stem cell population. We observed germ cell stimulatory activity only with the folates 10-formyl-THF-Glu_n and 5,10-methenyl-THF-Glu_n. We also showed that this role of folates in germ cell proliferation is independent of

its role in one-carbon metabolism. Interestingly, increasing the conversion of 10-formyl-THF to THF via increased expression of 10-formyltetrahydrofolate dehydrogenase has been shown to inhibit human neuroblastoma cell proliferation, without affecting purine synthesis in the cell, demonstrating the cell proliferative properties of 10-formyl-THF [20].

Folates and FR in lifespan

10-formyl-THF-Glu_n- and 5,10-methenyl-THF-Glu_n-induced germ cell stimulatory activity increases with larger numbers of poly-Glu. In *C. elegans*, folates are known to decrease lifespan [21], and we have observed a sharper decline in lifespan in wild-type animals with stimulatory folates compared to non-stimulatory folates (data not shown). Therefore, our data suggests that *C. elegans* use bacterial folates as a signal to indicate the presence or absence of food, and stimulatory folates from bacteria contribute to a critical binary decision between germ stem cells (GSC) proliferation, and lifespan. This inverse relationship appears to reflect an integral choice: the availability of preferred foods, relayed to GSCs by bacterial folates and insulin/IGF-like signaling, leads to increased GSC proliferation in order to maximize offspring production; conversely, food scarcity leads to the inhibition of GSC proliferation and the activation of lifespan extension pathways. Interestingly, metformin-induced longevity in *C. elegans* correlates with a shift in bacterial folate polyglutamylation, where consistently folates with n= 3 glutamates increased, while n= 5 glutamates decreased in all metformin-treated bacterial folates tested [21]. This suggests that folates with higher number of Glu species, which we showed increases germ cell proliferation, correlates with a reduction of lifespan.

Furthermore, expression of the *skn-1* transcription factor in the ASI neurons in the pharynx and the intestine is critical for metformin-induced longevity in *C. elegans* [21]. ASI neurons have been shown to sense satiety and are known to mediate diet-restriction-induced longevity [22, 23]. Therefore, polyglutamylated (n >3) folates from bacteria that induce germ cell proliferation, could act as a signal via ASI neuron-activation, or SKN-1 activation in the intestine for presence of food, thus accelerating aging; while metformin reduces polyglutamylation of folates in the bacteria, inducing a food deprivation-like state, mimicking dietary restriction (DR).

Lastly, we identified the *C. elegans* folate receptor (FR) homolog, FOLR-1 in being required for active folates to induce germ cell proliferation. Given the link between FR-mediated signaling and cancer discussed in Chapter 1, it is not surprising that FR is required for inducing germ cell proliferation in tumorous mutants. Data from this study, and from observations made in folate research using *C. elegans* as a model system, it is clear that folates induce germ cell proliferation and lifespan by acting via bacteria, and not by the folates that are directly absorbed by the animal [21, 24, 25]. Therefore, there is increasing evidence that bacterial folates affect *C. elegans* lifespan due to their role in molecular signaling.

Folate fortification and NTDs

As discussed in Chapter 1, many countries mandate the fortification of food with folic acid to prevent neural tube defects (NTDs) [26]. A sharp decline in NTD occurrence has been documented in countries after fortification [27]. However, recent work has questioned the protective effects of folate supplementation on NTD. Folic acid

supplementation was found to cause lethality in embryos that had defects in neural tube closure in mice, leading to miscarriage [28]. On the contrary, studies in humans have shown no link between folate supplementation and miscarriage [29]. However, in humans, neural tube closure would occur in the fourth week of pregnancy and could often go unnoticed as a miscarriage [30]. In fact, in a developed country like America, the diet is expected to provide a sufficient intake of folate [27]. However, improved folate intake is warranted in targeted subgroups, which include sexually active women of childbearing age, whereas other population groups are at risk of excessive intake and are warned to be cautious [31].

The recent paradigm for the interaction of folates with cancer is that folate deficiency results in an increased frequency of oncogenesis, but that once cancers are formed, excess folates may accelerate tumor growth [32]. Therefore, folate supplements should be taken by the public more cautiously, and not be generally considered as a healthy option [33-35].

Folate fortification and cancer

Mathematical Modeling on the effects of excess folates on cancer-related biomarkers provides biological support for the observations that excessive folic acid intake increases risk of both precursor lesions (i.e., colorectal adenomas) and cancer [36]. Folates are needed for *de novo* synthesis of nucleotides, which would in principle be needed for proliferating neoplastic cells. This, combined with the fact that there is an increase in the expression of folate receptors in several cancer types provides a plausible biological reason why high levels of folate may promote carcinogenesis [37]. As discussed in

Chapter 1, the human gut appears to have a very efficient capacity to convert reduced dietary folates to 5-methyl-THF but limited ability to reduce folic acid. Therefore, large amounts of unmodified folic acid circulate in the portal vein [38]. Thus, the human body relies on the liver for reducing folic acid, even though the liver's capacity to do so is limited and variable owing to its low and highly-variable DHFR activity. Chronic exposure of the liver to folic acid can induce saturation, further causing an increase in systemic circulation of unmetabolized folic acid [38]. Unmetabolized folic acid has recently been shown to be associated with reduced natural killer cell cytotoxicity, which could impair a first-line defense against malignant cells [37]. A large-scale clinical investigation probing the benefits of supplementation observed that folates increase the incidence of prostate and other cancers [37]. Moreover, in the same study, folates induced an increase in overall mortality as seen in patients who were taking folic acid supplements [38]. Low doses of folic acid increases *C. elegans* lifespan, but is toxic at higher levels and has the opposite effect, reducing lifespan [39, 40]. FR overexpression causes a decrease in cervical carcinoma cells in vitro and in vivo, only in the presence of low folate, arguing against having large amounts of unmodified folic acid circulating in the blood [41]. Folate also has a key role in DNA methylation, and alterations in methylation patterns including global and gene-specific hypomethylation appear to be important events in the prognosis of prostate cancer [38]. Results from a randomized clinical trial has shown that a prostate-specific membrane antigen, a transmembrane-carboxypeptidase with folate hydrolase activity which can increase uptake of folate in the cells, is overexpressed in nearly all prostate cancers, and is linked to increased cancer recurrence [37]. High folic acid levels can decrease plasma homocysteine levels, causing

chromosome damage and increase in cancer markers in men [42, 43]. Moreover, *E. coli* in the human gut can take up a breakdown product of folic acid (pABA-glu), which can increase bacterial folate pools tremendously, thus allowing production of stimulatory folates to cells and tissues [40, 44]. Considering the studies in *C. elegans* where increases in bacterial folate levels can reduce lifespan, folic acid supplements can accelerate aging via gut microflora [21, 24, 40, 45].

Folate fortification- alternate strategies

The commercial fortification of cereals, grains, and bread with folic acid has made folic acid the predominant source of folates, and has resulted in a rise in tissue and blood folate levels [34]. Therefore, global folic acid supplementation may not be the most ideal intervention to supply adequate folates to the subgroups who need them. A small dose of folinic acid can restore folates in *C. elegans* without affecting folate levels in their bacterial diet [24]. The cancer-promoting FRα, which is overexpressed in most cancers, has 139-fold lower affinity for folinic acid as compared to folic acid [46]. Pharmaceutical companies, mainly in Europe have started manufacturing folinic acid based folate supplements. However, no clinical studies are available for the dosage and timing for these drugs [30]. Furthermore, at acidic pHs in the stomach and intestine, folinic acid can convert to the stimulatory folate 5,10-methenyl-THF, and subsequently to 10-formyl-THF at neutral pH. Therefore, folinic acid may induce proliferation of existing cancers in the body.

It has been suggested that consideration could be given to replacing folic acid with 5-methyl-THF in countries that have mandatory programs of flour fortification [38].

The Food and Drug Administration in the United States and the European Food Standards Agency have already approved products containing a 5-methyl-THF calcium salt (Metafolin; Merck & Cie) and a 5-methyl-THF glucosamine salt (Quatrefolic; Gnosis) [38]. Microencapsulation of 5-methyl-THF to prevent losses from manufacture should be undertaken to retain 5-methyl-THF in voluntary fortified foods (eg, breakfast cereals), and efforts should be made to reduce the loss of 5-methyl-THF from subsequent processing (e.g. heat) of fortified products [38, 47]

Also, using high-folate-producing bacterial strains as part of the starter culture for yogurt production, yogurt with elevated levels of folate could be produced. It is expected that in combination with specific growth conditions and metabolic engineering approaches, the current contribution of yogurt of 10 to 20% to the average daily intake for folate could be substantially increased [48].

Dafachronic acid inhibits germ cell proliferation

Steroid signaling is very important during *C. elegans* development to sense the environment and make developmental decisions [49]. However, the role of steroid signaling in adults and its influence on lifespan is not well understood. Dafachronic acid (DA) made by the cytochrome P-450 DAF-9, and in larval stages, prevents dauer entry under favorable conditions of food. In adults, DA is produced under conditions of starvation or dietary restriction. Starvation conditions dramatically reduce the size of the *C. elegans* germline [49]. In Chapter 4, we described a role of the steroid hormone DA in inhibiting *C. elegans* germ cells cell-autonomously. We demonstrated that DA inhibits *C. elegans* germ cell proliferation in vitro, reduces the number of germline tumors in a

tumorous mutant strain, and reduces the number of proliferative germ cells in wild-type animals. We show that DA exerts its effects on germ cells cell-autonomously via the DAF-12 receptor. DA has been known to increase lifespan only in germline-less mutants [49]. Interestingly, DAF-12 is conspicuously expressed in the somatic gonad in adults, and is required for the extended lifespan of germline-less mutants [50, 51]. Therefore, DA may act via DAF-12 in the somatic gonad and the germ line differently to induce pleiotropic effects on germ cell proliferation and lifespan.

References

1. Kenyon, C., *A pathway that links reproductive status to lifespan in Caenorhabditis elegans.* Ann N Y Acad Sci, 2010. **1204**: p. 156-62.
2. Yanos, M.E., C.F. Bennett, and M. Kaeberlein, *Genome-Wide RNAi Longevity Screens in Caenorhabditis elegans.* Curr Genomics, 2012. **13**(7): p. 508-18.
3. Walston, J.D., *Sarcopenia in older adults.* Curr Opin Rheumatol, 2012. **24**(6): p. 623-7.
4. Sun, N., R.J. Youle, and T. Finkel, *The Mitochondrial Basis of Aging.* Mol Cell, 2016. **61**(5): p. 654-66.
5. Garatachea, N., et al., *Exercise attenuates the major hallmarks of aging.* Rejuvenation Res, 2015. **18**(1): p. 57-89.
6. Kujoth, G.C., et al., *Mitochondrial DNA mutations, oxidative stress, and apoptosis in mammalian aging.* Science, 2005. **309**(5733): p. 481-4.

7. Richter, E.A. and M. Hargreaves, *Exercise, GLUT4, and skeletal muscle glucose uptake.* Physiol Rev, 2013. **93**(3): p. 993-1017.

8. Viollet, B., et al., *Cellular and molecular mechanisms of metformin: an overview.* Clin Sci (Lond), 2012. **122**(6): p. 253-70.

9. Hamilton, B., et al., *A systematic RNAi screen for longevity genes in C. elegans.* Genes Dev, 2005. **19**(13): p. 1544-55.

10. Lee, S.S., et al., *A systematic RNAi screen identifies a critical role for mitochondria in C. elegans longevity.* Nat Genet, 2003. **33**(1): p. 40-8.

11. Pereira, C., et al., *Mitochondria-dependent apoptosis in yeast.* Biochim Biophys Acta, 2008. **1783**(7): p. 1286-302.

12. Wang, W., et al., *Mitochondrial fission triggered by hyperglycemia is mediated by ROCK1 activation in podocytes and endothelial cells.* Cell Metab, 2012. **15**(2): p. 186-200.

13. Lee, S.J., C.T. Murphy, and C. Kenyon, *Glucose shortens the life span of C. elegans by downregulating DAF-16/FOXO activity and aquaporin gene expression.* Cell Metab, 2009. **10**(5): p. 379-91.

14. Westermann, B., *Bioenergetic role of mitochondrial fusion and fission.* Biochim Biophys Acta, 2012. **1817**(10): p. 1833-8.

15. Bereiter-Hahn, J. and M. Voth, *Dynamics of mitochondria in living cells: shape changes, dislocations, fusion, and fission of mitochondria.* Microsc Res Tech, 1994. **27**(3): p. 198-219.

16. Chen, H., et al., *Mitofusins Mfn1 and Mfn2 coordinately regulate mitochondrial fusion and are essential for embryonic development.* J Cell Biol, 2003. **160**(2): p. 189-200.

17. Frank, S., et al., *The role of dynamin-related protein 1, a mediator of mitochondrial fission, in apoptosis.* Dev Cell, 2001. **1**(4): p. 515-25.

18. Regmi, S.G., S.G. Rolland, and B. Conradt, *Age-dependent changes in mitochondrial morphology and volume are not predictors of lifespan.* Aging (Albany NY), 2014.

19. Diot, A., K. Morten, and J. Poulton, *Mitophagy plays a central role in mitochondrial ageing.* Mamm Genome, 2016. **27**(7-8): p. 381-95.

20. Anguera, M.C., et al., *Regulation of folate-mediated one-carbon metabolism by 10-formyltetrahydrofolate dehydrogenase.* J Biol Chem, 2006. **281**(27): p. 18335-42.

21. Cabreiro, F., et al., *Metformin retards aging in C. elegans by altering microbial folate and methionine metabolism.* Cell, 2013. **153**(1): p. 228-39.

22. Gallagher, T., et al., *ASI regulates satiety quiescence in C. elegans.* J Neurosci, 2013. **33**(23): p. 9716-24.

23. Bishop, N.A. and L. Guarente, *Two neurons mediate diet-restriction-induced longevity in C. elegans.* Nature, 2007. **447**(7144): p. 545-9.

24. Virk, B., et al., *Folate Acts in E. coli to Accelerate C. elegans Aging Independently of Bacterial Biosynthesis.* Cell Rep, 2016. **14**(7): p. 1611-20.

25. Virk, B., et al., *Excessive folate synthesis limits lifespan in the C. elegans: E. coli aging model.* BMC Biol, 2012. **10**: p. 67.

26. Crider, K.S., L.B. Bailey, and R.J. Berry, *Folic acid food fortification-its history, effect, concerns, and future directions.* Nutrients, 2011. **3**(3): p. 370-84.

27. Dunlap, B., et al., *Folic acid and human reproduction-ten important issues for clinicians.* J Exp Clin Assist Reprod, 2011. **8**: p. 2.

28. Marean, A., et al., *Folic acid supplementation can adversely affect murine neural tube closure and embryonic survival.* Hum Mol Genet, 2011. **20**(18): p. 3678-83.

29. Gindler, J., et al., *Folic acid supplements during pregnancy and risk of miscarriage.* Lancet, 2001. **358**(9284): p. 796-800.

30. Cavalli, P., *Prevention of Neural Tube Defects and proper folate periconceptional supplementation.* J Prenat Med, 2008. **2**(4): p. 40-1.

31. Bailey, R.L., et al., *Total folate and folic acid intake from foods and dietary supplements in the United States: 2003-2006.* Am J Clin Nutr, 2010. **91**(1): p. 231-7.

32. Kim, Y.I., *Role of folate in colon cancer development and progression.* J Nutr, 2003. **133**(11 Suppl 1): p. 3731S-3739S.

33. Bailey, L.B., et al., *Biomarkers of Nutrition for Development-Folate Review.* J Nutr, 2015. **145**(7): p. 1636S-1680S.

34. Hou, Z., et al., *Identification and functional impact of homo-oligomers of the human proton-coupled folate transporter.* J Biol Chem, 2012. **287**(7): p. 4982-95.

35. Kelemen, L.E., *The role of folate receptor alpha in cancer development, progression and treatment: cause, consequence or innocent bystander?* Int J Cancer, 2006. **119**(2): p. 243-50.

36. Neuhouser, M.L., et al., *Mathematical modeling predicts the effect of folate deficiency and excess on cancer-related biomarkers.* Cancer Epidemiol Biomarkers Prev, 2011. **20**(9): p. 1912-7.

37. Figueiredo, J.C., et al., *Folic acid and risk of prostate cancer: results from a randomized clinical trial.* J Natl Cancer Inst, 2009. **101**(6): p. 432-5.

38. Patanwala, I., et al., *Folic acid handling by the human gut: implications for food fortification and supplementation.* Am J Clin Nutr, 2014. **100**(2): p. 593-9.

39. Rathor, L., et al., *Folic acid supplementation at lower doses increases oxidative stress resistance and longevity in Caenorhabditis elegans.* Age (Dordr), 2015. **37**(6): p. 113.

40. Nguyen, T.P. and C.F. Clarke, *Folate status of gut microbiome affects Caenorhabditis elegans lifespan.* BMC Biol, 2012. **10**: p. 66.

41. Sun, X.L., et al., *Transduction of folate receptor cDNA into cervical carcinoma cells using recombinant adeno-associated virions delays cell proliferation in vitro and in vivo.* J Clin Invest, 1995. **96**(3): p. 1535-47.

42. Fenech, M.F., I.E. Dreosti, and J.R. Rinaldi, *Folate, vitamin B12, homocysteine status and chromosome damage rate in lymphocytes of older men.* Carcinogenesis, 1997. **18**(7): p. 1329-36.

43. Fenech, M., C. Aitken, and J. Rinaldi, *Folate, vitamin B12, homocysteine status and DNA damage in young Australian adults.* Carcinogenesis, 1998. **19**(7): p. 1163-71.

44. Hussein, M.J., J.M. Green, and B.P. Nichols, *Characterization of mutations that allow p-aminobenzoyl-glutamate utilization by Escherichia coli.* J Bacteriol, 1998. **180**(23): p. 6260-8.

45. Onken, B. and M. Driscoll, *Metformin induces a dietary restriction-like state and the oxidative stress response to extend C. elegans Healthspan via AMPK, LKB1, and SKN-1.* PLoS One, 2010. **5**(1): p. e8758.

46. Selhub, J. and W.A. Franklin, *The folate-binding protein of rat kidney. Purification, properties, and cellular distribution.* J Biol Chem, 1984. **259**(10): p. 6601-6.

47. Tomiuk, S., et al., *Studies on the retention of microencapsulated l-5-methyltetrahydrofolic acid in baked bread using skim milk powder.* Food Chem, 2012. **133**(2): p. 249-55.

48. Sybesma, W., et al., *Effects of cultivation conditions on folate production by lactic acid bacteria.* Appl Environ Microbiol, 2003. **69**(8): p. 4542-8.

49. Aguilaniu, H., P. Fabrizio, and M. Witting, *The Role of Dafachronic Acid Signaling in Development and Longevity in Caenorhabditis elegans: Digging Deeper Using Cutting-Edge Analytical Chemistry.* Front Endocrinol (Lausanne), 2016. **7**: p. 12.

50. Antebi, A., et al., *daf-12 encodes a nuclear receptor that regulates the dauer diapause and developmental age in C. elegans.* Genes Dev, 2000. **14**(12): p. 1512-27.

51. Hsin, H. and C. Kenyon, *Signals from the reproductive system regulate the lifespan of C. elegans.* Nature, 1999. **399**(6734): p. 362-6.